



THE UNIVERSITY
of ADELAIDE

The role of nitroxyl in the development of neuropathic pain.

A thesis submitted in fulfilment for the degree of
DOCTOR OF PHILOSOPHY

In

The Discipline of Physiology
Adelaide Medical School
The University of Adelaide

By

Vasiliki Staikopoulos

September

2019

Table of Contents

Abstract	i
Thesis declaration	iii
Acknowledgements	iv
Publications arising from this thesis	vi
Additional studies and co-authored publications	vii
Research grants, awards and conference presentations	viii
Abbreviations	x
<u>Chapter 1. An introduction to neuropathic pain</u>	1
1.2 Definition and epidemiology of neuropathic pain.....	1
1.2.1 Neuropathic pain disease pathology.....	3
1.2.2 Peripheral nerve injury (PNI) & epidemiology.....	3
1.3 Pain pathology.....	4
1.3.1 Anatomical overview.....	4
1.3.2 Primary sensory afferents.....	6
1.3.3 Signal transduction.....	7
1.3.4 Acute pain – peripheral modulation.....	7
1.3.4.1 Nociceptor activation.....	8
1.3.5 Persistent pain – peripheral modulation.....	9
1.3.6 Acute pain -central modulation.....	10
1.3.6.1 Molecular changes.....	10
1.3.7 Persistent pain – central modulation.....	11
1.3.8 Acute pain – interneurons and descending disinhibition.....	12
1.3.9 Persistent pain - interneurons and descending disinhibition.....	13
1.3.10 Glial cell regulation of pain processing.....	13
1.3.10.1 Tetrapartite synapse.....	14
1.3.10.2 Microglia homeostatic regulation.....	14
1.3.11 Persistent pain – microglia modulation.....	15
1.3.12 Acute pain – astrocyte modulation.....	17
1.3.13 Persistent pain – astrocyte dysregulation.....	18
1.4 Reactive nitrogen species in neuropathic pain.....	19

1.4.1 NO function and endogenous production.....	19
1.4.2 Evidence of NO role in neuropathic pain.....	20
1.4.3 Downstream signalling mechanism of NO.....	22
1.4.4 Chemical biology of NO.....	23
1.5 Nitroxyl (HNO) involvement in neuropathic pain.....	25
1.5.1 Measuring endogenous nitric oxide and nitroxyl release.....	26
1.6 Animal models of neuropathic pain.....	28
1.6.1 Types of neuropathic pain animal models.....	28
1.6.1.1 Peripheral nerve injury models.....	30
1.6.2 Behavioural measures of nociception in animals.....	31
1.6.2.1 Tactile allodynia.....	32
1.7 References.....	34
Chapter 2. Current tools for detecting nitroxyl in biology.....	63
2.1 Abstract.....	63
2.2 The link between nitroxidative signalling and pain.....	63
2.3 Production of nitroxidative species by neurons, glia, and immune cells.....	64
2.3.1 NADPH oxidase.....	66
2.3.2 Nitric oxide synthases.....	67
2.3.3 Cellular respiration.....	68
2.4 Mechanisms of nitroxidative signaling in neuronal hyperexcitability.....	70
2.4.1 Nitroxidative species as neuromodulators in pain pathways.....	70
2.4.2 Nitroxidative species activate TRP channels.....	71
2.4.3 Nitroxidative species induce mitochondrial dysfunction.....	72
2.4.4 Nitroxidative species induce neuroinflammatory signalling.....	72
2.5 Endogenous regulators of nitroxidative signalling.....	77
2.5.1 Antioxidant defense.....	77
2.5.2 Anti-inflammatory cytokine and adenosine signalling.....	77
2.6 Opposition of opioid analgesia by nitroxidative species.....	78
2.7 Nitroxidative signaling as a therapeutic target for pathological pain.....	78
2.8 Concluding remarks.....	80

2.8.1 Outstanding questions.....	80
2.9 New and emerging tools to study nitroxidative species.....	81
2.10 Update of new tools since publication.....	86
2.10.1 Nitroxyl biochemistry.....	86
2.11 Summary.....	88
2.12 References.....	94

2.13 Thesis aims and hypotheses.....99

Chapter 3. Multi-coloured fluorescent sensing toolbox for selective detection of Nitroxyl in vitro and ex vivo.....105

3.1 Abstract.....	105
3.2 Introduction.....	105
3.3 Results – Chemistry.....	107
3.3.1 Design and synthesis of sensors 1-3.....	107
3.3.2 Spectroscopic characterisation of sensors 1 – 3.....	110
3.3.3 Kinetic, Stability and Selectivity Profiles.....	110
3.4 Results – application in biological systems.....	119
3.4.1 Stability and kinetics of Sensors 1 – 3 in biological buffer.....	119
3.4.2 HNO Sensors 1, 2 and 3 are not cytotoxic to microglial cells.....	119
3.4.3 Sensor 3 can detect exogenous and endogenous HNO in microglial cell lines.....	119
3.4.4 <i>Endogenous HNO may be produced by iNOS enzyme following LPS and LPA challenge</i>	121
3.4.5 Sensor 3 is taken up into BV2 cell mitochondria.....	122
3.5 Discussion.....	134
3.6 Conclusion.....	137
3.7 Methods – Chemistry.....	137
3.7.1 Synthesis of sensors 1 – 3.....	137
3.7.2 Fluorescence of sensors 1 – 3 with and without added AS.....	144
3.7.3 Limit of detection of sensor 3.....	144
3.7.4 Fluorescence of sensors 1 – 3 with and without added AS in buffers and cell media.....	144

3.7.5 Selectivity of sensors 1 – 3.....	144
3.7.6 Quantum yield calculations.....	145
3.8 Methods – biological validation.....	145
3.8.1 Chemicals and sensors.....	145
3.8.2 Cell culture.....	145
3.8.3 Cell viability and function in the presence of Sensors 1, 2 and 3.....	146
3.8.4 Detecting HNO in cell free media.....	146
3.8.5 Detecting HNO in BV2 cells.....	147
3.8.5.1 Detection and sub-cellular localisation of endogenous HNO using Sensor 3 in BV2 cells.....	147
3.8.6 Image analysis.....	148
3.8.7 Statistics.....	148
3.9 References.....	149
3.10 Supplementary data.....	157
3.10.1 Cell culture.....	157
3.10.2 Detection of endogenous HNO using sensor 1 in supernatant of H9C2 cells.....	157
3.10.3 Confocal experiments.....	158
3.10.4 Image analysis.....	158
3.10.5 Detecting HNO in plasma/red blood cells.....	159
3.10.6 Chronic constriction injury model.....	159
3.10.7 Myocardial ischemic reperfusion injury model.....	159
3.11 Results.....	160
3.11.1 Sensor 1 may detect endogenous HNO signal in blood of neuropathic pain animals.....	160
3.11.2 Sensor 1 may detect endogenous HNO in, in vitro and in vivo models of ischemic reperfusion injury.....	161
Chapter 4. Nitroxyl reduces Cathepsin B enzymatic activity in both in vitro and in vivo models of neuropathic pain.....	169
4.1 Abstract.....	169
4.2 Introduction.....	169

4.3 Methods.....	170
4.3.1 Chemicals and assays.....	170
4.3.2 Enzymatic assay to determine exogenous Cathepsin B activity.....	170
4.3.3 Cell culture.....	171
4.3.3.1 Cell experiments.....	171
4.3.4 Animal experiments.....	172
4.3.4.1 Experimental protocol.....	172
4.3.4.2 Graded chronic constriction injury (CCI) model.....	173
4.3.4.3 von Frey mechanical allodynia behavioural testing.....	173
4.3.4.4 Tissue collection and preparation.....	174
4.3.5 Cathepsin B enzyme assay.....	174
4.3.6 Western blotting.....	174
4.3.7 Immunohistochemistry.....	175
4.3.8 Live cell preparation and Cathepsin B staining.....	176
4.3.9 Confocal acquisition.....	176
4.3.10 Image analysis.....	177
4.3.11 Statistical analysis.....	177
4.4 Results.....	178
4.4.1 Nitroxyl deactivates Cathepsin B enzyme.....	178
4.4.2 Nitroxyl inhibits LPS derived Cathepsin B enzyme activity in BV2 cells.....	178
4.4.3 CB or IL-1 β protein levels are not altered by LPS treatment in BV2 cells.....	179
4.4.4 Nitroxyl reduces neuropathic pain symptoms in mice.....	180
4.4.5 Nitroxyl reduces Cathepsin B enzyme activity in mouse spinal cord.....	181
4.4.6 HNO reduces CX3CR1 expression but not Cathepsin B in mouse spinal cord of CCI injured animals.....	181
4.4.7 Nitroxyl treatment did not change Cathepsin B, MMP-2 and MMP- 9 protein levels.....	182
4.5 Discussion.....	193
4.6 Conclusion.....	196
4.7 References.....	197

Chapter 5. Graded peripheral nerve injury alters the progression and severity of microglial activity within the spinal cord of CX3CR1-GFP mice.	205
5.1 Abstract	205
5.2 Introduction	206
5.3 Methods	208
5.3.1 Animals	208
5.3.2 Experimental design	208
5.3.2.1 Surgery (spinal window)	208
5.3.2.2 Surgery (sensory cortex window)	210
5.3.3 Graded chronic constriction injury (CCI) model	210
5.3.4 von Frey mechanical allodynia behavioural testing	211
5.3.5 Confocal imaging of spinal cord	211
5.3.6 Photoacoustic microscopy of somatosensory cortex imaging	211
5.3.7 Confocal imaging	212
5.3.8 Photoacoustic imaging	212
5.3.9 Statistical analysis	213
5.4 Results	214
5.4.1 Development of graded mechanical allodynia following nerve injury	214
5.4.2 Microglial density, circularity, process length and movement following graded nerve injury	214
5.4.3 Sensory motor cortex oxygen levels increase due to injury	216
5.5 Discussion	222
5.6 Conclusion	226
5.7 References	227
Chapter 6. General discussion	234
6.1 Detection of endogenous nitroxyl in persistent pain models	234
6.2 Exogenous nitroxyl in persistent pain and its cystine interactions	237
6.3 Spinal microglial activation is dependent upon degree of injury	239
6.4 Concluding remarks	242
6.5 References	243

Appendix 1. Cathepsin B enzyme assay protocol (Sigma-Aldrich).....	247
Appendix 2. Publications arising from this thesis.....	253

Abstract

Neuropathic pain is a debilitating persistent (chronic) pain condition which affects 2% of the total population, characterised by spontaneous pain (stimulus independent), allodynia (pain generated from non-noxious stimuli) and hyperalgesia (heightened sense of pain to noxious stimuli). Unlike other types of pain such as nociceptive or inflammatory, neuropathic pain is maladaptive and therefore neither protects or supports healing or repair. It is defined as “*pain caused by a lesion or disease of the somatosensory nervous system*” and can develop following an array of aetiologies such as peripheral or central nerve lesions, diabetes, herpes zoster, HIV and cancer, to name a few. However, resolution of the underlying disease and/or healing of the injury often does not alleviate the associated neuropathic pain symptoms suggesting that central maladaptive plasticity may occur in people with neuropathic pain. Compounding this situation, this maladaptive plasticity often renders traditional analgesics used for nociceptive and inflammatory pain ineffective, thus reducing the treatment options available for neuropathic pain sufferers. The spinal mechanisms which lead to persistent pain development have yet to be fully elucidated. It is well understood that adaptations in the reactivity of spinal glial cells (microglia and astrocytes) may also contribute to central neuronal plasticity, by releasing inflammatory mediators such as nitric oxide and other reactive nitrogen species, that enhance excitatory and/or reduce inhibitory neuronal signalling (also referred to as neuro-immune signalling). Previous limitations in methodology have limited our understanding of longitudinal changes in spinal glial during critical developmental stages in persistent pain pathology. Whether there is a correlation between glial reactivity and neuropathic pain severity during the development of the disease model, has yet to be established. Therefore, the initial aim of this thesis was to determine if reactivity characteristics of spinal microglia may correlate with peripheral injury severity and subsequent neuropathic pain symptoms, in mouse models of persistent pain (Chapter 5).

Studies suggest that following peripheral injury, there may be alternative reactive nitrogen species, other than nitric oxide, released by highly reactive glial cells which may facilitate neural plasticity within the spinal cord. The recent development of novel fluorescent tools for measuring reactive nitrogen species, such as nitroxyl, have yet to be used to identify the endogenous presence of this reactive nitrogen species in neuropathic pain development. Therefore, the second aim of this thesis was to validate the use of a novel fluorescent probe

for the detection of endogenous nitroxyl in mouse models of persistent pain (Chapter 3). The role of nitroxyl in persistent pain development, has been complicated by recent reports whereby exogenous application of high concentration of this reactive nitrogen species, can act as therapeutic agent for persistent pain. The mechanism of action has yet to be fully elucidated, however nitroxyl is highly reactive towards thiols and metalloproteases which have been implicated in various persistent pain pathways. This led to the subsequent aim of this thesis, which was to determine whether the exogenous nitroxyl donor (Angelis's salt) may reduce allodynia via its ability to cleave active cysteine residues on lysosomal proteasomes and thus reduce their enzyme function (such as Cathepsin B) in persistent pain mouse models (Chapter 4).

The studies offered herein demonstrate that: both the onset time post-injury, and level of microglial reactivity is closely correlated with the severity of peripheral injury and subsequent allodynia; endogenous nitroxyl is produced in models of persistent pain (and other diseases) and can be detected in multiple imaging platforms using novel fluorescent probes; and exogenous nitroxyl donor can reduce both Cathepsin B enzyme activity and allodynia, however Cathepsin B inactivation does not directly account for the reduced allodynia and may not be the pathway involved in this phenomenon.

Collectively, these results highlight that there is a correlation between microglial reactivity and the severity of injury and subsequent allodynia which may suggest that physicians should consider the severity of the injury when prescribing treatment and at which timepoint post-injury to best intervene. In addition, novel tools developed at the ARC Centre of Excellence for Nanoscale Biophotonics, University of Adelaide, have provided a way to demonstrate that stimuli used in persistent pain models can generate endogenous nitroxyl which can be semi-quantitatively measured. Furthermore, exogenous nitroxyl donors may reduce allodynia via the in-activation of key thiols and metalloproteases which are critical to persistent pain development. With future research, these novel fluorescent probes may be used *in vivo* to measure the endogenous nitroxyl output in central glial cells in relation to peripheral injury severity. Furthermore, future work exploring the mechanisms by which exogenous nitroxyl is able to reduce allodynia, could provide a safe therapeutic tool for treating symptoms in neuropathic pain patients.

Thesis declaration

'I certify that this work contains no material which has been accepted for the award of any other degree or diploma in my name, in any university or tertiary institution and, to the best of my knowledge and belief, contains no material previously published or written by another person, except where due reference has been made in the text. In addition, I certify that no part of this work will, in the future, be used in a submission in my name, for any other degree or diploma in any university or other tertiary institution without the prior approval of the University of Adelaide and where applicable, any partner institution responsible for the joint-award of this degree.'

'I acknowledge that copyright of published works contained within this thesis resides with the copyright holder(s) of those works.'

'I also give permission for the digital version of my thesis to be made available on the web, via the University's digital research repository, the Library Search and also through web search engines, unless permission has been granted by the University to restrict access for a period of time.'

'I acknowledge the support I have received for my research throughout the provision of an Australian Government Research Training Program Scholarship.'

Vasiliki Staikopoulos

September 2019

Acknowledgements

First and foremost, I would like to dedicate this thesis to my two children, Georgio and Marina who have been a constant source of grounding along this journey. I thank you for your patience and support throughout these last few years.

To my superstar supervisors Prof Mark Hutchinson and Dr Elizabeth Beckett, I could not have completed this PhD without your amazing support, guidance and encouragement. I will be forever grateful for the opportunities you have provided me. To Mark, for always having my back and knowing when to give it a good push, working under your guidance these last few years has been inspirational. To Liz, one of the most humble and intelligent scientist I have had the pleasure of working under, your attention to detail and editing prowess is amazing. I thank you both immensely.

I give many thanks to all the members of the Neuroimmunopharmacology lab, who have supported me and been patient with me while I sat on the fence as both part-time lab manager and PhD student. Dr Sam Lee and Dr Jiajun Liu for collaborating with me and contributing towards my thesis experimentally and JJ for your statistical insight (Chapters 3 & 5). To Drs Sanam Mustafa, Kelsi Dodds and Juliana Bajic, thank you for being both an amazing support network to bounce ideas off and great friends for helping me make it through this journey unscathed.

To my ARC Centre of Excellence for Nanoscale Biophotonics (CNBP) collaborators, Prof Andrew Abell and Drs Xiaozhou (Micelle) Zhang, Philipp Reineck, Achini Vidanapathirana and Mr Ben Pullen thank you for all your support and contribution towards the work in this thesis (Chapter 3). It has been a pleasure working with you and getting to know you over the years. In particular, Michelle, thank you for persisting with making these nitroxyl probes and your input towards the experimental design of Chapters 3 & 4.

To my collaborators at Wuhan National Laboratory for Optoelectronics (WNLO, China), Profs Zhihong Zhang and Qingming Luo and Drs Sha Qiao, Xianlin Song and Xiaoqun Yang, thank you for your contribution towards my thesis (Chapter 5) in both the conception of the manuscript and the experiments. It was a pleasure working with you and getting to know you.

This collaboration was made possible thanks to the generous support of CNBP and HUST University (Huazhong University of Science and Technology, Wuhan, China).

To Dr Peter Grace, thank you for requesting my contribution towards the review in Chapter 2 and for your permission to include it as part of my thesis. It was a pleasure collaborating with you on this manuscript.

A big thank you to Dr Jane Sibbons from Adelaide Microscopy for all your amazing input and technical support with confocal imaging throughout my PhD.

I would like to acknowledge the amazing team at the University of Adelaide Laboratory Animal Services (especially Mrs Pacita Wissell, Ms Tiffany Boehm and Mr Nathan Stringer) for taking excellent care of the animals used in these studies.

I am very grateful for the University of Adelaide, ARC Centre of Excellence for Nanoscale Biophotonics scholarship for their financial support throughout my candidature and for providing travel funds which allowed me to attend both national and international conferences. I would also like to acknowledge both the amazing professional and research teams at CNBP, whom I have had the pleasure of working closely with over the last 6 years. The nurturing and supportive environment of CNBP, has allowed me to flourish both professionally and personally. I will always be grateful for the opportunities provided to me and the friendships I have made.

To all my family and friends who encouraged me and would check-in on me to make sure I was ok and was being supported throughout these last few years. Your messages and phone calls meant more to me than you could ever know. To my brother Peter and sister-in-law Nathalie, your love and support from afar is greatly appreciated. I am grateful for your encouragement. To Arthur Staikopoulos, thank you for encouraging me to peruse my PhD and get me started on this journey.

Finally, to my biggest supporters, mum and dad; Marina and Alex Alexandrou, you have had my back from day 1, my rock and my reality check. I could not have done this without your love and support. I am forever grateful to you and will never forget you always encouraging me to aim higher and work hard for what I want. Thank you for the bottom of my heart.

Publications and manuscripts in preparation arising from this thesis

Grace PM, Gaudet AD, Staikopoulos V, Maier SF, Hutchinson MR, Salvemini D, Watkins LR.

Nitroxidative Signaling Mechanisms in Pathological Pain. Trends Neurosci. 2016

Dec;39(12):862-879. doi: 10.1016/j.tins.2016.10.003. Review article.

Staikopoulos V, Zhang X, Liu, J, Lee SM, Abell A, Hutchinson MR. Multi-coloured fluorescent

sensing toolbox for selective detection of Nitroxyl in vitro and ex vivo. Nature Chemistry. 2019.

Manuscript in preparation.

Staikopoulos V, Qiao S, Liu J, Song X, Yang X, Luo Q, Hutchinson MR, Zhang Z. Graded

peripheral nerve injury alters the progression and severity of microglial activity within the spinal

cord of CX3CR1-GFP mice. Neurobiology of disease. 2019 Under review.

Additional studies and co-authored publications

During my PhD candidature, I contributed to several additional primary research papers and reviews that are not presented in my thesis. These publications are listed below.

Parker LM, Sayyadi N, Staikopoulos V, Shrestha A., Hutchinson MR, Packer NH. Visualizing neuroinflammation with fluorescence and luminescent lanthanide-based in situ hybridization. *Journal of Neuroinflammation*. 2019 March.

Grundy L, Harrington AM, Caldwell A, Castro J, Staikopoulos V, Zagorodnyuk VP, Brookes SJH, Spencer NJ, Brierley SM. Translating peripheral bladder afferent mechanosensitivity to neuronal activation within the lumbosacral spinal cord of mice. *Pain*. 2018 Dec 5. doi: 10.1097/j.pain.0000000000001453.

Beckett EAH, Staikopoulos V, Hutchinson MR. Differential effect of morphine on gastrointestinal transit, colonic contractions and nerve-evoked relaxations in Toll-Like Receptor deficient mice. *Sci Rep*. 2018 Apr 12;8(1):5923. doi: 10.1038/s41598-018-23717-4.

Wardill HR, Gibson RJ, Van Seville YZ, Secombe KR, Coller JK, White IA, Manavis J, Hutchinson MR, Staikopoulos V, Logan RM, Bowen JM. Irinotecan-Induced Gastrointestinal Dysfunction and Pain Are Mediated by Common TLR4-Dependent Mechanisms. *Mol Cancer Ther*. 2016 Jun;15(6):1376-86. doi: 10.1158/1535-7163.MCT-15-0990.

Jacobsen JHW, Parker LM, Everest-Dass AV, Schartner EP, Tsiminis G, Staikopoulos V, Hutchinson MR, Mustafa S. Novel imaging tools for investigating the role of immune signalling in the brain. *Brain Behav Immun*. 2016 Nov; 58:40-47. doi: 10.1016/j.bbi.2016.04.014. Review.

Research grants, awards, workshop attendance and conference presentations

Throughout my PhD candidature, I received awards and scholarships in recognition of, and to support, this work. I was also fortunate to attend multiple national and international conferences to present my research findings.

Scholarships

Australian Government – Australian Post-graduate award (2016) - \$26,288 p/a for 3 years

ARC Centre of Excellence for Nanoscale Biophotonics (CNBP) research graduate scholarship 2016-2018 \$6000 p/a for 3 years

Travel awards

Walter Duncan travel fund (2016) - \$500

School of Medicine, Neuroimmunopharmacology travel scholarship (2016) - \$1500

ANS Student travel award (2017) \$250

School of Medicine travel award (2018) \$1500

IASP Student travel award (2018) \$1300 (USD)

Entrepreneurship awards

University of Adelaide ECIC Tech eChallenge runner-up (2017) - \$10,000 prize

Australian-French Entrepreneurship challenge (2017) – winning prize 10-day study tour in Paris, France (all expenses paid)

ARC Centre of Excellence for Nanoscale Biophotonics (CNBP) Shark Tank (2018) - \$5000 prize

Positions held

CNBP Adelaide node, student representative on Executive Council - 2016

ANS Student Body Council, Deputy Chair - 2017/2018

Bio-Optics Australia (Start-up company), Co-founder – 2018

Competitive workshop attendance:

Frontiers in Neurophotonics Summer School, Laval University, Quebec, Canada – 2017

Australian-French Entrepreneurship challenge, Adelaide, South Australia – 2017

CSIRO ON Prime – Accelerator program, Adelaide, South Australia – 2017

Conference presentations:

Society of Photographic Instrumentation Engineers (SPIE) 2016 – Oral presentation

Society of Photographic Instrumentation Engineers (SPIE BiOS) 2016 – Poster presentation

Society for Neuroscience (SFN) 2017 – Poster presentation

Australasian Neuroscience Society (ANS) 2016/2017 – Poster presentation

International Association for the Study of Pain (IASP) 2018 - Poster presentation

Abbreviations

1400W	inducible nitric oxide synthase inhibitor
5HT	serotonin
ADP	adenosine diphosphate
AMPA	α -amino-3-hydroxy-5-methyl -4-isoxazolepropionic acid
ARE	antioxidant response element
AS	Angeli's salt
ASIC	acid sensing channel
ATF3	activating Transcription Factor 3
ATP	adenosine triphosphate
BCA	bicinchoninic acid
BDNF	brain derived neurotrophic factor
BH4	(6R)-5, 6, 7, 8-tetrahydro-L-biopterin
BK	bradykinin
Ca	calcium
CamKII	calmodulin dependent protein kinase II
Cat S	cathepsin S
CB	cathepsin B
CCI	chronic constriction injury
CCL2	C-C Motif Chemokine Ligand 2
CFA	complete Freuds adjuvant
cGKI	cGMP-dependent protein kinase I
cGMP	cyclic guanosine monophosphate
CGRP	calcitonin gene related peptide
CIPN	chemotherapy induced peripheral neuropathy
CNS	central nervous system
COX2	cyclooxygenase-II
Cs ₂ CO ₃	caesium carbonate

CX3CR1	C-X3-C Motif Chemokine Receptor 1/fractalkine
DAMP	danger associated molecular patterns
DAPI	4',6-diamidino-2-phenylindole
DCM	dichloromethane
DIC	differential interference contrast
DIC	N, N'-diisopropylcarbodiimide
DMAP	4-Dimethylaminopyridine
DMEM	Dulbecco's modified eagle media
DMSO	dimethyl sulphide
DN	diabetic neuropathy
DNA	deoxyribonuclease
DRG	dorsal root ganglion
DTT	Dithiothreitol
EAAT	excitatory amino acid transporter
EAE	experimental autoimmune encephalomyelitis
ECM	extracellular matrix
EDRF	endothelium derived relaxation factor
EDTA	ethylenediaminetetraacetic acid
FA	flavin adenine dinucleotide
FMN	flavin mononucleotide
fNIRS	functional near-infrared spectroscopy
FRET	Forster resonance energy transfer
GABA	γ - amino butyric acid
GAD68	glutamic acid decarboxylase isoform 65
GFAP	glial fibrillary acidic protein
GFP	green fluorescent protein
GSH	glutathione
GSNO	S-Nitrosoglutathione

H ₂ S	dihydrogen sulphide
HBSS	Hank's buffered saline solution
HbT	total haemoglobin
HCl	hydrogen chloride
HNO	nitroxyl
HPLC	high performance liquid chromatography
i.p.	intraperitoneal
IFN γ	interferon gamma
IKK β	inhibitor of nuclear factor kappa-B kinase
IL-1 β	interleukin 1 β
IL6	interleukin 6
KCC2	potassium-chloride co-transporter
LDH	lactate dehydrogenase
LPA	lysophosphatidic Acid
LPS	lipopolysaccharide
MAP	mitogen-activated protein
MAPK	mitogen-activated protein kinase
mETC	mitochondrial electron transport chain
Mg	magnesium
MgSO ₄	magnesium sulphate
MMP-2	matrix metalloprotease 2
MMP-9	matrix metalloprotease 9
MPC1	monocyte chemoattractant protein 1
MPO	myeloperoxidase
MPZ	myelin protein zero
mRNA	messenger ribonucleic acid
MTT	tetrazolium dye
N ₂	nitrogen

N ₂ O ₃	dinitrogen trioxide
Na ₂ SO ₄	sodium sulphate
NADPH	nicotinamide adenine dinucleotide phosphate
NaOH	sodium hydroxide
NFκB	nuclear factor kappa-light-chain-enhancer of activated B cells
NGF	nerve growth factor
NH ₂ OH	hydroxylamine
NLRP3	nucleotide-binding domain, leucine rich family, pyrin containing 3
NMDA	N-methyl-D-aspartate
NMR	nuclear magnetic resonance
NO	nitric oxide
NO ⁺	nitrosonium
NO ₂	nitrogen dioxide
NOS	nitric oxide synthase
NOX	NADPH oxidase
NR1	NMDA receptor 1
Nrf2	nuclear factor E2 related factor 2
NSAIDS	nonsteroidal anti-inflammatory drugs
O ₂	oxygen
OCT	optimal cutting temperature
OONO-	peroxynitrite
P2X	purinergic receptor
PA	photoacoustic amplitude
PAG	periaqueductal grey
PAM	photoacoustic tomography
PBS	phosphate buffered saline
PET	photoinduced electron transfer
PFA	paraformaldehyde

PGE ₂	prostaglandin E ₂
PGI ₂	prostaglandin I ₂
PKA	protein kinase A
PKC	protein kinase C
PMP22	peripheral myelin protein 22
PNB	phenyl-N-tert-butyl nitron
PNI	peripheral nerve injury
PNS	peripheral nervous system
PRF	phenol red free
RBC	red blood cells
RFU	relative fluorescence units
RNS	reactive nitrogen species
ROI	region of interest
ROS	reactive oxygen species
RVM	rostromedial medulla
s.c.	subcutaneous
S1HL	sensory 1 hindlimb region
SAHMRI	South Australian health and medical research institute
SCI	spinal cord injury
SDS	sodium dodecyl sulfate
SF	serum free
sGC	soluble guanylate cyclase
SO ₂	oxygen saturation
SOD	superoxide dismutase
SP	substance P
SPF	specific pathogen free
TGF	transforming growth factor
THF	tetrahydrofuran

TLR4	toll like receptor 4
TNF α	tumor necrosis factor α
TrkB	tyrosine receptor kinase B
TRP	transient receptor potential
TTX	tetrodotoxin resistant
WDR	wide dynamic range

Chapter 1. An introduction to neuropathic pain

This chapter introduces neuropathic pain and its pathogenesis following peripheral nerve injury and compares it with acute nociceptive pain, while focusing on contributions of the reactive nitrogen system within the spinal cord. An overview of the current tools used to study reactive nitrogen/oxygen species, and potential glial mechanisms underlying the associated pain behaviours, will also be presented. In conjunction with the literature on the reactive nitrogen species, nitroxyl and its contributions to pain, this offers the relevant background information used to formulate the aims and hypotheses explored throughout this thesis.

1.2 Definition and epidemiology of neuropathic pain

Neuropathic pain is a pathophysiological chronic pain state, defined as “pain caused by a lesion or disease of the somatosensory nervous system” (www.iasp-pain.org; 2018). This differs from acute nociceptive pain which as of August 2019, is described as an aversive sensory and emotional experience typically caused by, or resembling that caused by, actual or potential tissue injury (www.iasp-pain.org; 2019). Unlike other types of pain such as nociceptive or inflammatory, neuropathic pain is maladaptive and therefore neither protects or supports healing or repair (Costigan *et al.*, 2009). In the general population, neuropathic pain affects approximately 1-2% of adults (Bowsher, 1991; Bennett, 1997) however these values may be an underestimate due to exclusions based on symptoms more akin to nociceptive pain. In Australia alone the total annual economic cost of chronic pain in 2018 was estimated at more than \$139.3 billion, including \$48.3 billion productivity costs and \$12.2 billion direct health care costs (pinaustralia.org.au, Deloitte report March 2019). In the US, the economic burden is estimated at \$635 billion per annum (Gaskin & Richard, 2012).

Epidemiological studies of neuropathic pain need to overcome many barriers surrounding the criteria for categorizing and identifying neuropathic pain symptoms before we can have a clear understanding of the prevalence in the total population. It has been suggested that much of the challenge lies in determining what a “lesion” or “disease” of the nervous system is and whether one can diagnose neuropathic pain without proof of the former (Smith and Torrance, 2012). The second part of the challenge is once the lesion or disease has been confirmed, how do you identify those who do or do not have neuropathic pain? Neuropathic pain or even nociceptive pain is not a binary phenomenon but rather lies along a sensory spectrum that may or may not have neuropathic mechanisms driving the symptoms (Smith and Torrance,

2012). As neuropathic pain can be attributed to a myriad of clinical conditions, it questions the need to understand the prevalence and treatment of the resulting neuropathic pain. However, there are enough similarities in the way neuropathic pain affects the population and its treatment, that it should be considered a distinct clinical condition.

Many diseases can cause lesions resulting in neuropathic pain, for example, autoimmune disease (e.g. multiple sclerosis), metabolic diseases (e.g. diabetic neuropathy), infection (e.g. shingles, postherpetic neuralgia), vascular disease (e.g. stroke), HIV, cancer as well as peripheral and central nerve trauma (Campbell and Meyer, 2006). It is often regarded as an important co-morbidity associated with these diseases. However, neuropathic pain is also acknowledged as its own condition supported by the following set of set criteria (IASP revised). It is characterized by the presence of spontaneous pain (stimulus independent), allodynia (pain generated from non-noxious stimuli) and hyperalgesia (heightened sense of pain to noxious stimuli) with patients presenting with symptoms such as burning or freezing pain, stabbing pain, tingling pain, numbness and extreme sensitivity to touch. However, the clinical manifestation varies depending on the type of underlying disease, suggesting there may be different mechanisms leading to the neuropathy which may also be reflected in the variable response to therapy. In the clinical setting, the lack of consensus regarding the clinical definition and diagnostic criteria for neuropathic pain has made epidemiological studies difficult. Estimates of neuropathic pain prevalence vary greatly throughout the literature based on 1) the type of questionnaire used; 2) whether the study was measuring the overall population frequency of neuropathic pain based on estimates of the prevalence of the main etiological conditions or 3) if they were measuring the proportion of individuals with a primary lesion or disease that experience neuropathic pain (Smith & Torrance, 2012). For example, neuropathic pain affects approximately 25% of people with diabetes, about 20% of people with herpes zoster infections (postherpetic neuralgia) upon presentation of shingles rash and around 37% of patients with lower back pain. These estimates of prevalence vary greatly according to disease state and are generally higher than the overall prevalence in the general population. Associated risk factors to developing neuropathic pain include **female gender, older age, anatomical location of the lesion, manual work, poor socioeconomic lifestyle and poor general health** (Torrance *et al.*, 2006; Bouhassira *et al.*, 2008; Smith *et al.*, 2007). Future epidemiological studies into neuropathic pain prevalence would require a strict set of

criteria for case definition and established methods for diagnosis, together with longitudinal studies to identify risk factors throughout the population, independent of the primary disease state.

1.2.1 Neuropathic pain disease pathology

Peripheral nerve damage caused by mechanical trauma and primary diseases such as metabolic diseases, neurotoxic chemicals, infection, or tumor invasion cause lesions to the peripheral nerve have all been reported to lead to neuropathic pain. (Dworkin *et al*, 2003; Woolf and Mannion, 1999). Although the primary disease and/or initial tissue injury (whereby neurons become stimulated and potentially damaged) are thought to be responsible for initiating the cascade of maladaptive changes that lead to and sustain the neuropathic pain, resolution of the underlying disease and/or healing of the injury often does not alleviate the associated neuropathic pain symptoms. Understanding the mechanisms responsible for the maladaptive plasticity allows the therapeutic opportunity to prevent the development of neuropathic hypersensitivity and allow normalization of function in established neuropathic pain (Costigan *et al*, 2009).

1.2.2 Peripheral nerve injury (PNI) & epidemiology

Damage to peripheral nerves can result from various trauma including; motor vehicle accident, penetrating injury, gunshot wound, crush, compression, traction, ischemia, occupational injury, sports-related injury, and explosion-related injury (Robinson, 2000). The anatomic location of common injury sites includes, nerves in the upper limbs including the ulnar, median, and radial nerves, along with the brachial plexus, while in the lower limbs the sciatic and deep peroneal nerves are more frequently involved (Ciaramitaro *et al*, 2010; Eser *et al*, 2009; Kouyoumdjian, 2006; Noble *et al*, 1998). The prevalence of each of these etiologies varies globally and is summarized in table 1 below, with the majority of peripheral nerve injuries stemming from either motor vehicle accidents or iatrogenic (eg. surgery) causes. Based on these causes, the risk factors associated with traumatic **PNI are males aged 18-35** with predominantly partial nerve injuries (partial axonotmesis) most prominent in the ulna nerve in the upper extremities and sciatic nerve of the lower extremities. Which is different when compared to the risk factors described for neuropathic pain in general, in section 1.2.

Table 1: Prevalence of peripheral nerve injuries by clinical presentation

Country of origin	Number of cases	Highest prevalence	Subsequent causes	Percentage of NP	Reference
Italy	158	Motor vehicle accident (45%)	Workplace accident (15%)	50%	Ciaramitaro <i>et al.</i> , 2010
Puerto Rico	163	Domestic gun violence (35%)	Motor vehicle accidents (24%)	Not reported	Miranda and Torres, 2016
Turkey	938	Motor vehicle accidents (26%)	Iatrogenic (11%)	Not reported	Eser <i>et al.</i> , 2009
Switzerland	231	Elective surgery (55%)	Post-traumatic surgery (28%)	100% NP cases	Decrouy-Duruz <i>et al.</i> , 2018

1.3 Pain pathology

It is important to our survival to be able to detect noxious stimuli, which we sense as pain, in order to protect us against further damage and facilitate normal healing processes. Changes in pain processing pathways which lead to a hypersensitivity of the system in which pain surpasses the healing process and becomes chronic, is maladaptive and debilitating. Persistent or chronic pain can be initiated at either peripheral and/or central locations and result from the plasticity of central circuits and molecules which will be discussed in the following sections.

1.3.1 Anatomical overview

Nociceptive pain signalling is perceived via nociceptive neuronal fibres (also referred to as primary sensory afferents), of which there are various types that are differentially triggered by changes in mechanical, temperature or chemical stimuli (see section 1.3.2 for details). The cell body of these nociceptive neurons reside in the dorsal root ganglia (DRG) and their axons terminate within specific layers of the outer laminae (Lamina 1 – 5) of the dorsal horn within the spinal cord, depending on their class or subtype (Figure 1.1). Secondary neurons then relay information to various brain regions (reticular formation, periaqueductal grey (PAG), limbic system, hypothalamus, basal ganglia, the insular, cingulate and somatosensory cortices) via ascending spinothalamic, spinoreticular, spinohypothalamic and spinomesencephalic tracts (from peripheral inputs) or the trigeminal ganglia (from head/face inputs) (Willis *et al.*, 1999; Tracy, 2005). The brain can also influence pain perception by inhibitory descending control generated from the midbrain (PAG) and rostroventromedial medulla (RVM) acting on the dorsal horn of the spinal cord (Dafny, 1997). Cortical nociceptive processing occurs via the activation of several cortical and subcortical brain regions including: insula cortex, frontal and

pre-frontal cortices, primary and secondary somatosensory cortices (S1 and S2 respectively) as well as many other regions (Tracy, 2005). Additionally, S1 and S2 regions of the somatosensory cortex have a predominant role in early nociceptive processing and are able to discriminate the location and intensity of the painful stimulus. As such, clear differences in activation of S1 (Yucel et al., 2015) and S2 (Ferretti et al, 2004) has been reported between painful and nonpainful stimulation.

In addition to neuronal processes, other cells types are also involved in the modulation of pain signalling and can directly and indirectly influence the neuronal signal strength at the synaptic interface within the spinal cord. The following section will outline some of the anatomical structures and molecular pathways involved in acute nociceptive signalling and the dysregulations which follows peripheral nerve damage to drive more chronic neuropathic type pain. Further to this, we will introduce the role of reactive nitrogen species and how they are involved in chronic pain signalling.

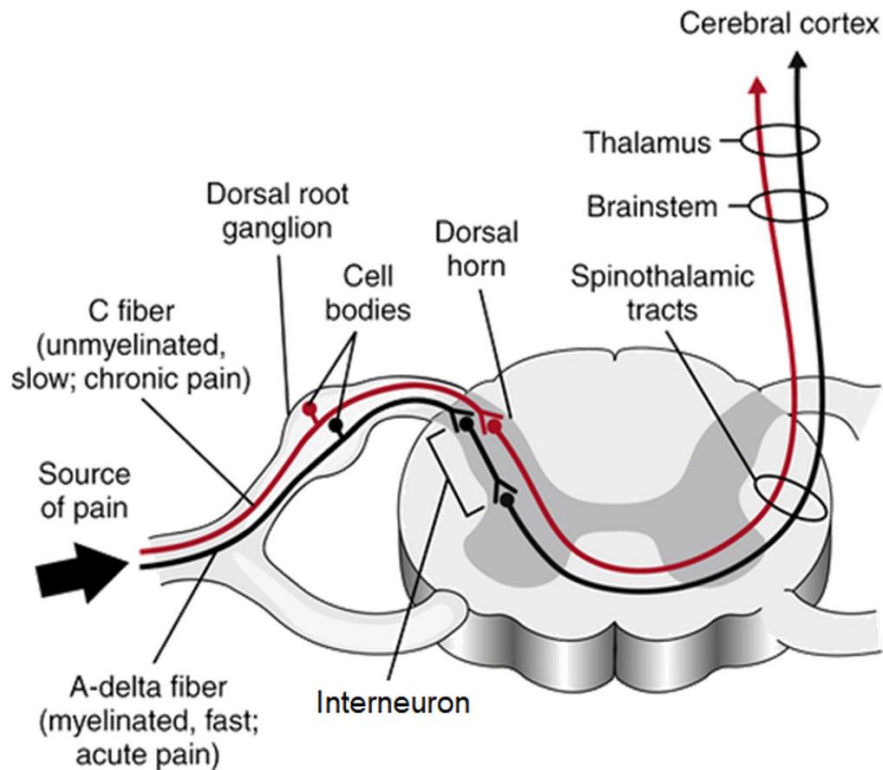


Figure 1.1 Anatomical overview of pain signalling. Neural responses begin as a transduction of signal at the periphery which is then transmitted along the A-delta and C fibres via their nerve cell bodies (which reside within the dorsal root ganglion) and terminate to form synapses with second order neurons in the outer laminae of the spinal dorsal horn. The second order fibres then project the nerve signals via tracts such as the spinothalamic tract, to higher processing centers into various brain regions where the perception of pain occurs. *Image modified from Cameron MH: Physical agents in rehabilitation: from research to practice, ed 3, St Louis, 2009, Saunders.*

1.3.2 Primary sensory afferents.

Primary sensory afferents or nociceptor fibres are pseudo-unipolar fibres with both peripheral and central terminals and a cell soma which resides in the dorsal root ganglion (DRG) or trigeminal neuron. There are 2 types of nociceptor fibres that are characterised based on whether they are myelinated (A δ type) or unmyelinated (C type). Each of these fibre types terminate into anatomically distinct laminae within the dorsal horn of the spinal cord with A δ -fibres terminating predominately in lamina I and lamina V of the dorsal horn and C-type fibres terminating throughout lamina I and dorsal part of lamina II (also referred to the Substantia gelatinosa) of the dorsal horn. These fibres can be further classified based on anatomical and electrophysiological properties (shown in Table 2). Briefly, small diameter C-fibres are slow

conducting and contribute to the dull ache and burning pain symptoms, compared to the myelinated A δ -fibres which are faster conducting and responsible for the “sharp and tingling” pain responses. The C-fibres can be further categorised based on their response to either mechanical, thermal or chemical stimuli. Polymodal C-fibres (also referred to as wide dynamic range (WDR) neurons) respond to all three stimuli (mechanical, thermal and chemical), whereas importantly, C-silent type fibres which generally respond to heat stimuli, but become mechanically sensitive after injury (Schmidt *et al.*, 1995). The presence of these complex fibre types means that humans can differentiate between different types of noxious stimuli and avoid particular dangers.

Table 2: Nerve Fibre types and their associated properties

Fibre class	Myelin	Diameter (mm)	Conduction velocity (m/s)	Spinal cord tract	Location	Function
A α	+	6-22	30-120	Ipsilateral dorsal column	Efferent to muscles	Motor
A β	+	6-22	30-120	Contralateral spinothalamic tract	Afferent from skin and joints	Tactile, proprioception
A γ	+	3-8	15-35	Ipsilateral dorsal column	Efferent to muscle spindles	Muscle tone
A δ	+	1-4	5-30	Contralateral spinothalamic tract	Afferent sensory nerves	Pain, cold, temperature, touch
sC	-	0.3-1.3	0.7-1.3	-	Postganglionic sympathetic	Various autonomic functions
dC	-	0.4-1.2	0.1-0.2	Contralateral spinothalamic tract	Afferent sensory nerves	Various autonomic functions & pain, warm, temperature, touch

Modified from: Seddighi A, et al (2016) Peripheral Nerve Injury: A review article. International Clinical Neuroscience Journal.

1.3.3 Signal transduction

Following the detection of noxious stimuli, pain signalling follows a clear pathway starting from the transduction of signal at the periphery, followed by transmission of signal via the DRG to the dorsal spinal cord, where the signal is modulated, prior to being projected via dorsal column and spinothalamic tracts to higher order brain centres. This section will focus on the transduction of signal at the periphery and the central modulation and compare the acute and chronic injury mechanisms.

1.3.4 Acute pain – peripheral modulation

As discussed in section 1.3.2, the peripheral terminals of the primary sensory neurons located within the peripheral tissue, transfer sensory information from the periphery to the dorsal horn

of the spinal cord. The specialised fibre subtypes transfer information about changes in mechanical, thermal and chemical stimuli via electrical signalling. Free endings of the nociceptive fibres transduce potentially noxious stimuli into depolarising currents, leading to ionic signalling (via action potential generation and propagation).

1.3.4.1 Nociceptor activation

Following acute noxious stimulation (such as heat, cold, mechanical or chemical), various mediators are released by the damaged peripheral tissue and signal the various nociceptors based on their receptor expression profile. This leads to channel opening at the terminals, allowing an influx of calcium to depolarize the cells and activate the signal transduction via an action potential. Damaged tissue can release bradykinin (BK) which is mediated via the B1/B2-type receptor (Whalley *et al.*, 1989) which activates protein kinase C (PKC), leading to an activation of sodium conductance via sodium channel activation (Dunn and Rang., 1990) and thus signal transduction. Further to this, tissue can also release adenosine triphosphate (ATP) and hydrogen ions (H⁺) which can activate terminals via P2X and acid-sensing channels (ASIC), respectively.

In cases where there is severe tissue damage and the noxious stimuli is prolonged, localised mast and macrophage cells can also release various peptides to directly or indirectly sensitise the peripheral nociceptor terminals, causing them to become hyperexcitable. This phenomenon occurs to help protect the damaged tissue whilst it is healing and can lead to hyperalgesia, a term describing the behaviour of a hyper-sensitivity to painful stimuli. It is generated by an increase in spontaneous activity, a lowered threshold for activation and increased and prolonged firing of peripheral nociceptors. Macrophages release inflammatory mediators such as cytokines interleukins -1b (IL-1b) and IL-6, tumour necrosis factor- α (TNF α) and other substances such as nerve growth factor (NGF) and BK. These mediators activate peripheral nerves via receptors IL-1-R (IL-1 β ligand), tyrosine kinase A receptor (TrkA; NFG ligand) and B1/B2 (BK ligand). Recruited mast cells also indirectly contribute to the sensitisation via the release of mediators such as prostaglandin E2 (PGE₂), prostaglandin I₂ (PGI₂), adenosine and serotonin (5-HT₂ & 5-HT₃) (Taiwo and Levine; 1988, 1990 and 1992), which activate their respective nociceptive receptors (Prostanoid receptor EP type (EP), ligand PGE₂; prostacyclin receptor (IP), ligand PGI₂; P2X receptor, ligand ATP; adenosine A1 receptor (A1r), ligand adenosine; 5-hydroxytryptamine receptor (5HT_r), ligand serotonin)

(Costigan and Woolf, 2000). C-fibre activation following peripheral inflammation, causes a release of substance P (SP), calcitonin gene-related peptide (CGRP), neurokinin A and nitric oxide (NO). This release of “inflammatory soup” leads to the activation of the C-silent type fibres which then contribute to the pain signalling peripheral input to the spinal cord (Chapman *et al.*, 2008). The function of NO release and how it contributes to pain signalling are discussed in detail in later sections (1.4 & 1.5). It should be noted, that as damage caused by acute noxious stimulus heals, the associated pain sensation reduces until no pain is detected.

1.3.5 Persistent pain – peripheral modulation

The most common types of nerve damage clinically presented following peripheral nerve injury is either stretch, laceration or compression injury (Ciaramitaro *et al.*, 2010). Following nerve compression injury (also referred to as entrapment injury), total loss of motor and sensory function may occur. The mechanical compression and ischemia which occurs immediately after injury provides a significantly stronger and longer lasting noxious stimulus compared to acute pain and is thought to contribute to the pathophysiology development of neuropathic pain. Local neutrophils and macrophages are attracted to the damaged nerve site by the release of chemo-attractants such as NGF, leukotriene-B4 and chemokine ligand CX3CL1 from the damaged nerve (Perkins and Tracey, 2000; Mueller *et al.*, 2001). Further release of chemokine ligands CCL2 and 3 from macrophages, together with the release of matrix metalloproteases (MMP-9) from denervated Schwann cells (peripheral astrocyte-like cells) and activated macrophages, disrupts the blood nerve barrier (Perrin *et al.*, 2005) thus facilitating the recruitment of monocytes from the peripheral blood. This invasion of immune cells is further supported by injured axons releasing vasoactive mediators SP, CGRP, BK and NO resulting in local hyperemia and swelling (Perrin *et al.*, 2005; Shubayev *et al.*, 2006). These vascular changes and subsequent influx of immune cells (macrophages, neutrophils and mast cells) over the first 48 hours, facilitate the removal of degenerating axons and myelin debris and enable Schwann cells to support the regeneration process of the injured axons (Stoll *et al.*, 2002). However, immune cells also release pro-inflammatory cytokines such as IL-1 β , IL6 and TNF α which can contribute to axonal damage and modulate spontaneous nociceptor activity in sensory neurons. Evidence to support a role for cytokines in persistent pain has been demonstrated by blocking the IL-1 β and IL6 signalling pathway which inhibits the development of spontaneous (ectopic) sensory

neuron firing and attenuates neuropathic like-behaviour (Arruda *et al.*, 2000; Wolf *et al.*, 2006). TNF α effects nociceptor neuronal activity via the TNF receptor 1 (TNFR1; which is upregulated on neurons following injury; George *et al.*, 2005) activating the p38 MAP kinase system, which increases the density and activation of tetrodotoxin resistant (TTX-R) sodium channels (Jin and Gereau, 2006) and contributes to the increased sensitivity and ectopic firing of the nociceptor fibers. Furthermore, the release of ATP from damaged tissue which act on purinergic receptors (P2X) expressed on neurons (P2X2 and P2X3 receptors) (Chen *et al.*, 2005; Jarvis *et al.*, 2002), also contributes to activation of TTX-R sodium channels. Purinergic receptors P2X3, P2X2/3 are upregulated in small diameter sensory nerve fibers in animal models of neuropathic pain (Novakovic *et al.*, 1999) and activation of these receptors by ATP, has an excitatory effect on nociceptors by the pre-synaptic release of glutamate (Gu and MacDermott, 1997). The mechanisms discussed here, provide support for a heightened transduction and transmission of signal following peripheral nerve injury, which causes an increased excitability and spontaneous firing rate of peripheral nociceptors which transmit signal to the DRG and dorsal horn of the spinal cord for further modulation.

1.3.6 Acute pain - Central Modulation

Following the transduction of signal from the peripheral terminals, the message is then relayed to the dorsal horn of the spinal cord where it can be modulated by a complex of excitatory and inhibitory interneurons and then projected to various regions of the brain for higher order perception, as well as the ventral region of the spinal cord to contribute to spinally-mediated nociceptive reflexes. The balance between excitation and inhibition is critical for maintaining normal sensory function. Synaptic inputs from peripherally derived nociceptive fibres can be modulated by changes in molecular signalling by both neuronal and non-neuronal cells within the dorsal horn and/or by descending inputs from the brain. Critically, these changes can lead to an overall increased state of hyperexcitability and enhanced nociceptive processing, which is referred to as central sensitization.

1.3.6.1 Molecular changes

Following peripheral activation, sensory fibres (including nociceptive A δ and C fibres) release pre-synaptic modulators glutamate, Substance-P and brain derived neurotrophic factor (BDNF), which act on ionotropic (NMDA & AMPA), metabotropic (mGluR, NK1) and tyrosine kinase (TrkB) post-synaptic receptors initiating a cascade of multiple signalling transduction

pathways. Glutamate binds to AMPA receptors which are non-selective cation channels and metabotropic receptors which are g-protein coupled receptors that then in turn either increase or decrease the channel activity of the ionotropic receptors to allow the influx of sodium, potassium and calcium ions into the cell which leads to depolarization. The depolarized cells can then generate fast excitatory postsynaptic potentials which ultimately encode the onset, duration, intensity, and location of peripheral noxious stimuli (Yoshimura and Nishi., 1993). An increased intensity or longer duration of nociceptor activation, results in the additional release of peptide and protein neuromodulators, which contributes to the generation of sustained depolarization (Sivilotti *et al.*, 1993; Doubell *et al.*, 1999; Miller and Woolf, 1996) and subsequent sensitisation of nociceptive fibres.

1.3.7 Persistent pain - Central Modulation

Following peripheral nerve injury, many adaptations occur within the dorsal horn of the spinal cord which lead to the development of neuropathic pain. Neuronal and glial cells alike, contribute to this phenomenon which cumulates in both increased neuronal excitability and synaptic plasticity which is referred to central sensitisation.

Following peripheral nerve injury, there is an increased release of the excitatory neurotransmitter glutamate from the pre-synaptic terminals (of the primary afferent A δ and C-fibres) within the outer lamina of the spinal cord. Unlike in acute pain signalling, the sustained release of glutamate leads to a depolarisation of post-synaptic neurons which could remove Mg²⁺ from blocking the NMDA receptor. The activation of post-synaptic NMDA receptors allows Ca²⁺ influx, which in turn activates calcium-sensitive intracellular signalling cascades that lead to phosphorylation of the NMDA receptor and other receptor-ion channels, resulting in increased excitability of post-synaptic neurons (Woolf and Salter, 2000; Krieger *et al.*, 2000). This phenomenon is referred to as “wind up” and once developed can potentiate sensory neurons to undergo phenotypic changes such that, tactile sensing fibres (A β) can now behave more like nociceptor fibres and contribute to the tactile hypersensitivity following peripheral nerve injury, which clinically manifests as allodynia (Ma *et al.*, 1996, 1998). Furthermore, the signalling events initiated by glutamatergic receptor activation include changes phosphorylation of receptor proteins which alter channel kinetics and more sustained actions due to second messenger-mediated alterations in gene expression. Such changes in transcription levels, lead to what is termed a potentiated or sensitised state and represents

longer term changes in primary sensory neurons within the dorsal horn which can progress to a persistent pain state.

One result of the calcium influx signalling cascade is the release of nitric oxide (NO) via enzyme neuronal-nitric oxide synthase (nNOS), which diffuses out of the neuron and can act as a neurotransmitter on adjacent pre- and post-synaptic nerve endings (Vincent, 1994). This leads to the increase in intracellular second messenger cyclic guanosine monophosphate (cGMP) via soluble guanylate cyclase (sGC) transduction. Details regarding NO involvement in persistent pain are further discussed in section 1.4 & 1.5. Activation of NMDA receptors also facilitates the recruitment of additional AMPA receptors to the membrane surface, thus increasing the sensitivity of the post-synaptic neuron and adding to synaptic potentiation of excitatory transmission in the spinal cord dorsal horn (Li and Zhuo, 1998; Li *et al.*, 1999), which in turn exacerbates responses to noxious stimuli and hence generates hyperalgesia.

1.3.8 Acute pain - Interneurons and descending disinhibition

Most neurons with cell bodies located within the outer laminae (I-III) of the spinal cord project locally onto motor neurons in the ventral horn of the spinal cord. These spinal interneurons can be divided into two main classes: excitatory (glutamatergic) or inhibitory (GABAergic or glycinergic). These neurons can be further characterised by their chemical, morphological, electrical and molecular phenotypes, which has been covered extensively in reviews elsewhere (Todd, 2010; Sengul and Watson, 2012). Briefly, GABAergic neurons release inhibitory neurotransmitter, γ -aminobutyric acid (GABA) which exerts its fast-inhibitory effects through ubiquitously expressed GABA_A receptors. Activation of these receptors results in the gating of chloride channels leading to membrane hyperpolarization and subsequent neuronal inhibition (Darlison, 2007). Further to this, there is also descending control from the brain centres which can contribute to the facilitation or inhibition of pain signalling. The midbrain periaqueductal grey (PAG) and the rostral ventromedial medulla (RVM) brain sites, provide inputs into both the superficial and deeper layers of dorsal horn laminae which influence nociceptive function (Fields *et al.*, 2006; Heinricher and Ingram, 2008). In normal pain states, noradrenaline release from descending fibres provide inhibitory control acting via α_2 -adrenergic receptors to inhibit the release of neurotransmitters from primary afferent neurons, thus minimising nociceptive transmission (Heinricher *et al.*, 2009).

1.3.9 Persistent pain - Interneurons and descending disinhibition

Following peripheral nerve injury, there is a decrease in the release of pre-synaptic GABA neurotransmitter in the spinal cord (Moore et al, 2002) which contributes to the hyperexcitability of the cells, in a similar fashion to releasing the breaks of a car while the accelerator is being applied at the same time (Sivilotti and Woolf., 1994). In addition to the increased excitatory signalling, mechanisms which normally regulate the inhibitory input of the synaptic response are suppressed following nerve injury. GABAergic neurons normally release inhibitory neurotransmitter GABA, which act on post-synaptic GABA_A receptors to cause hyperpolarisation of the cell and suppress firing of action potentials. However, following nerve injury there is a loss of inhibitory regulation in the outer layers of the dorsal horn, that is suggested to be driven by reduced GABA release at pre-synaptic neurons, rather than a loss of GABA_A receptors at post-synaptic neurons. This is supported by a significant decline of the enzyme responsible for synthesising GABA, GAD65 (glutamic acid decarboxylase: isoform 65) following nerve injury (Moore *et al*, 2002; Eaton *et al*, 1998). GAD65 is preferentially targeted to membranes and nerve endings where it normally synthesises GABA for vesicular release (Soghomonian and Martin, 1998). Further to this, in persistent pain states there is a switch in descending influence whereby the adrenergic inhibitory effect is suppressed and an increase in serotonin signalling via the ionotropic 5-HT₂ and 5-HT₃ receptors (located on terminals of small-diameter fibres) becomes dominant, leading to an overall increase in excitatory signalling (Colloca *et al*, 2017; Suzuki *et al*, 2004).

1.3.10 Glial cell regulation of pain processing

The modulation of neuronal synapses within the spinal cord also include other non-neuronal cell types such as microglia and astrocytes, which form a tightly regulated complex referred to as the “tetrapartite synapse”. The glial cells are responsible for monitoring and responding to synaptic neurotransmitter release and can actively contribute to the signal strength of incoming and outgoing neuronal activity. Glial involvement in acute pain signalling generated from noxious stimuli, is somewhat contentious, however the general consensus is that glial cell activation has no effect on normal responses to acute pain stimuli (Watkins *et al.*, 2001). This section will explore the homeostatic role of glial cells to form the basis for further understanding of the changes which occur during chronic pain development.

1.3.10.1 Tetrapartite synapse

The tetrapartite synapse describes a complex functional unit made up of a pre- and post-synaptic neuron, astrocyte and microglial cells (De Leo *et al.*, 2006). It is suggested that this unit contributes to the regulation of excessive excitatory signalling at the synapse, by moderating neurotransmitter release. Each of the glial cell types within the unit have their own distinct functional role that can alter with excessive incoming signal from the periphery, following noxious stimuli.

1.3.10.2 Microglia homeostatic regulation

Microglia are considered the resident immune-like cell of the CNS and are part of the tetrapartite synapse. They are in close proximity with both pre-synaptic neurons and astrocytes (Tremblay *et al.*, 2010) therefore perfectly placed to monitor neuronal firing activity and synaptic function. In the healthy CNS, microglia are very active and are constantly surveying the CNS tissue for signs of threat or damage (Nimmerjahn *et al.*, 2005) and are also involved in triggering apoptosis and clearing neuronal debris during CNS development, supporting survival and proliferation of neurons and regulating synaptic activity (Salter and Beggs, 2014). In their surveying state (often reported as their “resting” state), microglia have a complex and highly ramified morphology with long, thin and highly branched processes that extend and retract as they survey the surrounding tissue. The density of microglia, the velocity of process movement, the frequency at which extensions and retractions occur, process length and degree of ramification are all important components of baseline surveillance (Madry and Attwell, 2015). Microglial baseline motility and process length is enhanced by neurotransmitter signalling, such as ATP released from excited neurons or adjacent astrocytes which can amplify the ATP signal (Hamilton and Attwell, 2010; Anderson *et al.*, 2004; Cotrina *et al.*, 2000). These neurotransmitters act on ionotropic purine receptors (such as P2X4 and P2X7) on the cell surface of microglia (Boucsein *et al.*, 2003; Tsuda *et al.*, 2003; Chessell *et al.*, 2005; McGaraughty *et al.*, 2007), resulting in evoked process outgrowth toward the neurons and thus enhancing microglial-neuron contacts which can attenuate both spontaneous and evoked activity of previously highly active neurons (Li *et al.*, 2012). However, the mechanism for this process has not yet been elucidated.

Neuron-to-microglia communication occurs via ligands found on the cell surface on neurons, such as CX3CL1 (fractalkine), which can prevent the activation of microglia via their

chemokine receptor CX3CR1 (Zujovic *et al.*, 2000; Cardona *et al.*, 2006; Lauro *et al.*, 2008). The involvement of microglia in acute pain signalling has not been fully elicited with some reports suggesting that microglia are only activated following nerve damage but not inflammatory tissue injury (Basbaum *et al.*, 2009), however others have reported spinal microglial activation following acute formalin inflammation (Lin *et al.*, 2007; Sweitzer *et al.*, 1999).

1.3.11 Persistent pain - Microglia modulation

Following peripheral nerve injury, microglial cells are activated and recruited to form clusters around the nerve terminals of the injured nerve fibers in both the dorsal and ventral horn of the spina cord. This activated state begins approximately 2-3 days post injury and peaks around 7-9 days before tapering down in following weeks, however this is altered depending on type of injury (Smith, 2010). Nerve damage also triggers proliferation and activation of astrocytes within the spinal cord, however compared with microglia this begins and peaks later (approximately 1-3 days following injury) and can last substantially longer (Mika *et al.*, 2009). This suggests that microglial activation is required for the development of neuropathic pain following nerve injury whilst astrocyte activation is involved in the maintenance phase (Tanga *et al.*, 2004; Raghavendra *et al.*, 2003).

Technical constraints have limited longitudinal spinal glial activation studies in the spinal cord of animals. Much of the evidence to date has been generated by collecting tissue samples from multiple animals across different time points post-injury and comparing cellular and molecular markers, together with behavioural observations, between groups of animals. Differences in injury type, animal strain, molecular markers together with inherent individual behavioural differences, means that it is challenging to draw conclusions about the dynamic and temporal adaptations which glial cells undergo following nerve injury. Recent advancements in surgical techniques (Farrar *et al.*, 2012; Jahromi *et al.*, 2017; Fenrich *et al.*, 2012) as well as high resolution microscopy (Davalos and Akassoglou, 2012; Weinger *et al.*, 2015; Akassoglou *et al.*, 2017) means that we can now create windows into the spinal cord of animals to allow longitudinal observations of glial changes within individual animals post peripheral nerve injury and associate those changes and/or adaptations to behavioural responses throughout the development of neuropathic pain. More details regarding these techniques and recent outcomes are discussed in Chapter 5.

Signalling molecules released from the injured neurons can act on microglia to trigger; 1) migration, proliferation and activation 2) release of agents which contribute to synapse hyperexcitability and 3) release of cytokines and reactive nitrogen species which can contribute to neuronal cell death.

Under chronic pain conditions, CX3CL1 (fractalkine) ligand and others such as CCL1 and CCL2 released from injured neurons may be cleaved by either lysosomal cysteine protease Cathepsin S (Cat S) (Clark *et al.*, 2009) or metalloprotease 9 (MMP-9) (Kawasaki *et al.*, 2008) and activate the microglia via CX3CR1, CCR8 and CCR2 receptors, respectively (Biber *et al.*, 2008; Akimoto *et al.*, 2013; Thacker *et al.*, 2009) to cause the release of IL-1 β via p38/MAPK phosphorylation (Zhuang *et al.*, 2007). Activation of these receptors result in microglial activation (microgliosis) and subsequent release of cytokines and neurotrophic factors such as IL-1 β , IL6, BDNF and further facilitate migration of microglia to the terminals of injured neurons.

The signalling molecule ATP released by both neurons and astrocytes, acts on P2X4 and P2X7 receptors to cause the release of BDNF (leading to reduced GABAergic inhibition) and microglial activation/migration/proliferation, respectively through the intracellular influx of Ca²⁺ (Coull *et al.*, 2005; Trang *et al.*, 2009; Monif *et al.*, 2009; Zou *et al.*, 2012). P2X4 is located within lysosomal compartments of microglia (Qureshi *et al.*, 2007) and requires the activation of TLR4 receptors (Toll-like 4 receptor: pattern recognition receptors) to migrate to the cell surface (Boumechache *et al.*, 2009; Toulme *et al.*, 2010). Ligands such as saturated fatty acids, released by damaged neurons following nerve injury are through to further enhance the activation state, by binding and activating TLR4 receptors on microglia and contribute to the release of pro-inflammatory cytokines (IL-6, IL-18, TNF α , IL-1 β) and pro-inflammatory mediators (MMP-9, iNOS, NO, COX-2) via NF κ B (nuclear factor kappa-B) activation (Boumechache *et al.*, 2009; Toulme *et al.*, 2010). Interestingly, levels of cytokine mRNA (IFN- γ , IL-1, and TNF- α) are reduced in the spinal cord of injured TLR4-KO animals (Tanga *et al.*, 2005) and, in animal models of peripheral nerve injury, inhibition of TLR4 was associated with reduced allodynia (Hutchinson *et al.*, 2008).

The influx of intracellular Ca²⁺ caused by the activation of P2X4 and TLR4 receptors also leads to the release of reactive nitrogen species, such as NO, via the inducible nitric oxide synthase (iNOS) found in microglia. It is important to note here that macrophages (peripherally) and glia

(both microglia and astrocytes; centrally) are the biggest producers of nitric oxide (Ignarro, 1996; Stuehr *et al.*, 2004). More details regarding the effect of reactive nitrogen species in neuropathic pain are outlined in the section below. The release of pro-inflammatory cytokines by microglial cells can affect multiple mechanisms including; recruiting more microglia to injured terminals, activating and cross-talking with surrounding astrocytes and facilitating the hyperexcitability of nociceptive neurons (Taves *et al.*, 2013). Furthermore, the release of pro-inflammatory mediators contributes to the cleavage of extracellular matrix (ECM) proteins including cytokines to their active form. For example, following nerve injury MMP-9 is co-released with pro-IL-1 β into the ECM whereby it cleaves pro-IL-1 β to generate mature IL-1 β which can then activate ionotropic receptors on post-synaptic neurons (Kawasaki *et al.*, 2008; Schonbeck *et al.*, 1998).

Compared to nociceptive and inflammatory pain where spinal microglia are either not active at all or are only temporally activated while the injury persists then resolving back to their normal “resting” state, peripheral nerve injury can cause a long-term phenotypic change in microglia. Once activated, microglia can remain in this “primed” or “sensitised” active state and continue to significantly contribute to neuronal hyperexcitability, resulting in long term neuropathic pain (Perry, 2004; Nicoira *et al.*, 2012). This defining characteristic flags microglia as key contributors of, and hence potential therapeutic targets in, the development of neuropathic pain (Tsuda *et al.*, 2005).

1.3.12 Acute pain – Astrocyte modulation

Under normal conditions, astrocytes serve to protect the CNS and support synaptic activity by; 1) active clearance of extracellular glutamate, 2) regulate synaptic transmission by the release of neurotransmitter, 3) providing an energy source for neurons by ATP production via glucose transport (Lukovic *et al.*, 2015). Moreover, astrocytes also interact with blood vessels to regulate CNS blood flow and contribute to the maintenance of the blood brain barrier (Sofroneiw and Vinters, 2010). Glutamate clearance from the extracellular space is accomplished primarily by transporter-mediated uptake. Glutamate transporters (excitatory amino acid transporters: EAAT1 and EAAT2) are expressed by astrocytes, as well as other cell types in the CNS, including neurons, oligodendrocytes and microglia (Anderson and Swanson, 2000). However, astrocytic EAAT1 and EAAT2 have high affinity for glutamate and are the predominant glutamate uptake mechanism in the central nervous system (Rothstein *et al.*,

1996). Once glutamate is taken up by astrocytes, it is converted to glutamine via the glutamine-synthetase-pathway (Martinez-Hernandez *et al.*, 1977; Norenberg and Martinez-Hernandez, 1979) where it is released back to pre-synaptic neurons for uptake and conversion back to glutamate (Daikhin and Yudkoff, 2000). Centrally located astrocytes have been implicated in the development of hyperalgesia following acute peripheral inflammation. Following acute inflammatory stimulus (subcutaneous formalin injection) astrocytes expressing immunoreactive marker, glial fibrillary acidic protein (GFAP; a classic marker of astrocyte reactivity) were transiently increased within the superficial layers of rat dorsal horn, peaking at 45 minutes following injection and having resolved by 120 minutes (Qin *et al.*, 2006). Their function during this activated period may serve to clear the excess glutamate being released by pre-synaptic nociceptors until the noxious peripheral stimulus is cleared. However, the precise neuro-glial mechanism during acute noxious stimulation, requires further investigation.

1.3.13 Persistent pain - Astrocyte dysregulation

Following nerve injury, microglia and neurons release growth factors/cytokines (TNF α , IFN γ , IL-1, IL-6, IL-18 and others) and neurotransmitters (glutamate, noradrenaline, ATP) which lead to activation of astrocytes (astrogliosis). This can result in further release of cytokines (TNF α , IL-1 β , IL-6, IL-17) and other mediators (ATP, glutamate and PGE $_2$) as well as large amounts of NO, which contribute to increased expression and activation of ionotropic receptors (NMDA) on post-synaptic neurons, via PKA, PKC mediated phosphorylation of the NR1 subunit (Gao *et al.*, 2007), as well as neuronal cell death (Sofroniew, 2009; Milligan and Watkins, 2009; Miyoshi *et al.*, 2008; Chao *et al.*, 1996; Meng *et al.*, 2013; Guo *et al.*, 2007). These factors can also modulate microglial activity and increased migration to the site of injured nerve terminal via the release of ATP and subsequent intracellular Ca $^{2+}$ waves which propagate through a network of astrocytes via end feet gap junctions. These intracellular Ca $^{2+}$ waves are characteristic of astrocyte excitability and are triggered predominantly by ATP (Cotrina *et al.*, 1998), causing the release of Ca $^{2+}$ from intracellular stores (Sofroniew and Vinters, 2010). ATP acts via astrocytic P2X7 receptors, however, it has recently been noted that there are differential mechanisms for ATP triggered release of Ca $^{2+}$ waves versus ATP derived (calcium-independent) release of transmitters, glutamate and D-serine (Pan *et al.*, 2015; Volterra *et al.*, 2014). It is interesting to note however, that although astrocytes also expressed TLR on their

membrane (TLR2, 3, 4, 7 & 9) (Nicotra *et al.*, 2012), TLR activation is not required for priming ATP-P2X7 receptor activation, as observed in microglial cells (Facci *et al.*, 2014).

It has also been demonstrated that activation of astrocytes following nerve injury, leads to a reduced uptake of extracellular glutamate (via down regulation of the glutamate transporter EAAT2) thereby increasing neurotransmitter levels at the cleft which can lead to increased post-synaptic excitatory transmission (Sung *et al.*, 2003; Tawfik *et al.*, 2006).

Based on the above, there are multiple communication pathways between activated neurons, microglia and astrocytes that contribute to and assist in the development and maintenance of increased excitatory transmission associated with increased firing of nociceptors, which encompasses neuropathic pain. There are many potential targets for pharmacological intervention, however there are few that have been successfully translated from animal models to human trials. The remainder of this chapter will focus on a specific mediator released by both neurons and glia following nerve injury, NO and its protonated species, nitroxyl (HNO) which has been recently implicated as a potential target for neuropathic pain therapy.

1.4 Reactive nitrogen species in neuropathic pain

Following nerve injury, neurons and glia release NO both peripherally and centrally as part of the transduction and modulation process, respectively, hence contributing to the development of neuropathic pain. This section will discuss some of the proposed mechanisms of actions and highlight the disparate outcomes of endogenous versus exogenous influences of both NO and other reactive nitrogen species, in pain signalling.

1.4.1 NO function and endogenous production

Nitric oxide (NO) is a small gaseous molecule with a half-life of a several seconds which readily permeates cell membranes to elicit its action. It was identified in 1978 as being the potent endothelial vasodilator, EDRF (endothelium derived relaxation factor) and a key component of blood pressure regulation (Furchgott, 1988). Since that time, research has discovered NO is involved in many physiological systems including; cardiovascular, nervous system, immune response (including cytokine release) and wound healing (Moncada and Higgs, 1993). Within these systems, NO acts as a messenger molecule interacting with numerous molecular targets to regulate; vascular tone (by stimulating NO-sensitive guanylyl cyclase), neurotransmission, gene transcription and mRNA translation (e.g. by binding to iron-

responsive elements) and produces post-translational modifications of proteins (e.g. by ADP ribosylation) (Pfeiffer *et al.*, 1999; Forstermann and Sessa, 2012).

Endogenous NO is generated from amino acid L-arginine, by a group of enzymes known as nitric oxide synthase (NOS). There are three main isoforms of NOS which are differentially located throughout the body. Neuronal NOS (nNOS or NOS 1) is expressed by both peripheral and centrally located neurons (Forstermann and Sessa, 2012). Inducible NOS (iNOS or NOS 2) is localized to immune cells including microglia and astrocytes with the nervous system and endothelial NOS (eNOS or NOS 3) is, as the name suggests located predominantly throughout the vascular system. NO production is stimulated by an increase in intracellular Ca^{2+} which activates calmodulin to dimerize the NOS monomers and facilitate electron transfer within the reductase domain from co-substrate NADPH (nicotinamide-adenine-dinucleotide phosphate) to the oxygenase domain. This is enabled by co-factors; flavin adenine dinucleotide (FAD), flavin mononucleotide (FMN), (6R-)5,6,7,8-tetrahydro-L-biopterin (BH4) and molecular oxygen (O_2). The electrons are used to reduce and activate O_2 and to oxidize the main substrate, L-arginine to L-citrulline and NO. It is important to note here that nNOS and eNOS are constitutively expressed on their respective cells but require intracellular Ca^{2+} for activation, however, iNOS is only expressed on glial cells upon activation by endotoxins or cytokines and produces NO in a Ca^{2+} -independent manner (Forstermann and Sessa, 2012). This key difference will be further explored later in this section. Many of the physiological actions of NO have been extensively reviewed, however this section will focus on the role of NO in neuropathic pain.

1.4.2 Evidence of NO role in neuropathic pain

Numerous animal studies have shown that NO contributes to central sensitization during both inflammatory and neuropathic pain. However, NO does not appear to be involved in normal nociceptive pain signalling and/or perception (Schmidtko *et al.*, 2008). Therefore, blocking this pathway could act as a potential therapeutic target specifically for neuropathic pain. There is, however, some conflicting observation regarding NO as it has been shown to exhibit both pro- and anti-nociceptive effects. The body of work conducted over the years in an attempt to elucidate the role of NO in neuropathic pain, can be categorized into the following areas: assessing expression of the manufacturing NOS enzyme following nerve and/or tissue damage; inhibition of NO production, NO enzyme (NOS) knock-out animal models or NO

substrate or donor administration. During neuropathic pain, nNOS expression is primarily upregulated in DRG neurons (Schmidtko *et al*, 2009; 2015), leading to an increased number of nNOS-positive DRG neurons and enhanced nNOS immunoreactivity in their central terminals in the dorsal horn of the spinal cord (Zhang *et al*, 1993; Luo *et al*, 1999; Guan *et al*, 2007; Martucci *et al*, 2008).

Furthermore, iNOS has been shown to be induced in macrophages and Schwann cells both at the site and distal to the injury (Levy and Zochodne, 1998; Levy *et al*, 1999), as well as in microglia within the dorsal horn of the spinal cord (Mika *et al*, 2010, Martucci *et al*, 2008). Local inhibition of NO synthesis in the spinal cord by intrathecally (i.t.) administered non-specific NOS inhibitors (L-NAME and L-NMMA), led to a reduction of the nociceptive behaviour in several animal models of inflammatory and neuropathic pain (Meller and Gabhart, 1993). Experiments with more selective NOS isoform inhibitors such as L-NAME or 7-NI (nNOS inhibitors) and 1400W (iNOS inhibitor), identify key roles for nNOS and iNOS in the development and maintenance of neuropathic pain. Inhibiting these specific isoforms results in attenuation of mechanical allodynia and thermal hyperalgesia in animal models of neuropathic pain. (Guan., *et al*, 2007). However, studies using knock-out animal models of specific isoforms have shown only a moderate reduction in neuropathic pain pathophysiology which may be attributed to compensatory upregulation of other NOS isoforms (Hervera *et al.*, 2010) or the availability of functionally active splice variants (Eliasson *et al.*, 1997).

As inhibition or knock-out of NO synthase was shown to reduce pain, administration of NO substrate and donors were expected to have mainly a pro-nociceptive effect. This hypothesis was supported by many reports that observed an increase in hyperalgesia following intrathecal administration of NO donors (Ferreira *et al.*, 1999). However, there have also been reports of anti-nociceptive effects following intrathecal injection of the NO substrate, L-arginine (Haley *et al.*, 1992; Zhuo *et al.*, 1993). One rationale proposed for this dual pro- and anti-nociceptive effect is due to the concentration of NO present. In support of this idea, low dose administration of NO donors was shown to reduce pain symptoms in both animals and humans, however, high doses resulted in increased neuropathic pain effects (Sousa and Prado, 2001). Further to this, a study examining the use of exogenous producing NO donors in endothelial cell lines, determined that NO can elicit physiological effects at concentrations ranging from picomolar to molar values (Thomas, *et al.*, 2009). Although studies inhibiting NOS

activity support the role of NO in neuropathic pain, conflicting findings regarding NO donors could be attributed to various downstream signalling mechanisms.

1.4.3 Downstream signalling mechanism of NO

There are various mechanisms by which NO elicit its signal including activation of NO-sensitive soluble guanylyl cyclase (sGC), S-nitrosylation, tyrosine nitration and the interaction with superoxide to form peroxynitrite (Schmidtko A. 2015). Evidence suggests that the sGC pathway is the most important in neuropathic signalling. Following peripheral nerve injury, activation of post-synaptic NMDA receptors causes an influx of intracellular Ca^{2+} leading to the production of NO by nNOS and L-arginine. The resulting NO molecules can then pass through cell membranes to elicit their effect on sGC which catalyses the formation of cyclic guanosine 3'-5' monophosphate (cGMP) from guanosine 5'-triphosphate (GTP) (Figure 1.2). Cyclic GMP then can act as an intracellular messenger by activating specific protein kinases (PKG), phosphodiesterase's (PDEs) and potassium and other ion channels (Pfeiffer *et al.*, 1999). Previous studies have demonstrated that modulating this NO/sGC/cGMP/PKG pathway either by inhibiting sGC, PKG or using sGC knock-out animals (Schmidtko *et al.*, 2003; 2008), can reduce symptoms of neuropathic pain, providing further support of a role for NO in neuropathic pain signalling.

Although there have been many studies published over the years reporting NO action in neuropathic pain and other pathologies, it is important to consider that the chemistry of NO makes it a highly reactive radical in biological media which can yield many other highly reactive chemical by-products. Hence, establishing differential regulation of distinct nitroxidative species would be useful, as specific oxygen or nitrogen species have unique outcomes in the neuroinflammatory responses. Further to this, differentiating between the direct action of NO and other highly reactive intermediates is made more complex because they are hard to detect. Literature reporting purported generation and activity of NO in neuropathic pain and other pathologies, is previously implied using measurements of by-products (such as Griess reagent and others, for nitrate/nitrite detection) or by application of fluorescent probes. These methods are limited in their temporal and spatial resolution and are insufficient for defining concentrations and time courses of specific nitroxidative species. A recent review has outlined some of the more common used methods for detecting NO and intermediate species and gives some insight into potential novel detection methods (Grace *et al.*, 2016).

Overall, it is evident that upregulation of nitric oxide synthase and subsequent downstream effects occur after peripheral nerve injury. However, the specific effector NO species in neuropathic pain remains unclear, with some suggestion that activation may be occurring via oxidised or reduced forms of NO in biology (Paolucci *et al.*, 2007).

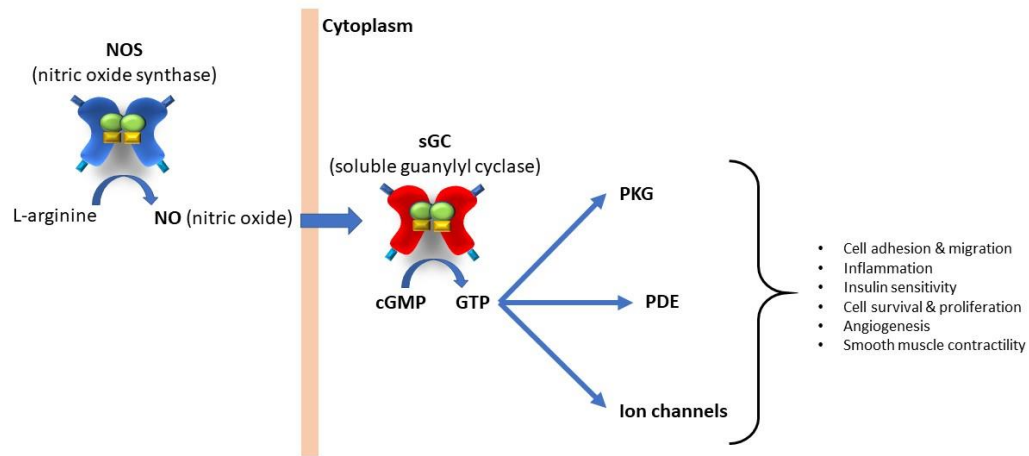


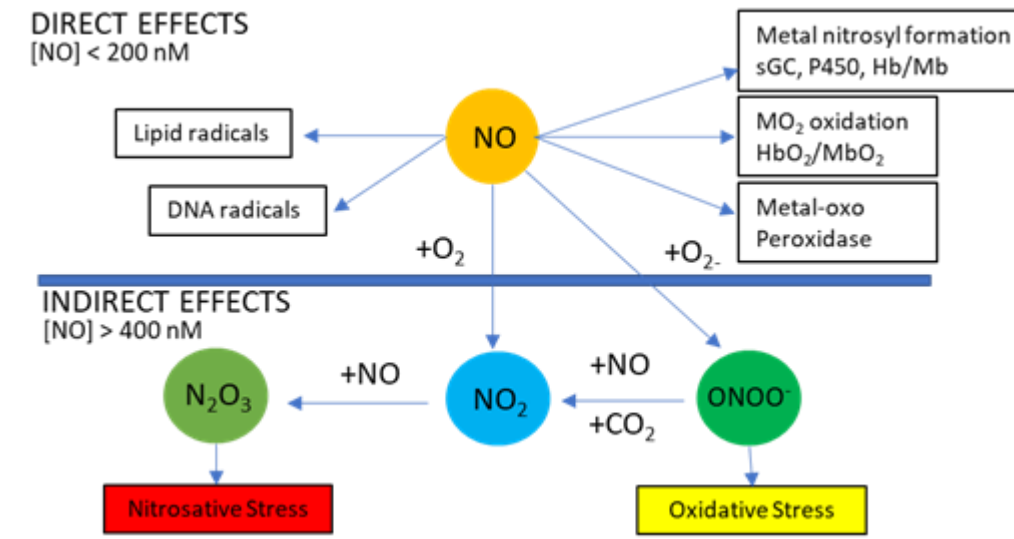
Figure 1.2 Signalling mechanisms of nitric oxide. The production of NO by nNOS and L-arginine. The resulting NO molecules can then pass through cell membranes to elicit their effect on sGC which catalyses the formation of cyclic guanosine 3'-5' monophosphate (cGMP) from guanosine 5'-triphosphate (GTP). Cyclic GMP then can act as an intracellular messenger by activating specific protein kinases (PKG), phosphodiesterase's (PDEs) and potassium and other ion channels to elicit various biological responses.

1.4.4 Chemical biology of NO

The challenge in pin-pointing the specific actions of NO comes from the enormous variety of chemical reactions and biological properties associated with it. There are excellent reviews covering the details of the chemical reactions of NO (Pfeiffer *et al.*, 1999; Meller & Gebhart, 1993), which are summarised in this section focusing on the differential signalling due to the varying concentrations of NO that can be endogenously generated. The chemical biology of NO can be divided into two categories: direct reactions and indirect reactions (Wink *et al.*, 1996). The direct effects of NO are those chemical reactions that occur fast enough to allow NO to directly react with a target molecule. In contrast, the indirect effects require that NO reacts with oxygen (O_2) or superoxide (O_2^-) to generate RNS, which subsequently react with the biological targets. Further to this, it is understood that the direct effects occur at low concentrations, while indirect effects occur at much higher concentrations of NO. The indirect effects can be separated further into nitrosative and oxidative stress (Wink and Mitchell, 1998),

whereby nitrosative stress implies the addition of a nitrosonium [NO⁺] equivalent to a thiol or amine and oxidative stress requires reactive oxygen species (OH radical, O₂⁻) which can create peroxynitrite (ONOO⁻) and nitrogen dioxide (NO₂). The balance between oxidation and nitrosation chemistry depends largely on the flux of NO (Figure. 1.3).

Figure 1.3: Direct versus indirect actions of NO



Modified from: Thomas DD *et al.*, (2009) 'The Chemical Biology of Nitric Oxide. Implications in Cellular Signalling.' *Free Radic Biol Med*; 45(1): 18–31.

The signalling pathways activated by NO appears to be highly dependent on its concentration, with different components being recruited over a broad (1000-fold) concentration range (Thomas *et al.*, 2009). In addition to concentration, temporal aspects of NO exposure are also important. Certain proteins respond immediately to NO exposure, while others require hours or even days to be activated. The concentration levels of NO and its associate species is thought to be regulated by the presence of O₂ and other reactive oxygen species (ROS) products, and vice versa, hence they can regulate each other's signalling behaviour. Many of the cellular responses elicited by NO have been determined both *in vitro*, and *in vivo* using endogenous activators and exogenous NO donors to control the local concentration. In vivo, macrophages (peripherally) and glia (centrally) are the biggest producers of nitric oxide (Ignarro, 1996; Stuehr *et al.*, 2004). The amount of NO produced from activated macrophages is dependent upon how they are stimulated. For example, different cytokines and proteins can trigger altered amounts of NO from cultured macrophages. Treatment with IFN γ + LPS (Lipopolysaccharide: TLR4 receptor agonist) yields the highest of NO release, with IFN γ pre-

treatment plus TNF α or IL-1 β stimulating 10-fold less, and treatment with TNF α or IL-1 β alone stimulating 30-fold less (Espey *et al.*, 2000). This profile suggests that NO generation and release is considerably potentiated when activation is mediated via the Toll-like receptors. This also contributes towards our understanding of how glial NO output is highly regulated in neuropathic pain conditions by the release of cytokines and other mediators following injury. However, as NO is involved in so many broad biological systems and has been demonstrated to have both detrimental and antioxidant effects, it may create many off-site effects if used as a therapeutic target for neuropathic pain. Other reactive nitrogen species have also been implicated as having a specific action in neuropathic pain, which may potentially serve as a better therapeutic target.

1.5 Nitroxyl (HNO) involvement in neuropathic pain

Aside from NO, many other reactive nitrogen species (peroxynitrite: ONOO $^-$, nitrogen dioxide: NO $_2$, dinitrogen trioxide: N $_2$ O $_3$) have been identified as being involved in physiological/pathophysiological functions, separate from that of NO. Reduced forms of NO (hydroxylamine: NH $_2$ OH) have also been examined to determine their biological activity and toxicity. One such species that has been identified is nitroxyl (HNO), the reduced, protonated form of NO (Miranda, 2005). Physiological effects of HNO, which to date have been identified using exogenous donors, include; potent vasodilation (Andrews *et al.*, 2015), increased cardiac output (Sabbah *et al.*, 2013), anti-alcoholism (DeMaster *et al.*, 1998) and recently implicated as an anti-nociceptive modulator of neuropathic and inflammatory pain (Longhi-Balbinot, DT., *et al.*, 2016; Zarpelon, AC., *et al.*, 2013). Longhi-Balbinot *et al.*, demonstrated that chronic administration of HNO donor, Angeli's salt was able to reduce chronic constriction injury (CCI; commonly used animal models of nerve entrapment) induced hyperalgesia by reducing the reactivity of spinal microglia and astrocytes together with expression of their associated cytokines. The authors suggested this analgesic affect was via the cGMP-PKG-K channel pathway after inhibition of these molecules were able to reverse the analgesic effects of Angeli's salt. HNO has also been implicated as an analgesic after pre-treatment with Angeli's salt was found to inhibit the induction of inflammatory pain responses, via the cGMP-PKG-K channel pathway (Staurengo-Ferrari *et al.*, 2014).

Interestingly, it has been proposed that HNO can alter NMDA receptor activity by modifying a thiol residue leading to a decrease in Ca $^{2+}$ influx (Kim *et al.*, 1999). As NMDA activation is

critical in the development of the increased post-synaptic excitatory signalling in neuropathic pain, this may provide an alternative mechanism of action. Further to this, HNO was also found to irreversibly inhibit the lysosomal cysteine protease Cathepsin B (Vaananen *et al.*, 2008).

Cathepsin B has been implicated in chronic pain by promoting the release and cleavage of IL-1 β in either a direct or indirect mechanism (Nakanishi, 2012). Pharmacological inhibition and gene knock-out of Cathepsin B showed reduced both tactile allodynia and IL-1 β level in models of inflammatory pain but not neuropathic pain (Sun *et al.*, 2012).

These studies were carried out using exogenous HNO donors therefore the question remains as to whether HNO is endogenously present. There has been much speculation regarding the possible chemical reactions that could result in endogenous HNO production. There are some thorough reviews that detail the proposed chemistry for the production and action of HNO in biology (Miranda, 2005; Fukuto *et al.*, 2005; Shoman and Aly, 2016). There are several potential endogenous pathways by which it may be created. It has been proposed that HNO can be formed via NOS when cofactor BH₄ is reduced (Adak *et al.*, 2000; Wei *et al.*, 2003), NH₂OH oxidation by a variety of heme proteins or reduction of NO to NO⁻ by cytochrome c leading to the formation of HNO at physiological pH, or by reaction with ubiquinol, manganese superoxide dismutase, and xanthine oxidase (Choe *et al.*, 2011). Currently there is no direct evidence to support the endogenous production of HNO in mammalian cells. Therefore, many of the proposed chemical reactions and physiological actions remain uncertain.

1.5.1 Measuring endogenous nitric oxide and nitroxyl release

Understanding the effects of concentration dependency of NO on physiological responses is important. However, NO's rapid diffusion, high reactivity, and short half-life make accurate and precise measurements challenging. Clearly any *in vitro* assessment should closely mimic the *in vivo* environment of the proposed application. It is important to also note that depending on the cellular location of the NO being produced, once diffused it will form a concentration gradient from the epicentre of release to the outer limit of the diffusion circumference meaning that the concentration at the point of production will be quickly diluted and may only elicit effects in close proximity to the source (Thomas *et al.*, 2009). Recently there has been an upsurge in the development of small molecular fluorescent probes for detecting NO and HNO. Common fluorescent probes use *o*-diaminofluorescein, a common reactive moiety for NO, can rapidly trap NO under aerobic conditions, and elicit fluorescence through suppression of

photoinduced electron transfer (PET). This concept was used to create a commercially available series of DAF probes for detecting, measuring and imaging NO in cell and tissues (Kojima *et al*, 1998). These probes have been well validated, and although next generation probes that are more stable, produce good quantum yield upon reacting with NO and stay with the cell, they are not always commercially available to apply to an immediate biological question.

Endogenous detection of HNO has also been difficult to resolve due to its physico-chemical nature. If not in the presence of thiols or metalloproteins, HNO reacts with itself to form a dimer that dehydrates to ultimately give nitrous oxide and water. This property alone requires nitroxyl to be introduced to systems by the use of donor molecules such as Angeli's salt ($\text{Na}_2\text{N}_2\text{O}_3$) (Shafirovich *et al*, 2002). HNO's reactivity with metalloproteins gave rise to Rosenthal and Lippard (2010) developing the first small-molecule fluorescent probe selective for HNO named Cull[BOT1]. This probe senses HNO in the 0.5-5 mM range and displays selectivity over other biological relevant species. Using this probe, faint intracellular HNO signals have been resolved in HeLa cells, however, the HNO donor Angeli's salt was required to raise intracellular fluorescence to quantifiable levels (Rosenthal *et al*, 2010). Furthermore, the wavelengths required to excite this probe are known to cause photobleaching and phototoxicity to live cells and tissue and led to the generation of another probe GCTPOC-1 (Zheng *et al*, 2015). Zheng, *et al* (2015) developed the first two-photon fluorescent turn-on HNO probe using tri-arylphosphine as the reactive site for HNO. The two-photon probe GCTPOC-1 has a large fluorescence enhancement, which makes it attractive for imaging HNO in living tissues with deep tissue penetration. Despite the development of these chemical probes, there are still some limitations for their general use in biology due to either low quantum yield for detection, rapid photobleaching, use of toxic wavelengths for detecting fluorophore, cell toxicity or low specificity for a specific RNS. As the next generation of RNS fluorescent probes are generated it will help advance our understanding of the biologically relevant concentrations, location and function in mammalian *in vitro* and *in vivo*. Current fluorescent probes and other assays used for the detection of short-lived molecules such as nitric oxide and its related reactive nitrogen species has recently been reviewed (Grace *et al.*, 2016) and outlines some of the advancements and limitations of current and next generation detection tools.

1.6 Animal models of Neuropathic pain

Neuropathic pain may develop either due to a disease state or trauma to peripheral or central nerves. Neuropathic pain is difficult to study in humans as the stimulus required to induce neuropathic pain is irreversible and as such, recruiting participants is understandably problematic and raises ethical issues. This necessitates the need to develop a well validated and easily reproducible animal model of neuropathic pain. The ideal models should result in reproducible sensory deficits such as allodynia, hyperalgesia and spontaneous pain over a sustained period, thus creating the opportunity to evaluate several pathophysiological conditions observed in humans, including responses to pharmacotherapies. This last point is critical as current pharmacotherapy for neuropathic pain has had limited success with little or no response to commonly used pain reducing drugs, such as NSAIDs and opiates (Woolf and Mannion, 1999). Consequently, there is a need to develop disease-modifying treatments as well as finding better targets for symptom management.

This section will focus on the types of animal models currently employed to study peripheral neuropathic pain and compare some of the benefits and limitations of each. Together with this, the various types of behavioural measures used to report the sensory deficits established within these models will be discussed.

1.6.1 Types of neuropathic pain animal models

Approximately 40 types of neuropathic pain animal models have been established that encompass the diverse aetiology and hence diverse manifestations of the neuropathy which include peripheral nerve injury, central pain and disease modifying models of neuropathy (Jaggi *et al.*, 2011). A list of neuropathic pain animal models has been provided in Table 3 with further details being covered in other reviews (Jaggi *et al.*, 2011). This section will focus on the most common peripheral nerve injury models currently used in literature and a more recent modified model that better represents the heterogeneity of neuropathic pain symptoms reported clinically.

Table 3: List of animal models of neuropathic pain

Name of model	Principle of injury	Species
Axotomy (complete sciatic nerve transection)	Complete sciatic nerve transection	Rats
Chronic constriction injury	Four loose ligatures around sciatic nerve	Rats, mice
Partial sciatic nerve ligation	Tight ligation of one-third to half of sciatic nerve	Rats, mice
Spinal nerve ligation	(i) Tight ligation of L5, L6 spinal nerves	Rats
	(ii) Tight ligation of L7 spinal nerve	Macaca fascicularis
Spared nerve injury	Axotomy of tibial and common peroneal nerves	Rats, mice
Tibial and sural nerve transection	Axotomy of tibial and sural nerves	Rats
Ligation of common peroneal nerve	Ligation of common peroneal nerve	Mice
Sciatic cryoneurolysis	Freezing of the sciatic nerve	Rats
Caudal trunk resection	Resection of caudal trunk	Rats, mice
Sciatic inflammatory neuritis	Injection of zymosan, HMG, TNF α around sciatic nerve	Rats, mice
Cuffing-induced sciatic nerve injury	Implantation of polyethylene cuff around sciatic nerve	Rats, mice
Photochemical-induced sciatic nerve injury	Thrombosis in small vessels supplying sciatic nerve by photosensitizing dye and laser	Rats, mice
Laser-induced sciatic nerve injury	Radiation mediated reduction in blood supply to sciatic nerve	Rats
Weight drop or contusive spinal cord injury	Dropping a weight over the exposed spinal cord	Rats, mice
Excitotoxic spinal cord injury	Intraspinal injections of excitatory amino acids	Rats, mice
Photochemical spinal cord injury	Thrombosis in blood vessels supplying the spinal cord by photosensitizing dye and laser	Rats
Spinal hemisection	Laminectomy of T11-T12 segments	Rats
Drug-induced		
(a) Anti-cancer agents	Direct injury of drugs to the nerves of peripheral nervous system	Rats, mice, guinea pigs
(b) Anti-HIV agents		Rabbits, rats
Diabetes-induced	Persistent hyperglycaemia-induced changes in the nerves	Rats, mice
(a) Streptozotocin-induced		
(b) Generic models		
Bone cancer pain models	Inoculation of cancerous cells into respective bones	
(a) Femur, calcaneus, tibial, humerus bone cancer pain		Rats, mice
(b) Neuropathic cancer pain	Growing a tumour in vicinity of sciatic nerve	Mice
(c) Skin cancer pain	Injection of melanoma cells in plantar region of hind paw	Mice
HIV-induced neuropathy	Delivery of HIV-1 protein gp120 to sciatic nerve	Rats
Post-herpetic neuralgia		
(a) Varicella Zoster virus	Injection of viral infected cells in the footpad	Rats, mice
(b) Herpes simplex virus	Depletion of capsaicin-sensitive afferents with resiniferotoxin	Rats
(c) Non-viral model		Rats

Chronic ethanol consumption/withdrawal	Administration of ethanol over extended period (approx.70 days)	Rats
Pyridoxine-induced	Administration of high dose pyridoxine for long period	Dogs, rats
Trigeminal neuralgia	Compression of trigeminal ganglion chronic constriction injury to infra-orbital nerve	Rats
Orofacial pain	Injection of formalin, carrageenan into temporomandibular joints and maxilla	Rats, mice
Acrylamide-induced	Administration of acrylamide for prolonged period	Rats

Adapted from: Jaggi AS, Jain V, Singh N. (2011) *Animal models of neuropathic pain. Fundamental & Clinical Pharmacology*; 25: 1–28.

1.6.1.1 Peripheral nerve injury models

The first model generated to study neuropathic pain was established in the 1970's by Wall *et al.*, which involved a complete transect of the sciatic nerve (Wall *et al.*, 1979). This model resulted in neuroma development and autotomy behaviour (self-mutilation of digits on injured hind-paw), which best represented amputee patients and their associated phantom pain. This work contributed significantly to the pathophysiological mechanisms of chronic pain, which are quite distinct from acute noxious pain, however it only represented a small percentage of clinical neuropathic pain cases. By the late 1980's Bennett and Xie (Bennett and Xie, 1988) generated a model of peripheral mononeuropathy, known as chronic constriction injury (CCI) that became one of the most commonly used animal models of nerve entrapment. The model involves loosely tying four gut ligatures around the mid-thigh level of the sciatic nerve, until a brief twitch in the foot is observed. This results in intraneural oedema, swelling and local axonal damage leading to Wallerian degeneration of the axons. The associated behaviours include signs of spontaneous pain including; mild autotomy, guarding, excessive licking, limping of ipsilateral hind paw and flicking of injured hind-paw. These behaviours appear to develop approximately 7 days post-injury and peak around 14 days lasting up to 2 months. Subsequent models were later developed by Seltzer *et al.*, (Partial sciatic nerve ligation: Seltzer *et al.*, 1990) and Kim and Chung (L5/L6 spinal nerve ligation: Kim and Chung, 1992) that mimic human symptoms of causalgia (burning pain). In the partial sciatic nerve ligation model, the dorsal third to a half of the sciatic nerve is tightly ligated just distal to the point at which posterior biceps semitendinosus nerve branches. Signs of spontaneous pain include paw guarding and licking on the injured side. These behaviour changes are reported approximately a week following injury and persist for up to 6 weeks. The L5/6 spinal nerve ligation is a more involved surgery, however, easier to reproduce between animals than the

aforementioned sciatic models. It involves separating out the L5 and L6 spinal nerves and tightly ligating each nerve individually just distal the DRG. Behavioural changes attributed to spontaneous pain, allodynia and hyperalgesia are present in these animals 24-48 hours following injury and persist for up to 16 weeks. These models have contributed significantly to the understanding of the pathophysiological mechanisms underlying neuropathic pain and provided a platform to measure the potential of therapeutic agents. Although these models can generate behaviours which are closely analogous to human symptoms, a major limitation is that they represent a binary model of pain (present versus absent). Clinically, patients present with a range of pain sensitivities suggesting that pain sensory experiences fall along a spectrum. However, it should be noted that although the injury model is binary there is growing evidence to suggest that measuring complex behaviours (such as emotional symptoms anhedonia, motivation and depression) in rats may be more closely related to changes in the degree of neuroimmune activation following peripheral nerve injury, as opposed to only measuring mechanical responses for signs on allodynia (Fiore & Austin, 2019).

In 2010, Grace *et al*, developed an animal model of neuropathic pain which was a modification of the Bennett and Xie CCI sciatic injury model. This involved modifying the number of ligatures tied around the sciatic nerve, from 0 to 4, but ensuring that each animal was exposed to 4 pieces of suture to control for the immune response to the suture itself. The additional sutures were placed beneath the skin prior to closing the wound. This study identified a 'dose-response' relationship, demonstrating that varying the number of sutures both delayed the onset of allodynia and altered the absolute level of allodynia accordingly. In animals with ligatures, mechanical allodynia was observed from day 3 post injury and persisted until day 29. The authors also reported a graded relationship between the associated molecular changes in the spinal glia of these animals and the number of nerve ligations. This model provided an alternative system to detect subtle pathophysiological and molecular changes following pharmacological intervention at sub-maximal pain thresholds.

1.6.2 Behavioural measures of nociception in animals

One major limitation of using animal models to learn about neuropathic pain is their inability to verbally communicate their sensory experiences. Therefore, experimenters often rely on tactile measures and obvious physiological or behavioural changes to determine altered states of

nociception, which can be somewhat subjective and can introduce observer bias. This makes it somewhat difficult to compare animal outcomes with clinical presentation of symptoms.

However, there are a number of techniques adopted over the years (Table 4) which have allowed for researchers to observe these pathophysiological changes in a more reproducible way (Deuis *et al.*, 2017). It is important to point out however, that each of these methods have their limitations which have been extensively reviewed elsewhere (Mogil, 2009). The most common phenomena tested for the presence of “pain-like” behaviours in animals include observation of spontaneous pain characteristics (over grooming, autotomy, vocalisation, reduced mobility), or stimulus invoked responses such as tactile allodynia and mechanical and thermal hyperalgesia. There are many reportable elements within each of these observations, however tactile allodynia which is one of the most common phenomena reported and will be the focus of this next section.

Table 4: Methods to evaluate pain behaviours

Stimulus evoked pain like behaviours			
<u>Stimulus</u>	Phenomenon tested	Method	Reference
Mechanical pressure	Mechanical allodynia	Manual von Frey	von Frey, 1896
Mechanical pressure	Mechanical allodynia	Electronic von Frey	Martinov <i>et al.</i> , 2013
Mechanical pressure	Mechanical hyperalgesia	Randall-Selitto test	Randal and Selitto, 1957
<u>Heat stimulus</u>	Heat allodynia	Tail flick test	D'Amour and Smith, 1941
<u>Heat stimulus</u>	Heat allodynia	Hot plate test	Woolfe & Macdonald, 1944
<u>Heat stimulus</u>	Heat allodynia / hypoalgesia	Hargreaves test	Hargreaves <i>et al.</i> , 1988
<u>Heat stimulus</u>	Heat allodynia / hypoalgesia	Thermal probe test	Deuis and Vetter, 2016
<u>Cold stimulus</u>	Cold allodynia	Cold plate test	Allchome <i>et al.</i> , 2005
<u>Cold stimulus</u>	Cold allodynia	Acetone evaporation test	Carlton <i>et al.</i> , 1994
<u>Cold stimulus</u>	Cold allodynia / hyperalgesia	Cold plantar test	Brenner <i>et al.</i> , 2012
<u>Thermal stimulus</u>	Thermal sensitivity	Thermal preference test	Mogrich <i>et al.</i> , 2005
Non-stimulus evoked nociception test			
Automated behaviours	Spontaneous pain	Grimace scale	Langford <i>et al.</i> , 2010
Automated behaviours	Spontaneous pain	Burrowing	Deacon, 2006
Automated behaviours	Spontaneous pain	Weight bearing/gait analysis	Schott <i>et al.</i> , 1994
Automated behaviours	Spontaneous pain	Automated behaviours	Brodkin <i>et al.</i> , 2014

Adapted from Deuis JR, Dvorakova LS and Vetter I (2017) *Methods Used to Evaluate Pain Behaviors in Rodents. Front. Mol. Neurosci; 10(284): 1-17*

1.6.2.1 Tactile allodynia

Tactile allodynia is the phenomenon of pain generated by a touch stimulus, which is otherwise considered non-noxious in non-pathological states. This is quantified in rodents by a withdrawal response from an applied stimulus (such as von Frey filament), that does not

normally evoke a withdrawal response. In most studies reporting tactile allodynia, von Frey filaments (also known as Semmes-Weinstein (S-W) monofilaments) are utilized to assess mechanical sensitivity. These filaments were designed to assess tactile sensation in humans (Bell-Krotoski, 1987) and have been successfully used in rodent models over the years (Chaplan *et al.*, 1994). The monofilaments are generally selected in either random or increasing logarithmic stiffness and are applied perpendicular to the surface with enough force to cause the filament to buckle. The dwell time (1-10 seconds) or number of applications (1 – 10) per filaments varies depending upon the method employed, but the resulting measure is always counted once the animal withdraws the hind-paw (or exhibits vocalization in the case of face measurements). The outcomes reported vary depending upon; the weight and/or species of the animal, if the animal is restrained or freely moving, if application is from the plantar or dorsum aspect of the paw (Ren, 1999); if the experimenter is measuring graded response or binary (Grace *et al.*, 2010) or if the experimenter is assessing male or female subjects (Nicotra *et al.*, 2014; Mogil, 2009). These variations in methodological approach to tactile assessment means caution is required when comparing between studies. For example, dwell time differences of filament application may be activating different mechanisms, with Bove *et al.*, (2006) suggesting that longer application times may trigger the itch response, rather than pain. Further to this, many methods were developed examining only male animal cohorts and when employed to compare male to female cohorts, reported baseline difference prior to intervention (Mogil, 2009) inferring that female animals exhibit inherently lower pain thresholds than their male counterparts. This was challenged by Nicotra *et al.*, (2014) that suggested the tactile testing methods employed in previous 'male v female' studies may not best represent the clinical pain scenario. They were able to demonstrate a refined preclinical tactile allodynia test that was sensitive enough to determine post-injury male and female difference in a graded injury model, taking into consideration the oestrus phase of the cycling females, using phasic application of lower threshold filaments (Nicotra *et al.*, 2014). This methodology is well suited for measuring responses in animal models of graded injury (Grace *et al.*, 2010) which generates more subtle and clinically relevant changes than binary models previously described. As patient's pain experiences often fall along a spectrum, this graded model is important for better translation of both pain experiences and treatment response from animal to human subjects, and vice versa.

1.7 References

Adak S, Wang Q, and Stuehr DJ. (2000) Arginine conversion to nitroxide by tetrahydrobiopterin-free neuronal nitric-oxide synthase - implications for mechanism. *J Biol Chem*; 275: 33554–33561.

Akassoglou K, Merlini M, Rafalski VA, Real R, Liang L, Jin Y, Dougherty SE, De Paola V, Linden DJ, Misgeld T and Zheng B. (2017) In Vivo Imaging of CNS Injury and Disease. *The Journal of Neuroscience*; 37(45): 10808 –10816.

Akimoto N, Ifuku M, Mori Y and Noda M. (2013) Effects of chemokine (C–C motif) ligand 1 on microglial function. *Biochemical and Biophysical Research Communications*; 436: 455–461.

Allchorne AJ, Broom DC and Woolf CJ. (2005). Detection of cold pain, cold allodynia and cold hyperalgesia in freely behaving rats. *Mol. Pain*; 1: 36. doi: 10.1186/1744-8069-1-36

Anderson CM and Swanson RA. (2000) Astrocyte Glutamate Transport: Review of Properties, Regulation, and Physiological Functions. *Glia*; 32: 1–14.

Anderson CM, Bergher JP and Swanson RA. (2004) ATP-induced ATP release from astrocytes. *J. Neurochem.* 88, 246–256 54.

Andrews KL, Lumsden NG, Farry J, Jefferis AM, Kemp-Harper BK, and Chin-Dusting JP. (2015) 'Nitroxyl: a vasodilator of human vessels that is not susceptible to tolerance,' *Clinical Science*; 129(2): 179–187.

Arruda JL, Sweitzer S, Rutkowski MD. and De Leo JA. (2000) Intrathecal anti-IL-6 antibody and IgG attenuates peripheral nerve injury-induced mechanical allodynia in the rat: possible immune modulation in neuropathic pain. *Brain Res*; 879: 216–225.

Basbaum AI, Bautista DM, Scherrer G, Julius D. (2009) Cellular and molecular mechanisms of pain. *Cell*; 139(20): 267-284.

Bell-Krotoski JA. (1987) Repeatability of the Semmes-Weinstein monofilaments. *J. Hand Surg*; 12:155–161.

Bennett GJ and Xie Y-K. (1988) A peripheral mononeuropathy in rat that produces disorders of pain sensation like those seen in man. *Pain*; 33(1): 87-107.

Bennett GJ. (1997) Neuropathic pain: an overview. In: Borsook D, editor. *Molecular biology of pain*. Seattle: IASP Press: 109–13.

Biber K, Vinet J and Boddeke HW. (2008) Neuron-microglia signaling: chemokines as versatile messengers. *J. Neuroimmunol*; 198: 69–74.

Boucsein C, Zacharias R, Färber K, Pavlovic S, Hanisch U-K and Kettenmann H. (2003) Purinergic receptors on microglial cells: functional expression in acute brain slices and modulation of microglial activation in vitro. *Eur. J. Neurosci*; 17: 2267–2276.

Bouhassira D, Lanteri-Minet M and Attal N. (2008) Prevalence of chronic pain with neuropathic characteristics in the general population. *Pain*; 136: 380–7.

Boumechache M, Masin M, Edwardson JM, Górecki DC, Murrell-Lagnado R. (2009) Analysis of assembly and trafficking of native P2X4 and P2X7 receptor complexes in rodent immune cells. *J Biol Chem*; 284(20): 13446-54.

Bouvier M, Szatkowski M, Amato A & Attwell D. (1992) The glial cell glutamate uptake carrier counter transports pH-changing anions. *Nature*; 360: 471-474.

Bove G. (2006) Mechanical sensory threshold testing using nylon monofilaments: the pain field's "tin standard." *Pain*; 124: 13–17. doi:10.1016/j.pain.2006.06.020

Bowsher D. (1991) Neurogenic pain syndromes and their management. *Br Med Bull*; 47: 644–66.

Brenner DS, Golden JP and Gereau RW. (2012). A novel behavioral assay for measuring cold sensation in mice. *PLoS One*; 7:e39765. doi: 10.1371/journal.pone.0039765

Brodkin J, Frank D, Grippo R, Hausfater M, Gulinello M, Achterholt N, Gutzen C. (2014) Validation and implementation of a novel high-throughput behavioural phenotyping instrument for mice. *J. Neurosci. Methods*; 224: 48–57. doi: 10.1016/j.jneumeth.2013.12.010

Campbell JN and Meyer RA. (2006) Mechanisms of Neuropathic Pain. *Neuron*; 52(1): 77–92.

Cardona AE, Piroo EP, Sasse ME, Kostenko V, Cardona SM, Dijkstra IM, Huang D, Kidd G, Dombrowski S, Dutta R, Lee J-C, Cook DN, Jung S, Lira SA, Littman DR and Ransohoff RM. (2006) Control of microglial neurotoxicity by the fractalkine receptor. *Nat. Neurosci*; 9: 917–924.

Carlton SM, Lekan HA, Kim SH and Chung JM. (1994). Behavioral manifestations of an experimental model for peripheral neuropathy produced by spinal nerve ligation in the primate. *Pain*; 56: 155–166. doi: 10.1016/0304-3959(94)90090-6

Chao CC, Hu S, Sheng WS, Bu D, Bukrinsky MI, Peterson PK. (1996) Cytokine-stimulated astrocytes damage human neurons via a nitric oxide mechanism. *Glia*; 16(3): 276–84.

Chaplan, SR, Bach FW, Pogrel JW, Chung JM, Yaksh TL. (1994) Quantitative assessment of tactile allodynia in the rat paw. *J. Neurosci. Methods*; 53: 55–63.

Champan CR, Tuckett RP, Song CW. (2008) Pain and stress in a systems perspective: reciprocal neural, endocrine and immune interactions. *J Pain*; 9: 122-45.

Chen Y, Li GW, Wang C, Gu Y and Huang LY. (2005) Mechanisms underlying enhanced P2X receptor-mediated responses in the neuropathic pain state. *Pain*; 119: 38–48.

Chessell IP, Hatcher JP, Bountra C, Michel AD, Hughes JP, Green P, Egerton J, Murfin M, Richardson J, Peck WL, Grahames CBA, Casulad MA, Yiangoud Y, Birche R, Anand P, Buellf GN. (2005) Disruption of the P2X7 purinoceptor gene abolishes chronic inflammatory and neuropathic pain. *Pain*; 114: 386–396.

Choe CU, Lewerenz J, Gerloff C, Magnus T and Donzelli S. (2011) 'Nitroxyl in the Central Nervous System' *Antioxid. Redox Signal*; 14: 1699–1711.

Ciaramitaro P, Mondelli M and Logullo F. (2010) Traumatic peripheral nerve injuries: epidemiological findings, neuropathic pain and quality of life in 158 patients. *J Peripher Nerv Syst*; 15:120-127.

Clark AK, Yip PK, Malcangio M (2009) The liberation of fractalkine in the dorsal horn requires microglial cathepsin S. *J Neurosci*; 29: 6945–6954.

Colloca L, Ludman T, Bouhassira D, Baron R, Dickenson AH, Yarnitsky D, Freeman R, Truin A, Attal N, Finnerup NB, Eccleston C, Kalso E, Bennett DL, Dworkin RH and Raja SN. (2017) *Nature Reviews Disease Primers* volume 3, Article number: 17002.

Costigan M, Scholz J and Woolf CJ. (2009) Neuropathic Pain: A Maladaptive Response of the Nervous System to Damage. *Annu Rev Neurosci*; 2009(32): 1–32.

Costigan M, Woolf CJ. (2000) Pain: molecular mechanisms. *J Pain*; Suppl. 3: 35-44.

Cotrina ML, Lin JH, Alves-Rodrigues A, Liu S, Li J, Azmi-Ghadimi H, Kang J, Naus CCG and Nedergaard M. (1998) Connexins regulate calcium signaling by controlling ATP release. *Proc Natl Acad Sci USA*; 95: 15735–40.

Cotrina ML, Lin JH-C, López-García JC, Naus CCG and Nedergaard M. (2000) ATP-mediated glia signaling. *J. Neurosci*; 20: 2835–2844.

Coull JA, Beggs S, Boudreau D, Boivin D, Tsuda M, Inoue K, Gravel C, Salter MW, De Koninck Y. (2005) BDNF from microglia causes the shift in neuronal anion gradient underlying neuropathic pain. *Nature*; 438: 1017–1021.

D'Amour FE and Smith DL. (1941). A method for determining loss of pain sensation. *J. Pharmacol. Exp. Ther*; 72: 74–79.

Dafny, N. Pain modulation and mechanisms. (1997) *Neuroscience Online: An Electronic Textbook for the Neurosciences*.

Daikhin Y and Yudkoff M. (2000) Compartmentation of Brain Glutamate Metabolism in Neurons and Glia.

Darlison MG. (2007) Inhibitory Regulation of Excitatory Neurotransmission. Chapter 1: Regulation of Excitation by GABAA Receptor Internalization (ed) Nancy J. Leidenheimer. DOI 10.1007/400.

Davalos D and Akassoglou K. (2012) In vivo imaging of the mouse spinal cord using two-photon microscopy. *J Vis Exp*; 59: e2760. doi: 10.3791/2760.

De Leo JA, Tawfik VL, LaCroix-Fralish ML. (2006) The tetrapartite synapse: path to CNS sensitization and chronic pain. *Pain*; 122:17–21.

Deacon RM. (2006) Burrowing in rodents: a sensitive method for detecting behavioral dysfunction. *Nat. Protoc*; 1: 118–121. doi: 10.1038/nprot.2006.19

Decrouy-Duruz V, Christen T and Raffoul W. (2018) Evaluation of surgical treatment for neuropathic pain from neuroma in patients with injured peripheral nerves. *J Neurosurg*; 128: 1235–1240.

DeMaster EG, Redfern B, and Nagasawa HT. (1998) "Mechanisms of inhibition of aldehyde dehydrogenase by nitroxyl, the active metabolite of the alcohol deterrent agent cyanamide," *Biochemical Pharmacology*; 55(12): 2007–2015.

Deuis JR and Vetter I. (2016). The thermal probe test: a novel behavioural assay to quantify thermal paw withdrawal thresholds in mice. *Temperature*; 3: 199–207. doi: 10.1080/23328940.2016.1157668

Deuis JR, Dvorakova LS and Vetter I (2017) Methods Used to Evaluate Pain Behaviors in Rodents. *Front. Mol. Neurosci*; 10(284): 1-17.

Doubell TP, Mannion RJ, Woolf CJ. (1999) The dorsal horn: State-dependent sensory processing, plasticity and the generation of pain, in Wall PD, Melzack R (eds): *Textbook of Pain*. London, Churchill Livingstone; 165-182

Dunn PM, Rang HP (1990) Bradykinin-induced depolarization of primary afferent nerve terminals in the neonatal rat spinal cord in vitro. *Br J Pharmacol*; 100: 656-660.

Dworkin RH, Backonja M, Rowbotham MC, Allen RR and Argoff CR. (2003) Advances in neuropathic pain: diagnosis, mechanisms, and treatment recommendations. *Arch. Neurol*; 60: 1524–34.

Eaton MJ, Plunkett JA, Karmally S, Martinez MA and Montanez K. (1998) Changes in GAD- and GABA- immunoreactivity in the spinal dorsal horn after peripheral nerve injury and promotion of recovery by lumbar transplant of immortalized serotonergic precursors. *J Chem Neuroanat*; 16: 57–72.

Eliasson MJ, Blackshaw S, Schell MJ, Snyder SH (1997) Neuronal nitric oxide synthase alternatively spliced forms: prominent functional localizations in the brain. *Proc Natl Acad Sci U S A*; 94:3396–3401.

Eser F, Aktekin LA, Bodur H and Atan C. (2009) Etiological factors of traumatic peripheral nerve injuries. *Neurol India*; 57: 434-437.

Espey MG, Miranda KM, Pluta RM, Wink DA. (2000) Nitrosative capacity of macrophages is dependent on nitric-oxide synthase induction signals. *J. Biol. Chem*; 275: 11341–11347.

Facci L, Barbierato M, Marinelli C, Argentini C, Skaper SD & Giusti P (2014) Toll-Like Receptors 2, -3 and -4 Prime Microglia but not Astrocytes Across Central Nervous System Regions for ATP-Dependent Interleukin-1b Release. *Sci. Rep*; 4: 6824.

DOI:10.1038/srep06824.

Farrar MJ, Bernstein IM, Schlafer DH, Cleland TA, Fetcho JR and Schaffer CB. (2012) Chronic in vivo imaging in the mouse spinal cord using an implanted chamber. *Nature methods*; 9(3): 297–302.

Fenrich KK, Weber P, Hocine M, Zalc M, Rougon G and Debarbieux F. (2012) Long-term in vivo imaging of normal and pathological mouse spinal cord with subcellular resolution using implanted glass windows *J Physiol*; 590(16): 3665–3675.

Ferreira J, Santos AR, Calixto JB (1999) The role of systemic, spinal and supraspinal L-arginine/nitric oxide-cGMP pathway in thermal hyperalgesia caused by intrathecal injection of glutamate in mice. *Neuropharmacology*; 38: 835–842.

Ferretti A, Del Gratta C, Babiloni C, Caulo M, Arienzo D, Tartaro A, Rossini PM and Romani GL. (2004) Functional topography of the secondary somatosensory cortex for nonpainful and painful stimulation of median and tibial nerve: an fMRI study. *Neuroimage*; 23: 1217-1225.

Fields HL, Basbaum AI, Heinricher MM. (2006) Central nervous system mechanisms of pain modulation. In: McMahon, S., Koltzenburg, M. (Eds.), *Wall and Melzack's Textbook of Pain*, 5th ed. Elsevier, London: 125–142.

Fiore NT, Austin PJ. (2019) Peripheral nerve injury triggers neuroinflammation in the medial prefrontal cortex and ventral hippocampus in a subgroup of rats with coincident affective behavioural changes. *Neuroscience*; 416: 147-187.

Forstermann U and Sessa WC. (2012) 'Nitric oxide synthases: regulation and function.' *European Heart Journal*; 33: 829–83.

Fukuto JM, Switzer CH, Miranda KM and Wink DA. (2005) NITROXYL (HNO): Chemistry, Biochemistry, and Pharmacology. *Annu. Rev. Pharmacol. Toxicol*; 45: 335–55.

Furchgott RF (1988). Studies on relaxation of rabbit aorta by sodium nitrite: the basis for the proposal that the acid-activatable inhibitory factor from retractor penis is inorganic nitrite and the endothelium derived relaxing factor is nitric oxide. In Vanhoutte PM, Ed. *Vasodilatation: Vascular Smooth Muscle Peptides, Autonomic Nerves, and Endothelium*. New York: Raven Press; 1988:401– 414.

Gao X, Kim HK, Chung JM, Chung K. (2007). Reactive oxygen species (ROS) are involved in enhancement of NMDA-receptor phosphorylation in animal models of pain. *Pain*; 131: 262–271.

Gaskin DJ, Richard P. (2012) The Economic Costs of Pain in the United States. *The Journal of Pain*; 13 (8): 715 DOI: [10.1016/j.jpain.2012.03.009](https://doi.org/10.1016/j.jpain.2012.03.009)

George A, Buehl A, Sommer C. (2005) Tumor necrosis factor receptor 1 and 2 proteins are differentially regulated during Wallerian degeneration of mouse sciatic nerve. *Exp Neurol*; 192: 163-166.

Grace PM, Gaudet AD, Staikopoulos V, Maier SF, Hutchinson MR, Salvemini D, and Watkins LR, (2016) Nitroxidative signaling mechanisms in pathological pain. *Trends Neurosci*; 39(12): 862–879. doi:10.1016/j.tins.2016.10.003

Grace PM, Hutchinson MR, Maier SF, Watkins LR. (2014) Pathological pain and the neuroimmune interface. *Nature Reviews Immunology*; 14: 217–231.

Grace PM, Hutchinson MR, Manavis J, Somogyi AA, Rolan PE (2010) A novel animal model of graded neuropathic pain: Utility to investigate mechanisms of population heterogeneity. *Journal of Neuroscience Methods*; 193(1): 47-53.

Gu JG and MacDermott, AB. (1997). Activation of ATP P2X receptors elicits glutamate release from sensory neuron synapses.

Guan Y, Yaster M, Raja SN, Tao YX (2007) Genetic knockout and pharmacologic inhibition of neuronal nitric oxide synthase attenuate nerve injury-induced mechanical hypersensitivity in mice. *Mol Pain*; 3: 29.

Guo W, Wang H, Watanabe M, Shimizu K, Zou S, LaGraize SC, Wei F, Dubner R, Ren K. (2007) Glial-cytokine-neuronal interactions underlying the mechanisms of persistent pain. *J Neurosci*; 27: 6006–6018.

Haley JE, Dickenson AH, Schachter M (1992) Electrophysiological evidence for a role of nitric oxide in prolonged chemical nociception in the rat. *Neuropharmacology*; 31: 251–258.

Hamilton NB and Attwell D. (2010) Do astrocytes really exocytose neurotransmitters? *Nat. Rev. Neurosci*; 11: 227–238.

Hargreaves K, Dubner R, Brown F, Flores C and Joris J. (1988). A new and sensitive method for measuring thermal nociception in cutaneous hyperalgesia. *Pain*; 32: 77–88. doi: 10.1016/0304-3959(88)90026-7

Heinricher MM and Ingram SL. (2008) The brainstem and nociceptive modulation. In: Bushnell, M.C., Basbaum, A.I. (Eds.), *The Senses, a Comprehensive Reference. Pain, Vol. 5*. Academic Press, San Diego: 593–626.

Heinricher MM, Tavares I, Leith JL, Lumb BM. (2009) Descending control of nociception: specificity, recruitment and plasticity. *Brain Res Rev*; 60: 241-25.

Hervera A, Negrete R, Leanez S, Martin-Campos JM, Pol O. (2010) The spinal cord expression of neuronal and inducible nitric oxide synthases and their contribution in the maintenance of neuropathic pain in mice. *PLoS One*; 5:e14321

Hiroshi N. (2012). Involvement of Microglial Cathepsin B in Pro-Interleukin-1 β Processing and Persistent Pain, Inflammation, Chronic Diseases and Cancer - Cell and Molecular Biology, Immunology and Clinical Bases, Dr Mahin Khatami (Ed.), ISBN: 978-953-51-0102-4.

<https://www.iasp-pain.org/Education/Content.aspx?ItemNumber=1698#Pain>

Hutchinson MR, Zhang Y, Brown K, Coats BD, Shridhar M, Sholar PW, Patel PJ, Crysdale NY, Harrison JA, Maier SF, Rice KC and Watkins LR (2008) Non-stereoselective reversal of neuropathic pain by naloxone and naltrexone: involvement of toll-like receptor 4 (TLR4) *European Journal of Neuroscience*; 28: 20–29.

Ignarro LJ. (1996) Physiology and pathophysiology of nitric oxide. *Kidney Int Suppl*; 55: S2–S5. *J. Nutr*; 130: 1026S–1031S.

Jaggi AS, Jain V, Singh N. (2011) Animal models of neuropathic pain. *Fundamental & Clinical Pharmacology*; 25: 1–28.

Jahromi NH, Tardent H, Enzmann G, Deutsch U, Kawakami N, Bittner S, Vestweber D, Zipp F, Stein JV and Engelhardt B. (2017) A Novel Cervical Spinal Cord Window Preparation Allows for Two-Photon Imaging of T-Cell Interactions with the Cervical Spinal Cord Microvasculature during Experimental Autoimmune Encephalomyelitis. *Front. Immunol*;
<https://doi.org/10.3389/fimmu.2017.00406>.

Jarvis MF, Burgard EC, McGaraughty S, Honore P, Lynch K, Brennan TJ, Subieta A, van Biesen T, Cartmell J, Bianchi B, Niforatos W, Kage K, Yu H, Mikusa J, Wismer CT, Zhu CZ, Chu K, Lee C-H, Stewart AO, Polakowski J, Cox BF, Kowaluk E, Williams M, Sullivan J, Faltynek C. (2002) A-317491, a novel potent and selective non-nucleotide antagonist of P2X3 and P2X2/3 receptors, reduces chronic inflammatory and neuropathic pain in the rat. *Proc. Natl. Acad. Sci. USA*; 99: 17179–17184.

Jin X, Gereau RWt. (2006) Acute p38-mediated modulation of tetrodotoxin resistant sodium channels in mouse sensory neurons by tumor necrosis factor-alpha. *J Neurosci*; 26: 246-255.

Kawasaki Y, Xu ZZ, Wang X, Park JY, Zhuang Z-Y, Tan P-H, Gao Y-J, Roy K, Corfas G, Lo EH and Ji RR. (2008) Distinct roles of matrix metalloproteases in the early- and late-phase development of neuropathic pain. *Nat Med*; 14: 331–336.

Kawasaki Y, Xu ZZ, Wang X, Park JY, Zhuang ZY, Tan PH. (2008) Distinct roles of matrix metalloproteases in the early- and late-phase development of neuropathic pain. *Nat. Med*; 14: 331–336.

Kim SH and Chung JM. (1992) An experimental model for peripheral neuropathy produced by segmental spinal nerve ligation in the rat. *Pain*; 50(3): 355-363.

Kim WK; Choi YB; Rayudu PV; Das P; Asaad W; Arnelle DR; Stamler JS; Lipton SA. (1999) Attenuation of NMDA Receptor Activity and Neurotoxicity by Nitroxyl Anion, NO⁻. *Neuron*; 24(2): 461-469.

Kojima H, Nakatsubo N, Kikuchi K, Kawahara S, Kirino Y, Nagoshi H, Hirata Y, Nagano T. (1998) 'Detection and imaging of nitric oxide with novel fluorescent indicators: diaminofluoresceins. *Anal. Chem*; 70: 2446–2453.

Kouyoumdjian JA. (2006) Peripheral nerve injuries: a retrospective survey of 456 cases. *Muscle Nerve*; 34: 785-788.

Krieger P, Hellgren-Kotaleski J, Kettunen P and El Manira AJ. (2000) Interaction between Metabotropic and Ionotropic Glutamate Receptors Regulates Neuronal Network Activity. *Journal of Neuroscience*; 20 (14): 5382-5391

Langford DJ, Bailey AL, Chanda ML, Clarke SE, Drummond TE, Echols S, Glick S, Ingrao J, Klassen-Ross T, LaCroix-Fralish ML, Matsumiya L, Sorge RE, Sotocinal SG, Tabaka JM, Wong D, van den Maagdenberg AMJM, Ferrari MD, Craig KD & Mogil JS. (2010). Coding of facial expressions of pain in the laboratory mouse. *Nat. Methods*; 7: 447–449. doi: 10.1038/nmeth.1455

Lauro C, Di Angelantonio S, Cipriani R, Sobrero F, Antonilli L, Brusadin V, Ragozzino D and Limatola C. (2008) Activity of adenosine receptors type 1 is required for CX3CL1-mediated neuroprotection and neuromodulation in hippocampal neurons. *J. Immunol*; 180: 7590–7596.

Levy D, Höke A, Zochodne DW. (1999) 'Local expression of inducible nitric oxide synthase in an animal model of neuropathic pain. *Neurosci Lett*; 260(3): 207-9.

Levy D. and Zochodne DW., (1998) 'Local nitric oxide synthase activity in a model of neuropathic pain.' *European Journal of Neuroscience*; 10(5): 1846–1855.

Li P, Kerchner GA, Sala C, Wei F, Huettner JE, Sheng M, Zhuo M. (1999) AMPA receptor-PDZ interactions in facilitation of spinal sensory synapses. *Nat Neurosci*; 2:972-977.

Li P, Zhuo M. (1998) Silent glutamatergic synapses and nociception in mammalian spinal cord. *Nature*; 393: 695-698.

Li Y, Du X-F, Liu C-S, Wen Z-L and Du J-L. (2012) Reciprocal regulation between resting microglial dynamics and neuronal activity in vivo. *Dev. Cell* 23, 1189–1202.

Lin T, Li K, Zhang FY, Zhang ZK, Light AR, Fu KY. (2007) Dissociation of spinal microglia morphological activation and peripheral inflammation in inflammatory pain models. *J Neuroimmunol*; 192: 40-48.

Longhi-Balbinot DT, Rossaneis AC, Pinho-Ribeiro FA, Bertozzi MM, Cunha FQ, Alves-Filho JC, Cunha TM, Peron JPS, Miranda KM, Casagrande R and Verri Jr. WA, (2016) 'The nitroxyl donor, Angeli's salt, reduces chronic constriction injury-induced neuropathic pain'. *Chemico-Biological Interactions*; doi: 10.1016/j.cbi.2016.06.009.

Lukovic D, Stojkovic M, Moreno-Manzano, V, Jendelova, P, Sykova E, Bhattacharya SS and Erceg S. (2015) Reactive Astrocytes and Stem Cells in Spinal Cord Injury: Good Guys or Bad Guys? *Stem Cells*; 33:1036–1041.

Luo ZD, Chaplan SR, Scott BP, Cizkova D, Calcutt NA, Yaksh TL (1999) Neuronal nitric oxide synthase mRNA upregulation in rat sensory neurons after spinal nerve ligation: lack of a role in allodynia development. *J Neurosci*; 19: 9201–9208.

Ma Q-P, Allchorne AJ, Woolf CJ. (1998) Morphine, the NMDA receptor antagonist MK801 and the tachykinin NK1 receptor antagonist RP67580 attenuate the development of inflammation-induced progressive tactile hypersensitivity. *Pain*; 77: 49-57.

Ma Q-P, Woolf CJ. (1996) Progressive tactile hypersensitivity: An inflammation-induced incremental increase in the excitability of the spinal cord. *Pain*; 67: 97-106.

Madry C and Attwell D. (2015) Receptors, Ion Channels, and Signaling Mechanisms Underlying Microglial Dynamics. *The journal of biological chemistry*; 290(20): 2443–12450.

Martinez-Hernandez A, Bell KP & Norenberg MD. (1977) Glutamine synthetase: glial localization in brain. *Science*; 195: 1356–1358.

Martinov T, Mack M, Sykes A, Chatterjea D. (2013) Measuring Changes in Tactile Sensitivity in the Hind Paw of Mice Using an Electronic von Frey Apparatus. *J. Vis. Exp*; 82: e51212, doi:10.3791/51212

Martucci C, Trovato AE, Costa B, Borsani E, Franchi S, Magnaghi V, Panerai AE, Rodella LF, Valsecchi AE, Sacerdote P, Colleoni M (2008) The purinergic antagonist PPADS reduces pain related behaviours and interleukin-1beta, interleukin-6, iNOS and nNOS overproduction in central and peripheral nervous system after peripheral neuropathy in mice. *Pain*; 137: 81–95.

McGaraughty S, Chu KL, Namovic MT, Donnelly-Roberts DL, Harris RR, Zhang XF, Shieh CC, Wismer CT, Zhu CZ, Gauvin DM, Fabiyi AC, Honore P, Gregg RJ, Kort ME, Nelson DW, Carroll WA, Marsh K, Faltynek CR, Jarvis MF. (2007) P2X7-related modulation of pathological nociception in rats. *Neuroscience*; 146: 1817–1828.

Meller ST, Gebhart GF (1993) Nitric oxide (NO) and nociceptive processing in the spinal cord. *Pain*; 52(2): 127-136.

Meng X, Zhang Y, Lao L, Saito R, Li A, Bäckman CM, Berman BM, Ren K, Wei PK, Zhang RX. (2013) Spinal interleukin-17 promotes thermal hyperalgesia and NMDA NR1 phosphorylation in an inflammatory pain rat model. *Pain*; 154: 294–305.

Mika J, Osikowicz M, Rojewska E, Korostynski M, Wawrzczak-Bargiela A, Przewlocki R, Przewlocka B. (2009) Differential activation of spinal microglial and astroglial cells in a mouse model of peripheral neuropathic pain. *European Journal of Pharmacology*; 623: 65–72.

Mika J, Rojewska E, Makuch W, Przewlocka B. (2010) 'Minocycline reduces the injury-induced expression of prodynorphin and pro-nociception in DRG in rat model of neuropathic pain.' *Neuroscience*; 165: 1420–1428.

Miller BA, Woolf CJ. (1996) Glutamate-mediated slow synaptic currents in neonatal rat deep dorsal horn neurons in vitro. *J Neurophysiol*; 76:1465-1476.

Milligan ED, Watkins LR (2009) Pathological and protective roles of glia in chronic pain. *Nat Rev Neurosci*; 10: 23–36.

Miranda GE and Torres RY. (2016) Epidemiology of traumatic peripheral nerve injuries evaluated with electrodiagnostic studies in a tertiary care hospital clinic. *Puerto Rico Health Sciences Journal*; 35(2): 76.

Miranda KM. (2005) The chemistry of nitroxyl (HNO) and implications in biology. *Coordination Chemistry Reviews*; 249: 433–455.

Miyoshi K, Obata K, Kondo T, Okamura H, Noguchi K. (2008) Interleukin-18-mediated microglia/astrocyte interaction in the spinal cord enhances neuropathic pain processing after nerve injury. *J Neurosci*; 28(48): 12775–87.

Mogill JS. (2009) Animal models of pain: progress and challenges. *Nature Reviews: Neuroscience*; 10: 284-294.

Moncada S, Higgs A. (1993) The L-arginine-nitric oxide pathway. *N Engl J Med*; 329: 2002-2012.

Monif M, Reid CA, Powell KL, Smart ML, Williams DA. (2009) P2X7 receptor drives microglial activation and proliferation: a trophic role for P2X7R pore. *J Neurosci*; 29: 3781–91.

Moore KA, Kohno T, Karchewski LA, Scholz J, Baba H and Woolf CJ. (2002) Partial Peripheral Nerve Injury Promotes a Selective Loss of GABAergic Inhibition in the Superficial Dorsal Horn of the Spinal Cord. *The Journal of Neuroscience*; 22(15): 6724–6731.

Moqrich A, Hwang SW, Earley TJ, Petrus MJ, Murray AN, Spencer KS, Andahazy M, Story GM and Patapoutian A. (2005) Impaired thermosensation in mice lacking TRPV3, a heat and camphor sensor in the skin. *Science*; 307: 1468–1472. doi: 10.1126/science. 1108609

Mueller M, Wacker K, Ringelstein EB, Hickey WF, Imai Y and Kiefer R. (2001) Rapid response of identified resident endoneurial macrophages to nerve injury. *Am. J. Pathol*; 159: 2187–2197.

Nicotra L, Loram LC, Watkins LR and Hutchinson MR. (2012) Toll-like receptors in chronic pain. *Experimental Neurology*; 234: 316–329.

Nimmerjahn A, Kirchhoff F, Helmchen F. (2005) Resting microglial cells are highly dynamic surveillants of brain parenchyma in vivo. *Science*; 308: 1314-1318.

Noble J, Munro CA, Prasad VS and Midha R. (1998) Analysis of upper and lower extremity peripheral nerve injuries in a population of patients with multiple injuries. *J Trauma*; 45: 116-122.

Norenberg, MD and Martinez-Hernandez A. (1979) Fine structural localization of glutamine synthetase in astrocytes of rat brain. *Brain Res*; 161: 303–310

Novakovic SD, Kassotakis LC, Oglesby IB, Smith JAM, Eglen RM, Ford APDW and Hunter JC. (1999) Immunocytochemical localization of P2X3 purinoceptors in sensory neurons in naive rats and following neuropathic injury. *Pain*; 80 (1–2): 73-282.

Pain Australia Deloitte report - <https://www.painaustralia.org.au/static/uploads/files/the-cost-of-pain-in-australia-final-report-12mar-wfxbrfyboams.pdf>

Pan HC, Chou YC, Sun SH. (2015) P2X7 R-mediated Ca⁽²⁺⁾-independent d-serine release via pannexin-1 of the P2X7 R-pannexin-1 complex in astrocytes. *Glia*; 63: 877–893.

Paolucci N, Jackson MI, Lopez BE, Miranda K, Tocchetti CG, Wink DA, Hobbs AJ, Fukuto JM., (2007) 'The pharmacology of nitroxyl (HNO) and its therapeutic potential: Not just the janus face of NO.' *Pharmacology & Therapeutics*; 113: 442–458.

Perkins NM and Tracey DJ. (2000) Hyperalgesia due to nerve injury: role of neutrophils. *Neuroscience*; 101: 745–757.

Perrin FE, Lacroix S, Aviles-Trigueros M & David S. (2005) Involvement of monocyte chemoattractant protein-1, macrophage inflammatory protein-1a and interleukin-1b in Wallerian degeneration. *Brain*; 128: 854–866.

Perry VH. (2004) The influence of systemic inflammation on inflammation in the brain: implications for chronic neurodegenerative disease. *Brain Behav. Immun*; 18: 407–413.

Pfeiffer S, Mayer B, Hemmens B. (1999) 'Nitric oxide: chemical puzzles posed by a biological messenger.' *Angew Chem Int Ed*; 38: 1714–31.

Qin M, Wang JJ, Cao R, Zhang H, Duan L, Gao B, Xiong YF, Chen LW, Rao ZR (2006) The lumbar spinal cord glial cells actively modulate subcutaneous formalin induced hyperalgesia in the rat. *Neurosci Res*; 55: 442–450.

Qureshi OS, Paramasivam A, Yu JC and Murrell-Lagnado RD. (2007) Regulation of P2X4 receptors by lysosomal targeting, glycan protection and exocytosis. *J. Cell. Sci*; 120: 3838–3849.

Raghavendra V, Tanga F and De Leo JA. (2003) Inhibition of Microglial Activation Attenuates the Development but Not Existing Hypersensitivity in a Rat Model of Neuropathy *J. Pharmacol. Exp. Ther*; 306: 624–630.

Randall LO and Selitto JJ. (1957). A method for measurement of analgesic activity on inflamed tissue. *Arch. Int. Pharmacodyn. Ther*; 111: 409–419.

Ren K. (1999) An Improved Method for Assessing Mechanical Allodynia in the Rat. *Physiology & Behavior*; 67(5): 711–716.

Robinson LR. (2000) Traumatic injury to peripheral nerves. *Muscle Nerve*; 23: 863-873.

Rosenthal SJ and Lippard J. (2010) 'Direct detection of nitroxyl in aqueous solution using a tripodal copper (II) BODIPY complex.' *Am. Chem. Soc*; 132: 5536.

Rothstein JD, M Dykes-Hoberg, CA Pardo, LA Bristol, L Jin, RW Kuncl, Y Kanai, MA Hediger, Y Wang, JP Schielke and DF Welty (1996) Knockout of glutamate transporters reveals a major role for astroglial transport in excitotoxicity and clearance of glutamate. *Neuron* 16, 675-686.

Sabbah HN, Tocchetti CG, Wang M, Daya S, Gupta RC, Tunin RS, Mazhari R, Takimoto E, Paolucci N, Cowart D, Colucci WS. And Kass DA. (2013) 'Nitroxyl (HNO) a Novel Approach for the Acute Treatment of Heart Failure.' *Circ Heart Fail*; 6(6): 1250–1258.

Salter MW and Beggs S. (2014) Sublime Microglia: Expanding Roles for the Guardians of the CNS. *Cell*; 158: 15-24.

Schmidt R, Schmelz M, Forster C, Ringkamp M, Torebjork E, Handwerker H. (1995) Novel classes of responsive and unresponsive C nociceptors in human skin. *J Neurosci*; 15: 333-341.

Schmidtko A, Tegeder I, Geisslinger G (2009) 'No, no pain? The role of nitric oxide and cGMP in spinal pain processing. *Trends Neurosci*; 32(6): 339–346.

Schmidtko A, Wei Gao W, König P, Heine S, Motterlini R, Ruth P, Schlossmann J, Koesling D, Niederberger E, Tegeder I, Friebe A and Geisslinger G. (2008) 'cGMP produced by NO-sensitive guanylyl cyclase essentially contributes to inflammatory and neuropathic pain by using targets different from cGMP-dependent protein kinase I.' *J. Neurosc*; 28: 8568–8576.

Schmidtko A. (2015) Nitric Oxide-Mediated Pain Processing in the Spinal Cord. *Handbook of Experimental Pharmacology*; 227: 103-117.

Schmidtko A; Ruth P; Geisslinger G; Tegeder I. (2003) Inhibition of cyclic guanosine 5'-monophosphate-dependent protein kinase I (PKG-I) in lumbar spinal cord reduces formalin-induced hyperalgesia and PKG upregulation. *Nitric Oxide*; 8: 89–94.

Schönbeck U, Mach F and Libby P. (1998) Generation of biologically active IL-1 beta by matrix metalloproteinases: a novel caspase-1-independent pathway of IL-1 beta processing. *J Immunol*; 161: 3340–3346.

Schött E, Berge OG, Angeby-Möller K, Hammarström G, Dalsgaard CJ, and Brodin E. (1994). Weight bearing as an objective measure of arthritic pain in the rat. *J. Pharmacol. Toxicol. Methods*; 31: 79–83. doi: 10.1016/1056-8719(94)90046-9

Seddighi A, Nikouei A, Seddighi AS, Zali AR, Tabatabaei Sm, Sheykhi AR, Yourdkhani F, Naeimain S. (2016) Peripheral nerve injury: a review article. *International Clinical Neuroscience Journal*: 3(1); 1-6.

Seltzer Z, Dubner R Shirc Y. (1990) A novel behavioral model of neuropathic pain disorders produced in rats by partial sciatic nerve injury. *Pain*; 43(2): 205-218.

Sengul G and Watson C. (2012) *Spinal Cord: Connections Chapter 7 The Human Nervous System, Third Edition*: 233-258. DOI: 10.1016/B978-0-12-374236-0.10007-0

Shafirovich V. and Lymar SV. (2002) 'Nitroxyl and its anion in aqueous solutions: Spin states, protic equilibria, and reactivities toward oxygen and nitric oxide.' *Proc. Natl. Acad. Sci*; 99: 7340.

Shoman ME and Aly OM. (2016) Nitroxyl (HNO): A Reduced Form of Nitric Oxide with Distinct Chemical, Pharmacological, and Therapeutic Properties. *Oxidative Medicine and Cellular Longevity*; Article ID 4867124.

Shubayev VI, Angert M, Dolkas J, Campan WM, Palenscar K and Myers RR. (2006) TNF α -induced MMP-9 promotes macrophage recruitment into injured peripheral nerve. *Mol. Cell. Neurosci*; 31: 407–415.

Sivilotti L, Woolf CJ. (1994) The contribution of GABAA and glycine receptors to central sensitization: disinhibition and touch-evoked allodynia in the spinal cord. *J Neurophysiol*; 72: 169–179.

Sivilotti LG, Thompson SWN, Woolf CJ. (1993) The rate of rise of the cumulative depolarization evoked by repetitive stimulation of small-calibre afferents is a predictor of action potential windup in rat spinal neurones in vitro. *J Neurophysiol*; 69:1621-1631.

Smith BH and Torrance N. (2012) Epidemiology of Neuropathic Pain and Its Impact on Quality of Life. *Curr Pain Headache Rep*; 16: 191–198.

Smith BH, Torrance N, Bennett MI and Lee AJ. (2007) Health and quality of life associated with chronic pain of predominantly neuropathic origin in the community. *Clin J Pain*; 23: 143–9.

Smtih HS. (2010) Activated microglia in nociception. *Pain Physician*; 13: 295-304.

Sofroniew MV (2009) Molecular dissection of reactive astrogliosis and glial scar formation. *Trends Neurosci*; 32: 638–647.

Sofroniew MV and Vinters HV. (2010) Astrocytes: biology and pathology. *Acta Neuropathol*; 119:7–35.

Soghomonian JJ and Martin DL. (1998) Two isoforms of glutamate decarboxylase: why? Trends Pharmacol Sci; 19: 500–505.

Sousa AM, Prado WA (2001) The dual effect of a nitric oxide donor in nociception. Brain Res; 897: 9–19.

Staufeno-Ferraria L, Zarpelona AC, Longhi-Balbinota DT, Marchesib M, Cunhac TM, Alves-Filhoc JC, Cunhac FQ, Ferreirac SH, Casagrande R, Miranda KM, and Verri Jr. WA. (2014) Nitroxyl inhibits overt pain-like behavior in mice: Role of cGMP/PKG/ATP-sensitive potassium channel signaling pathway. Pharmacological Reports; 66(4): 691-698.

Stoll G, Jander S and Myers RR. (2002) Degeneration and regeneration of the peripheral nervous system: from Augustus Waller's observations to neuroinflammation. J. Peripher. Nerv. Syst; 7: 13–27.

Stuehr DJ, Santolini J, Wang ZQ, Wei CC, Adak S. (2004) Update on mechanism and catalytic regulation in the NO synthases. J Biol Chem; 279: 36167–36170.

Sun L, Wu Z, Hayashi Y, Peters C, Tsuda M, Inoue K and Nakanishi H. (2012) Microglial Cathepsin B Contributes to the Initiation of Peripheral Inflammation-Induced Chronic Pain. The Journal of Neuroscience; 32(33): 11330 –11342.

Sung B, Lim G, Mao J. (2003) Altered expression and uptake activity of spinal glutamate transporters after nerve injury contribute to the pathogenesis of neuropathic pain in rats. J. Neurosci; 23: 2899–2910.

Suzuki R, Rygh LJ and Dickenson AH. (2004) Bad news from the brain: descending 5-HT pathways that control spinal pain processing Neuropathic pain. TRENDS in Pharmacological Sciences; 25(12): 613-617.

Sweitzer SM, Colburn RW, Rutkowski M, De Leo JA. (1999) Acute peripheral inflammation induces moderate glial activation and spinal IL-1 β expression that correlates with pain behaviour in the rat. *Brain Research*; 829(1–2): 209-221.

Taiwo YO, Levine JD (1988) Characterization of the arachidonic acid metabolites mediating bradykinin and noradrenaline hyperalgesia. *Brain Res*; 458: 402-406.

Taiwo YO, Levine JD (1990) Direct cutaneous hyperalgesia induced by adenosine. *Neuroscience*; 38:757-762.

Taiwo YO, Levine JD (1992) Serotonin is a directly-acting hyperalgesic agent in the rat. *Neuroscience*; 48: 85-490.

Tanga FY, Nutile-McMenemy N and De Leo JA (2005) The CNS role of Toll-like receptor 4 in innate neuroimmunity and painful neuropathy. *Proc. Natl Acad. Sci. USA*; 102: 5856–5861.

Tanga FY, Raghavendra V and De Leo JA. (2004) Quantitative real-time RT-PCR assessment of spinal microglial and astrocytic activation markers in a rat model of neuropathic pain. *Neurochem. Int*; 45: 397–407.

Taves S, Berta T, Chen G and Ji RR. (2013) Microglia and spinal cord synaptic plasticity in persistent pain. *Neural Plasticity*; Article ID 753656. <http://dx.doi.org/10.1155/2013/753656>

Tawfik VL, Lacroix-Fralish M., Bercury KK, Nutile-McMenemy N, Harris BT, De leo JA, (2006) Induction of astrocyte differentiation by propentofylline increases glutamate transporter expression in vitro: heterogeneity of the quiescent phenotype. *Glia*; 54: 193–203.

Thacker MA, Clark AK, Bishop T, Grist J, Yip PK, Moon LD, Thompson SW, Marchand F and McMahon SB. (2009) CCL2 is a key mediator of microglia activation in neuropathic pain states. *Eur J Pain*; 13: 263–272.

Thomas DD, Ridnour LA, Isenberg JS, Flores-Santana W, Switzer CH, Donzellie S, Hussain P, Vecoli C, Paolucci N, Ambs S, Colton C, Harris C, Roberts DD. and Wink DA., (2009) 'The Chemical Biology of Nitric Oxide. Implications in Cellular Signaling.' *Free Radic Biol Med*; 45(1): 18–31.

Todd AJ. (2010) Neuronal circuitry for pain processing in the dorsal horn. *Nature Reviews Neuroscience*;11: 823-836.

Torrance N, Smith BH, Bennett MI, Lee AJ. (2006) The epidemiology of chronic pain of predominantly neuropathic origin. Results from a general population survey. *J Pain*; 7: 281–9.

Toulme E, Garcia A, Samways D, Egan TM, Carson MJ, Khakh BS. (2010) P2X4 receptors in activated C8-B4 cells of cerebellar microglial origin. *J Gen Physiol*; 135(4):333-53

Tracy I. (2005) Nociceptive processing in the human brain. *Curr Opin in Neurobiology*; 15: 478-487.

Tracey I and Bushnell M. (2009) How neuroimaging studies have challenged us to rethink: is chronic pain a disease? *J Pain*; 10: 1113-20.

Trang T, Beggs S, Wan X and Salter MW. (2009) P2X4-receptor-mediated synthesis and release of brain-derived neurotrophic factor in microglia is dependent on calcium and p38-mitogen-activated protein kinase activation. *J. Neurosci*; 29: 3518–3528.

Tremblay ME, Lowery RL, and Majewska AK. (2010) Microglial interactions with synapses are modulated by visual experience *PLoS Biol*; 8(11): e1000527. doi: 10.1371/journal.pbio.1000527

Tsuda M, Shigemoto-Mogami Y, Koizumi S, Mizokoshi A, Kohsaka S, Salter MW and Inoue K. (2003) P2X4 receptors induced in spinal microglia gate tactile allodynia after nerve injury. *Nature*; 424: 778–783.

Tsuda M, Inoue K, Salter MW. (2005) Neuropathic pain and spinal microglia: a big problem from molecules in 'small' glia. *Trends in Neurosciences*; 28(2): 101-107.

Väänänen AJ, Salmenperä P, Hukkanen M, Miranda KM, Harjula A, Rauhala P, Kankuri E. (2008) Persistent susceptibility of cathepsin B to irreversible inhibition by nitroxyl (HNO) in the presence of endogenous nitric oxide. *Free Radical Biology & Medicine*; 45: 749–755.

Vincent, S. R. (1994). Nitric oxide: a radical neurotransmitter in the central nervous system. *Prog. Neurobiol*; 42: 129–160.

Volterra A, Liaudet N, Savtchouk I. (2014) Astrocyte Ca²⁺ signalling: an unexpected complexity. *Nat Rev Neurosci*; 15: 327–335.

von Frey MH (1896). Untersuchungen u ¨ber Sinnesfunction der Menschlichen Haut: Druckenempfindung und Schmerz. *Abhl Sach Akad Wissensch Leipzig* 23:175–266.

Wall PD, Devor M, Inbal R, Scadding JW, Schonfeld D, Seltzer Z, Tomkiewicz MM. (1979) Autotomy following peripheral nerve lesions: experimental anesthesia dolorosa. *Pain*; 7: 103–111.

Watkins LR, Milligan ED and Maier SF. (2001) Glial activation: a driving force for pathological pain *TRENDS in Neurosciences*; 24 (8): 450-455.

Wei CC, Wang ZQ, Hemann C, Hille R, and Stuehr DJ. (2003) 'A tetrahydrobiopterin radical forms and then becomes reduced during N-omega-hydroxyarginine oxidation by nitric oxide synthase.' *J Biol Chem*; 278: 46668–46673.

Weinger JG, Greenberg ML, Matheu MP, Parker I, Walsh CM, Lane TE, Cahalan MD. (2015) Two-photon imaging of cellular dynamics in the mouse spinal cord. *J Vis Exp*; 96: e52580 doi: 10.3791/52580.

Whalley ET, Clegg S, Steward JM, Vavrek RJ (1989) Antagonism of the analgesic action of bradykinin on the human blister base. *Adv Exp Med Biol*; 247A: 261-268.

Willis WD, Al-Chaer ED, Quast MJ, Westlund KN. (1999) A visceral pain pathway in the dorsal column of the spinal cord. *Proc Natl Acad Sci U S A*; 96(14):7675.

Wink DA, Hanbauer I, Grisham MB, Laval F, Nims RW, Laval J, Cook JC, Pacelli R, Liebmann J, Krishna MC, Ford MC, JB M. (1996) The Chemical Biology of NO. Insights into Regulation, Protective and Toxic Mechanisms of Nitric Oxide. *Current Topics in Cellular Regulation*; 34: 159–187.

Wink DA, Mitchell JB. (1998) Chemical biology of nitric oxide: Insights into regulatory, cytotoxic, and cytoprotective mechanisms of nitric oxide. *Free Radic Biol Med*; 25: 434–456.

Wolf G, Gabay E, Tal M, Yirmiya R and Shavit Y. (2006) Genetic impairment of interleukin-1 signaling attenuates neuropathic pain, autotomy, and spontaneous ectopic neuronal activity, following nerve injury in mice. *Pain*; 120: 315–324.

Woolf CJ and Mannion RJ. (1999) Neuropathic pain: aetiology, symptoms, mechanisms, and management. *Lancet*; 353: 1959–64.

Woolf CJ, Salter MW. (2000) Neuronal plasticity: increasing the gain in pain. *Science*; 288: 1765-1769.

Woolfe G and Macdonald AD. (1944). The evaluation of the analgesic action of pethidine hydrochloride (Demerol). *J. Pharmacol. Exp. Ther*; 80: 300–307.

Yoshimura M, Nishi S. (1993) Blind patch-clamp recordings from substantia gelatinosa neurons in adult rat spinal cord slices: Pharmacological properties of synaptic currents. *Neuroscience*; 53: 519-526.

Yucel, M.A., Aasted, C.M., Petkov, M.P., Borsook, D., Boas, D.A., and Becerra, L. (2015). Specificity of Hemodynamic Brain Responses to Painful Stimuli: A functional near-infrared spectroscopy study. *Sci. Rep.* 5, 9469.

Zarpelon AC, Souza GR, Cunha TM, Schivo IRS, Marchesi M, Casagrande R, Pinge-Filho P, Cunha FQ, Ferreira SH, Miranda KM and Verri Jr. WA, (2013) 'The nitroxyl donor, Angeli's salt, inhibits inflammatory hyperalgesia in rats.' *Neuropharmacology*; 71: 1–9.

Zhang X, Verge V, Wiesenfeld-Hallin Z, Ju G, Bredt D, Synder SH, Hokfelt T (1993) Nitric oxide synthase-like immunoreactivity in lumbar dorsal root ganglia and spinal cord of rat and monkey and effect of peripheral axotomy. *J Comp Neurol*; 335: 563–575.

Zheng K, Lin W, Cheng D, Chen H, Liub Y and Liub K. (2015) A two-photon fluorescent turn-on probe for nitroxyl (HNO) and its bioimaging application in living tissues. *Chem. Commun*; 51: 5754.

Zhuang ZY, Kawasaki Y, Tan PH, Wen YR, Huang J and Ji RR. (2007) Role of the CX3CR1/p38 MAPK pathway in spinal microglia for the development of neuropathic pain following nerve injury-induced cleavage of fractalkine. *Brain Behav. Immun*; 21: 642–651.

Zhuo M, Meller ST, Gebhart GF (1993) Endogenous nitric oxide is required for tonic cholinergic inhibition of spinal mechanical transmission. *Pain*; 54: 71–78.

Zou J, Vetreano RP and Crews FT. (2012) ATP-P2X7 receptor signaling controls basal and TNF α -stimulated glial cell proliferation. *Glia*; 60: 661–73.

Zujovic V, Benavides J, Vigé X, Carter C and Taupin V. (2000) Fractalkine modulates TNF α -secretion and neurotoxicity induced by microglial activation. *Glia*; 29: 305–315.

This page has been left deliberately blank

Statement of Authorship

Title of Paper	Nitroxidative Signaling Mechanisms in Pathological Pain.	
Publication Status	<input checked="" type="checkbox"/> Published	<input type="checkbox"/> Accepted for Publication
	<input type="checkbox"/> Submitted for Publication	<input type="checkbox"/> Unpublished and Unsubmitted work written in manuscript style
Publication Details	Trends Neurosci. 2016 Dec;39(12):862-879. doi: 10.1016/j.tins.2016.10.003. Review	

Principal Author

Name of Principal Author (Candidate)	Dr Peter M Grace		
Contribution to the Paper	Contributed to the conception, writing and editing of the manuscript.		
Overall percentage (%)	40%		
Certification:	This paper reports on original research I conducted during the period of my Higher Degree by Research candidature and is not subject to any obligations or contractual agreements with a third party that would constrain its inclusion in this thesis. I am the primary author of this paper.		
Signature		Date	09/03/2019

Co-Author Contributions

By signing the Statement of Authorship, each author certifies that:

- i. the candidate's stated contribution to the publication is accurate (as detailed above);
- ii. permission is granted for the candidate to include the publication in the thesis; and
- iii. the sum of all co-author contributions is equal to 100% less the candidate's stated contribution.

Name of Co-Author	Andrew David Gaude		
Contribution to the Paper	Contributed to the writing and editing of the manuscript. 15%		
Signature		Date	13 September 2019

Name of Co-Author	Vasiliki Staikopoulos		
Contribution to the Paper	Contributed to the writing of the manuscript. 15%		
Signature		Date	2 SEP 2019

Please cut and paste additional co-author panels here as required.

Name of Co-Author	Steven F Maier		
Contribution to the Paper	Contributed to the editing of the manuscript. 5%		
Signature		Date	09/03/19

Name of Co-Author	Mark R Hutchinson		
Contribution to the Paper	Contributed to the editing of the manuscript. 5%		
Signature		Date	3/9/2019

Name of Co-Author	Daniela Salvemini		
Contribution to the Paper	Contributed to the editing of the manuscript. 5%		
Signature		Date	Sept 6, 2019

Name of Co-Author	Linda R Watkins		
Contribution to the Paper	Contributed to the writing and editing of the manuscript. 15%		
Signature		Date	Sept 3, 2019

Chapter 2. Current tools for detecting nitroxyl in biology

This chapter has been peer-reviewed and formally published as a contribution to a collaborative review paper [Grace PM et al. (2016) *Trends in Neuroscience*, Vol 39, Issue 12, P862-879].

2.1 Abstract

Tissue injury can initiate bidirectional signaling between neurons, glia and immune cells that creates and amplifies pain. While the ability for neurotransmitters, neuropeptides, and cytokines to initiate and maintain pain has been extensively studied, recent work has identified a key role for reactive oxygen and nitrogen species (nitroxidative species), including superoxide, peroxynitrite, and hydrogen peroxide. In this review, we describe how nitroxidative species are generated after tissue injury, and the mechanisms by which they enhance neuroexcitability in pain pathways. Finally, we discuss potential therapeutic strategies for normalizing nitroxidative signaling, which may also enhance opioid analgesia, to help to alleviate the enormous burden of pathological pain.

2.2 The link between nitroxidative signalling and pain

Investigation of oxidative processes, such as rusting, began with the “phlogiston theory”, developed by Georg Ernest Stahl during the scientific revolution, which postulated that a fire-like element (phlogiston) is released during combustion. Oxidation was formally linked to biology during the early 20th Century, when it was found to underpin cellular metabolism [1–3]. The connection between reactive oxygen species (ROS) and altered sensory processing was empirically identified around the same time [4]. Since then, research has shown that prolonged, unchecked increases in reactive oxygen and nitrogen (nitroxidative) species after infection or tissue damage can promote cytotoxicity and inflammation. These processes can cause peripheral and central sensitization, which underlie pathological pain (see Glossary) [5,6]. Thus, restoring nitroxidative balance in peripheral and central nervous systems (PNS, CNS) is a possible therapeutic approach for ameliorating neuropathology [6–10].

In this review, we summarize recent research on how nitroxidative species participate in neuroimmune signalling throughout the neuraxis to drive pathological pain. We additionally discuss potential therapeutic strategies for normalizing nitroxidative signalling by activating

endogenous antioxidant systems, which may also enhance opioid analgesia. As pathological pain is often intractable to current therapies, new strategies to normalize nitroxidative signalling may help to alleviate the enormous burden of pain [11].

2.3 Production of nitroxidative species by neurons, glia, and immune cells

The role of nitroxidative signalling in pain has been studied using rodent experimental models of inflammatory pain (e.g. intraplantar complete Freund's adjuvant (CFA), formalin) and neuropathic pain (e.g. peripheral nerve injury (PNI), chemotherapy-induced peripheral neuropathy (CIPN), diabetic neuropathy (DN), spinal cord injury (SCI), experimental autoimmune encephalomyelitis (EAE)), which have recently been reviewed elsewhere [12].

There are numerous endogenous sources of ROS and nitric oxide (NO) that are engaged during pain processing [13]. Nicotinamide adenine dinucleotide phosphate (NADPH) oxidases, NO synthases and mitochondrial respiration are among the best characterized ROS/NO producers and will be discussed here (Figs. 2.1 and 2.2).

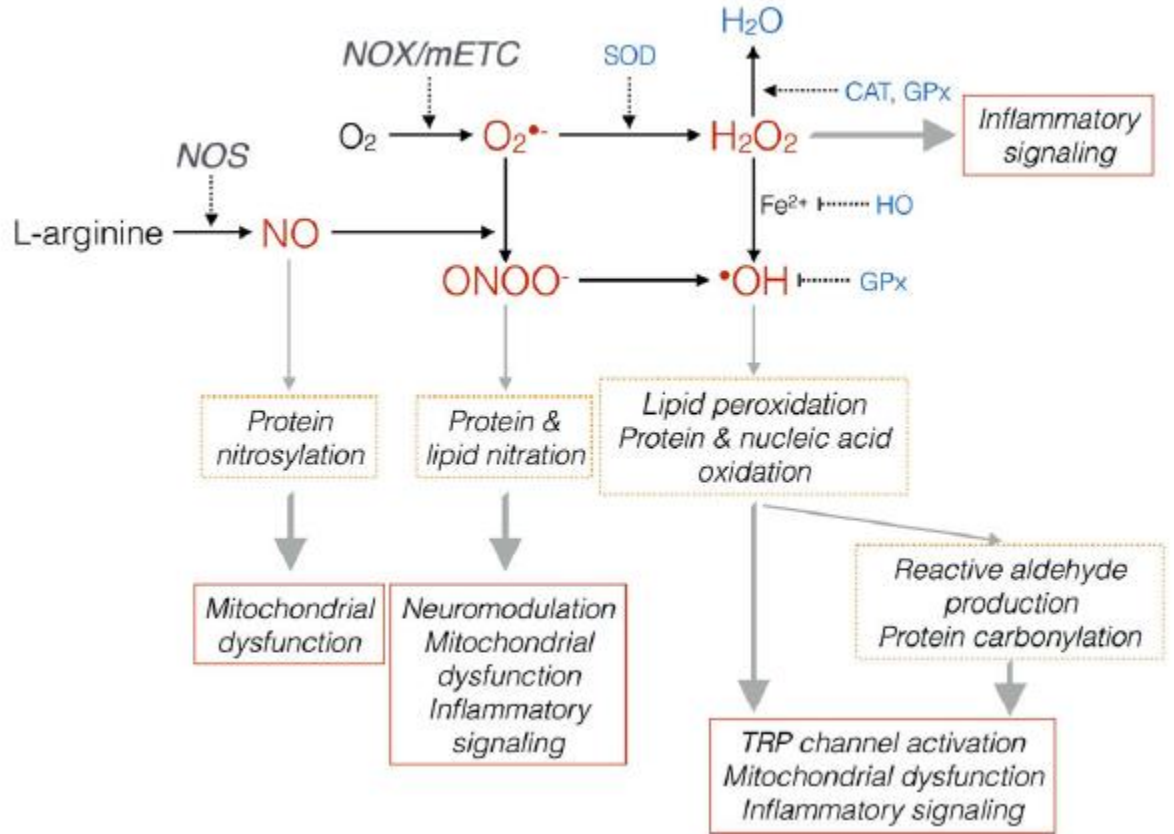


Figure 2.1 Induction of nitroxidative species after tissue injury

Nitroxidative species can induce posttranslational modifications of proteins and lipids, which subsequently drive pathological pain by modulating nociceptive neurotransmission, activating TRP channels, inducing mitochondrial dysfunction, and induce inflammatory signaling. In healthy cells, endogenous antioxidant systems prevent nitroxidative damage. Cell damage/pathology can perturb this balance, driving accumulation of potentially damaging nitroxidative species. O_2 : oxygen; NO : nitric oxide; $O_2^{\bullet-}$: superoxide; $ONOO^-$: peroxynitrite; H_2O_2 : hydrogen peroxide; $\bullet OH$: hydroxyl radical; H_2O : water; NOX: NADPH oxidase; NOS: nitric oxide synthase; mETC: mitochondrial electron transport chain; SOD: superoxide dismutase; CAT: catalase; GPx: glutathione; HO: heme oxygenase.

2.3.1 NADPH oxidases

NADPH oxidases (NOX) are membrane-bound enzyme complexes. They transport electrons donated from cytosolic NADPH to generate extracellular or luminal superoxide anions or hydrogen peroxide, that can be transported into the cytosol via aquaporin channels [13,14]. In contrast to other sources of ROS that are generated as a by-product of catabolism, ROS generation is the primary function of NOX. There are seven members in the NOX family; NOX1, 2, and 4 have been implicated in pathological inflammatory and neuropathic pain models [13,15,16]. NOX1 and 2 are expressed at the cellular membrane and produce superoxide anions following phosphorylation of cytosolic subunits [17]. NOX4 is expressed on organelles, such as the endoplasmic reticulum, and constitutively produces hydrogen peroxide [17].

NOX1 is inducibly expressed by microglia, neurons, astrocytes, and macrophages in the dorsal root ganglion (DRG) and CNS [17–19]. Nociceptive hypersensitivity induced by the inflammatory stimuli formalin and carrageenan is attenuated in Nox1 deficient mice [18]. NOX1-derived ROS induce translocation of PKC α to the membrane to enhance Transient Receptor Potential (TRP) V1 activity in DRG neurons [18], a change consistent with pain amplification (Fig. 2.2). In contrast, another study showed that NOX1 mRNA failed to upregulate in the DRG following peripheral nerve injury (PNI) [20]. These results indicate that DRG NOX1 may have a preferential role in inflammatory versus neuropathic pain.

NOX2 is predominantly expressed by phagocytic cells—peripheral macrophages and CNS microglia [13]. PNI induces a rapid upregulation of NOX2 mRNA by DRG macrophages and spinal microglia, which is correlated with increased intracellular superoxide [20,21]. PNI-induced nociceptive hypersensitivity was attenuated in Nox2 deficient mice [20,21]. Nox2 deficiency attenuated TNF, but not IL-1, mRNA expression, as well as expression of the neuronal injury marker ATF3 in DRG (Fig. 2.2) [20]. However, Nox2 deficiency did not influence macrophage recruitment to the injured DRG, suggesting a role for NOX2 in macrophage function rather than chemotaxis [20]. Nox2 deficiency attenuated PNI-induced Iba1 expression and the attendant expression of pro-inflammatory cytokines TNF and IL-1 α in the spinal dorsal horn [21]. As these studies were performed in global knockouts, it is still unclear whether alterations in the DRG and dorsal horn are subject to NOX-dependent

changes in macrophage function at the injury site. In contrast to NOX1, NOX2 activity in monocytes appears to play no role in inflammatory pain [22].

NOX4 is expressed by DRG neurons—both myelinated (A-fibers) and unmyelinated (C-fibers) DRG neurons—and by microglia, astrocytes and macrophages [13,23,24]. Nociceptive hypersensitivity following PNI is attenuated in Nox4 deficient mice, with attenuation of hydrogen peroxide at the sciatic nerve injury site [23]. These results are supported by the absence of NOX4 upregulation in the DRG after PNI [20]. The myelin proteins MPZ and PMP22 are decreased at the sciatic nerve injury site over time in an NOX4-dependent fashion, suggesting that myelin degeneration by hydrogen peroxide may maintain neuropathic pain (Fig. 2.2). However, attenuated damage at the injury site did not alter expression of the nitroxidative stress and neuroinflammation indices at the spinal dorsal horn or DRG (microglia proliferation, hydrogen peroxide levels) [23]. This contrasts with other studies showing that such processes are dependent on manipulations at the sciatic nerve [25–27]. Finally, a role for NOX4 may be limited to neuropathic, rather than inflammatory pain [23].

Together, these data suggest that NOX1, 2, and 4 isoforms contribute to pathological pain. Future studies could expand the role of various NOX isoforms to other sites in the neuraxis, and well as identifying a role for other NOX isoforms in pain. These data may help to guide development of therapeutics that target the activity of specific NOX isoforms to reduce nitroxidative stress and pain.

2.3.2 Nitric oxide synthases

NO is a diffusible gas mediator that is synthesized from L-arginine by one of three nitric oxide synthase (NOS) isoforms: NOS1 (neuronal), 2 (inducible), and 3 (endothelial). NO and all three NOS isoforms have a well-established role in nociception (Fig. 2.2) [28]. It easily passes through membranes to directly impact nearby cells.

NOS1 is constitutively expressed in the cytosolic compartment of postsynaptic terminals of neurons, and of stressed Schwann cells, and requires calcium for its activation [29–31]. In abnormal pain states, N-methyl-D-aspartate (NMDA) receptors are activated, resulting in calcium influx and activation of NOS1 [28]. Nociceptive hypersensitivity induced by PNI and CIPN is attenuated by genetic ablation and pharmacological inhibition of NOS1 [32–35]. NOS2 is a cytosolic isoform that is widely expressed in many immune cells and in glia. Transcription of NOS2 is initiated by Toll like receptors (TLRs) and, once translated, is

constitutively active—that is, unlike NOS1 and 3, its activity is independent of calcium [28]. NOS2 inhibition attenuates nociceptive hypersensitivity associated with inflammatory and neuropathic pain models [15,36,37].

NOS3 is best known for its expression in the cardiovascular system as a regulator of vascular tone. NOS3 is a membrane-bound enzyme that is constitutively expressed; however, it requires the interaction of calcium and calmodulin for its activation [28]. NOS3 expression is increased in the DRG after subcutaneous administration of CFA, and is correlated with allodynia, suggestive of increased NOS3 activity [38]. CFA-induced inflammatory pain is attenuated by NOS3 inhibition [38].

2.3.3 Cellular respiration

One critical function of mitochondria is energy metabolism. The mitochondrial electron transport chain (mETC) is a series of five molecular complexes through which electrons are transported to synthesize ATP from ADP. Premature electron leakage can occur during cellular respiration, particularly at Complexes I and III, resulting in superoxide production (Fig. 2.2) [39]. Mitochondrial ROS are elevated in spinal neurons, microglia and astrocytes in neuropathic pain models [21,40,41]. Furthermore, blocking the mETC attenuates hyperalgesia associated with a range of inflammatory and neuropathic pain models [42–45]. However, a direct link between mETC-dependent pain and mitochondrial ROS has yet to be shown. These results suggest that cellular respiration is increased, but is inefficient due to enhanced ROS-generating electron leakage from the mETC, as ATP production by sciatic nerves is impaired during CIPN [46].

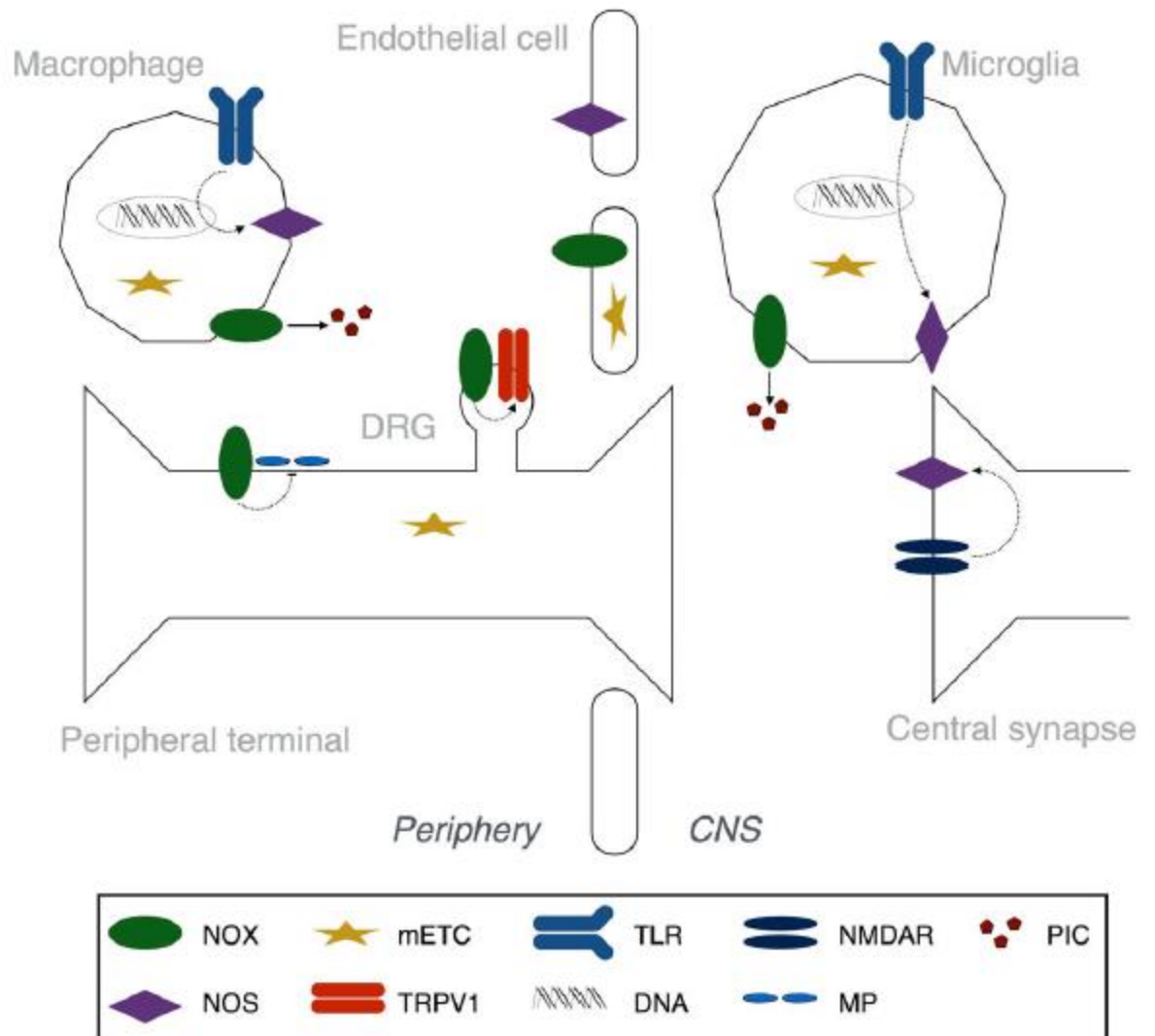


Figure 2.2 Sources of nitroxidative species after tissue injury

Principal sources of nitroxidative species include NADPH oxidase (NOX), nitric oxide synthase (NOS), and electron leakage from the mitochondrial electron transport chain (mETC). The NOX1, 2, and 4 isoforms are differentially expressed across cell types and tissues after injury. NOX1-derived reactive oxygen species induce enhance Transient Receptor Potential (TRP) V1 activity in dorsal root ganglia (DRG) neurons. NOX2 activity in macrophages and microglia drives mRNA expression of proinflammatory cytokines (PIC) in DRG the spinal dorsal horn. NOX4 expression at the site of peripheral nerve injury decreases expression of myelin proteins (MP). The three NOS isoforms—NOS1 (neuronal), 2 (inducible), and 3 (endothelial)—are also differentially expressed by cell type. In abnormal pain states, N-methyl-D-aspartate receptors (NMDARs) are activated, resulting in calcium influx and activation of NOS1. Transcription of NOS2 is initiated by Toll like receptors (TLRs). These enzymes and processes have a well-established role in pathological pain.

2.4 Mechanisms of nitroxidative signalling in neuronal hyperexcitability

Injury or disease can provoke intense, repeated, and sustained activity of primary afferent (sensory) neurons. This activity, together with the release of mediators from reactive glia and immune cells, elicits well-characterized changes in neuronal and biochemical processing at peripheral terminals and central synapses [5,47–50]. This is termed ‘sensitization’, and results in nociceptive hypersensitivity. Here, we discuss how nitroxidative signalling engages neurons in pain pathways, leading to peripheral and central sensitization (Figs. 2.1 and 2.3).

2.4.1 Nitroxidative species as neuromodulators in pain pathways

Nitroxidative species can directly increase the excitability of nociceptive neurons. Intraplantar administration of superoxide, peroxynitrite, or intrathecal delivery of the ROS donor tert-butyl hydroperoxide (tBOOH) is sufficient to induce nociceptive hypersensitivity in naïve rats [51–54]. These studies demonstrated that ROS activates calcium calmodulin-dependent protein kinase II (CamKII) in glutamatergic spinal neurons and induced presynaptic inhibition of GABAergic interneurons (disinhibition). Furthermore, hydrogen peroxide enhanced the frequency and amplitude of action potentials of DRG neurons from neuropathic rats (Fig. 2.3) [55].

In neuropathic pain models, administration of the non-selective ROS scavenger phenyl-N-tert-butyl nitron (PBN), selective small molecule superoxide and peroxynitrite decomposition catalysts such as M40403, FeTMPyP5+ and MnTE-2-PyP5+, or selective peroxynitrite decomposition catalysts such as SRI6 and SRI110 attenuated nociceptive hypersensitivity [15,51,53,54,56–58]. Accordingly, PBN attenuated injury-induced hyperexcitability of spinal dorsal (sensory) horn “pain” responsive neurons and phosphorylation of CamKII [51,57], an effect consistent with pain normalization. Several mechanisms of enhanced excitatory signalling have been identified. Hydrogen peroxide can activate cGKI, resulting in increased neurotransmitter release from the terminals of primary afferent neurons in the dorsal horn [59,60]. Peroxynitrite and ROS disrupt glutamate homeostasis leading to potentiation of synaptic currents and calcium influx, and ultimately excitotoxicity [56,61]. Mechanisms include nitration and phosphorylation of several NMDA receptor subunits, as well as inhibition of glutamine synthetase and the glutamate transporter GLT-1 that limit the synaptic half-life of glutamate [15,56,62,63]. Nitroxidative products also induce disinhibition after PNI, as PBN normalized the decrease in GAD-67+ GABAergic dorsal horn neurons, and increased GABA

release (Fig. 2.3) [53,64]. Together, these data suggest that nitroxidative species directly enhance neuroexcitability in pain pathways.

2.4.2 Nitroxidative species activate TRP channels

The TRP family of nonselective cation channels plays a vital role in the molecular integration of multiple endogenous and exogenous sensory stimuli [65]. Several of these channels, expressed at the peripheral and central terminals and cell bodies of primary afferent neurons, are activated by nitroxidative species and products. TRP channel activation by nitroxidative species can also initiate neurogenic inflammation—recruitment and activation of immune cells following release of neuropeptides by neurons—which is a key process underlying pathological pain (Fig. 2.3) [5,66]. Here, we focus on known roles of TRPA1, TRPM2, and TRPV1.

TRPA1 is a chemoreceptor expressed exclusively by peptidergic C-fibers [65]. Nitroxidative species induce protein carbonylation, and membrane phospholipid peroxidation and nitration, and subsequent production of reactive aldehydes such as acrolein (Fig. 2.1). These products all share the ability to induce nociceptive hypersensitivity by directly activating TRPA1 [67–72]. Acrolein is elevated in the DRG and spinal cord after SCI, and blockade with hydralazine or phenelzine partially attenuated allodynia [73,74]. Moreover, nociceptive hypersensitivity induced by CIPN was abolished in *Trpa1* deficient mice, or with a TRPA1 antagonist [75]. In this model, the chemotherapeutic bortezomib did not directly activate TRPA1, suggesting that ROS may act as an intermediate [75].

TRPM2 is expressed by neurons, and abundantly by immune cells, including monocytes/macrophages, neutrophils and T cells, and microglia. This channel is directly activated by hydrogen peroxide, and cytosolic ADP-ribose that is generated after nitroxidative damage to mitochondria [76–81]. Furthermore, TRPM2 activation is critical for activation of spinal microglia and for macrophage infiltration into the spinal cord after PNI [82]. TRPM2 also activates ERK MAPK and induces nuclear translocation of NF- κ B, resulting in production of proinflammatory cytokines and chemokines [76,77,81,83,84]. Consequently, pharmacological and genetic studies have demonstrated that TRPM2 contributes to inflammatory and neuropathic nociceptive hypersensitivity [77–79,82,85].

TRPV1 is found on unmyelinated, slowly conducting neuronal C-fibers, and is an essential component underlying injury-elicited thermal hyperalgesia and nociceptive hypersensitivity [65]. TRPV1 expression is upregulated by an exogenous ROS donor (tBOOH), and is a target

of oxidation and nitration events that increase responsiveness of the channel [18,86–88].

Moreover, linoleic acid metabolites, created during production of eicosanoids, are endogenous TRPV1 agonists when oxidized, and contribute to nociceptive signaling [89,90].

2.4.3 Nitroxidative species induce mitochondrial dysfunction

Mitochondria have pivotal roles in a variety of cellular functions, including energy metabolism, calcium homeostasis, lipid synthesis, and apoptosis. As noted above, cellular respiration can be elevated under neuropathic pain conditions, with an attendant elevation of ROS derived from neuronal and microglial mitochondria [21,40,41]. Together with nitroxidative species derived from NOX and NOS enzymes, these species disrupt mitochondrial homeostasis via several mechanisms, leading to bioenergetic crisis (due to impaired mETC efficiency) and degeneration of primary afferents (Fig. 2.3) [91].

Mitochondrial DNA is a target of oxidation and nitration, while peroxidated lipid end-products, such as reactive aldehydes, can form covalent modifications (adducts) with an array of mitochondrial proteins, including antioxidants [92,93]. Together, these changes impair the structural integrity and function of mitochondria. Nitroxidative species can also trigger release of pro-apoptotic factors from mitochondria. For example, NO can disrupt mitochondrial dynamics (fission and fusion; responsible for maintaining metabolic homeostasis) that results in translocation of Bcl-2-associated X protein from the cytosol to the organelle membrane, where it activates apoptosis pathways [94–96]. Activation of apoptosis pathways contributes to neuropathic pain, as inhibition of several caspase enzymes attenuates vincristine- and dideoxycytidine-induced nociceptive hypersensitivity [97]. Neuropathic pain is associated with impaired mitochondrial function, and nociceptive hypersensitivity is accordingly attenuated by pharmacologically normalizing mitochondrial dynamics or preventing mitotoxicity [46,98–100].

2.4.4 Nitroxidative species induce neuroinflammatory signalling

Pro-inflammatory mediators released by glial and immune cells increase neuroexcitability in pain pathways after injury (e.g. TNF, IL-1 β , BDNF) [5,50,101–103]. Several mechanisms include enhanced glutamate release, increased AMPA receptor expression, phosphorylated NMDA receptor subunits, and downregulated astrocyte glutamate transporters [5]. These proinflammatory mediators can also induce disinhibition of neuronal excitability by attenuating GABA and glycine release from interneurons and inhibitory descending projections, and downregulating KCC2 on postsynaptic terminals [5].

Nitroxidative species regulate the production of proinflammatory mediators during pathological pain. For example, NFκB and p38 MAPK are responsible for the production of a wide array of proinflammatory mediators in immune cells. Nitroxidative products degrade/inhibit IκB and MAPK phosphatases, resulting in activation of NFκB and p38 that both mediate inflammatory and neuropathic pain [52,104–107]. Furthermore, nitroxidative species may promote release of neuron-to-glia signals, such as matrix metalloproteases (MMPs) (Fig. 2.3) [108].

Nitroxidative species also elicit proinflammatory responses via toll-like receptor (TLR) signalling. TLRs bind a variety of endogenous ligands (danger associated molecular patterns: DAMPs), including DNA and N-formyl peptides from nitroxidatively damaged mitochondria, to trigger innate immune responses that contribute to pathological pain [5,109]. ROS serve a vital role as second messengers for TLR signalling. A rapid (minutes) respiratory burst occurs upon activation of TLR2 and 4, which is mediated by a direct interaction with the intracellular domains of NOX1, 2, and 4 enzymes. This NOX activity is essential for downstream NFκB- and p38 MAPK-dependent cytokine production [110–114]. Furthermore, activation of NOX enzymes by TLR signalling induces transcription of TLRs, and promotes membrane expression in lipid rafts, which is necessary for efficient signalling [111,115,116]. In concert with disruption of blood-brain barrier tight junctions by nitroxidative species, the TLR2-NOX1 interaction also upregulates adhesion molecules via CCL3 to facilitate transendothelial cell migration, which contributes to nociceptive hypersensitivity after PNI (Fig. 2.3) [102,110,117]. ROS have been implicated in the activation of NLRP3 inflammasomes [118]—protein complexes responsible for the proteolytic activation of IL-1 β , a pro-inflammatory cytokine with a well-established role in pathological pain [5,101,119]. Among the various sensor molecules that trigger formation of inflammasomes, NLRP3 has been most widely investigated, and has a recently described role in neuropathic pain [120]. The relative contributions of ROS to the activation versus priming of NLRP3 inflammasomes remains to be elucidated [119].

Mitochondria are key participants in the activation of NLRP3 inflammasomes; they are a source of ROS that can directly activate NLRP3, as well as oxidized mitochondrial DNA that can also activate NLRP3 (Fig. 2.3) [118,121–123]. Furthermore, TRPM2 activation by nitroxidative species induces a calcium flux that activates the NLRP3 inflammasome [124].

Finally, there is a reciprocal relationship between nitroxidative species and inflammatory signalling. For example, the transcription of NOX and NOS enzymes is upregulated by TLR4 and 9 signalling, and by NFkB and p38 activation [19,125–129]. The purinergic receptor P2X7, which has a documented role in pathological pain, also induces ROS production [5,120,130]. ATP signalling through P2X7R activates NOX2 in a calcium and p38-dependent fashion [131–133].

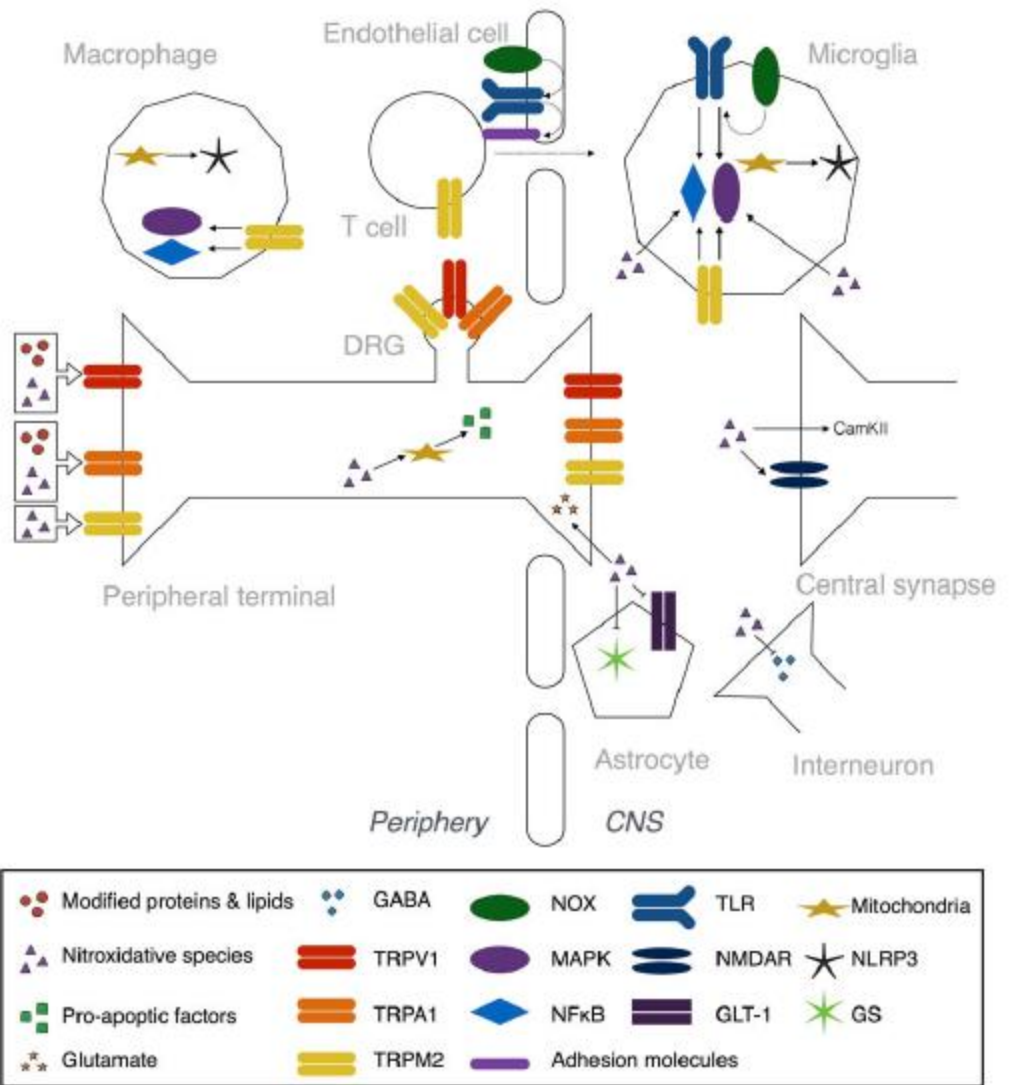


Figure 2.3 Nitroxidative mechanisms of neuroexcitability after tissue injury

Reactive nitroxidative species, such as hydrogen peroxide and peroxynitrite, and modified proteins and lipids, like carbonylated proteins, peroxidated and nitrated lipids, and reactive aldehydes, all contribute to peripheral and central sensitization after tissue injury. These processes drive pathological pain. Several of the Transient Receptor Potential (TRP) family of nonselective cation channels are activated by nitroxidative species and modified proteins and lipids (see Nitroxidative species activate TRP channels). TRPA1 is expressed by peptidergic C-fibers, and is activated by modified proteins and lipids. TRPM2, which is expressed by neurons, monocytes/macrophages, microglia, and T cells, is directly activated by nitroxidative species. TRPM2 also activates intracellular signaling pathways, including mitogen activated protein kinase (MAPK) and nuclear translocation of nuclear factor κ -light-chain-enhancer of activated B cells (NF κ B) pathways. TRPV1 is found on C-fibers and is directly activated by some modified proteins and lipids, as well as being a target of oxidation and nitration events by nitroxidative species that increase responsiveness of the channel. Reactive nitroxidative species can directly modulate neuroexcitability in central synapses by promoting glutamate release from primary afferent terminals, by activating calcium calmodulin-dependent protein kinase II (CamKII) in glutamatergic spinal neurons, and by inhibiting GABAergic interneurons (see Nitroxidative species as neuromodulators in pain pathways). Nitroxidative species also disrupt glutamate homeostasis by nitration and phosphorylation of NMDA receptor (NMDAR) subunits, as well as inhibiting glutamine synthetase (GS) and the glutamate transporter GLT-1. Mitochondrial DNA is a target of oxidation and nitration, while some nitroxidative species can form adducts with many mitochondrial proteins, which together impairs the structural integrity and function of mitochondria (see Nitroxidative species induce mitochondrial dysfunction). Nitroxidative species can also trigger release of pro-apoptotic factors from mitochondria by disrupting organelle dynamics. Nitroxidative species induce production of proinflammatory mediators, and can activate NF κ B and MAPK intracellular signalling pathways (see Nitroxidative species induce neuroinflammatory signalling). Toll like receptors (TLRs) bind a variety of endogenous danger signals, including those released from nitroxidative-damaged mitochondria, to activate NF κ B and MAPKs. NOX-derived ROS are second messengers for NF κ B- and p38 MAPK-dependent TLR signalling, and TLR expression. The TLR2-NOX1 interaction also upregulates adhesion molecules via CCL3, which facilitates transendothelial cell migration into the CNS. Mitochondria-derived ROS also activate NLRP3 inflammasomes, which are protein complexes responsible for the proteolytic activation of IL-1 β .

2.5 Endogenous regulators of nitroxidative signaling

Under healthy conditions, nitroxidative species and antioxidants exist in a balanced state, as nitroxidative products play a vital physiological role in cellular processes (e.g. signal transduction, pathogen defense [134–136]). In response to increased production of nitroxidative species during injury or infection, antioxidant and regulatory systems are activated in an attempt to recover homeostasis (Fig. 2.1) [14].

2.5.1 Antioxidant defense

Transcription of antioxidant genes is a critical step in controlling nitroxidative signalling. One key transcription factor is nuclear factor E2-related factor 2 (Nrf2). Nrf2 is expressed in CNS and PNS neurons, macrophages, Schwann cells, astrocytes, and microglia [137–139]. Under homeostatic conditions, cytosolic Nrf2 is sequestered by the protein Keap1 and ubiquitinated for degradation. However, in the presence of oxidants and electrophiles Nrf2 is released from Keap1 and translocates to the nucleus [140]. Nrf2 binds to the antioxidant response element (ARE) promoter region to elicit expression of 200+ antioxidant genes, including superoxide dismutases (SOD1: cytosolic; SOD2: mitochondrial), catalase, glutathione, and heme-oxygenases [140]. Another transcription factor, forkhead box, class O (FoxO), is also responsible for the production of SOD2 and catalase [141]. Many of these antioxidants are ubiquitously expressed, and their catabolic function is summarized in Figure 2.1 [142].

These endogenous antioxidant systems collaborate to detoxify reactive nitroxidative species (Fig. 2.1). Evidence is mixed whether neuroinflammatory or traumatic events increase nervous system antioxidant levels [143–152]. This likely reflects a temporally- and injury-specific antioxidant response, and the fact that injury-induced nitroxidative species can negatively regulate antioxidant production [15,76]. Antioxidant system activation can limit pathological pain: deletion of SOD1 exacerbates neuropathic pain, while exogenous antioxidants attenuate nociceptive hypersensitivity in a range of inflammatory and neuropathic pain models [37,108,153–155]. Similarly, heme-oxygenases, which elicit expression of various antioxidants, protects cells and could improve inflammation and neuropathic pain [21]. Therefore, therapies that increase antioxidant systems could resolve neuroinflammation and pain symptoms.

2.5.2 Anti-inflammatory cytokine and adenosine signalling

Cytokines such as IL-10 and TGF β counter-regulate proinflammatory signalling and contribute to the resolution of neuropathic pain hypersensitivity [5,156,157]. One mechanism of action is

regulation of nitroxidative signaling. For example, IL-10 and TGF β inhibit NOX2 activity and promote antioxidant production [158–160]. This is a reciprocal relationship, as antioxidants can also drive production of anti-inflammatory cytokines [161,162]. Adenosine signalling is also anti-nociceptive in pathological pain models [163–165]. Signalling through A2A and A3 receptors inhibits NOX activity, and drives production of anti-inflammatory cytokines and antioxidants [163,166,167].

2.6 Opposition of opioid analgesia by nitroxidative species

Opioid analgesics remain the cornerstone of management of moderate-to-severe pain.

However, the clinical utility of opioids is limited by tolerance, which is characterized by dose escalation due to reduced sensitivity to an opioid agonist, as well as hyperalgesia, a paradoxical increase in pain sensitivity due to opioid exposure [168,169]. Recent evidence has identified a role for nitroxidative signalling in these phenomena [6,170].

NOX activity is elevated by morphine, and genetic or pharmacological disruption of these enzymes attenuates tolerance and hyperalgesia [171–173]. Superoxide and peroxynitrite have been implicated as downstream mediators, as decomposition catalysts also attenuate tolerance and hyperalgesia [174–176]. It remains unclear how morphine engages these enzymes, but it may be mediated by classical μ -opioid receptors and/or TLR4 [168]. The pronociceptive mechanisms of nitroxidative species, described above, may act as an opponent process of neuronally-mediated opioid analgesia to create tolerance, or may overshadow analgesia to induce hyperalgesia. Therefore, correcting nitroxidative imbalance may improve the clinical profile of opioids [170].

Nitroxidative signaling also disrupts endogenous opioid analgesia in supraspinal sites that is engaged to inhibit spinal nociception via descending projections. For example, induction of peroxynitrite during inflammatory pain results in nitration of met-enkephalin in the rostral ventromedial medulla (RVM), which reduces opioid receptor binding affinity [177]. This may be normalized by intra-RVM microinjections of FeTMPyP5+, which was antinociceptive in inflammatory and neuropathic pain models [177].

2.7 Nitroxidative signaling as a therapeutic target for pathological pain

Under pathological conditions, endogenous antioxidant responses can be insufficient, leading to an accumulation of toxic nitroxidative species. As mentioned above, unchecked increases in nitroxidative species can promote cytotoxicity and inflammation via cascading pronociceptive

signalling. Therefore, discovering therapeutic treatments that enhance cellular antioxidant capacity could help achieve nitroxidative balance to recover homeostasis.

Initial efforts to combat increases in nitroxidative species in a wide range of neurological disorders used direct antioxidant compounds (e.g. vitamins C and E, co-enzyme Q). The consensus view is that the possible beneficial effects are outweighed by unfavorable pharmacokinetic and pharmacodynamic profiles [13,178,179]. A variety of redox-active therapeutics are being developed to overcome these issues and are effective in treating cancer-induced bone pain, inflammatory, and neuropathic pain, and can also potentiate opioid analgesia [9,10,180].

Newer approaches have instead aimed to inhibit sources of nitroxidative species, stimulate endogenous antioxidants, and prevent nitroxidative damage [13,178]. To this end, inhibitors of specific NOX and NOS isoforms, and ROS toxifiers such as MPO, are being developed and may prove effective for pain treatment [13,181]. As noted above, A2A and A3 adenosine receptor agonists attenuate spinal NOX activity and promote antioxidant production, with a concomitant decrease in neuropathic pain [163–165]. Another promising approach is the development of small molecules that catalyze the clearance of reactive aldehydes [182]. Indirect antioxidants augment the redox response without being antioxidants themselves. For example, sulforaphane, resveratrol, and curcumin induce nuclear translocation of Nrf2, a transcription factor responsible for the production of a wide array of antioxidants, and attenuate nociceptive hypersensitivity in neuropathic pain models [21,183–186]. Non-pharmacological approaches may also function in this capacity. For example, exercise increases Nrf2 expression and promotes the expression of antioxidants in the CNS as well as peripherally [187–189]. Consequently, voluntary wheel running has been shown to both prevent and reverse neuropathic pain [187,190].

Finally, ROS have a role in normal physiological processes [134–136], and there is some evidence that ROS may have protective effects after injury. For example, inflammation induced by endotoxin is exacerbated in NADPH-impaired mice, relative to their wild-type counterparts [191]. In another study, yeast survival to hydrogen peroxide stress was dependent on superoxide [192]. Further work is required to determine whether reactive oxygen species may also have a protective role after sterile nervous system injury. However, agents have been developed to spare superoxide (e.g. peroxytrite decomposition catalysts SRI110 and SRI6

[15]), and such approaches may prove to be important for restoring homeostasis after nervous system injury.

2.8 Concluding remarks

Nitroxidative species are generated by mitochondria and by NOX and NOS enzymes. They enhance neuroexcitability in pain pathways through direct neuronal interactions, and indirectly by impairing mitochondria and inducing neuroinflammation. Normalizing nitroxidative signalling may be an alternative strategy to help to alleviate the enormous burden of pathological pain, which affects ~20% of the population, and is poorly treated [11,193,194]. There are several areas of basic science research that may move us towards that goal (see 2.8.1 Outstanding Questions).

Despite the extensive research implicating nitroxidative species in pathological pain states, no studies to date have quantified the critical relationships between real-time local cellular creation of nitroxidative species, their concentration at the effect site, or the distribution of their direct effect. This challenge has not been overcome owing to the volatility of these nitroxidative species and hence the very short life-time in vivo and ex vivo. Several new technologies are being developed to address these issues and are discussed in section 2.9.

Lessons from the failure of direct antioxidants to improve clinical disease need to be recognized within the pain field; the effects of direct antioxidants on preclinical pain models continue to be reported, despite the strong probability that the results will not translate clinically. Several studies suggest that more robustly engaging antioxidant systems after injury can help alleviate pain: for instance, in animal pain models, increasing action of master antioxidant transcription factors Nrf2 or FoxO, or activating the heme-oxygenase system show promising pain-relieving effects. Future studies could explore whether combinatorial strategies aimed at boosting multiple antioxidants or targeting both antioxidant and nitroxidative systems simultaneously dampen inflammation and pain. Nitroxidant dysregulation clearly contributes to neuropathology; thus, discovering new targets and therapies that restore nitroxidative balance could help relieve pathological pain.

2.8.1 Outstanding Questions•

- How ubiquitous are nitroxidative signalling mechanisms within the neuraxis, beyond the classical sites already tested (peripheral nerve injury site, DRG, spinal cord)?

- Are nitroxidative signalling mechanisms common or different between different preclinical pain models?
- What is the relationship between the antioxidant and anti-inflammatory cytokine systems?
- Do indirect antioxidants have improved translational potential for treatment of pathological pain?

2.9 New and emerging tools to study nitroxidative species – the following section was contributed by Vasiliki Staikopoulos and edited by Prof Mark Hutchinson.

Colorimetric and fluorescent methods for detecting the “shadow” of the presence of nitroxidative species production is well established by the quantification of attendant cellular events (e.g. oxidative stress such as lipid peroxidation (TBARS) [195]; and DNA damage (8-Oxoguanine: 8-OxoG) [196,197]) or the quantification of more stable metabolites (e.g. nitrite/nitrate using Griess reaction [198]). These methods are not only limited in their temporal and spatial resolution, but also due to their insufficient ability to define concentrations and time courses of specific nitroxidative species. Establishing differential regulation of distinct nitroxidative species would be useful, as specific oxygen or nitrogen species have unique outcomes in the neuroinflammatory responses. A recent example demonstrated that specifically targeting peroxynitrite reduced inflammatory progression via NLRP3 inflammasome-dependent IL-1 β /IL-18 release following ICH induced inflammatory injury [199]. Thus, new biosensors are required to improve our mechanistic understanding of how nitroxidative species affect the nervous system.

The chemistry of fluorescent probes for specific detection of both ex vivo and in vivo production of nitroxidative species has grown rapidly. A range of approaches and hence biosensors have been created that exploit platform sensing modalities, such as photoinduced electron transfer (PET) and Förster resonance energy transfer (FRET) signalling. Additionally, composite biosensors that incorporate a sensor functionalised to a nanoparticle (gold particles, UCNP and QDots) are used to detect and/or measure ROS/RNS species (detailed in Table 1). Such ROS species probes can quantify hypochlorite [200,201], hydroxyl [202,203], superoxide [204], hydrogen peroxide [205] and singlet oxygen [206]. Biosensors for nitric oxide [207,208], nitroxyl [209–211], peroxynitrite [212] are also being developed.

These probes detect targeted species either in cell-lines, in ex vivo tissue, or in in vivo models of inflammation. However, these biosensor tools require further optimization. Further refining biosensors will help improve the stability of the probe; the brightness of the fluorescing molecule; the specificity to defined species; the sensitivity of detection; and the consumption of the probe in the sensing process. Thus, real-time continued visualisation and/or quantification of nitroxidative species within the CNS of a behaving preclinical rodent model of pathological pain remains an elusive goal.

The ultimate nitroxidative species biosensor would have real-time sensing capacity, with signal brightness that detected subcellular localisation of the nitroxidative species; ideally, this probe would not be consumed/bleached in the sensing process allowing for repeated measurements in vivo. Next generation probes will address some of these limitations. For instance, a redox sensitive fluorescent protein (rxRFP1), whose fluorescence intensity is positively related to the extent of oxidation of the probe, can detect varying amounts of oxidative stress within separate cellular compartments [213]. Further refining these tools will enable an improved understanding of how certain species contribute to oxidative or nitrosative stress and will allow researchers to define how spatiotemporal regulation of nitroxidative activity contributes to pathological pain.

Table 2.1 Probes able to detect specific ROS and RNS species, *in vitro*, *ex vivo* or *in vivo*.

ROS Species	Probe type	Imaging platform used	Tested in vitro	Tested ex vivo/ in vivo	ROS/RNS stimulation	Ref
<u>Hypochlorite</u>	Iridium (III) complex-based two-photon phosphorescent probe.	Two-photon laser scanning fluorescence microscope & Confocal laser microscope	HeLa cells/ RAW 264.7 cells	Zebrafish	10mM NaClO (<i>HeLa</i>) 1mg/mL LPS (<i>RAW 264.7</i> & <i>Zebrafish</i>)	[201]
<u>Hypochlorite</u>	Rhodamine-based hydrazide protein fluorescent probe	Fluorescence microscope	HeLa cells		50µM OCI-	[200]
<u>Hydroxyl</u>	Ratiometric fluorescence biosensor (gold particles conjugated with organic fluorophore)	Confocal laser microscope	HeLa cells		10µg/mL LPS	[203]
<u>Hydroxyl</u>	Ratiometric fluorescence biosensor (upconversion nanoparticles conjugated with organic fluorophore)	Fluorescence microscope equipped with 980nm laser.	HeLa cells	Mouse liver	500ng/mL PMA (<i>in vitro</i>) 1-4mg LPS/100g body weight (<i>in vivo</i>)	[202]
<u>Superoxide</u>	Fluorescein protein based fluorescent probe	Confocal laser microscope	HCT116/ BV-2/ RAW 264.7 cells	Zebrafish	500ng/mL LPS & 50ng/mL IFN-γ (<i>in vitro</i>) PMA 200 ng/mL or antimycin A 500 nM (<i>in vivo</i>)	[204]

<u>Hydrogen Peroxide</u>	Chemo-selective fluorescent naphthylimide peroxide probe	Two-photon laser scanning fluorescence microscope	RAW 264.7 cells	Mouse lung & skin	1µg/ml LPS (<i>in vitro</i>) 20µg LPS (<i>in vivo</i>)	[205]
<u>Singlet Oxygen</u>	Far-red silicon-rhodamine based chemical fluorescent probe	Fluorescence microscope with 640nm laser	HeLa cells/ RAW 264.7 cells		Photosensitizers: 150µg/mL 5-ALA 5µM TMPyP4	[206]
RNS Species						
<u>Nitric oxide</u>	Chemo-selective copper (II) based fluorescence probe	Confocal laser microscope	HeLa cells/ RAW 264.7 cells		50-200µM DEA-NONOate (HeLa) 200ng/mL LPS (RAW 264.7)	[208]
<u>Nitric oxide</u>	Far-red two-photon chemical fluorescent probe	Two-photon laser scanning fluorescence microscope	HeLa cells/ RAW 264.7 cells	Mouse liver	25µM NOC-9 (HeLa) 20µg/mL LPS, 200U/mL IFN- γ and 0.5mg/mL L-arginine (RAW 264.7) 1-4mg/ml LPS (<i>in vivo</i>)	[207]
<u>Nitroxyl</u>	FRET-based ratio-metric chemical fluorescent probe	Confocal laser microscope	HeLa cells		100µM AS	[211]

<u>Nitroxyl</u>	Near infra-red chemical fluorescent probe	Confocal laser microscope & In Vivo Imaging System	RAW 264.7 cells	Mouse (<i>in vivo</i>)	100µM AS (<i>RAW 264.7</i>) 500µM AS (<i>i.p. Mouse</i>)	[210]
<u>Nitroxyl</u>	Lysosome-targetable near infra-red chemical fluorescent probe	Confocal laser microscope & In Vivo Imaging System	RAW 264.7 cells	Mouse (<i>in vivo</i>)	200µM AS (<i>RAW 264.7</i>) 1mM AS (<i>i.p. Mouse</i>)	[209]
<u>Peroxynitrite</u>	Boronate-based chemical fluorescent probe	Confocal laser microscope	HeLa cells/ RAW 264.7 cells		5 & 20µM Peroxynitrite solution (<i>HeLa</i>) 1µg/mL LPS, 50ng/ml IFN- γ 2.5ng/ml PMA (<i>RAW 264.7</i>)	[212]

LPS: Lipopolysaccharide (produces endogenous ROS/RNS); **PMA:** phorbol 12-myristate-13-acetate (activates protein kinase C *in vivo* and *in vitro*); **IFN- γ :** Interferon gamma (produces endogenous ROS/RNS); **Antimycin A:** Produces endogenous ROS/RNS by driving apoptosis; **5-ALA:** 5-Aminolevulinic acid (drug used in photodynamic therapy, known to produce singlet oxygen); **TMPyP4:** 5, 10, 15, 20-tetra-(N-methyl-4-pyridyl)porphyrin (drug used in photodynamic therapy, known to produce singlet oxygen); **DEA-NONOate:** 2-(N,N-Diethylamino)-diazonolate 2-oxide (Nitric Oxide donor); **NOC-9:** 6-(2-Hydroxy-1-methyl-2-nitrosohydrazino)-N-methyl-1-hexanamine (Nitric Oxide donor); **AS:** Angeli's salt (Nitroxyl donor)

2.10 Update of new tools since publication

Since publishing this article, [Grace PM *et al.* (2016) Trends in Neuroscience, Vol 39, Issue 12, P862-879] there have been approximately 41 new papers released (research and reviews papers combined) reporting on nitroxyl fluorescent probes as of 6 July, 2019 (*Web of Science*; search terms “nitroxyl” + “fluorescent” + “probe”). A subset of these articles have been summarised in table 2.2 below highlighting the expanding selection of probe types which are becoming available to try and overcome some of the innate challenges of working with fluorescent substances in biology. However, this is still very much a chemistry dominated field, with very few papers being published showing a translation of this technology into identifying nitroxyl presence in biological systems, at this point in time. This section will provide an update in the latest development of chemical tools being generated to measure nitroxyl *in vitro*, *ex vivo* and *in vivo* and outline the benefits and limitations of using these methods for accurate and practical detection in biology.

2.10.1 Nitroxyl biochemistry

Investigating nitroxyl in biology has been problematic due to its spontaneous dimerisation in solution, with its final products yielding nitrous oxide (N₂O) and water (H₂O) (Equation 1) (Shafirovich and Lymar, 2002).



Therefore, to study the effects of nitroxyl in biology, most of the literature have reported using the exogenous donors Angeli's salt (sodium trioxodinitrate, Na₂N₂O₃). The highly reactive nitroxyl, which unlike NO, can act as a strong electrophile and be readily oxidised, can also target thiols, thiol proteins (Fukuto *et al.*, 2009; Liochev *et al.*, 2003; Smulik--Izydorczyk *et al.*, 2014; Miranda *et al.*, 2003) and metalloproteins (such as superoxide dismutase (SOD) and cytochrome c) (Murphy *et al.*, 1991; Liochev *et al.*, 2001, 2002). Although several mechanisms have been proposed, the highly reactive property of nitroxyl has meant that there has been no unequivocal evidence to support its formation *in vivo* to date. The most supported proposed mechanism of endogenous nitroxyl formation is during the nitric oxide synthase-mediated oxidation of N^ω-hydroxyl-L-arginine (Fukuto *et al.*, 1992; Schmidt *et al.*, 1996; Pufahl *et al.*, 1995; Hobbs *et al.*, 1994; Adak *et al.*, 2000; Tantillo *et al.*, 2000; Pagliaro, 2003). The lack of

evidence to support these mechanisms is due to the highly reactive nature of nitroxyl, making detection challenging. Several methods have been previously attempted to measure nitroxyl in biological systems such as; electrochemical analysis (Suarez *et al.*, 2013), mass spectrometry (Cline *et al.*, 2011), electron paramagnetic resonance (EPR) spectroscopy (Adachi *et al.*, 2008) and fluorescent probes. Fluorescent probes utilise the highly reactive nature of nitroxyl with various compounds (metal complexes, metalloporphyrins, thiols, phosphines or nitroso compounds) to detect and report the presence of the elusive nitrogen species (Smulik-Izdorczyk *et al.*, 2018). As previously discussed, fluorescent probes are highly sensitive and often used for the detection of many reactive species in biology. They are versatile as they can be excited in range of wavelengths which do not interfere with endogenous biological fluorophores and even near-infrared wavelengths that allow for deep penetration of light for detecting nitrogen species *in vivo* (Smulik-Izdorczyk *et al.*, 2018; Dong *et al.*, 2018).

Fluorescence quantum yield (Φ) is a measure of the efficiency of photon emission through fluorescence, which is the loss of energy by a substance that has absorbed light via emission of a photon (Lakowicz, 2006). This is a key factor in characterising the brightness of a fluorophore which is often determined in water or solvent based samples. However, the fluorescence quantum yield of a probe can be affected in biological samples by the solvent polarity throughout extracellular and sub-cellular regions, the proximity and concentration of quenching species (such as reactive nitrogen and oxygen species) and the pH of the environment (Lakowicz, 2006). These elements must be taken into consideration when designing fluorophores for measuring in biological systems.

There is a growing list of fluorogenic probes designed for the detection of nitroxyl which are categorised into four classes based on their reaction chemistry; (Smulik-Izdorczyk *et al.*, 2018; Dong *et al.*, 2018).

1. Copper (II) based fluorescent probes: nitroxyl reacts with Cu^{2+} ions to form NO and Cu^+ .
2. Arylphosphine based fluorescent probes: reacts with nitroxyl to form phosphine oxides and aza-ylides.
3. Nitroxide based fluorescent probes: reduced by nitroxyl to form hydroxylamines.
4. 2-Mercapto-2-methylpropionic acid based fluorescent probes: react with nitroxyl to form *N*-hydroxysulfenamide.

Generally, in each of these classes the reaction with nitroxyl causes the liberation of a fluorophore, thus most of these probes are considered “turn on” probes. The advantage of using any of these probes is that they are generally a one-step direct reaction with nitroxyl to yield the observed fluorescence response. However, the biggest disadvantage is the non-specificity of the probes when used in biological systems. Many of the probes can react with other species (such as thiols, oxygen, hydrogen sulphide, hydrogen peroxide) either once they are reduced by nitroxyl or competitively. Further to this, there is also the consideration of the nitroxyl scavenger glutathione, which can interfere with the system by either quickly removing any endogenous nitroxyl generated before it can react with the probes or reacting itself with the probe (Smulik-Izydorczyk *et al.*, 2018). Further research is required in this field to produce, not only sensitive and bright probes, but tools that are highly specific and reversible to allow for real-time monitoring in living systems.

2.11 Summary

It is clear that fluorescent probes are a valuable tool for detecting and measuring highly reactive nitrogen species in support of understanding their mechanistic role in neuropathic pain and other diseases. As with many other tools for measuring reactive nitrogen and oxygen species, the extent as to which these methods accurately report the specific species targeted without directly or indirectly interfering with the biological system being observed, is contentious. Currently, there is no probe available that can accurately measure endogenous nitroxyl production *in vivo* in a mammalian system. Due to the vastly complex biochemistry of nitric oxide, nitroxyl and other reactive nitrogen species, many factors need to be carefully considered when deciding on the appropriate fluorescent probe to select for addressing aims directed at understanding the *in vivo* role of these species in neuropathic pain states.

It is also evident that design and chemical synthesis of these probes, together with the selected wavelength and electron transfer rate of the attached fluorophore are also a major determining factor in the successful use of these tools in biological systems. While many studies by chemists have created probes with good specificity, high quantum yield, high sensitivity and readily reactive to their target molecule, they fall short in reproducing these results in the complex milieu which makes up biological systems. Therefore, the use of current nitroxyl fluorescent probes, may be inadequate to explore the role of nitroxyl in pathologies such as neuropathic pain. For future studies, there is a need to create and thoroughly validate

a highly stable, bright, sensitive and specific nitroxyl probe that can withstand the highly complex mix of potentially reactive molecules which make up biological cells and tissue.

Table 2.2 Probes able to detect nitroxyl, *in vitro*, *ex vivo* or *in vivo* post 2016.

ROS Species	Probe chemistry	Imaging platform	<i>In vitro</i> model	<i>Ex vivo/ In vivo</i> model	Nitroxyl stimulus	$\lambda_{em}/\lambda_{ex}$ (nm) wavelength	Ref
Nitroxyl	A coumarin-based HNO probe featuring a 2-mercaptoacetate trigger	Confocal microscope (details not reported)	Human breast adenocarcinoma cell line (MDA-MB-231)		AS (250 to 1000 μ M)	505/525	Pino <i>et al.</i> , 2017
Nitroxyl	Staudinger reaction chemistry-based bio-orthogonal probe with coumarin fluorophore	Confocal laser scanning microscope Two-photon fluorescence microscope (details not reported)	HeLa cells		AS (0–100 mM) DEA NONOate	405/470–500	Sunwoo <i>et al.</i> , 2017
Nitroxyl	HNO-responsive ratiometric two-photon fluorescence probe based on benzo-[h]chromene-rhodol dyes with FRET reporter	Two-photon confocal microscope (details not reported)	HeLa cells & Human umbilical vein cells (HUVECs)	Ex vivo rat liver & brain tissue	AS 500 μ M NaHS 500 μ M and DEA-NONOate 500 μ M AS 2mM N-methyl-D-aspartic acid (NMDA) and NaHS solution 1 mM	750/540 fluorescence ratio (F540/F470)	Zhou Y <i>et al.</i> , 2017
Nitroxyl	Merocyanine skeleton as the NIR fluorescent platform and 2-	Olympus FV1000 confocal laser	Human hepatocellular		AS 80 mM	635/655-755	Gong <i>et al.</i> , 2016

	(diphenylphosphino)benzoyl group as the HNO recognition moiety	scanning microscope (Japan).	carcinoma (SMMC-7721)				
Nitroxyl	Aza-BODIPY as fluorescent signal transducer, triphenylphosphonium cationic as mitochondria navigator, and diphenylphosphino-benzoyl as HNO-response unit.	Laser scanning confocal microscope (details not reported)	RAW264.7 cells BV-2 cells	Ex vivo, synovial membrane tissue of ankle joint In vivo mouse	AS 100 μ M NOC-5 and/or NaHS LPS 1 μ g/ml AS 500 μ M	680/730	Huang <i>et al.</i> , 2019
Nitroxyl	“Turn off” probe - copper(II) complex, Cu(II)-AbTCA, as a sensor for nitroxyl detection	TCS-SP5-X AOBS confocal scanning microscope (Leica, Wetzlar, Germany)	EAHY-44926 cells RAW 264.7 cells	In vivo Zebra fish	AS 200 μ M DEA NONOate and sodium ascorbate AS 200 μ M	375/450	Palanisamy <i>et al.</i> , 2018
Nitroxyl	NIR fluorescent turn-on probe (DCX-TPP) DCX-OH, consisted of a dicyanomethylene-4H-chromene conjugated to a xanthene moiety	Fluorescence microscopy (details not reported)	HeLa cells Raw264.7 cells		AS (0, 10, 50 and 100 μ M) SNP 2 mM NaASc 2 mM	360/500	Zhang CX <i>et al.</i> , 2019
Nitroxyl	Naphthalene-based fluorescent probe for HNO 2- (Diphenylphosphino) benzoate	Olympus FV1200-MPE multiphoton laser scanning confocal microscope (Japan)	Human hepatocellular liver carcinoma (HepG2)		AS 50 mM	370/556	Ma <i>et al.</i> , 2019
Nitroxyl	Caged D-luciferin with a	In vivo imaging	fLuc transfected		AS 50 & 100 mM	390/543	Li <i>et al.</i> , 2019

	(diphenylphosphino)-benzoate moiety	system (details not reported)	Human breast adenocarcinoma cell line (MDA-MB-231 cells)	In vivo, fLuc-transfected MDA-MB-231 tumor-bearing nude mice	AS 1 mM		
Nitroxyl	Synthesized [CuII-DQ468] as anHNO probe upon a dansyl-quinoline platform	fluorescence microscope (Leica DM3000, Germany)	Human hepatocellular liver carcinoma (HepG2)		AS 10 μ M	520/580–630	Maiti <i>et al.</i> , 2019
Nitroxyl & GSSH	Dual-site fluorescent probe NCF containing two individual reactive sites; organophosphine for HNO detection and the double bond between TCF and naphthaline for GSH addition	Olympus IX81 confocal laser scanning microscope (Japan)	Human hepatocellular liver carcinoma (HepG2)		AS 50 μ M	750/432	Nie <i>et al.</i> , 2019
Nitroxyl	Two-photon fluorophore 6-acetyl-2-naphthol bound to 2-(Diphenylphosphino)-benzoate as the HNO recognition moiety	Two-photon fluorescence microscope (details not reported).	HeLa cells	Ex vivo, fresh liver tissue slices (species not reported)	AS 20 and 50 mM NaASc 2.0 mM and SNP 2.0 mM AS 100 mM	488/550	Zhang P <i>et al.</i> , 2019

Nitroxyl	Mitochondrial-targeting moiety triphenylphosphonium, HNO recognition moiety of 2-(diphenylphosphino)-benzoate attached to the rhodol fluorescent platform	Nikon A1MP confocal microscope	HeLa cells		AS 30 mM	488/550	Ren <i>et al.</i> , 2017
----------	---	--------------------------------	------------	--	----------	---------	--------------------------

LPS: Lipopolysaccharide (produces endogenous ROS/RNS); **DEA-NONOate:** 2-(N,N-Diethylamino)-diazene 2-oxide (Nitric Oxide donor); **NOC-5:** 3-(Aminopropyl)-1-hydroxy-3-isopropyl-2-oxo-1-triazene (Nitric Oxide donor); **AS:** Angeli's salt (Nitroxyl donor); **SNP:** Sodium nitroprusside (Nitric oxide donor); **NaHS:** Sodium hydrosulphide (H₂S donor); **NaAsc:** Sodium ascorbate (electron donor); **RA model:** Rheumatoid arthritis model.

2.12 References

Adachi Y, Nakagawa H, Matsuo K, Suzuki T, Miyata N. (2008) Photoactivatable HNO releasing compounds using the retro-Diels-Alder reaction. *Chem. Commun*; (41): 5149–5151.

Adak S, Wang Q, Stuehr DJ. (2000) Arginine conversion to nitroxide by tetrahydrobiopterin-free neuronal nitric-oxide synthase. Implications for mechanism. *J.Biol. Chem*; 275(43): 33554–33561.

Cline MR, Tu C, Silverman DN, Toscano JP. (2011) Detection of nitroxyl (HNO) by membrane inlet mass spectrometry. *Free Radic. Biol. Med*; 50(10): 1274–1279.

Dong B, Kong X, Lin W. (2018) Reaction-Based Fluorescent Probes for the Imaging of Nitroxyl (HNO) in Biological Systems. *ACS Chem. Biol*; 13: 1714–1720.

Fukuto JM, Bianco CL, Chavez TA. (2009) Nitroxyl (HNO) signalling. *Free Radic. Biol. Med*; 47(9): (2009) 1318–1324.

Fukuto JM, Wallace GC, Hsieh R, Chaudhuri G. (1992) Chemical oxidation of N-hydroxyguanidine compounds. Release of nitric oxide, nitroxyl and possible relationship to the mechanism of biological nitric oxide generation. *Biochem. Pharmacol*; 43(3): 607–613.

Gong X, Yang X-F, Zhong Y, Chen Y, Li Z. (2016) A mitochondria-targetable near-infrared fluorescent probe for imaging nitroxyl (HNO) in living cells. *Dyes and Pigments*; 131: 24-32.

Hobbs AJ, Fukuto JM, Ignarro LJ. (1994) Formation of free nitric oxide from L-arginine by nitric oxide synthase: direct enhancement of generation by superoxide dismutase. *Proc. Natl. Acad. Sci. USA*; 91(23): 10992–10996.

Huang Y, Zhang X, He N, Wang Y, Kang Q, Shen D, Yu F, Chen L. (2019) Imaging of HNO anti-inflammatory effects via a near-infrared fluorescent probe in cell and in rat gouty arthritis models. *Journal of Materials Chemistry B*; 7(2): 305-313.

Lakowicz JR. (2006). Effects of Solvents on Fluorescence Emission Spectra. Principles of Fluorescence Spectroscopy, 3rd Edn. New York, NY: Springer US: 187-215.

Li J-B, Wang Q, Liu H-W, Yin X, Hu X-X, Yuan L, Zhang X-B. (2019) Engineering of a bioluminescent probe for imaging nitroxyl in live cells and mice. Chemical Communications; 55(12): 1758-1761.

Liochev SI, Fridovich I. (2001) Copper,zinc superoxide dismutase as a univalent NO(-) oxidoreductase and as a dichlorofluorescein peroxidase. J. Biol. Chem.; 276(38): 35253–35257.

Liochev SI, Fridovich I. (2002) Nitroxyl (NO-): a substrate for superoxide dismutase. Arch. Biochem. Biophys; 402(2): 166–171.

Liochev SI, Fridovich I. (2003) The mode of decomposition of Angeli's salt ($\text{Na}_2\text{N}_2\text{O}_3$) and the effects thereon of oxygen, nitrite, superoxide dismutase, and glutathione. Free Radic. Biol. Med; 34(11): 1399–1404.

Ma Q, Xu J, Mao G, Guo X, Liang B, Bai Y, Wang C. (2019) A highly sensitive and selective fluorescent probe for nitroxyl based on a naphthalene derivative. Analytical Methods; 11(6): 832-843.

Maiti D, Islam ASM, Dutta A, Sasmal M, Prodhan C, Ali M. (2019) Dansyl-appended CuII-complex-based nitroxyl (HNO) sensing with living cell imaging application and DFT studies. Dalton Transactions; 48(8): 2760-2771.

Miranda KM, Paolocci N, Katori T, Thomas DD, Ford E, Bartberger MD, Espey MG, Kass DA, Feelisch M, Fukuto JM, Wink DA. (2003) A biochemical rationale for the discrete behavior of nitroxyl and nitric oxide in the cardiovascular system. Proc. Natl. Acad. Sci. USA; 100(16): 9196–9201.

Murphy ME, Sies H. (1991) Reversible conversion of nitroxyl anion to nitric oxide by superoxide dismutase. *Proc. Natl. Acad. Sci. USA*; 88(23): 10860–10864.

Nie L, Gao C, Shen T, Jing J, Zhang S, Zhang X. (2019) Dual-Site Fluorescent Probe to Monitor Intracellular Nitroxyl and GSH-GSSG Oscillations. *Analytical chemistry*; 91(7): 4451-4456.

Pagliari P. (2003) Differential biological effects of products of nitric oxide (NO) synthase: it is not enough to say NO. *Life Sci*; 73(17): 2137–2149.

Palanisamy S, Wang Y-L, Chen Y-J, Chen C-Y, Tsai F-T, Liaw W-F, Wang Y-M. (2018) In Vitro and in Vivo Imaging of Nitroxyl with Copper Fluorescent Probe in Living Cells and Zebrafish. *Molecules*; 23(10): 2551.

Pino NW Davis J, Yu Z, Chan J. (2017) NitroxylFluor: A Thiol-Based Fluorescent Probe for Live-Cell Imaging of Nitroxyl. *J. Am. Chem. Soc*; 139(5): 118476-18479.

Pufahl RA, Wishnok JS, Marletta MA. (1995) Hydrogen peroxide-supported oxidation of NG-hydroxy-L-arginine by nitric oxide synthase. *Biochemistry*; 34(6): 1930–1941.

Ren M, Deng B, Zhou K, Wang J-Y, Kong X, Lin W. (2017) A targetable fluorescent probe for imaging exogenous and intracellularly formed nitroxyl in mitochondria in living cells. *Journal of Materials Chemistry B*; 5(10): 1954-1961.

Schmidt HHHW, Hofmann H, Schindler U, Shutenko ZS, Cunningham DD, Feelisch M. (1996) No· NO from NO synthase. *Proc. Natl. Acad. Sci. USA*; 93(25): 14492–14497.

Shafirovich V, Lyamar SV. (2002) Nitroxyl and its anion in aqueous solutions: spin states, protic equilibria, and reactivities toward oxygen and nitric oxide. *Proc. Natl. Acad. Sci. USA*; 99 (11): 7340–7345.

Smulik-Izydorczyk R, Debski D, Zielonka J, Michalowski B, Adamus J, Marcinek A, Kalyanaraman B, Sikora A. (2014) Nitroxyl (HNO) reacts with molecular oxygen and forms peroxynitrite at physiological pH. *Biological Implications. J. Biol. Chem*; 289(51): 35570–35581.

Smulik-Izydorczyk R, Dębowska K, Pięta J, Michalski R, Marcinek A, Sikora A. (2018) Fluorescent probes for the detection of nitroxyl (HNO). *Free Radical Biology and Medicine*; 128: 69–83.

Suarez SA, Bikiel DE, Wetzler DE, Marti MA, Doctorovich F. (2013) Time-resolved electrochemical quantification of azanone (HNO) at low nanomolar level. *Anal.Chem*; 85(21): 10262–10269.

Sunwoo K, Bobba KN, Lim J-Y, Park T, Podder A, Heo JS, Lee SG, Bhuniya S, Kim JS. (2017) A bio-orthogonal 'turn-on' fluorescent probe for tracking mitochondrial nitroxyl formation. *Chemical Communications*; 53(10): 1723-1726.

Tantillo DJ, Fukuto JM, Hoffman BM, Silverman RB, Houk KN. (2000) Theoretical studies on N-hydroxy-L-arginine and derived radicals: implications for the mechanism of nitric oxide synthase. *J. Am. Chem. Soc*; 122(3): 536–537.

Zhang C-X, Xiang M-H, Liu X-J, Wang F, Yu R-Q, Jiang J-H. (2019) Development of large Stokes shift, near-infrared fluorescence probe for rapid and bioorthogonal imaging of nitroxyl (HNO) in living cells. *Talanta*; 193: 152-160.

Zhang P, Lian P, Wang X, Li X, Wei C, Li X. (2019) A 6-acetyl-2-naphthol based two-photon fluorescent probe for the selective detection of nitroxyl and imaging in living cells. *Analytical Methods*; 11(10): 1299-1303.

Zhou Y, Zhang X, Yang S, Li Y, Qing Z, Zheng J, Li J, Yang R. (2017) Ratiometric Visualization of NO/H₂S Cross-Talk in Living Cells and Tissues Using a Nitroxyl-Responsive Two-Photon Fluorescence Probe. *Analytical chemistry*; 89(8): 4587-4594.

This page has been left intentionally blank

Thesis aims and hypotheses

The introductory chapters (Chapter 1 and 2) of this thesis aimed to highlight that neuropathic pain is a highly complex pathophysiological state that can be derived from many disease states. It is very likely that processes of peripheral and central sensitisation contribute to the observed pain symptoms. Furthermore, both neuronal and glial cells contribute to the development of disease via changes in activation state and the subsequent release of molecules, such as reactive nitrogen species, which can affect the overall excitability of post-synaptic neurons and contribute to the pain symptoms. However, current methods utilised to detect these species are inadequate, non-specific, degrade quickly and not sensitive enough to measure endogenous products in biological systems.

The aim of the first primary research study (Chapter 3) in this thesis was therefore:

- To validate a novel designed nitroxyl turn-on fluorescence probe that allows for the studies of nitroxyl species in biological systems, without the interference of other nitrogen species (Aim 1).

Based on the current understanding of the limitations of previously designed fluorescent nitroxyl probes, we hypothesise that:

- The current novel probe will readily pass into different cell types without inducing metabolic stress or toxicity of the cell; and
- Where nitroxyl is assumed to be present either by endogenous generation or exogenous application of nitroxyl, the probe will generate a high enough fluorescent quantum yield to be detected by confocal microscopy and/or plate reader spectroscopy.

Further, recent literature suggests that exogenous administration of reactive nitrogen species, nitroxyl, may inhibit the development of neuropathic pain symptoms via similar pathways to nitric oxide. It is also been suggested that nitroxyl is highly reactive with cysteine residues on cathepsin enzymes, which regulate modulation of pain signalling in both inflammatory and neuropathic pain.

The second primary research study (Chapter 4) therefore aimed:

- To determine the ability of nitroxyl to alter Cathepsin B enzyme activity and downstream signalling using both *in vitro* and *in vivo* mouse models of neuropathic pain reported in Chapter 1 as the Grace model of chronic constriction injury (Aim 2).

Based on the current understanding of the role of Cathepsin B enzyme activity in modulating glial release of cytokines in models of chronic pain, and recent suggestion of nitroxyl inhibition in chronic pain, we hypothesise:

- The reactive nitrogen species, nitroxyl will directly reduce Cathepsin B enzyme activity; and
- Nitroxyl administration will alter pain states of animals with developed neuropathic pain via a Cathepsin B enzyme pathway.
- Nitroxyl administration will alter key proteins, within the lumbar spinal cord which are involved in the release of cytokine, IL-1 β .

At present, studies investigating neuropathic pain spinal glial modulation have primarily focused on static end point measurements of molecular changes at multiple time points throughout the progression of the pathophysiology. However, it is now well established the innate neuroimmune responses in the spinal cord are highly dynamic and variable and can

occur quickly following peripheral injury leading to central sensitisation and progression to neuropathic pain symptoms long term. This includes changes in the cellular characteristics of microglia within the spinal cord which may be correlated with the intensity of the peripheral injury and subsequent symptoms. Further to this, changes in cerebral haemodynamic blood flow and oxygenation may be a surrogate measure of neuronal activity. Clinical studies have reported changes in somatosensory cortex which correlate with pain intensity from neuropathic pain patients, however this has not previously been explored in animal models.

Hence, the aims of the third primary research study (Chapter 5) were:

- To determine whether the expression and cellular characteristic of spinal microglia are altered prior to the development of neuropathic pain symptoms, using the clinically relevant mouse model of peripherally induced neuropathic pain reported in Chapter 1 as the Grace model of chronic constriction injury (Aim 3).
- To determine whether haemodynamic blood flow and oxygenation are altered following the development of neuropathic pain symptoms, using the above-mentioned animal model (Aim 4).

Given that an increase in spinal glial reactivity has been reported to correlate with heightened neuropathic pain sensations, and peripheral nerve lesions can vary in size of the damaged area, we hypothesise:

- Microglial expression will be increased in the lumbar spinal cord of mice with sciatic nerve lesions; and
- The alterations in microglial reactivity will be relative to the extent of the lesion developed with increasing injury.

As increased blood flow and oxygenation has been previously reported to correlate with pain sensations in humans, we hypothesise:

- Haemodynamic blood flow and oxygenation of blood will be increased in the primary somatosensory cortex of mice with established allodynia.

Statement of Authorship

Title of Paper	Multi-coloured fluorescent sensing toolbox for selective detection of Nitroxyl in vitro
Publication Status	<input type="checkbox"/> Published <input type="checkbox"/> Accepted for Publication <input type="checkbox"/> Submitted for Publication <input checked="" type="checkbox"/> Unpublished and Unsubmitted work written in manuscript style
Publication Details	Prepared for submission to Nature Chemistry

Principal Author

Name of Principal Author (Candidate)	Vasiliki Staikopoulos			
Contribution to the Paper	Manuscript conception, experimental design and data generation of biological component, co-wrote manuscript, statistical analysis and figure generation.			
Overall percentage (%)	60%			
Certification:	This paper reports on original research I conducted during the period of my Higher Degree by Research candidature and is not subject to any obligations or contractual agreements with a third party that would constrain its inclusion in this thesis. I am the primary author of this paper.			
Signature	<table border="1"> <tr> <td>_____</td> <td>Date</td> <td>2/9/2019</td> </tr> </table>	_____	Date	2/9/2019
_____	Date	2/9/2019		

Co-Author Contributions

By signing the Statement of Authorship, each author certifies that:

- i. the candidate's stated contribution to the publication is accurate (as detailed above);
- ii. permission is granted for the candidate to include the publication in the thesis; and
- iii. the sum of all co-author contributions is equal to 100% less the candidate's stated contribution.

Name of Co-Author	Xiaozhou Zhang			
Contribution to the Paper	Manuscript conception, experimental design and data generation of chemistry component, co-wrote manuscript and figure generation.			
Signature	<table border="1"> <tr> <td>_____</td> <td>Date</td> <td>4/9/19</td> </tr> </table>	_____	Date	4/9/19
_____	Date	4/9/19		

Name of Co-Author	Philipp Reineck			
Contribution to the Paper	Generated data and figures on quantum yield.			
Signature	<table border="1"> <tr> <td>_____</td> <td>Date</td> <td>05/08/2019</td> </tr> </table>	_____	Date	05/08/2019
_____	Date	05/08/2019		

Please cut and paste additional co-author panels here as required.

Name of Co-Author	Sam Man Lee		
Contribution to the Paper	Generated data and figures on cardiomyocyte experiments.		
Signature		Date	05/09/2019

Name of Co-Author	Elizabeth Beckett		
Contribution to the Paper	Assisted in manuscript conception and revised manuscript.		
Signature		Date	3/9/2019

Name of Co-Author	Andrew Abell		
Contribution to the Paper	Assisted in manuscript conception and revised manuscript.		
Signature		Date	12/9/2019

Name of Co-Author	Mark R Hutchinson		
Contribution to the Paper	Assisted in manuscript conception and revised manuscript.		
Signature		Date	3/9/2019

Name of Co-Author			
Contribution to the Paper			
Signature		Date	

Chapter 3. Multi-coloured fluorescent sensing toolbox for selective detection of Nitroxyl in vitro and ex vivo.

This chapter has been prepared as a manuscript for submission as a primary research paper in Nature Chemistry and is set out in the following heading order: Abstract, Results, Discussion, Conclusion, Methods, References. [Staikopoulos V, Zhang X, Liu, J, Lee SM, Abell A, Hutchinson MR. Multi-coloured fluorescent sensing toolbox for selective detection of Nitroxyl in vitro and ex vivo. Manuscript in preparation]

3.1 Abstract:

The endogenous detection of nitroxyl (HNO), the reduced and protonated derivative of nitric oxide (NO), would greatly contribute to the understanding of the role of this species in biological systems. In this study we show the design and synthesis of 3 super-bright, highly sensitive, specific and non-cytotoxic arylphosphine based fluorescent nitroxyl sensors and their ability to detect endogenous nitroxyl *in vivo*. We show the presence of endogenously produced nitroxyl in murine microglial cell line, BV2 and H9C2 cells following stimulation, using both spectroscopy and confocal microscopy. We propose that of these sensors, Sensor 3 (rhodol 4 on a 2-(diphenylphosphanyl)benzoate backbone) shows the most sensitivity in detecting endogenous nitroxyl following stimulation, in the presence of biological media such as HBSS and DMEM. Herein, we provide a validated tool for measuring nitroxyl in biological systems.

3.2 Introduction

Nitroxyl is the protonated product of the one-electron reduced nitric oxide and has its own unique chemical properties resulting in specific biological functions. Nitroxyl can lead to potent vasodilation (Andrews *et al.*, 2015), increased cardiac output (Sabbah *et al.*, 2013), alter post-ischemic myocardial injury (Ma *et al.*, 1999; Pagliaro *et al.*, 2003; Takahira *et al.*, 2001), be used to treat alcoholism (DeMaster *et al.*, 1998), and acts as an anti-nociceptive modulator of neuropathic and inflammatory pain (Longhi-Balbinot *et al.*, 2016; Zarpelon *et al.*, 2013). The chemical properties and reactivity of HNO is distinct from NO, and although they have similar biological targets (thiols, thiol protein and metalloproteins), the mechanisms of interaction and resulting products are distinctly different (Fukuto *et al.*, 2005, 2009, 2012, 2013, 2019). The role for nitroxyl in biological systems has been established through the use of donor species such as Angeli's salt and Piloty's acid (Shoman *et al.*, 2016). Furthermore, proposed

endogenous production has been speculated based on chemical reactions and the use of scavengers (Miranda et al., 2005). Despite the growing body of evidence supporting the biochemistry of nitroxyl, it remains unclear if nitroxyl is generated *in vivo* and the mechanism involved. A reliable method for detecting nitroxyl *in vivo* is required to help answer these questions. The use of fluorescent probes for detecting reactive nitrogen species *in vitro* and *in vivo* is growing due to their high sensitivity, simple use, non-invasive nature, spatiotemporal resolution and wide range of wavelengths. This makes them ideal candidates for detecting HNO in complex biological environments. Several classes of HNO-sensitive fluorescent probes have been previously generated with various mechanisms of detection and limitations (Smulik-Izydorczyk et al., 2018). These classes of probes are based on the reaction of nitroxyl with chemicals such as; copper (II), nitroxide, 2-Mercapto-2-methylpropionic acid and arylphosphine. With probes based on the reduction of Cu(II) (Rosenthal & Lippard, 2010; Royzen et al., 2013; Zhou et al., 2011) other biological reductants such as ascorbate or glutathione can cause interference, limiting their applications in biological studies.

Arylphosphine based probes rely on the reaction between HNO and triaryl-phosphine to yield the aza-ylide intermediate and lead to subsequent ester aminolysis (Reisz et al., 2009; Kawai et al., 2013) to the original fluorophores. These chemosensors are highly selective for HNO over other cellular reductants and have resulted in several probes being designed (Mao et al., 2014; Liu et al., 2014; Zheng et al., 2015; Kawai et al., 2013; Jing et al., 2014; Miao et al., 2015; Zhang et al., 2015).

Here we report a new, highly sensitive and biostable tri-arylphosphine-based fluorescent chemosensor **3** (Scheme 3.1), for selective detection of HNO in cells and blood samples and demonstrate the use of this sensor to image exogenous and endogenous HNO in cellular and animal models of neuropathic pain and myocardial ischemic reperfusion. This sensor, together with two other highly selective sensors (**1** and **2**, Scheme 3.1), form a multicoloured sensing toolkit for HNO that encompass a wide range of common wavelengths (480 nm – 560 nm) used in sensing studies. All chemo-sensors in this toolkit demonstrated good ability to detect HNO in various aqueous buffers and cellular media without the use of organic solvent, and low cytotoxicity to common cell lines, such as BV2 (mouse microglia) and H9C2 (rat cardiomyocytes). The excellent biocompatibility of this toolkit makes it suitable for a wide range of biological studies. These probes were applied for imaging exogenous and endogenous HNO

following LPS (inflammatory mediator) or LPA (de-myelinating agent) challenge of BV2 cells and in pilot studies using animal models of neuropathic pain and myocardial ischemia-reperfusion injury (supplementary data).

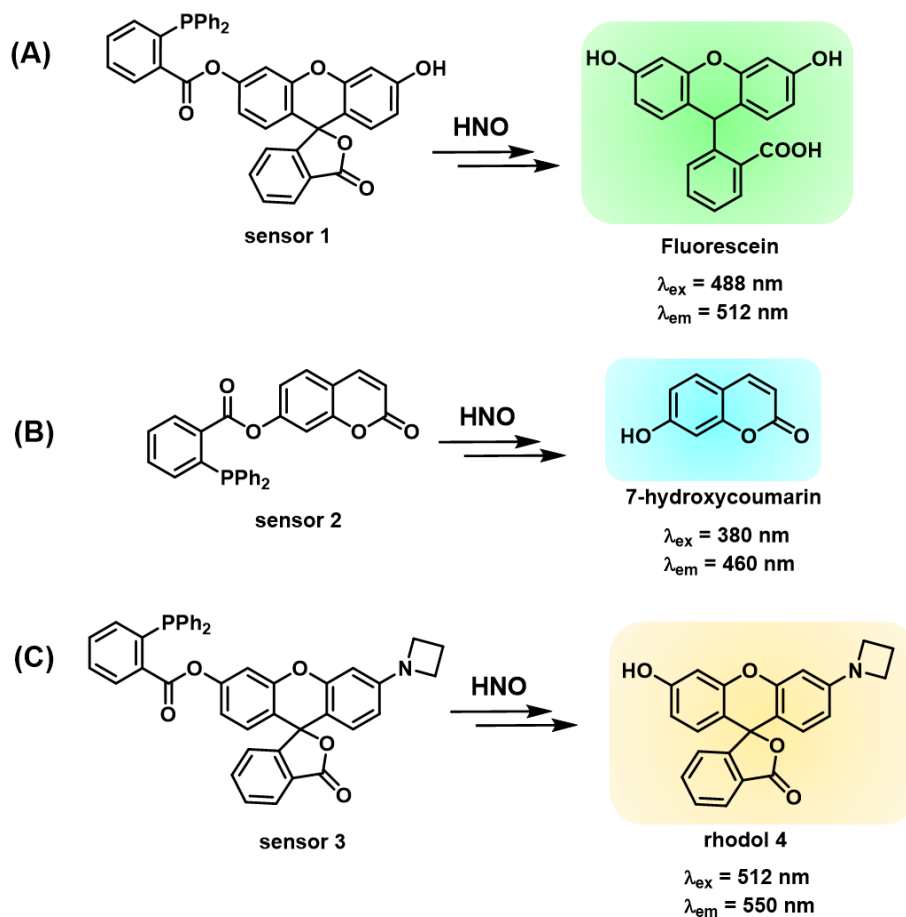
3.3 RESULTS – Chemistry

3.3.1 Design and synthesis of sensors 1-3.

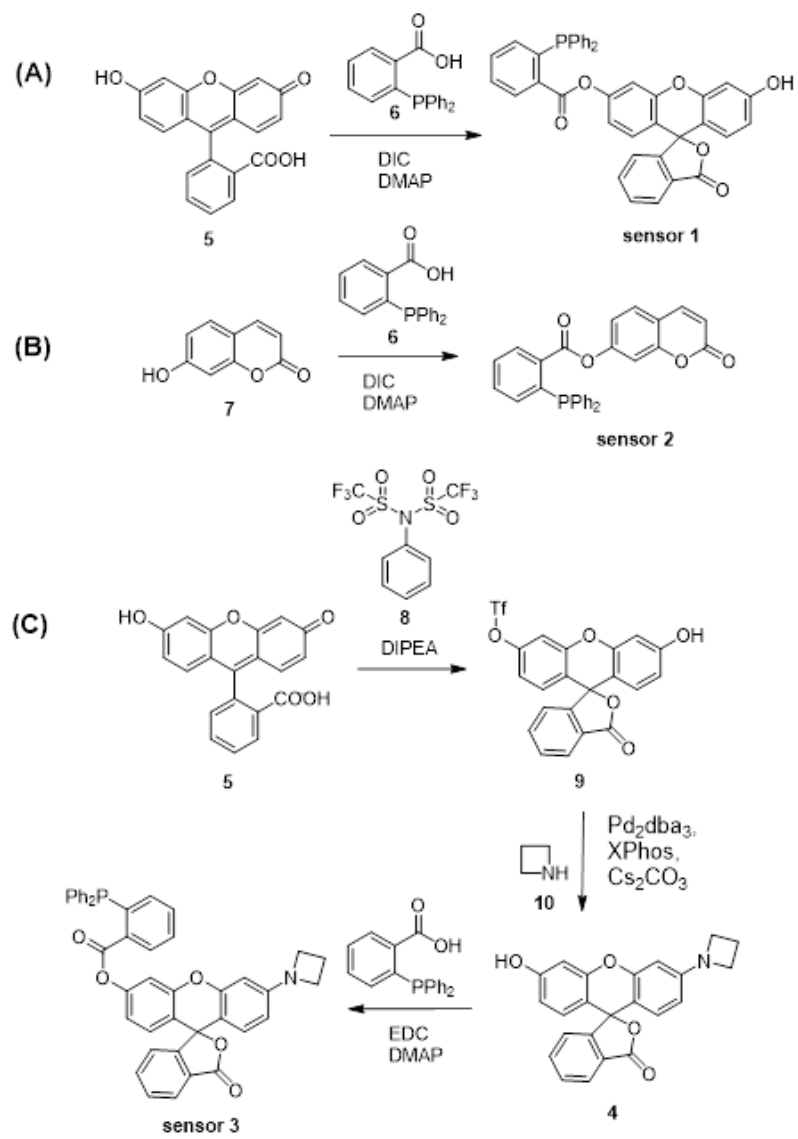
Sensors 1 - 3 consist of a triarylphosphine group conjugated with three distinctive fluorophores, fluorescein, coumarin and a mono-substituted rhodol 4, to selectively detect intracellular HNO (Scheme 3.1 A-C). The attachment of this moiety is reported to quench the fluorescence of the fluorophore, (Reisz *et al.*, 2009) and upon the reaction with HNO, releases the free fluorophore to give a measurable increase in fluorescence. This in turn leads to detection by fluorescence spectroscopy and confocal microscopy. This reaction is bio-orthogonal as phosphines are abiotic and essentially unreactive toward other biomolecules inside or near cells. The fluorophores were selected to represent a wide range of common wavelengths used in sensing studies. Importantly, the three sensors encompass wavelength ranges commonly used in chemical sensing, with sensor 2 emitting in the blue range ($\lambda_{em} = 460$ nm), sensor 1 in the green range ($\lambda_{em} = 512$ nm) and sensor 3 in the yellow range ($\lambda_{em} = 550$ nm). In particular, sensor 3 reacts with HNO to form the fluorescent rhodol 10, with superb brightness and high biostability to allow detection of subtle changes in concentrations of HNO in cells and tissues. In addition, this fluorophore emits in a wavelength region ($\lambda_{em} = 550$ nm) where biological samples typically have weaker autofluorescence. This ensures that sensing of HNO can be achieved with minimal background fluorescence and hence further enhances sensitivity. Together these sensors form a multi-coloured fluorescent sensing tool kit that can be used in conjunction with a broad range of biosensing techniques including green-fluorescent protein, fluorescent antibodies, nucleus stain and mitochondria stain.

Sensors 1 - 3 were synthesised as shown in Scheme 3.2. Briefly, fluorescein (5) or 7-hydroxycoumarin (7) was subjected to esterification with 2-(diphenylphosphino) benzoic acid (6) to give sensor 1 or 2 in 44% and 28% yield respectively. Sensor 3 was synthesised from fluorescein (5). Fluorescein was monoprotected with triflate to afford compound 9, which was subsequently coupled with azetidine (10) under the catalysis of Pd₂dba₃ and XPhos to give

rhodol 4. Esterification of rhodol 4 with 2-(diphenylphosphino) benzoic acid (6) gave sensor 3 in 8% yield. All sensors were purified by HPLC.



Scheme 3.1 (A) Structure of sensor 1 (fluorescein-based) and its reaction with HNO; (B) structure of sensor 2 (coumarin-based) and its reaction with HNO; (C) structure of sensor 3 (rhodol based) and its reaction with HNO.



Scheme 3.2. Synthesis of (A) sensor 1, (B) sensor 2 and (C) sensor 3

3.3.2 Spectroscopic characterisation of sensors 1 - 3.

The spectroscopic properties of sensors **1 - 3** were assessed in water. First, the fluorescence of sensors **1 - 3** with and without Angeli's salt (AS) was measured in an airtight cuvette to demonstrate their ability to sense HNO in solution. AS is a common donor to generate HNO in aqueous environment. Briefly, a solution of the sensor (2 μM for sensor **1** and **3**, 5 μM for sensor **2**) in 5% DMSO in water was purged with N_2 for 10 min before mixing with AS (0-100 μM) in 10 mM NaOH. Final concentration of NaOH was 0.5 mM. Sensor **3** ($\lambda_{\text{ex}} = 512$ nm and $\lambda_{\text{em max}} = 550$ nm) provides a 120-fold increase in fluorescence upon addition of 100 μM AS, the largest turn-on response amongst all three sensors (Figure 1C). In comparison, sensors **1** and **2** gave a 30-fold and 12-fold increase in a similar experiment (Figure 1A and B). Sensors **1** and **2** were also found to have typical fluorescence emission profiles of fluorescein and coumarin respectively, with $\lambda_{\text{ex}} = 488$ nm and $\lambda_{\text{em max}} = 512$ nm for sensor **1**, and $\lambda_{\text{ex}} = 380$ nm, $\lambda_{\text{em max}} = 460$ nm for sensor **2**. (Figure 3.1A and B). The standard curves of calibration of sensors 1-3 were derived (Figure 3.1 inserts) to provide a first step towards the quantification of HNO concentration. Briefly, the fluorescence of sensors **1 - 3** increased with increasing concentration of AS, with sensors **1** and **3** following a trend of one-phase association and sensor **2** following a linear trend. The quantum yield of each sensor was determined in the presence of 100 μM Angeli's salt. All three sensors demonstrated very high quantum yield ($\Phi_{\text{sensor1}} = 0.9$, $\Phi_{\text{sensor2}} = 0.85$, $\Phi_{\text{sensor3}} = 0.77$) with sensor **1** being the highest (Figure 3.2). This is expected as sensor **1** reacts with HNO to give fluorescein, which has a reported quantum yield of 0.93 in 0.1 M NaOH. The high quantum yield ensures high sensitivity of these chemosensors for HNO detection in biological studies. In addition, the limit of detection of sensor **3** was 100 nM (Figure 3.3), which is the lowest amongst the three sensors reported herein, and to our best knowledge, one of the lowest reported in literature. Overall, sensor **3** provides the optimal sensing profile that combines low detection limit and large fluorescence turn-on response. This warrants good sensitivity towards HNO and fluorescence read-out. Thus, sensor **3** is the optimal tool assessed here for detecting HNO levels in biological environments.

3.3.3 Kinetic, Stability and Selectivity Profiles

The kinetic profiles of the sensors were next investigated to examine their stability in water and rate of reaction with AS. Briefly, a similar solution of sensor was prepared using above mentioned conditions and mixed with AS (200 μM) in 10 mM NaOH. Fluorescence of both samples was

continuously monitored for 60 min (Figure 3.4 a-c). Sensor 1 reacts with AS faster than sensor 2 and 3, taking 10 min to reach the saturation of fluorescence signal, while sensors 2 and 3 taking more than 10 min. The fast rate of reaction of sensor 1 is desirable to capture this particularly unstable analyte as HNO is oxidised rapidly to corresponding RNS in biological environments (reaction rates with; HNO ($k = 8 \times 10^6 \text{ M}^{-1} \text{ s}^{-1}$), NO ($k = 5.8 \times 10^6 \text{ M}^{-1} \text{ s}^{-1}$), oxygen ($k = 3 \times 10^3 \text{ M}^{-1} \text{ s}^{-1}$)) (Miao et al, 2016). At a concentration of 1 μM , sensor 1 showed a 67-fold increase in fluorescence compared to 0 μM , sensor 2 showed a 19-fold increase in fluorescence and sensor 3 showed the highest fluorescence increase with a 368-fold increase (Figure 3.4 d-f). Interestingly, at 100 nM concentration, sensor 1 showed a 5.5-fold increase in fluorescence compared to 0 μM , sensor 2 showed a 3-fold increase in fluorescence and sensor 3 showed a 38-fold increase. The high turn-on fluorescence of sensor 3 makes it more sensitive for measuring potentially low concentrations of endogenous HNO. This data was used to determine the optimal concentration of sensor and incubation time to use in our subsequent *in vitro* work. The stability of the sensors in common biological buffers (PBS and HBSS) and cell media (DMEM, DMEM serum-free (SF), DMEM phenol-red free (PRF) and DMEM serum-free and phenol-red free (SF PRF)) was investigated to examine their applicability in cell-based experiments. The sensor was dissolved in buffer or media containing 1% DMSO followed by the addition of NaOH (final concentration 0.5 mM) or AS (100 μM , in 10 mM NaOH). The sample was incubated for 10 min in the dark and the resulting fluorescence was measured and shown in Figure 3.5. All three sensors were found to retain sensing ability in the tested buffers and media, with sensor 3 providing the most ideal sensing profile. PBS buffer gave a similar sensing profile compared to sensors in water, with sensor 1, 2 and 3 giving a 32-fold, 7-fold and 65-fold increase in fluorescence upon addition of AS respectively. Incubation in HBSS resulted in decreased fluorescence response in sensors 1 and 2 while enhancing the response of sensor 3. Incubation in cell media resulted in a decrease in sensitivity for all three sensors. Sensor 3 is shown to be the most compatible with cell media, with the retained ability to produce a 40-fold fluorescence response in DMEM PRF. In comparison, sensors 1 and 2 gave lower fluorescence response (12-fold and 4-fold) in DMEM-related media. This demonstrates that sensor 3 is optimal for cell-based experiments.

Next, sensors 1-3 were assayed against a range of biologically relevant RNS (NO, NO₂⁻, NO₃⁻, N₃⁻, ONOO⁻), amino acids (Cys, Arg), small molecules (ascorbate, H₂S, GSH, GSNO), and ROS

(H₂O₂, OH) to define the selectivity profile. All three sensors clearly show good selectivity for AS (Figure 3.6), with sensor 3 showing the optimal selectivity and is non-reactive to all species tested. Importantly, the sensors display an excellent selectivity for AS over all other tested RNS, NO in particular. This is critical as RNS always co-exist in biological environments and thus the ability to detect HNO amongst a complex mixture of RNS is highly desirable. Both sensor 1 and sensor 2 showed minimal affinity to arginine. This is important as arginine is the precursor of RNS and thus the ability to distinguish between these species is critical to accurate sensing of intracellular HNO. Sensor 1 is also found to react with H₂S to a limited extent, which is consistent with literature. However, due to the low concentration of H₂S present in cells, the weak affinity to H₂S is not expected to disrupt the applicability of sensor 1 in biosensing. Collectively, sensor 3 demonstrates excellent fluorescence turn-on response to AS, superb brightness, low detection limit, high compatibility with cell media and excellent selectivity. Therefore, this sensor is selected for all subsequent cell-based studies.

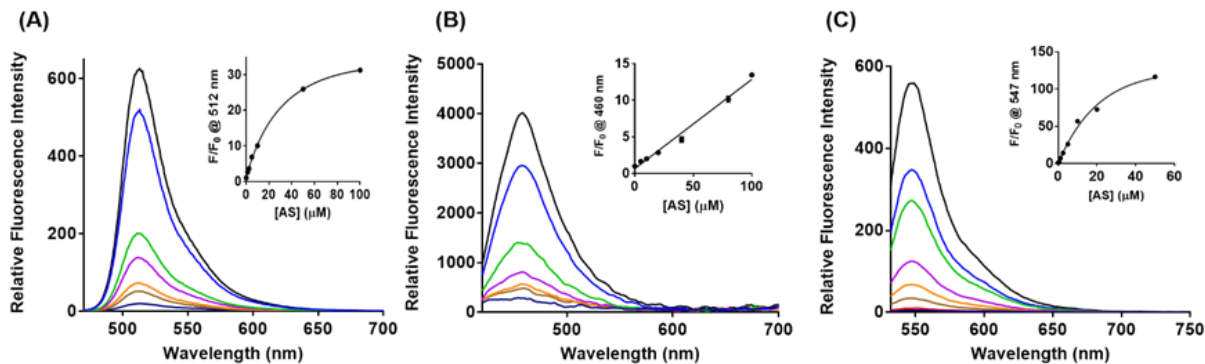


Figure 3.1 Sensor 3 has highest ‘turn-on’ fluorescence response to 100 μM AS.

(A) Fluorescence emission profiles of sensor 1 (2 μM) with and without Angelis salt (AS, 0-100 μM), a donor of HNO, $\lambda_{\text{ex}} = 488 \text{ nm}$. Insert: standard curve of calibration of sensor 1 (2 μM) with AS (0-100 μM) where the concentration of AS (x-axis) is plotted against the fluorescence intensity at 512 nm (y-axis); (B) fluorescence emission of sensor 2 (5 μM) with and without AS (0-100 μM), $\lambda_{\text{ex}} = 380 \text{ nm}$. Insert: standard curve of calibration of sensor 2 (5 μM) with AS (0-100 μM) where the concentration of AS (x-axis) is plotted against the fluorescence intensity at 460 nm (y-axis). (C) fluorescence emission of sensor 3 (2 μM) with and without AS (0-100 μM), $\lambda_{\text{ex}} = 512 \text{ nm}$. Insert: standard curve of calibration of sensor 3 (2 μM) with AS (0-100 μM) where the concentration of AS (x-axis) is plotted against the fluorescence intensity at 547 nm (y-axis).

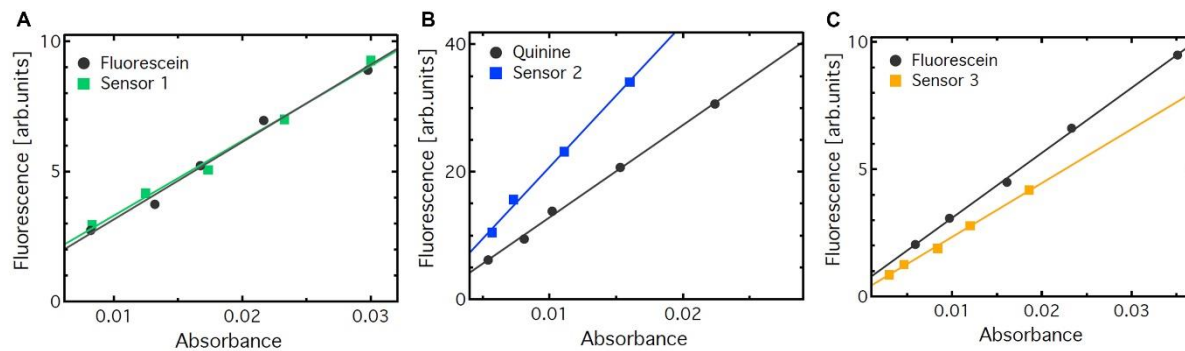


Figure 3.2. Sensor 1 give highest quantum yield of all 3 sensors.

The integrated fluorescence depends linearly on the absorbance for (A) Fluorescein (black circles) and Sensor 1 (green squares) ($\Phi_{\text{Sensor 1}} = 0.9$). (B) Quinine (black circles) and Sensor 2 (blue squares) ($\Phi_{\text{Sensor 2}} = 0.85$) and (C) Fluorescein (black circles) and Sensor 3 (yellow squares) ($\Phi_{\text{Sensor 3}} = 0.77$).

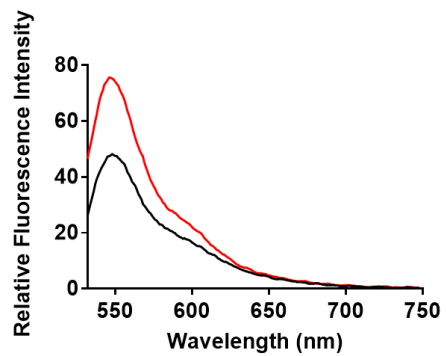


Figure 3.3. Sensor 3 has lowest detection limit of all 3 sensors.
Fluorescence of sensor 3 (1 μ M) with AS (100 nM) (red) and without AS (black).

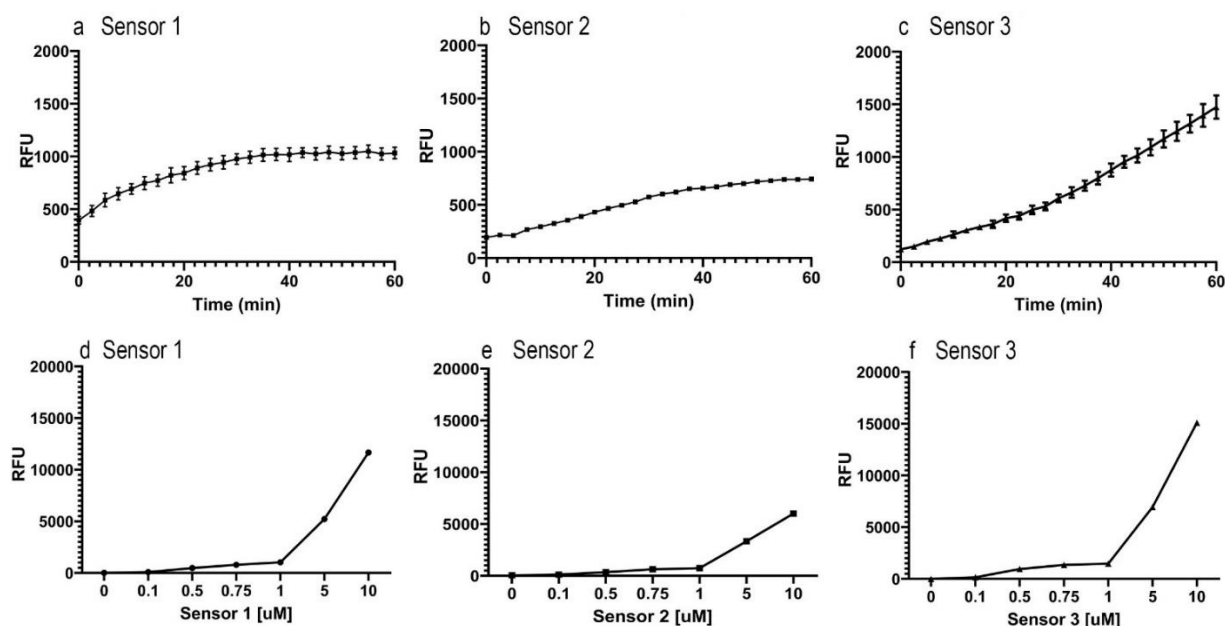


Figure 3.4 Sensor 1 - 3 kinetics in the presence of Angeli's salt in HBSS solution.

Data showing the time it takes for each sensor 1 (a), 2 (b) and 3 (c) to saturate fluorescence over time in the presence of Angeli's salt (200 μM). At a concentration of 1 μM, Sensor 1 reached saturation of fluorescent signal by 10 min, Sensors 2 and 3 took longer than 10 min to reach saturation. The fluorescence at 1 hour following the addition of Angeli's salt (200 μM) for increasing concentrations of Sensor 1 (d), Sensor 2 (e) and Sensor 3 (f). At a concentration of 1 μM, Sensor 1 showed a 67-fold increase in fluorescence compared to 0 μM, Sensor 2 showed a 19-fold increase in fluorescence and Sensor 3 showed the highest fluorescence increase with a 368-fold increase.

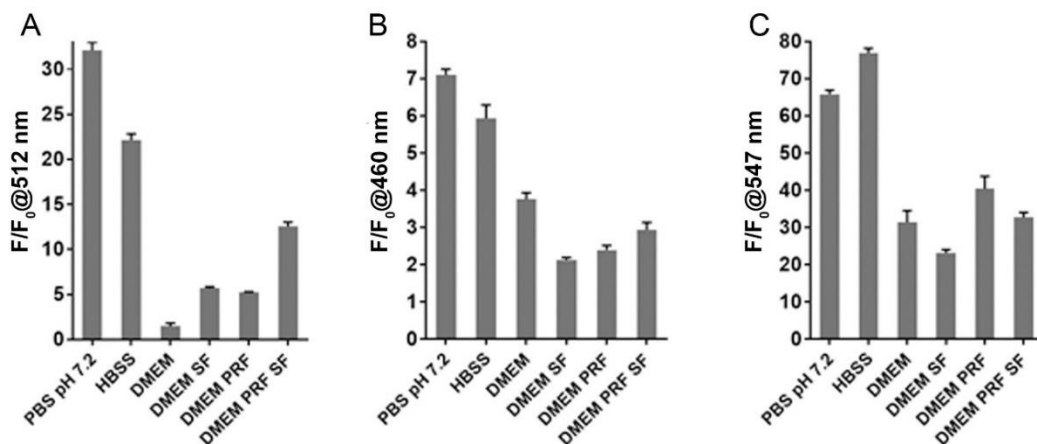


Figure 3.5. Sensor 3 shows highest fluorescent signal in biological buffers and media following AS.

Fluorescence of sensors 1 (A), 2 (B) and 3 (C) in buffers (PBS pH 7.2, HBSS pH 7.2) and cell media (DMEM, DMEM SF, DMEM PRF, DMEM SF PRF) with 100 μ M AS.

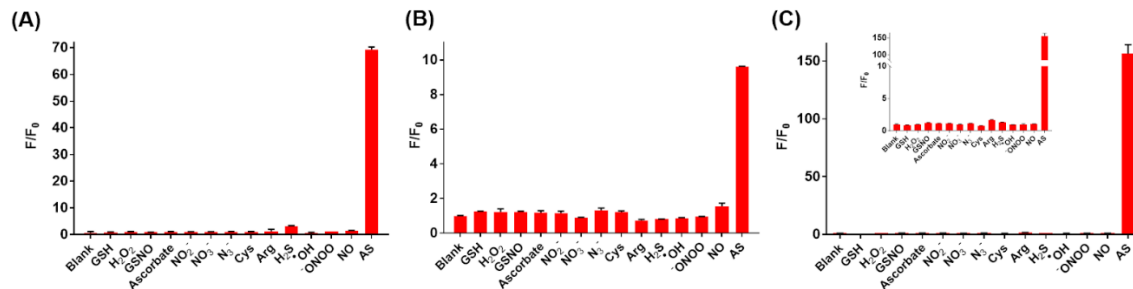


Figure 3.6. Sensor 3 shows optimal selectivity profile against a range of biologically relevant species.

Sensor 1 (2 μM) was separately incubated with each species (as denoted on the x-axis, 100 μM) for 10 min in the dark before measuring the fluorescence at $\lambda_{\text{ex/em}} = 488/512 \text{ nm}$; Sensor 2 (5 μM) was separately incubated with each species (as denoted on the x-axis, 100 μM) for 10 min in the dark before measuring the fluorescence at $\lambda_{\text{ex/em}} = 380/455 \text{ nm}$. All experiments were performed in 0.5-1% DMSO in water. Sensor 3 (2 μM) was separately incubated with each species (as denoted on the x-axis, 100 μM) for 10 min in the dark before measuring the fluorescence at $\lambda_{\text{ex/em}} = 512/550 \text{ nm}$. All experiments were performed in 0.5-1% DMSO in water.

3.4 RESULTS – application in biological systems

3.4.1 Stability and kinetics of Sensors 1 – 3 in biological buffer

The fluorescent stability of all 3 sensors in biological buffer (HBSS) were assessed by spectroscopy. Angeli's salt (AS) was used as a donor of HNO and tested at concentrations ranging from 0 to 200 μM (Figure 3.7). All 3 Sensors were tested at 2.5, 5 and 10 mM and measured for up to an hour. Sensors 1 and 2 display a similar 'turn-on' fluorescent profile across all concentrations of probe and donor, and the starting baseline increased in proportion to the sensor concentration. Sensor 2 appeared to be the least stable in AS concentration ranges between 100 – 200 μM . The time taken for the fluorescence signal to peak before plateauing was 20 minutes for Sensors 1 and 2, and 10 minutes for Sensor 3 making it the fastest responder of all 3 probes. Together with the kinetic data and fluorescent characteristics in biological buffers and media (Section 3.3.3) we were able to determine a concentration range (1 – 3 μM) and incubation time (at least 10 min) to proceed with future biological experiments.

3.4.2 HNO Sensors 1, 2 and 3 are not cytotoxic to microglial cells.

Following the evaluation of Sensors 1-3 in biological media samples, Trypan Blue and MTT experiments were conducted to evaluate the cell viability and cytotoxicity of Sensors 1-3 (Figure 3.8). BV2 cells were incubated with 1-10 μM of Sensors 1, 2 or 3, for either 1.5 hours for cell viability assay using Trypan blue (Figure 3.8 a-c) or up to 48 hours for MTT (Figure 3.8 d-f). The results indicate the all three sensors are of low toxicity towards living cells at concentrations below 10 μM , within 24 hours of exposure. Therefore, further qualifying our concentration range of 1 - 3 μM for Sensor 3 was for subsequent spectroscopy and confocal imaging studies.

3.4.3 Sensor 3 can detect exogenous and endogenous HNO in microglial cell lines

As sensor 3 was shown to be the brightest and most stable in biological media of all 3 probes, this sensor was selected to carry-out the following experiments. The presence of both exogenous and endogenous HNO in BV2 microglia cells was examined by spectroscopy and confocal microscopy. Exogenous donor AS was used to observe the activation of Sensor 3 and used as a positive sensor control in the following experiments. BV2 cells were treated with inflammatory agent lipopolysaccharide (LPS, 0 – 1000 ng/ml) for 24 hours to stimulate the endogenous production of reactive nitrogen species (RNS), such as HNO. The supernatant

was removed and added to 3 μM of Sensors 3 and incubated for 15 min before being measured by spectroscopy detect fluorescence signal pertaining to endogenous HNO (Figure 3.9). Sensor 3 was able to detect HNO levels above baseline following LPS treatment. Next, we wanted to determine if we could measure signal coming from within the cells using spectroscopy. BV2 cells or culture media alone, were co-incubated with 2 μM of Sensor 3 and either LPS (100, 500 or 1000 ng/ml) or control treatment (AS; 200 μM , AS; 200 μM + L-cysteine 1 mM or L-cysteine 1 mM only) and measured every 5 minutes for 24 hours at 37°C (Figure 3.10). After 10 hours, it was observed that the fluorescence signal started to decline, as these are 'turn-on' probes, we suspected that there may be degradation of signal occurring and therefore disregarded any readings beyond this time point. We subtracted the signal produced by the media alone from the signal produced by the cells in media and reported the difference. We observed an increase in Sensor 3 RFU in the presence of increasing concentration of LPS (Figure 3.10, a) between 4 – 10 hours of treatment. A simple linear regression was calculated to determine the effect of LPS concentration on endogenous nitroxyl production over time. For each concentration of LPS, there was a significant change in slope compared to control (LPS 100 ng/ml; $F(1,13) = 26.86$, $p < 0.001$, $r^2 = 0.67$; LPS 500 ng/ml, $F(1,13) = 217$, $p < 0.0001$, $r^2 = 0.943$; LPS 1000 ng/ml, $F(1,13) = 5.512$, $p < 0.035$, $r^2 = 0.29$). Interestingly, it appears that there was an inverse relationship between the concentration of LPS and the Sensor 3 fluorescent signal with the lowest concentration of LPS (100 ng/ml) producing the highest signal as determined by the slope (control: -0.81 ± 35.98 ; LPS 100 ng/ml: 211.6 ± 40.83 ; LPS 500 ng/ml: 160.9 ± 10.93 ; LPS 1000 ng/ml: 70.44 ± 30). The control treatments (Figure 3.10, b) indicated that most of the fluorescent signal produced by AS is derived in the media and may be absorbed by the cells. HNO scavenger, L-cysteine (1 mM) was able to diminish approximately 91% of the signal produced by AS, indicating that Sensor 3 signal was specific to HNO as observed by a change in slope being shifted closer to baseline (AS: 341.3 ± 47.22 ; AS + L-cysteine: 29.63 ± 1.07). Confocal microscopy imaging was carried out to assess the ability for each sensor to be taken up by BV2 cells. BV2 cells were incubated with 1 μM of Sensor 3 for 30 min prior to confocal imaging (Figure 3.11). Eleven minutes of video capture at 40x magnification was taken at the appropriate wavelength. Following 1 min of recording baseline values either LPS (500 ng/ml), AS (200 μM) or vehicle control (0.01M NaOH) was added to the well, followed by a further 10 minutes of recording. To

determine if the increase in fluorescent signal was due to HNO, control wells were pre-treated for 30 minutes with L-cysteine (1 mM) prior to the addition of AS. To determine the change in fluorescence signal, 20 randomly selected BV2 cells were outlined using ImageJ (v1.52p, National Institute of Health, USA) from the DIC image, then the mask applied to the 515 nm channel and the mean pixel intensity was measured for those cells at each frame. The baseline values (1 min pre-treatment time) of were subtracted from the brightest frame in the captured series at approximately the 10-minute time point and the data expressed as the percentage change in fluorescence (reported as 'random fluorescence units': RFU) from the baseline frame. The data shows that acute LPS treatment ($p < 0.0001$) and HNO donor AS ($p < 0.0001$) both increased fluorescence signal compared to control (Sensor 3 only) (control: 13.59 ± 0.86 RFU; LPS: 25.58 ± 0.96 RFU; AS: 49.26 ± 1.2). Pre-treatment with L-cysteine (1 mM) was able to prevent the AS derived signal (LC: -9.718 ± 0.8 RFU), indicating that the Sensor 3 probe is specific to HNO. Together this data suggest that Sensor 3 is sensitive enough to detect endogenous HNO signal from BV2 cells using both spectroscopy and confocal microscopy.

3.4.4 Endogenous HNO may be produced by iNOS enzyme following LPS and LPA challenge.

To determine the mechanism deriving the endogenous signal within BV2 cells, a series of spectroscopy and confocal microscopy experiments were carried out using 24-hour treatment of stimuli LPS, Lysophosphatidic Acid (LPA) and controlled using iNOS enzyme inhibitor, 1400W (Figure 3.12). LPA is a bioactive lipid species which is thought to be involved in signalling during neuropathic pain development and can act at receptors found on microglial cells causing them to become activated (Yung et al., 2015). Twenty-four-hour treatment with LPS (500 ng/ml) (4196 ± 489 RFU) significantly increased Sensor 3 fluorescence when compared to 'Sensor only' controls (2721 ± 142 RFU, $p < 0.05$). Furthermore, pre-incubation with 1400W (1861 ± 64 RFU) significantly prevented the HNO signal compared to both LPS ($p < 0.001$) (Figure 3.12, A) and the 'Sensor only' control ($p < 0.01$) which suggests that the homeostatic baseline fluorescent levels observed in sensory only control, may also be derived from iNOS production. However, 24 hour-LPA (1 μ M) treatment (2750 ± 298 RFU) did not produce a higher fluorescence signal compared to 'Sensor only' (2721 ± 142 RFU) and pre-incubation with 1400W did not reduce the LPA signal (1953 ± 77.7 RFU) (Figure 3.12, A) when

measured by spectroscopy. Control data (Figure 3.12, B) indicates that Sensor 3 is specific to HNO as (200 μ M) significantly increased Sensor 3 RFU signal ($28,589 \pm 4636$ RFU) ($p < 0.001$), which was almost totally abolished by L-cysteine pre-treatment (8912 ± 175 RFU). Confocal microscopy determined that both LPS (500 ng/ml) (47.72 ± 2.5 RFU, $p < 0.0001$) and LPA treatment (1 μ M) (58.05 ± 2.2 RFU, $p < 0.0001$) were able to increase the RFU of Sensor 3 within BV2 cells (Figure 3.13; A & B) when compared to 'Sensor only' control (32.07 ± 0.56 RFU) (Figure 3.13; D) which was reduced when cells were pre-incubated with 1400W (iNOS inhibitor) (LPS: 5.69 ± 0.18 RFU, LPA: 23.36 ± 0.5 RFU, $p < 0.0001$) (Figure 3.13; A' & B'). AS also increased signal within cells (109 ± 3.2 RFU, $p < 0.0001$) (Figure 3.13; C) which was prevented by pre-incubation of L-cysteine (16.65 ± 0.4 , $p < 0.0001$) (Figure 3.13; C'). This data suggests that endogenous HNO signal in LPS and LPA treated BV2 cells is derived from iNOS enzyme.

3.4.5 Sensor 3 is taken up into BV2 cell mitochondria

Sub-cellular localisation of Sensor 3 within AS treated BV2 cells was determined by confocal microscopy using a mitochondria specific stain (Figure 3.14). Confocal imaging determined that AS activated Sensor 3 appears more punctate around the nucleus of cells (Figure 3.14; A, A') in a similar location to Mitotracker Deep Red (Figure 3.14; B, B'). Overlay of the 2 channels shows the co-localisation of signal (in yellow) (Figure 3.14; D, D') suggesting that Sensor 3 is taken up predominately by mitochondria within BV2 cells.

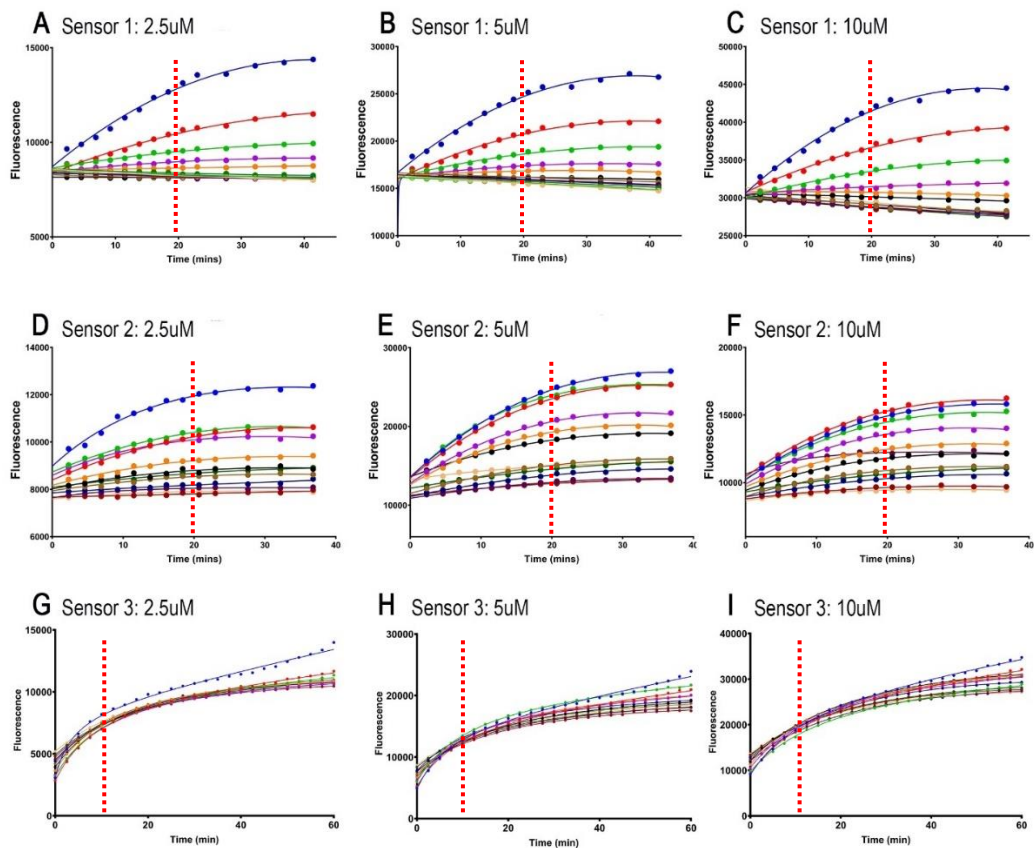


Figure. 3.7 Fluorescence relationship between HNO Sensor concentration (1 – 3) and HNO donor, Angeli's salt in buffer.

A-C) Fluorescence intensity of Sensor 1 (concentrations; 2.5, 5 and 10 μM) over 1 hour with increasing amounts of AS (0 – 200 μM). D-F) Sensor 2 with increasing amounts of AS (0 – 200 μM). G-I) Sensor 3 with increasing amounts of AS (0 μM ; blue line – 200 μM ; light pink line), all in Hank's balanced salt solution (HBSS). Peak signal time shown by red dotted line.

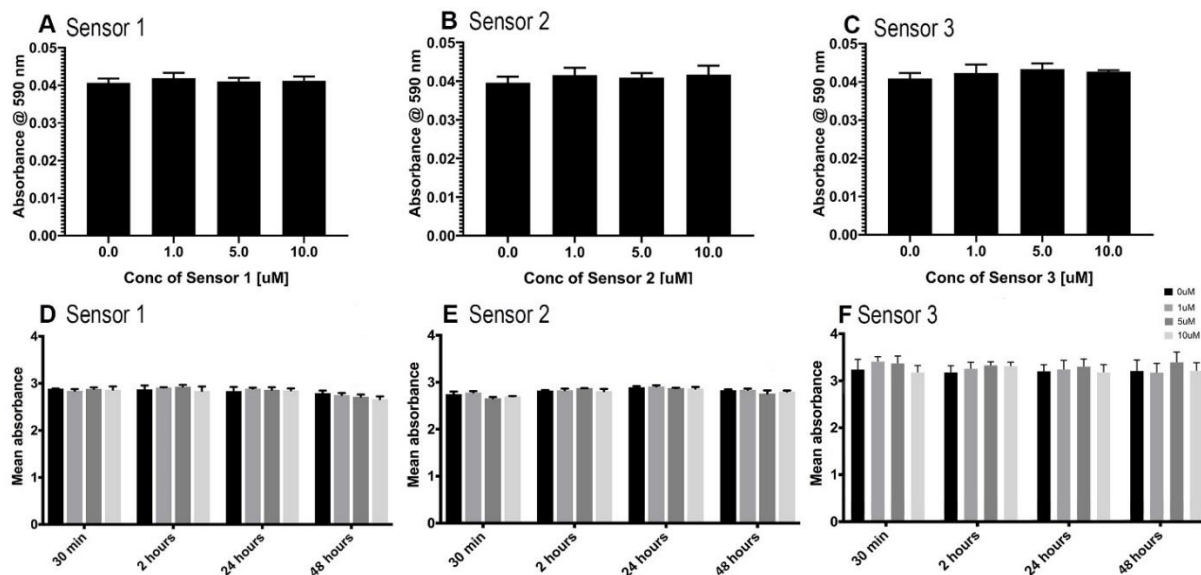


Figure 3.8 The effect of Sensors 1, 2 & 3 on cell toxicity and viability

Data showing the toxicity of sensor 1 (a), 2 (b) and 3 (c) with increasing concentrations following a 1.5-hour incubation in BV2 cells. There was no toxic effect observed of the sensors at any of the concentrations following the incubation. There also was no effect on cell viability (change in cell metabolism) in the presence of increasing concentrations of either sensor 1 (d), 2 (e) or 3 (f) for up to 48 hours. This data was used to determine which concentration of sensor and incubation time to use in our *in vitro* work.

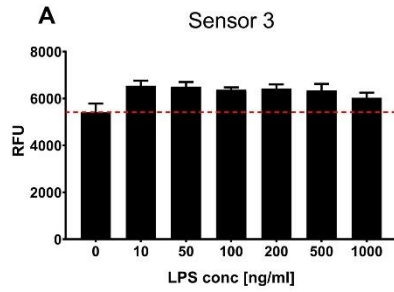


Figure 3.9 Sensor 3 detects endogenous HNO released into the supernatant by BV2 cells following 24-hour LPS treatment.

Data showing the fluorescent levels detected by spectrophotometer for sensors 3 (A) following 24 hours incubation of increasing concentrations of LPS, in BV2 cells. Sensor 3 appeared sensitive enough to detect endogenous HNO levels above control (0 ng/ml LPS; indicated by red dotted line) at all concentrations of LPS. Data reported at 'random fluorescence units' (RFU), $n = 3$.

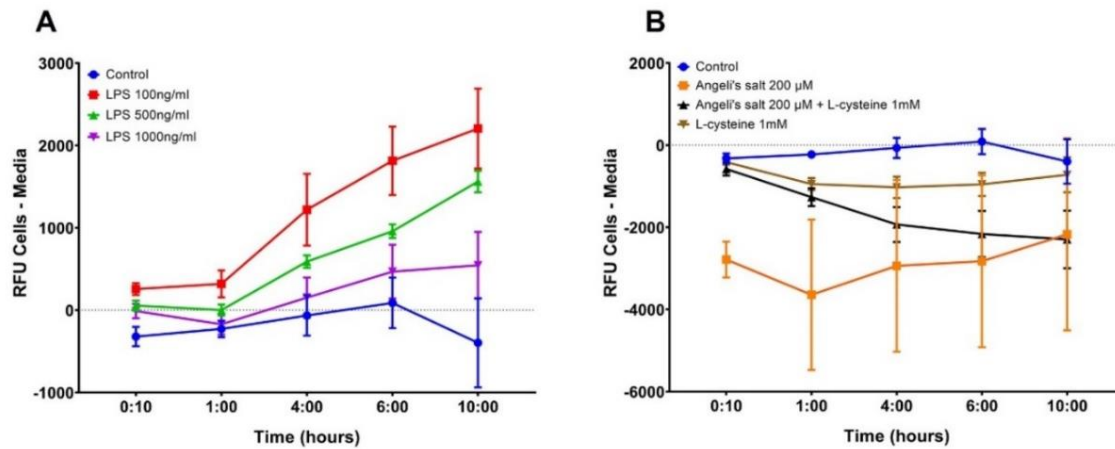


Figure 3.10 Sensor 3 detects increasing endogenous HNO in BV2 cells stimulated with LPS.

Data showing the relative fluorescent units (RFU) of Sensor 3 detected over time by spectrophotometer. The RFU values from the Media only samples, were subtracted from the Cell samples to differentiate the signal coming from the cells only. Line graph A shows the increasing level of endogenous HNO in the presence of LPS (100 ng/ml: red line, 500 ng/ml: green line and 1000 ng/ml: purple line) when compared to control (0 ng/ml: blue line). The LPS signal peaked at 10 hours post-incubation for all concentrations. (LPS 100 ng/ml; $F(1,13) = 26.86$, $p < 0.001$, $r^2 = 0.67$; LPS 500 ng/ml, $F(1,13) = 217$, $p < 0.0001$, $r^2 = 0.943$; LPS 1000 ng/ml, $F(1,13) = 5.512$, $p < 0.035$, $r^2 = 0.29$) Line graph B shows that the control conditions (0 ng/ml LPS: blue line, HNO exogenous donor Angeli's salt: orange line, HNO scavenger L-cysteine pre-incubation: black line and L-cysteine: brown line) generated a signal that was predominantly derived from the media. $n = 3$.

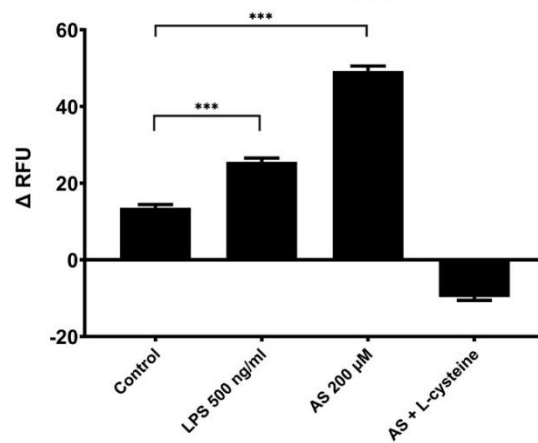
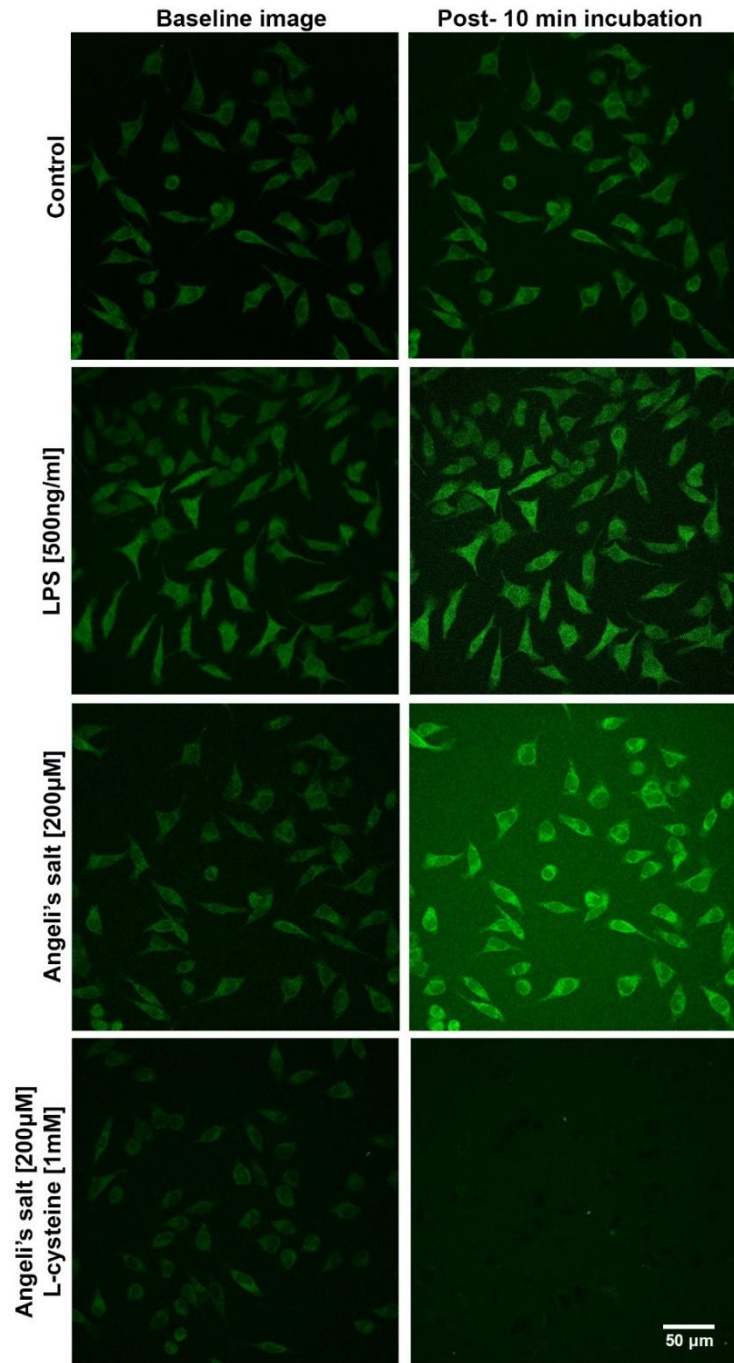


Figure 3.11 Sensor 3 can detect endogenous HNO produced in BV2 cells generated by acute LPS challenge.

Representative confocal images (40x) showing the fluorescence intensity of Sensor 3 (1 μ M) captured immediately following a 15 min incubation in BV2 cells and then again 10 min following the addition of the treatments; vehicle (0.01 M NaOH), Angeli's salt 200 μ M (HNO donor), Angeli's salt 200 μ M plus L-cysteine 1 mM (HNO scavenger) and LPS 500 ng/ml. The change in fluorescence signal from baseline (1-minute pre-treatment) to the brightest frame (~10 min post-treatment) were determined and show that both acute Angeli's salt and LPS challenge can increase the fluorescence signal and hence HNO output from BV2 cells, compared to control. Pre-incubation with HNO scavenger, L-cysteine, attenuated the Angeli's salt derived fluorescence signal of Sensor 3, which suggests the fluorescence signal is specific to HNO. Scale bar = 50 μ m. (***) $p < 0.0001$.

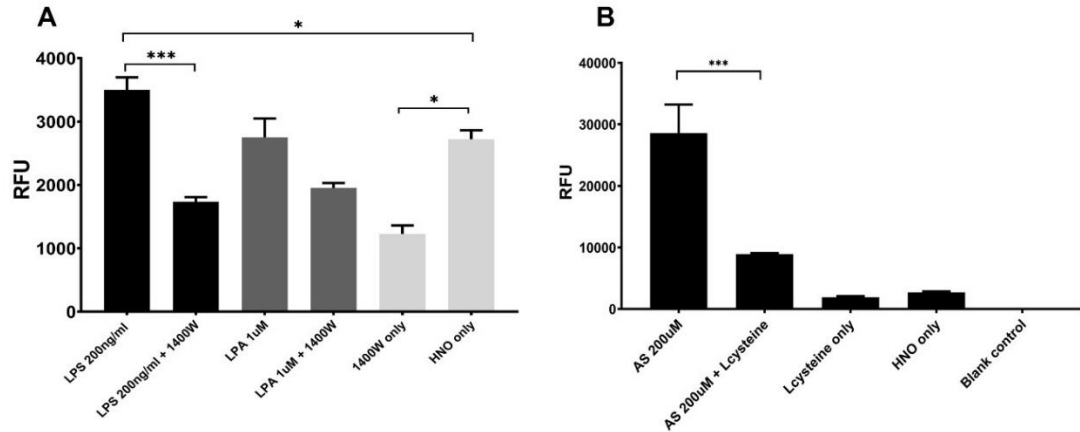


Figure 3.12 LPS may cause an increase of endogenous HNO production via iNOS enzyme.

Bar graphs showing the RFU from spectrophotometer readings of Sensor 3 in BV2 cells ($n = 3$) following 24-hour incubation of LPS (black bars) and LPA (dark grey bars) (A). LPS treatment (500 ng/ml) significantly increased Sensor 3 RFU compared to control (HNO only) ($*p < 0.05$). However, pre-treatment with iNOS inhibitor 1400W, showed reduced RFU compared with LPS alone ($***p < 0.001$). LPA (1 μ M) treatment did not increase the Sensor 3 signal when compared to HNO only control. Pre-incubation with 1400W significantly attenuated Sensor 3 fluorescent signal when compared to control conditions (light grey bars) ($*p < 0.01$), but not LPA treatment ($n = 3$). Graph B shows that the signal derived from Sensor 3 is HNO specific due to the signal increase following application of Angeli's salt (HNO donor: 200 μ M) ($***p < 0.001$) which could be scavenged by L-cysteine (HNO scavenger: 1 mM).

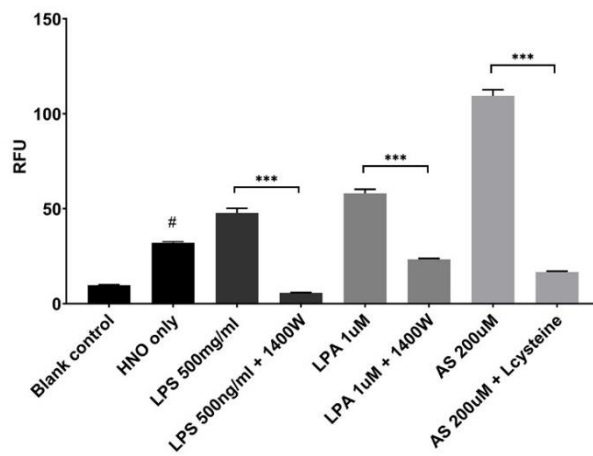
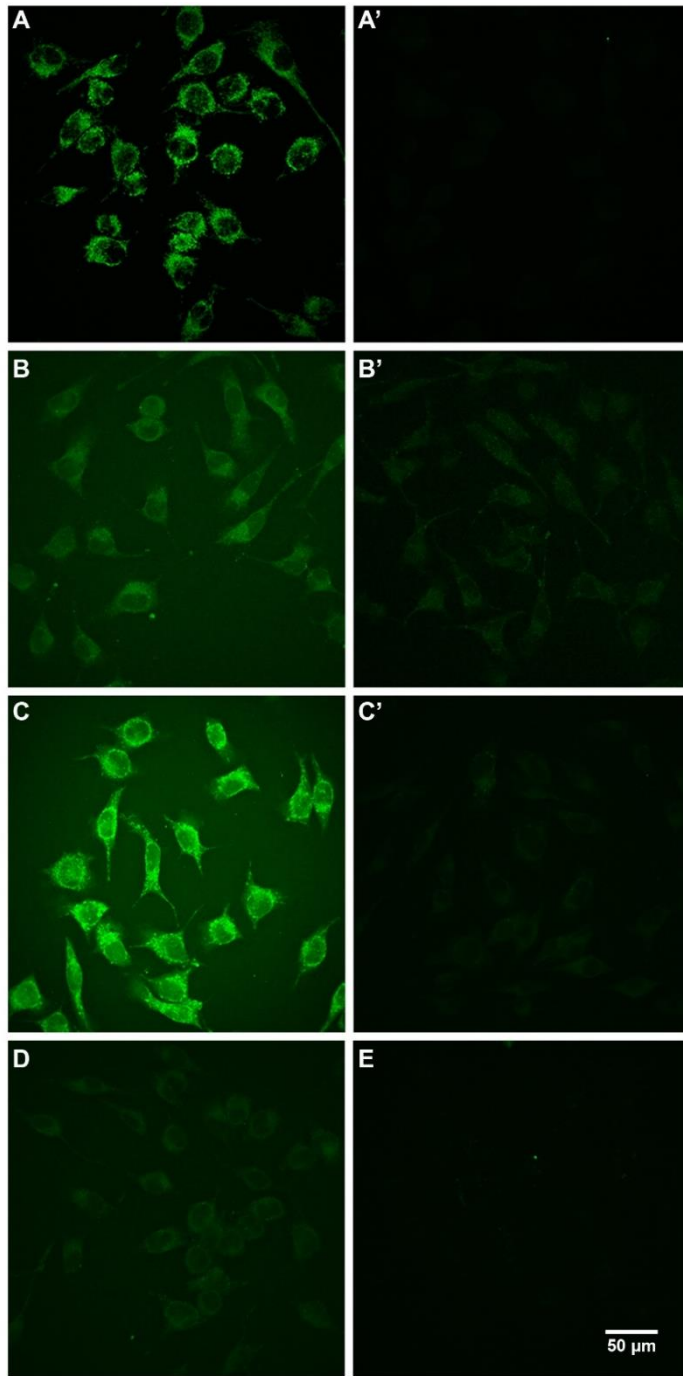


Figure 3.13 Confocal data indicates LPS and LPA may cause an increase of endogenous HNO production via iNOS enzyme.

Representative confocal images (40x) showing the fluorescence intensity of Sensor 3 (1 μ M) captured immediately following a 15 min incubation in BV2 cells. Cells were treated for 24 hours with inflammatory mediator LPS (A; 500 ng/ml) or de-myelination agent, LPA (B; 1 μ M) for 24 hours, with or without iNOS inhibitor 1400W (A' and B' respectively). Control conditions included incubating naïve cells with Sensor 3 alone (D; HNO only), adding HNO donor (C; Angeli's salt, 200 μ M) with or without HNO scavenger (D'; L-cysteine, 1 mM) and imaging naïve cells without any Sensor 3 (E; blank controls). The bar graph below shows the mean RFU measured from 20 cells within each image. LPS and LPA treated cells had significantly higher RFU compared to HNO only control (#p < 0.0001), and pre-treatment with 1400W attenuated this signal in both LPS (**p < 0.0001) and LPA (**p < 0.0001) treatment groups. The increased signal following application of Angeli's salt (HNO donor: 200 μ M, p < 0.0001) which could be scavenged by L-cysteine (HNO scavenger: 1 mM, **p < 0.0001) indicated that Sensor 3 signal is specific to HNO in these conditions. Scale bar = 50 μ m, n = 3.

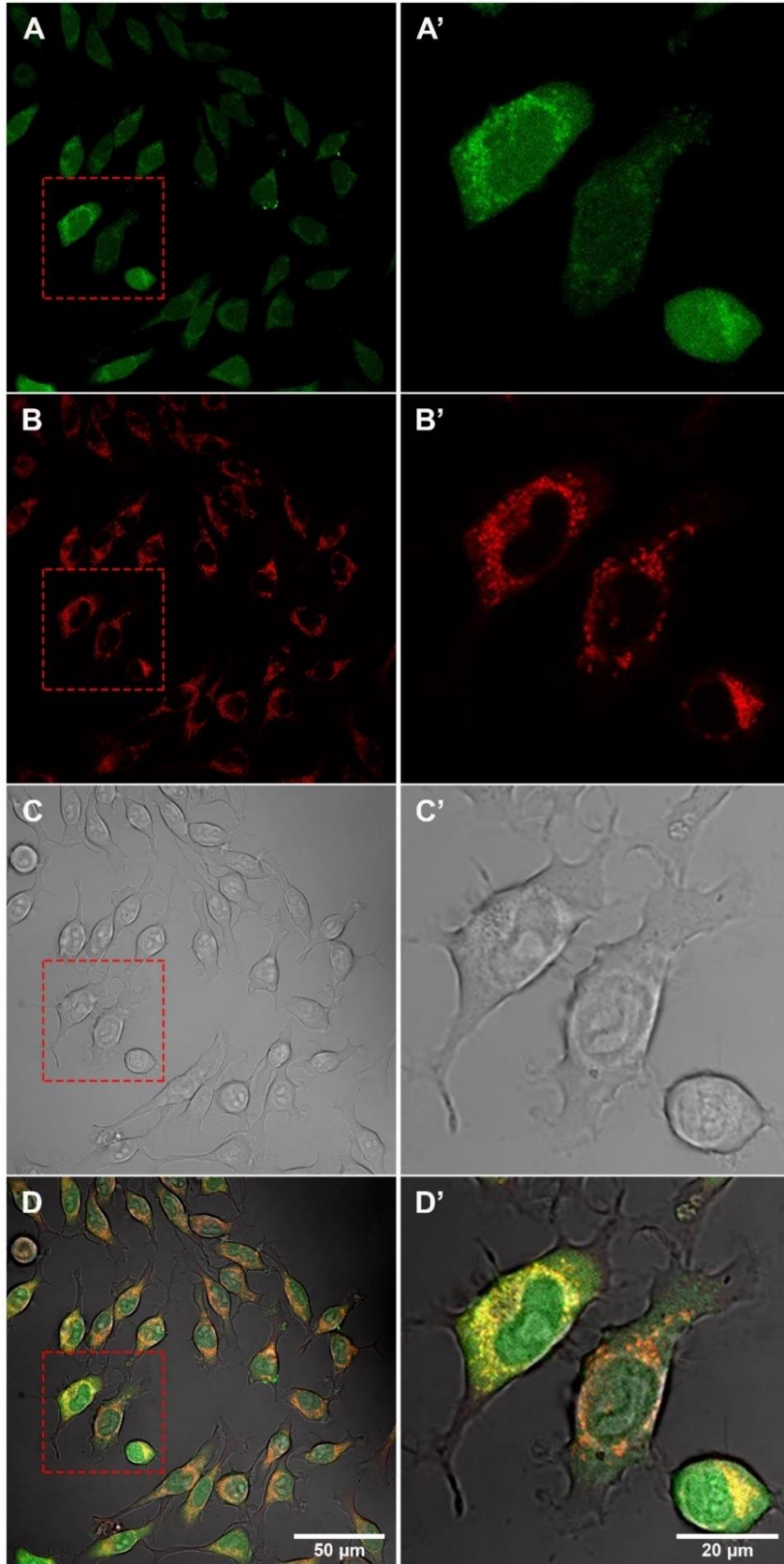


Figure 3.14 Sensor 3 localises to mitochondria within BV2 cells

Confocal images (60x) showing Sensor 3 (A, A': 1 μM), Mitotracker Deep Red (B, B'), DIC contrasted (C, C') and merged composite of all 3 (D, D') represented in BV2 cells. BV2 cells were incubated with Sensor 3 for 15 min then replaced with HBSS and Mitotracker Deep Red for a further 15 min. The Mitotracker solution was washed with HBSS, then Angeli's salt (200 μM) added to the cells to activate Sensor 3. Uptake of Sensor 3 was seen throughout the whole of the BV2 cells, however following AS addition, there was an increased fluorescence signal within the mitochondria observed as yellow overlay in image D and D' insert. Scale bar = 50 μm (A – D), scale bar = 20 μm (A' – D').

3.5 Discussion

Previous literature has shown distinct chemical and physiological properties of the one-electron reduced, protonated form of NO, nitroxyl (Miranda et al., 2005; Kemp-Harper, 2011; Fukuto et al., 2005, 2011). Endogenous production of nitroxyl is suggested to occur via several possible mechanisms such as; NOS activation in the absence of the cofactor tetrahydrobiopterin (BH₄) (Wei. CC., et al. 2003), hydroxylamine (NH₂OH) oxidation by a variety of heme proteins, reduction of NO to NO⁻ by cytochrome c (Choe, CU., et al, 2011), or by reaction with either ubiquinol (Poderoso et al., 1999), manganese superoxide dismutase (Niketic et al., 1999), or xanthine oxidase (Saleem et al., 2004). Furthermore, potential mechanisms of HNO generation in microglial cells includes; iNOS enzyme, reduction hydroxylamine (NH₂OH) to HNO via myeloperoxidase (MPO), the conversion of S-nitrosothiols to HNO by dithiols (Choe et al., 2011) or by the interaction between H₂S and NO (Yong et al., 2010). However, there is only indirect evidence to support the endogenous generation of HNO *in vivo* and therefore the development of analytical tools to assess this is paramount.

Fluorescent probes are high sensitivity, simple to use, non-invasive, have good spatiotemporal resolution and can be developed in a wide range of wavelengths, thus making excellent candidates for detecting HNO. Many fluorescent probes have been developed over recent years based on different chemical reactions to HNO, however, the Arylphosphine based probes have demonstrated the highest selectivity and the least interference from other potential reducing agents in biological systems (Smulik-Izydorczyk et al., 2018).

In the current study we have demonstrated the generation of a suite of bright, highly sensitive and very stable triarylphosphine based HNO fluorescent probes, with Sensor 3 detection limit the lowest reported to our knowledge. Using LPS, LPA or hypoxia challenge, we have observed the presence of endogenous HNO in BV2 and H9C2 cells using Sensor 3 by both spectroscopy and confocal microscopy.

Our study found that all the sensors were able to detect HNO generated by AS in biological buffers and media, with HBSS buffer and DMEM phenol red free (DMEM-PRF) media yielding the best fold increase for Sensor 3. This is important for live imaging studies which require the cells to be imaged in their conditioned media and stimulated to produce endogenous HNO signal. Many studies reporting the generation of HNO probes that can detect intracellular signal via the use of HNO donors such as Angeli's salt (Miao et al, 2015; Dong et al., 2018),

following the uptake of probe and therefore require the removal of excess probe by washing. This method may be misleading in determining the sensitivity of the probe, as the timing and concentration of the endogenous signal may be significantly slower and lower than what is produced by AS, and hence below the limit of detection for many probes.

Our study found that BV2 cells challenged with LPS (100-1000 ng/ml) showed increased intracellular HNO fluorescence which began at 4 hours and peaked approximately 10 hours post-incubation. This is supported by Parka *et al.*, (2015) which reported increased iNOS mRNA level between 6 – 12 hours and protein levels around 12 hours post LPS treatment (Parka *et al.*, 2015). Interestingly, the HNO fluorescence signal was inversely proportional to the LPS concentration. This phenomenon may be explained by a previous report showing an inflammatory response in monocytes to low-dose LPS (100 pg/ml), while a high-dose LPS (1 µg/ml) caused inflammatory tolerance (Yuan *et al.*, 2016). However, this is in contrast to another study which found that in BV2 cells ROS continued to increase with increasing doses of LPS up to 1 µg/ml, before showing a decrease at 1.5 µg/ml (Gaikwad *et al.*, 2015). This may be explained by the different cell types used in these studies, however it requires a thorough investigation as the range of LPS used in literature varies from pg/ml to µg/ml ranges which may elicit different downstream activation pathways of its target TLR4 receptor or off target effects (Yuan *et al.*, 2016). This differential effect was further demonstrated in a review of dose and timing of *in vivo* LPS administration in rodents (Lopes, 2016). We were also able to detect increases in HNO fluorescence of Sensor 3 with acute LPS (10-15 minutes) treatment of BV2 cells which was not present in control cells. However, the mechanism of HNO production following such a short time exposure to LPS is yet to be elucidated and requires further investigation. We observed a significant reduction of HNO fluorescence in BV2 cells pre-treated with iNOS inhibitor 1400W, prior to 24-hour incubation with LPS or LPA treatment, which suggests that endogenous HNO is generated via iNOS activation. Both LPS (Kim *et al.*, 2004; Pocock *et al.*, 2001) and LPA (Plastira *et al.*, 2016) have been shown to increase iNOS expression and release of NO in BV2 cells. Further to this, studies suggest that iNOS can produce HNO in the absence of co-factor BH₄ (Wei *et al.*, 2003), which implicates iNOS as a potential source of HNO *in vivo*. However, as the measure of BH₄ was beyond the scope of this study, we are unable to speculate its involvement in our findings.

We were able to localise HNO sensor 3 to the mitochondria of the BV2 cells via the use of live cell stain, Mitotracker Deep Red. The localisation of HNO probes within mitochondria has been previously reported (Ren et al., 2017; Gong et al., 2016) and supports our findings. Further to this, the generation of ROS and RNS has been suggested to also be localised to the mitochondria of cells (Ren et al., 2017; Gong et al., 2016; Sunwoo et al., 2017).

Two pilot studies were carried out using sensor 1 to measure blood levels of endogenous HNO in animal models of neuropathic pain and myocardial ischemia-reperfusion injury (supplementary data sections 3.10 & 3.11). This study reported for the first time the potential detection of HNO in red blood cell fractions of neuropathic pain animals (Supplementary figure 3.15). Interestingly, using Sensor 1 we observed a trending non-significant increase in fluorescent signal using spectroscopy which was not present in control samples. This finding was unexpected as many previous studies measuring RNS describe methods by which the plasma fraction is measured for RNS, not the red blood cells (Bryan et al., 2007). One explanation for these findings may be due the time point of blood collection. Although allodynia in these animals was still present at day 28, the peak systemic inflammation caused by the injury occurs much earlier on. Therefore, future experiments should consider taking blood samples at 1-3 days post injury. Furthermore, caution is required when measuring circulating RNS as the short-lived half-life and potentially low circulating levels of nitroxyl and other species, may be below the limit of detection for many methods. However, these super bright sensors can detect down to 100 nM of HNO and could potentially be used to measure *in vivo* samples, however further investigation is required.

Using a cellular model of ischemic-reperfusion injury, H9C2 cells showed increased intracellular HNO fluorescence following the replacement of oxygenated media and/or buffer, after a period of hypoxia (Supplementary figure 3.16). This is the first study to our knowledge that has demonstrated endogenous production of HNO in myocardial-like cells. Further to this, using sensor 1 we were able to detect elevated levels of HNO fluorescent signal in plasma fractions of blood samples taken immediately at the onset of reperfusion to the heart following at 30-minute period of ischemia, when compared with pre-ischemia (Supplementary figure 3.17). Samples were collected from a catheter inserted into the jugular vein directly into a syringe pre-loaded with sensor 1. Previous studies have identified a dual role for nitroxyl in myocardial ischemia-reperfusion, whereby administration of AS just prior to reperfusion causes

an increase in myocardial injury (Ma et al., 1999), however pre-ischemic administration is protective (Pagliaro et al., 2003; Irvine et al., 2008). Further investigation is required to validate this model and understand the role the endogenous nitroxyl may be having following reperfusion.

3.6 Conclusion

The validation of these super bright, highly specific and stable HNO fluorescent sensors in biological systems provides evidence to support the use of these tools to further our understanding of the role of endogenous nitroxyl. Since the first fluorogenic nitroxyl probe was synthesised in 2007 by Tennyson *et al.*, there has been a flourish of subsequent HNO probes designed and synthesised. However, this is the first study to report such an extensive validation in multiple biological systems using both spectroscopy and confocal microscopy for detection. These triacylphosphine based sensors described here show excellent potential for detecting HNO *in vivo* in future studies and furthering our understanding of the role of this endogenously produced reactive nitrogen species.

3.7 METHODS – Chemistry (This section was contributed by collaborator Dr. Xiaozhou Zhang)

3.7.1 Synthesis of sensors 1-3

3'-hydroxy-3-oxo-3H-spiro[isobenzofuran-1,9'-xanthen]-6'-yl 2-(diphenylphosphanyl)benzoate (sensor 1). To a solution of fluorescein (5) (1 g, 3.00 mmol) in anhydrous DMF (20 mL) under N₂ was added 2-(diphenylphosphino)benzoic acid (6) (760 mg, 2.48 mmol), DIC (520 mg, 4.12 mmol) and DMAP (126 mg, 2.80 mmol). The mixture was stirred under N₂ at room temperature for 21 h before H₂O (50 mL) was added. The aqueous phase was extracted with ethyl acetate (3 * 50 mL) and the combined organic layer was washed with H₂O (50 mL) and brine (100 mL). The organic layer was dried over Na₂SO₄ and concentrated in vacuo to give the crude product as a yellow oil (2.093 g). The mixture was purified by flash column chromatography to afford pure sensor 1 as a yellow solid (845 mg, 44%). ¹H NMR (500 MHz, DMSO-*d*₆) δ 10.21 (s, 1H), 8.02 (d, *J* = 7.8 Hz, 1H), 7.98 (d, *J* = 7.9 Hz, 1H), 7.83 – 7.78 (m, 2H), 7.77 – 7.68 (m, 2H), 7.62 – 7.49 (m, 10H), 7.39 (dd, *J* = 13.0, 7.8 Hz, 1H), 7.35 – 7.30 (m, 2H), 6.88 (d, *J* = 8.7 Hz, 1H), 6.79 (d, *J* = 8.7 Hz, 1H), 6.74 (s, 1H), 6.59 (s, 2H). ¹³C NMR (126 MHz, DMSO-*d*₆) δ 171.7, 162.8, 155.5, 154.7, 154.0, 138.9, 136.7, 136.2, 135.2, 134.5, 133.4, 132.0, 128.9,

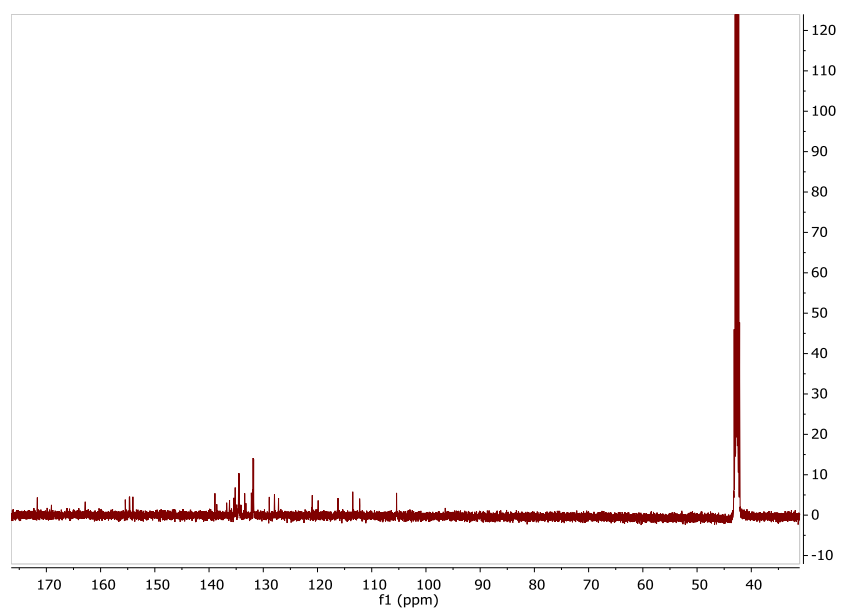
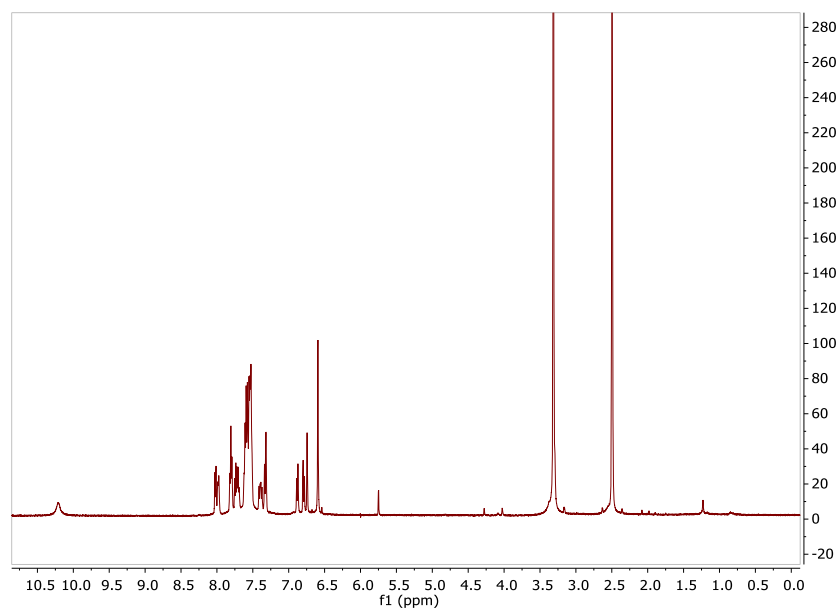
127.9, 121.0, 119.9, 116.2, 113.5, 112.2, 105.4. HRMS (m/z) for [C₃₉H₂₅O₆P]⁺ calculated 620.1389, found 620.1389.

2-oxo-2H-chromen-7-yl 2-(diphenylphosphanyl)benzoate (sensor 2). To a solution of 7-hydroxycoumarin (7) (91 mg, 0.56 mmol) in anhydrous DCM (20 mL) under N₂ was added 2-(diphenylphosphino)benzoic acid (6) (205 mg, 0.67 mmol), DIC (92 mg, 0.73 mmol) and DMAP (61 mg, 0.50 mmol). The mixture was stirred under N₂ at room temperature for 21 h before H₂O (20 mL) was added. The aqueous phase was extracted with ethyl acetate (3 * 20 mL) and the combined organic layer was washed with H₂O (20 mL) and brine (50 mL). The organic layer was dried over Na₂SO₄ and concentrated in vacuo to give the crude product as a brown oil (130 mg). The mixture was purified by flash column chromatography to afford pure sensor 2 as a white solid (70 mg, 28%). ¹H NMR (500 MHz, CDCl₃) δ 8.29 – 8.23 (m, 1H), 7.67 (d, *J* = 9.6 Hz, 1H), 7.55 – 7.46 (m, 2H), 7.43 (d, *J* = 8.0 Hz, 1H), 7.39 – 7.28 (m, 10H), 7.06 – 6.98 (m, 1H), 6.95 – 6.86 (m, 2H), 6.39 (d, *J* = 9.5 Hz, 1H). ¹³C NMR (126 MHz, CDCl₃) δ 167.3, 163.0, 157.3, 155.7, 145.5, 144.5, 139.9, 136.6, 135.6, 135.2, 134.2, 131.6, 131.3, 121.2, 119.3, 118.7, 113.2. HRMS (m/z) for [C₂₈H₁₉O₄P]⁺ calculated 450.1021, found 450.1015.

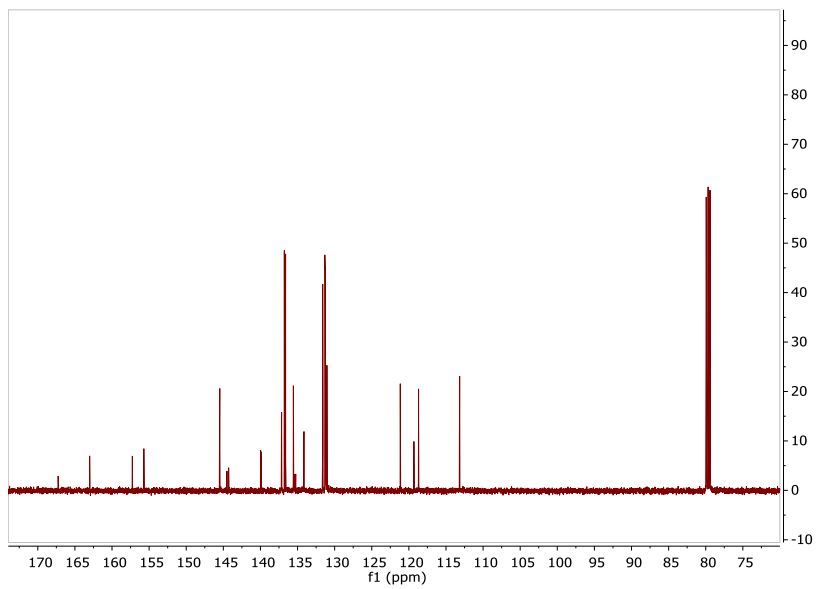
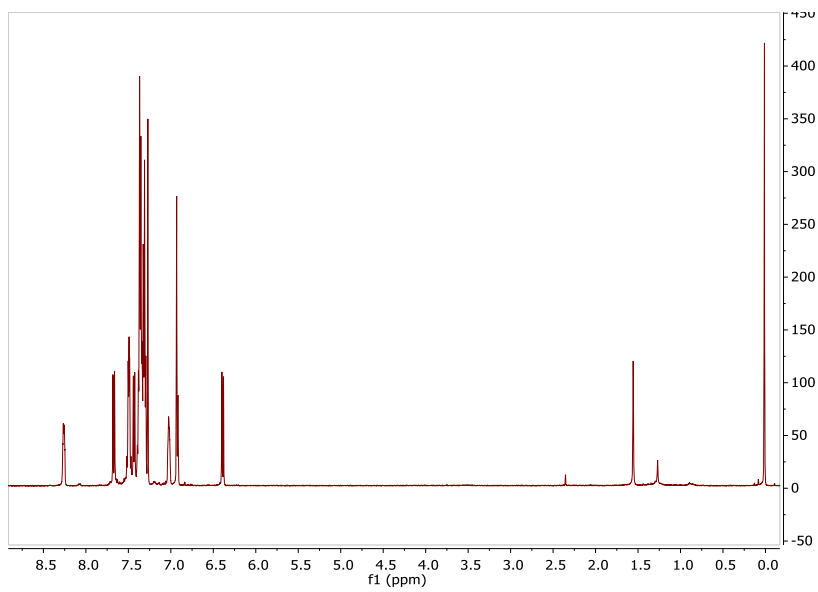
3'-(azetidin-1-yl)-6'-hydroxy-3H-spiro[isobenzofuran-1,9'-xanthen]-3-one (4). To a dry solution of fluorescein (5) (1 g, 3.00 mmol) in anhydrous DMF (7.5 mL) was added phenyl triflimide (9) (1.08 g, 3.00 mmol). The mixture was stirred under N₂ and DIPEA (1.56 mg, 12.04 mmol) was added dropwise. The mixture was further stirred under N₂ for 48 h at room temperature and acidified to pH 1 with 1 M HCl. The mixture was extracted with ethyl acetate (3 * 50 mL) and the combined organic layer was washed with H₂O (50 mL), dried over MgSO₄, and concentrated in vacuo to give crude product white solid (800 mg), which was used without further purification. To a solution of compound 8 (150 mg, 0.32 mmol), Pd₂dba₃ (30 mg, 0.03 mmol), XPhos (46 mg, 0.1 mmol) and Cs₂CO₃ (295 mg, 0.9 mmol) in anhydrous 1,4-dioxane (2.5 mL) under N₂ was added azetidine (44 mg, 0.78 mmol). The mixture was stirred under N₂ at 100 °C for 20 h and diluted with MeOH (20 mL). The volatiles were removed in vacuo to give the crude product as a dark red oil (849 mg). The mixture was purified by column chromatography to give rhodol 4 as a red solid (88 mg, 73%). ¹H NMR (500 MHz, Methanol-*d*₄) δ 8.11 (m, 1H), 7.83 – 7.64 (m, 2H), 7.27 (d, *J* = 7.5 Hz, 3H), 6.86 – 6.75 (m, 2H), 6.67 (d, *J* = 2.4 Hz, 1H), 6.41 (dd, *J* = 4.6, 2.6 Hz, 2H), 4.11 (m, 4H), 2.48 (p, *J* = 7.4, 2H).

3'-(azetidin-1-yl)-3-oxo-3H-spiro[isobenzofuran-1,9'-xanthen]-6'-yl 2-(diphenylphosphanyl)benzoate (sensor 3). Rhodol 4 (88 mg, 0.24 mmol), 2-(diphenylphosphino)benzoic acid (73 mg, 0.24 mmol), EDC (110 mg, 0.71 mmol) and DMAP (29 mg, 0.24 mmol) was dissolved in anhydrous THF (2 mL). The mixture was stirred under N₂ at room temperature for 20 h. The mixture was acidified to pH 1 with 1 M HCl and extracted with DCM (2 * 20 mL). The combined organic layer was washed with H₂O (20 mL) and brine (50 mL), dried over Na₂SO₄ and concentrated in vacuo to give the crude product as a pink oil (97 mg). The crude mixture was purified by rp-HPLC to afford sensor 3 as a pale pink solid (12 mg, 8%). ¹H NMR (500 MHz, CDCl₃) δ 8.33 – 8.16 (m, 1H), 8.01 (d, *J* = 7.5 Hz, 1H), 7.63 (m, 2H), 7.47 (m, 2H), 7.38 – 7.22 (m, 10H), 7.17 (d, *J* = 7.5 Hz, 1H), 7.05 – 6.92 (m, 2H), 6.71 (d, *J* = 8.7 Hz, 1H), 6.61 – 6.54 (m, 2H), 6.21 (s, 1H), 6.12 (d, *J* = 8.7, 1H), 3.93 (t, *J* = 7.3 Hz, 4H), 2.40 (p, *J* = 7.3 Hz, 2H). ¹³C NMR (126 MHz, CDCl₃) δ 172.1, 167.4, 156.3, 155.8, 155.0, 154.7, 154.3, 144.3, 144.1, 140.2, 140.1, 137.5, 137.1, 136.8, 136.7, 135.7, 135.3, 134.0, 132.2, 131.5, 131.5, 131.3, 131.2, 131.2, 131.1, 131.0, 129.5, 127.6, 126.8, 119.7, 113.0, 110.7, 109.5, 100.2, 86.1, 54.7, 19.3. HRMS (*m/z*) for [C₂₈H₁₉O₄P]⁺ calculated 659.1862, found 659.1860.

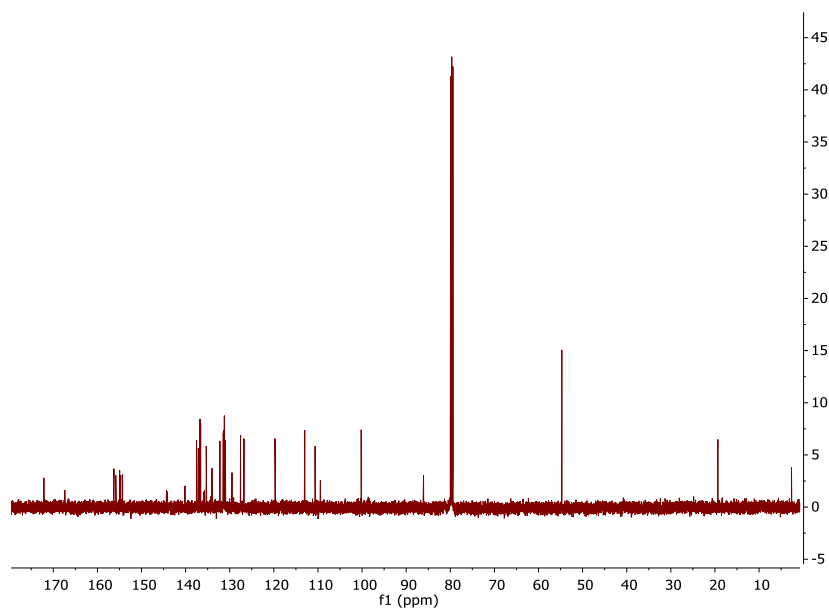
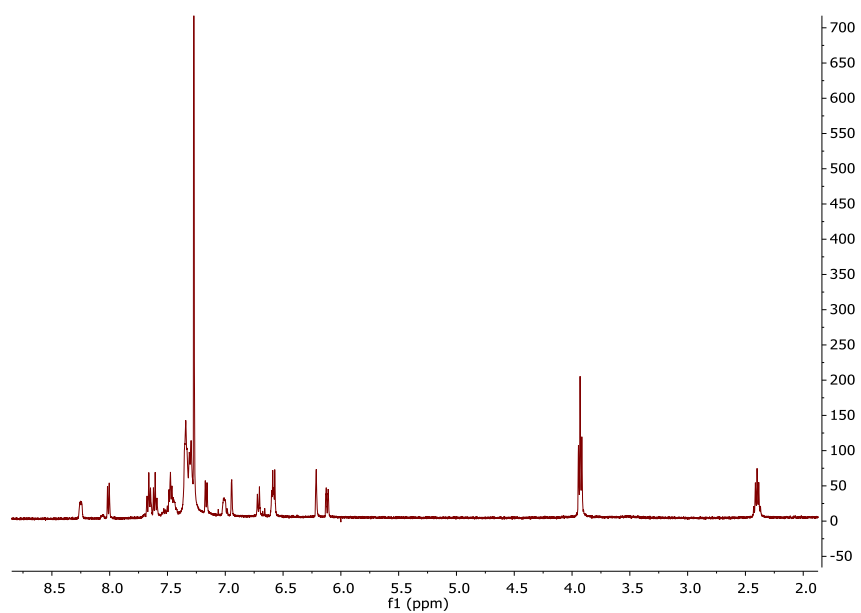
NMR of sensor 1



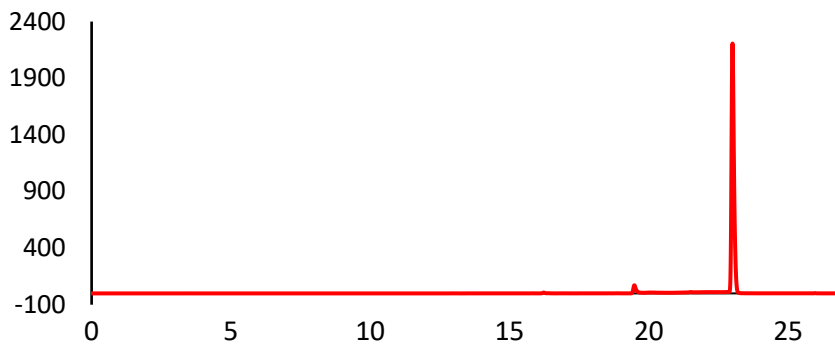
NMR of sensor 2



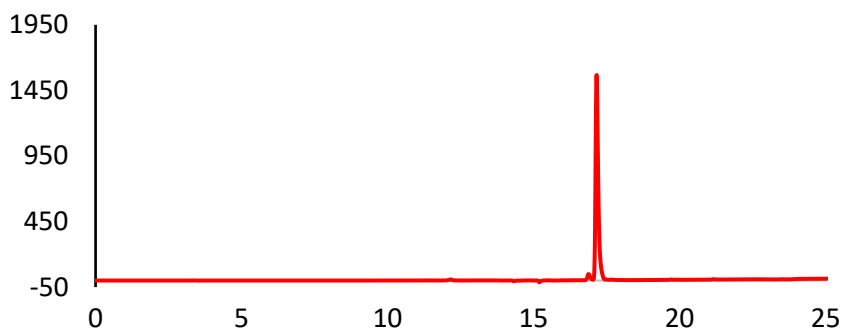
NMR of sensor 3



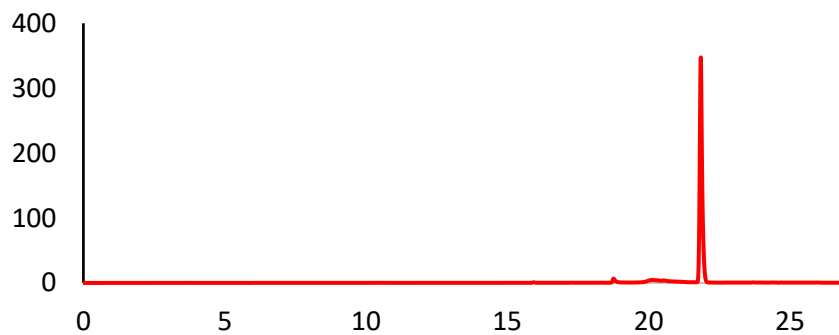
HPLC trace ($\lambda = 220$ nm) of sensor 1



HPLC trace ($\lambda = 220$ nm) of sensor 2



HPLC trace ($\lambda = 220$ nm) of sensor 3



3.7.2 Fluorescence of sensors 1-3 with and without added AS.

A solution of sensors 1-3 (2 μM for sensors 1 and 3 and 5 μM for sensor 2) in 1% DMSO in water (2 mL) was prepared in a sealed container and purged with N_2 for 30 min. Varying concentrations of AS ($[\text{AS}] = 0\text{--}100\ \mu\text{M}$) in 10 mM NaOH (20 μl) was added and the mixture was incubated in the sealed container for 10 min in the dark at room temperature. All concentrations of sensors 1-3 and AS reported are final concentrations of the solution after mixing. The resultant fluorescence (sensor 1: $\lambda_{\text{ex}} = 488\ \text{nm}$; sensor 3: $\lambda_{\text{ex}} = 512\ \text{nm}$) spectra of sensors 1 and 3 with each concentration of GSH was recorded on a Cary Eclipse Fluorescence Spectrophotometer. The fluorescence spectra of sensor 2 ($\lambda_{\text{ex}} = 380\ \text{nm}$) was similarly measured on a microplate reader. The maximum fluorescence intensity of each spectrum was plotted against AS concentration in μM to produce a standard curve of calibration for sensors 1-3. A linear trendline was fitted to the plot by GraphPad Prism 7.0.

3.7.3 Limit of detection of sensor 3.

A solution of sensor 3 (1 μM) in 1% DMSO in water (2 mL) was prepared in a sealed container and purged with N_2 for 30 min. AS (10 μM) in 10 mM NaOH (20 μL) was added and the mixture was incubated in the sealed container for 10 min in the dark at room temperature. The resultant fluorescence ($\lambda_{\text{ex}} = 512\ \text{nm}$) spectrum was recorded on a Cary Eclipse Fluorescence Spectrophotometer.

3.7.4 Fluorescence of sensors 1-3 with and without added AS in buffers and cell media.

A solution of sensors 1-3 (2 μM for sensors 1 and 3 and 5 μM for sensor 2) in 1% DMSO in various buffers (PBS and HBSS) and cell media (DMEM, DMEM serum-free (SF), DMEM phenol-red free (PRF) and DMEM SF PRF) (2 mL) was prepared in a sealed container and purged with N_2 for 30 min. AS (100 μM) in 10 mM NaOH (20 μL) was added and the mixture was incubated in the sealed container for 10 min in the dark at room temperature. The resultant fluorescence (sensor 1: $\lambda_{\text{ex/em}} = 488\ \text{nm}/512\ \text{nm}$; sensor 2: $\lambda_{\text{ex/em}} = 380\ \text{nm}/460\ \text{nm}$; sensor 3: $\lambda_{\text{ex/em}} = 512\ \text{nm}/550\ \text{nm}$) was measured on the microplate reader (Figure S2). The intensity was plotted in GraphPad Prism 7.0 as bar graphs. The experiment was conducted in triplicate.

3.7.5 Selectivity of sensors 1-3.

In a black 96-well plate, sensors 1-3 (2 μM for sensors 1 and 3 and 5 μM for sensor 2) was separately mixed with solutions (100 μM) of various biologically relevant species (NO , NO_2^- ,

NO₃⁻, N₃⁻, ONOO⁻, Cys, Arg, ascorbate, H₂S, GSH, GSNO, H₂O₂ and ·OH) in 1% DMSO in H₂O. The mixtures were incubated in the dark for 30 min before fluorescence (sensor 1: λ_{ex/em} = 488 nm/512 nm; sensor 2: λ_{ex/em} = 380 nm/460 nm; sensor 3: λ_{ex/em} = 512 nm/550 nm) of each mixture was measured on the plate reader. The experiments were carried out in triplicate.

3.7.6. Quantum Yield Calculations

The integrated fluorescence intensity is calculated as a sum of the intensities over the emission spectra for each sample. The integrated fluorescence intensity from a blank was subtracted and the plot of the integrated fluorescence intensity as a function of absorbance should show a linear relationship. The slope of the linear fit for the standards, a_r , is used to calculate the quantum yield of the fluorescent protein, Φ_s . According to the equation:

$$\Phi_s = \Phi_R \frac{a_s}{a_r} \left(\frac{n_s}{n_r} \right)^2 \quad (1)$$

where a_r is the quantum yield of the standard (Fluorescein; $\Phi = 0.93$ (Sjöback et al., 1995), Quinine; $\Phi = 0.55$ (Eaton, 1988)), a_s is the slope of the linear fit for the integrated fluorescence intensity of the fluorescent protein as a function of absorbance, and n_s and n_r are the refractive indices of the fluorescent protein and the standard solutions, respectively. Graph pad Prism was used for all linear fitting and calculations.

3.8 METHODS – Biological validation

3.8.1 Chemicals and Sensors

LPS (Lipopolysaccharides from Escherichia coli O111:B4, L2630), L-cysteine (L-cysteine Hydrochloride; C7477) and LPA (Oleoyl-L- α -lysophosphatidic acid sodium salt; L7260), were supplied by Sigma-Aldrich and Angeli's Salt (AS; 82230), carboxy-PTIO (cPTIO; 81540) and 1400W (1400W hydrochloride; 81520) from Cayman Chemicals. HNO sensors 1, 2 & 3 was synthesised and provided by Dr. Xiaozhou Zhang, School of Sciences, University of Adelaide. Details provided in section 3.7 of this thesis chapter.

3.8.2 Cell culture

Immortalized BV2 cells from a murine microglial cell line (BV2) were cultured in Dulbecco's modified Eagle's medium (DMEM; Sigma-Aldrich) supplemented with 10% fetal bovine serum (FBS; Gibco, ThermoFisher-Scientific), 100 IU/ml penicillin, 100 µg/ml streptomycin, (Penicillin-streptomycin; Sigma-Aldrich) 2 mM L-glutamine (Gibco, ThermoFisher-Scientific) and 100 µg/ml Normocin (InvivoGen). Cells were maintained at 37 °C in a saturated humidity

atmosphere containing 95% air and 5% CO₂ and used for assays when 75-80% confluent. To prepare samples for spectrophotometer experiments, 10,000 cells/ml of BV2 cells were seeded in a 96 well plate in 200 µl of media per well. Cells were grown to approximately 75-80% confluency prior to carrying out experiments. On the day of experimentation Sensors were added to wells and allowed to incubate for 15 - 30 min prior to the addition of stimulus (unless otherwise specified below).

3.8.3 Cell viability and function in the presence of Sensors 1, 2 and 3.

A trypan blue spectrophotometric assay (Uliasz et al., 2000) was used to measure the effect of 1.5 hours exposure to Sensors 1, 2 and 3 on BV2 cell death, before using them for HNO detection. Briefly, BV2 cells were exposed to 4 concentrations [0, 1, 5 & 10 µM] of each Sensor (1, 2 or 3) for 1.5 hours before removing media and replaced with a 0.05% Trypan blue solution in PBS (0.01M) and incubated (37°C) for 15 minutes. Cells were then gently washed 3x with ice cold PBS (0.01M) before adding 200 µl of 1% SDS solution (sodium dodecyl sulfate made in PBS) and contents gently triturated. Finally, 175 µl of the SDS/trypan solution was transferred into a clean 96 well culture plate and the absorbance read at 590 nm on a spectrophotometer.

Cytotoxicity of Sensors 1, 2 & 3 were further assessed using MTT (dimethylthiazol-diphenyltetrazolium bromide; Sigma-Aldrich) assay. For the cytotoxicity experiments, 3 x 10⁴ cells/ml BV2 cells were seeded into a 96 well culture plate and incubated for 24 hours at 37°C with 5% CO₂ until cells were 75-80% confluent. Four time points of exposure were used; 30 minutes, 2 hours, 24 hours and 48 hours in the presence of 4 concentrations [0, 1, 5 & 10 µM] of each Sensor. At the end of the incubation, the supernatant was removed and used for the LDH assay and to the cells, 100 µl of MTT solution (0.25mg/ml) was quickly added to each well and the plate incubated for 2 hours at 37 °C with 5% CO₂. After the incubation period, the MTT solution was removed and 100 µl of DMSO (dimethyl sulfoxide) added to each well for 10 minutes and the plate gently agitated. The absorbance was then measured on a spectrophotometer at 570 nm.

3.8.4 Detecting HNO in cell free media

The following series of experiments were all measured using a BioTek SynergyMx spectrophotometer. Measurements were taken at appropriate excitation/emission wavelengths for each Sensor (Sensor 1 $\lambda_{ex/em}$ = 470/512 nm, Sensor 2 $\lambda_{ex/em}$ = 387/456 nm, Sensor 3 $\lambda_{ex/em}$

= 518/550 nm). The relationship between Sensor concentration and HNO concentration was assessed in HBSS (Gibco, ThermoFisher-Scientific) buffer. Three concentrations of each Sensor [2.5, 5 & 10 μM] were assessed with increasing concentrations of AS were added [0, 0.195, 0.39, 0.78, 1.562, 3.125, 6.25, 12.5, 25, 50, 100 & 200 μM] and measurements taken every 2.5 minutes for 40-60 minutes total time. In a separate series of experiments, spectrophotometric fluorescent measurements for each Sensor [at 1 μM] were assessed in HBSS over 1 hour in the presence of 200 μM Angeli's salt. In another series of experiments, the limit of detection for each Sensor in the presence of Angeli's salt [200 μM] was determined in HBSS. Angeli's salt was added increasing concentrations of each Sensor [0, 0.1, 0.5, 0.75, 1, 5 & 10 μM] and measured after 1-hour incubation time.

3.8.5 Detecting HNO in BV2 cells

The presence of Sensors 3 in BV2 cells was observed using spectrophotometric and confocal microscopic analysis in the presence of Angeli's salt or relative treatment (described below) used to stimulate endogenous HNO, to determine the cellular localisation of HNO-activated Sensor 3 fluorescence.

3.8.5.1 Detection and sub-cellular localisation of endogenous HNO using Sensor 3 in BV2 cells.

LPS (Kim et al., 2004) is known to induce increased iNOS enzyme expression and subsequent NO and other reactive nitrogen species production in BV2 cells and was used as potential driver of endogenous HNO production in this study. BV2 cells (triplicates) were co-incubated with increasing concentrations of LPS (100, 500 and 1000 ng/ml) and Sensor 3 (2 μM) for 24 hours and spectral measurements taken at appropriate peak wavelength every 5 minutes for 24 hours. Control cells were incubated with 200 μM Angeli's salt, with and without 1 mM L-cysteine, to demonstrate the increase and reduction of fluorescence in the presence of HNO donor and scavenger, respectively. Negative control wells included cells without any stimuli or absence (HNO Sensor only) of Sensor 3 (blank control). These experimental conditions were repeated (triplicate) in wells containing media only, and the values of the media on wells were subtracted from the values measured with the cells and the difference reported.

In a separate series of experiments, both LPS and LPA were used as endogenous HNO stimuli in BV2 cells. BV2 cells (triplicates) were co-incubated with either increasing concentrations of LPS (200, 500 and 1000 ng/ml) or LPA (1 & 2 μM) for 24 hours. In parallel

experiments, cells were pre-incubated for 2 hours with 1400W (10 μ M) prior to the addition of LPS or LPA, to demonstrate the reduction of fluorescence in the presence of an iNOS inhibitor. Control cells were incubated with 200 μ M Angeli's salt, with and without 1 mM L-cysteine following the addition of Sensor 3, to demonstrate the increase and reduction of fluorescence in the presence of HNO donor and scavenger, respectively. Negative control wells included cells without any stimuli or absence (HNO Sensor only) of Sensor 3 (blank control). Following the 24-hour LPS/LPA incubation, Sensor 3 (2 μ M) was added to each well (except blank control wells) and incubated for 30 minutes prior to measuring the unwashed cells on the spectrometer using a top down spiral read.

3.8.6 Image analysis

The Sensor 3 Olympus FV3000 images were analysed for mean pixel intensity of the intracellular fluorescence of 20 randomly selected cells and were compared for the change in mean fluorescence intensity following a 10-minute incubation to baseline images (acute LPS treatment experiments). Images captured following 24-hours incubation with LPS/LPA \pm 1400W were also analysed for mean pixel intensity of the intracellular fluorescence of 20 randomly selected cells and were compared between treatments and to controls outlined above.

3.8.7 Statistics

Data were analysed using GraphPad Prism software (GraphPad Software, Inc. La Jolla, CA, USA). Shapiro-Wilk or Kolmogorov-Smirnov normality test was used to test the normality of data distribution. One-way ANOVA was used to compare three or more groups and the *p-values* for significant differences were derived from relevant post-hoc test for multiple comparisons. Two-way ANOVA was used to compare multiple treatments across groups and the *p-values* for significant differences were derived from relevant post-hoc test for multiple comparisons. Where applicable, linear regression was used to determine the slope of a line. All data are reported as mean \pm standard error of the mean (SEM), along with the individual data points where relevant to demonstrate biological variability.

3.9. References

Adak S, Wang Q, Stuehr DJ. (2000) Arginine Conversion to Nitroxide by Tetrahydrobiopterin-free Neuronal Nitric-oxide Synthase. *J. Biol. Chem.* 275, 33554–33561.

Andrews KL, Irvine JC, Tare M, Apostolopoulos J, Favaloro JL, Triggle CR, Kemp-Harper BK. (2009) A role for nitroxyl (HNO) as an endothelium-derived relaxing and hyperpolarizing factor in resistance arteries. *Br. J. Pharmacol*; 157: 540–550.

Andrews KL, Lumsden NG, Farry J, Jefferis AM, Kemp-Harper BK, and Chin-Dusting JP. (2015) 'Nitroxyl: a vasodilator of human vessels that is not susceptible to tolerance,' *Clinical Science*; 129(2): 179–187.

Bryan NS, Grisham MB. (2007) Methods to detect nitric oxide and its metabolites in biological samples. *Free Radical Biology & Medicine*; 43: 645–657.

Choe CU, Lewerenz J, Gerloff C, Magnus T and Donzelli S. (2011) Nitroxyl in the Central Nervous System. *Antioxid. Redox Signal*; 14: 1699–1711.

DeMaster EG, Redfern B, and Nagasawa HT. (1998) "Mechanisms of inhibition of aldehyde dehydrogenase by nitroxyl, the active metabolite of the alcohol deterrent agent cyanamide," *Biochemical Pharmacology*; 55(12): 2007–2015.

Dong B, Kong X, Lin W. (2018) Reaction-Based Fluorescent Probes for the Imaging of Nitroxyl (HNO) in Biological Systems. *ACS Chem. Biol*; 13: 1714–1720.

Eaton DF. (1988) Reference Materials for Fluorescence Measurement. *Pure & Appl. Chem*; 60: 1107.

Ellis A, Li CG, Rand MJ. (2000) Differential actions of L-cysteine on responses to nitric oxide, nitroxyl anions and EDRF in the rat aorta. *Br. J. Pharmacol*; 129: 315–322.

Fukuto JM, Bartberger MD, Dutton AS, Paolocci N, Wink DA, Houk KN (2005). The physiological chemistry and biological activity of nitroxyl (HNO): the neglected, misunderstood and enigmatic nitrogen oxide. *Chem Res Toxicol*; 18: 790–801.

Fukuto JM, Bianco CL, Chavez TA (2009). Nitroxyl (HNO) signaling. *Free Radic Biol Med*; 47: 1318–1324.

Fukuto JM, Carrington SJ, Tantillo DJ, Harrison JG, Ignarro LJ, Freeman BA, Chen A, Wink DA. (2012). Small molecule signaling agents: the integrated chemistry and biochemistry of nitrogen oxides, oxides of carbon, dioxygen, hydrogen sulfide, and their derived species. *Chem Res Toxicol*; 25: 769–793.

Fukuto JM, Carrington SJ. (2011) HNO Signaling Mechanisms. *Antioxidants and redox signalling*; 14(9): 1649-1657.

Fukuto JM, Cisneros CJ, Kinkade RL (2013). A comparison of the chemistry associated with the biological signaling and actions of nitroxyl (HNO) and nitric oxide (NO). *J Inorg Biochem*; 118: 201–208.

Fukuto JM, Switzer CH, Miranda KM, Wink DA. (2005) NITROXYL (HNO): Chemistry, Biochemistry, and Pharmacology. *Annu. Rev. Pharmacol. Toxicol*; 45: 335–55.

Fukuto JM. (2019) A recent history of nitroxyl chemistry, pharmacology and therapeutic potential. *British Journal of Pharmacology*; 176: 135–146.

Gaikwad S, Patel D, Naveen CR, Rajput RA. (2015) The critical role of JNK and p38 MAPKs for TLR4 induced microglia-mediated neurotoxicity. *European Journal of Experimental Biology*; 5(8): 34-42.

Gerő D. (2016) The Hypoxia-Reoxygenation Injury Model. Book chapter 3: Hypoxia and Human disease. <http://dx.doi.org/10.5772/65339>

Gong X, Yang XF, Zhong Y, Chen Y, Li Z. (2016) A mitochondria-targetable near-infrared fluorescent probe for imaging nitroxyl (HNO) in living cells. *Dyes and Pigments*; 131: 24-32.

Grace PM, Hutchinson MR, Manavis J, Somogyi AA, Rolan PE (2010) A novel animal model of graded neuropathic pain: Utility to investigate mechanisms of population heterogeneity. *Journal of Neuroscience Methods*; 193(1): 47-53.

He X, Azarov I, Jffers A, Presley T, Richardon J, King SB, Gladwin MT, Kim-Shapiro DB. (2008) The potential of Angeli's salt to decrease nitric oxide scavenging by plasma hemoglobin. *Free radical biology and medicine*; 44(7): 1420-1432.

Hrabie JA, Klose JR, Wink DA, Keefer LK. (1993) New nitric oxide-releasing zwitterions derived from polyamines. *The Journal of Organic Chemistry*; 58:1472–1476.

Hu L, Wang J, Zhu H, Wu X, Zhou L, Song Y, Zhu S, Hao M, Liu C, Fan Y, Wang Y, Li Q. (2016) Ischemic postconditioning protects the heart against ischemia–reperfusion injury via neuronal nitric oxide synthase in the sarcoplasmic reticulum and mitochondria. *Cell Death and Disease*; 7: e2222.

Irvine JC, Ritchie RH, Favaloro JL, Andrews KL, Widdop RE, Kemp-Harper BK. (2008) Nitroxyl (HNO): the Cinderella of the nitric oxide story. *Trends in Pharmacological Sciences*; 29(12): 601-608.

Jing XT, Yu FB, Chen LX. (2014) Visualization of nitroxyl (HNO) in vivo via a lysosome-targetable near-infrared fluorescent probe. *Chem. Commun*; 50(91): 14253–14256.

Kawai AK, Ieda N, Aizawa K, Suzuki T, Miyata N, Nakagawa H. (2013) A reductant resistant and metal-free fluorescent probe for nitroxyl applicable to living cells. *J. Am. Chem. Soc*; 135(34): 12690–12696.

Kemp-Harper BK. (2011) Nitroxyl (HNO): A Novel Redox Signaling Molecule. *Antioxidants and redox signalling*; 14(9): 1609-1613.

Kim SS, Kong PJ, Kim BS, Sheen DH, Nam SY, Chun W. (2004) Inhibitory action of minocycline on lipopolysaccharide-induced release of Nitric Oxide and Prostaglandin E2 in BV2 microglial cells. *Arch Pharm Res*; 27(3): 314-318.

Liu C, Wu H, Wang Z, Shao C, Zhu B, Zhang X. (2014) A fast-response, highly sensitive and selective fluorescent probe for the ratio-metric imaging of nitroxyl in living cells. *Chem. Commun*; 50(45): 6013–6016.

Longhi-Balbinot DT, Rossaneis AC, Pinho-Ribeiro FA, Bertozzi MM, Cunha FQ, Alves-Filho JC, Cunha TM, Peron JPS, Miranda KM, Casagrande R and Verri Jr. WA, (2016) 'The nitroxyl donor, Angeli's salt, reduces chronic constriction injury-induced neuropathic pain'. *Chemico-Biological Interactions*; doi: 10.1016/j.cbi.2016.06.009.

Lopes PC. (2016) LPS and neuroinflammation: a matter of timing. *Inflammopharmacol*; 24: 291-293.

Ma XL, Gao F, Liu GL, Lopez BL, Christopher TA, Fukuto JM, Wink DA, Feelisch M. (1999) Opposite effects of nitric oxide and nitroxyl on post-ischemic myocardial injury. *Proc. Natl. Acad. Sci. U.S.A.*; 96: 14617–14622.

Mao GJ, Zhang XB, Shi XL, Liu HW, Wu YX, Zhou LY, Tan W, Yu RQ. (2014) A highly sensitive and reductant-resistant fluorescent probe for nitroxyl in aqueous solution and serum. *Chem. Commun*; 50(43): 5790–5792.

Miao Z, King SB. (2016) Recent advances in the chemical biology of nitroxyl (HNO) detection and generation. *Nitric Oxide*; 57: 1-14.

Miao Z, Reisz JA, Mitroka SM, Pan J, Xian M, King SB. (2015) A selective phosphine based fluorescent probe for nitroxyl in living cells. *Bioorg. Med. Chem. Lett*; 25(1): 16–19.

Miranda KM. (2005) The chemistry of nitroxyl (HNO) and implications in biology. *Coordination Chemistry Reviews*; 249: 433–455.

Niketic V, Stojanovic S, Nikolic A, Spasic M, Michelson AM. (1999) Exposure of Mn and FeSODs, but not Cu/ZnSOD, to NO leads to nitrosonium and nitroxyl ions generation which cause enzyme modification and inactivation: an in vitro study. *Free Radical Biol. Med*; 27: 992–996.

Pagliari P, Mancardi D, Rastaldo R, Penna C, Gattullo D, Miranda KM, Feelisch M, Wink DA, Kass DA, Paolocci N. (2003) Nitroxyl affords thiol-sensitive myocardial protective effects akin to early preconditioning. *Free Radic. Biol. Med*; 34: 33–43.

Park J, Min JS, Kim B, Chae UB, Yun JW, Choi MS, Kong IK, Chang KT, Lee DS. (2015) Mitochondrial ROS govern the LPS-induced pro-inflammatory response in microglia cells by regulating MAPK and NF- κ B pathways. *Neuroscience Letters*; 584: 191–196.

Plastira I, Bernhart E, Goeritzer M, Reicher H, Kumble VB, Kogelnik N, Wintersperger A, Hammer A, Schlager S, Jandl K, Heinemann A, Kratky D, Malle E, Sattler W. (2016) 1-Oleoyl-lysophosphatidic acid (LPA) promotes polarization of BV-2 and primary murine microglia towards an M1-like phenotype. *Journal of Neuroinflammation*; 13: 205.

Pocock JM, Liddle AC. (2001) Microglial signalling cascades in neurodegenerative disease. *Prog. Brain Res*; 132: 555- 565.

Poderoso JJ, Carreras MC, Schopfer F, Lisdero CL, Riobo NA, Guilivi C, Boveris AD, Cadenas E. (1999) *Free Radical Biol. Med*; 26: 925–935.

Reisz JA, Klorig EB, Wright MW, King SB. (2009) Reductive phosphine-mediated ligation of nitroxyl (HNO). *Org Lett*; 11: 2719–21.

Ren M, Deng B, Zhou K, Wang JY, Kong X, Lin W. (2017) A targetable fluorescent probe for imaging exogenous and intracellularly formed nitroxyl in mitochondria in living cells. *J. Mater. Chem. B*; 5: 1954-1961.

Rosenthal J, Lippard SJ. (2010) Direct detection of nitroxyl in aqueous solution using a tripodal copper(II) BODIPY complex. *J Am Chem Soc*; 132: 5536–7.

Royzen M, Wilson JJ, Lippard SJ. (2013) Physical and structural properties of [Cu(BOT1)Cl]Cl, a fluorescent imaging probe for HNO. *J Inorg BioChem*; 118: 162–170.

Sabbah HN, Tocchetti CG, Wang M, Daya S, Gupta RC, Tunin RS, Mazhari R, Takimoto E, Paolucci N, Cowart D, Colucci WS. and Kass DA. (2013) 'Nitroxyl (HNO) a Novel Approach for the Acute Treatment of Heart Failure.' *Circ Heart Fail*; 6(6): 1250–1258.

Saleem M, Ohshima H. (2004) Xanthine oxidase converts nitric oxide to nitroxyl that inactivates the enzyme *Biochemical and Biophysical Research Communications*; 315(2): 455-462.

Shoman ME and Aly OM. (2016) Nitroxyl (HNO): A Reduced Form of Nitric Oxide with Distinct Chemical, Pharmacological, and Therapeutic Properties. *Oxidative Medicine and Cellular Longevity*; Article ID 4867124.

Sjöback R, Nygren J, Kubista M. (1995) Absorption and Fluorescence Properties of Fluorescein. *Spectrochimica Acta Part A: Molecular and Biomolecular Spectroscopy*; 51: L7.

Smulik-Izydorczyk R, Dębowska K, Pięta J, Michalski R, Marcinek A, Sikora A. (2018) Fluorescent probes for the detection of nitroxyl (HNO). *Free Radical Biology and Medicine*; 128: 69–83.

Sunwoo K, Bobba KN, Lim JY, Park T, Podder A, Heo JS, Lee SG, Bhuniya S, Kim JS. (2017) A bioorthogonal 'turn-on' fluorescent probe for tracking mitochondrial nitroxyl formation. *Chem. Commun*; 53: 1723.

Switzer CH, Flores-Santana W, Mancardi D, Donzelli S, Basudhar D, Ridnour LA, Miranda KM, Fukuto JM, Paolocci N, Wink DA. (2009) The emergence of nitroxyl (HNO) as a pharmacological agent. *Biochimica et Biophysica Acta*; 1787: 835-840.

Takahira R, Yonemura K, Fujise Y, Hishida A. (2001) Dexamethazone attenuates neutrophil infiltration in the rat kidney in ischemia/reperfusion injury: the possible role of nitroxyl. *Free Radic. Biol. Med*; 31: 809–15.

Tennyson AG, Do L, Smith RC, Lippard SJ. (2007) Selective fluorescence detection of nitroxyl over nitric oxide in buffered aqueous solution using a conjugated metallopolymer. *Polyhedron*; 26: 4625–4630.

Uliasz TF, Hewett SJ. (2000) A microtiter trypan blue absorbance assay for the quantitative determination of excitotoxic neuronal injury in cell culture. *Journal of Neuroscience Methods*; 100: 157–163.

Wang P & Zweier JL. (1996) Measurement of nitric oxide and peroxynitrite generation in the postischemic heart. *J Biol Chem*; 271 (46): 29223-29230.

Wei CC, Wang ZQ, Hemann C, Hille R, Stuehr DJ. (2003) A Tetrahydrobiopterin Radical Forms and then Becomes Reduced during N-Hydroxyarginine Oxidation by Nitric-oxide Synthase. *J. Biol. Chem*; 278: 46668-46673.

Wu Y, Yin X, Wijaya C, Huang MH, McConnell BK. (2011) Acute myocardial infarction in rats. *J Vis Exp*; 16(48): 2464.

Yong QC, Hu LF, Wang S, Huang D, Bian JS. (2010) Hydrogen sulfide interacts with nitric oxide in the heart: possible involvement of nitroxyl. *Cardiovasc. Res*; 88(3): 482–491.

Yuan R, Geng S, Li L (2016) Molecular Mechanisms That Underlie the Dynamic Adaptation of Innate Monocyte Memory to Varying Stimulant Strength of TLR Ligands. *Front. Immunol.* 7:497.

Yung YC, Stoddard NC, Mirendil H, Chun J. (2015) Lysophosphatidic Acid Signaling in the Nervous System. *Neuron*; 85(4): 669-682.

Zarpelon AC, Souza GR, Cunha TM, Schivo IRS, Marchesi M, Casagrande R, Pinge-Filho P, Cunha FQ, Ferreira SH, Miranda KM and Verri Jr. WA, (2013) 'The nitroxyl donor, Angeli's salt, inhibits inflammatory hyperalgesia in rats.' *Neuropharmacology*; 71: 1–9.

Zhang H, Liu R, Tan Y, Xie WH, Lei H, Cheung HY, Sun H. (2015) A FRET-based ratiometric fluorescent probe for nitroxyl detection in living cells. *ACS Appl. Mater. Interfaces*; 7(9): 5438–5443.

Zheng KB, Lin WY, Cheng D, Chen H, Liu Y, Liu KY. (2015) A two-photon fluorescent turn-on probe for nitroxyl (HNO) and its bioimaging application in living tissues. *Chem. Commun*; 51(26): 5754–5757.

Zhou Y, Liu K, Li JY, Fang Y, Zhao TC, Yao C. (2011) Visualization of nitroxyl in living cells by a chelated copper(II) coumarin complex. *Org Lett*; 13: 1290.

3.10 SUPPLEMENTARY DATA

METHODS

3.10.1 Cell culture

H9C2 cells are a rat cardio-myoblast cell line and were maintained in accordance to manufacturer's instructions. Briefly, H9C2 cells were cultured in ATCC-formulated Dulbecco's Modified Eagle's Medium (ATCC, Australia), supplemented with 10% fetal bovine serum (FBS; Gibco, ThermoFisher-Scientific) and maintained at 37 °C in a saturated humidity atmosphere containing 95% air and 5% CO₂ and used for assays when 75% confluent. To prepare cells for experimentation, 2.5 x 10⁴ cells/ml were seeded (quadruplicates) either in 96 well cell culture plates or 4 well ibidi slides and allowed to adhere overnight at 37 °C.

3.10.2 Detection of endogenous HNO using sensor 1 in supernatant of H9C2 cells

Hypoxia-reoxygenation injury is a commonly used cell-based model of ischemia-reperfusion injury. Hypoxia is induced by incubating the cells with hypoxic gas mixture/buffers, causing energetic failure due to the lack of oxygen and driving anaerobic metabolism and can lead to oxidative stress (Gerő, 2017). The replacement of hypoxic conditions, back to that of normoxic is akin to the reperfusion of oxygenated blood *in vivo* and can cause an immediate and significant spike in NO levels which is thought to drive the myocardial tissue injury (Hu et al., 2016). H9C2 cells (2.5 x 10⁴ cells/ml; quadruplicates) were seeded in 96 well culture plates and allowed to adhere overnight at 37°C. Cells were exposed to either media or hypoxic buffer for 2 hours at 37°C. Samples of the supernatant (50 µl) were taken and added to 5 µM of sensor 1 in a second 96 well culture plate, the remaining supernatant was removed and replaced with either media or normoxic buffer (Table 1) and left to incubate for 1-2 minutes before a second sample (50 µl) was transferred to 5 µM of sensor 1 and read using a spectrophotometer at $\lambda_{ex/em} = 470/512$ nm. The values of the second sample were subtracted from the first value to determine the difference in fluorescence signal.

Table 1

<u>Combo</u>	Treatment 1	Treatment 2
<u>1</u>	Media	Media
<u>2</u>	Hypoxic buffer	Media
<u>3</u>	Hypoxic buffer	Normoxic buffer
<u>4</u>	Media	Normoxic buffer

3.10.3. Confocal Experiments

For H9C2 confocal imaging experiments, cells (2.5×10^4 cells/ml) were seeded on 4 well ibidi slides in 700 μ l of media per well and allowed to adhere overnight at 37°C. Sensor 1 (2 μ M) was added to the cells for 30 minutes in the presence of the first treatment. After the incubation period a z-series 60x magnification image was captured on SP5 Leica scanning confocal system, with a 512 x 512-pixel image size. The treatment 1 buffer was then removed and replaced with the second treatment solution and allowed to incubate for 1-2 minutes before a second confocal image was captured of the same field of view for comparison (Table 2). Sensor 1 was detected using 488 nm/512 nm (emission/excitation) wavelength.

Table 2

<u>Combo</u>	Treatment 1	Treatment 2
<u>1</u>	Media	Media
<u>2</u>	Normoxic buffer	Media
<u>3</u>	Media	Normoxic buffer
<u>4</u>	Hypoxic buffer	Normoxic buffer

3.10.4 Image analysis

The Sensor 1 Leica SP5 confocal time series images were analysed for mean pixel intensity on a per cell basis over time using Image J (FIJI version 1.52d). An AVI file was created from the 60x magnification image stacks and 20 random cells were selected per series and masked using the DIC image as reference. H9C2 were analysed for mean pixel intensity of the intracellular fluorescence of 20 randomly selected cells and the random fluorescence units (RFU) were compared between treatments.

3.10.5 Detecting HNO in plasma/ red blood cells

All animal care and handling procedures were approved by Animal Ethics Committee of the University of Adelaide. All procedures were performed in accordance with the Australian Code for the Care and Use of Animals for Scientific Purpose (2013). Ethics application M-2017-005 (Chronic constriction injury), M-2016-039a (Myocardial ischemic reperfusion injury).

3.10.6 Chronic constriction injury model

In a pilot study using an animal model of neuropathic pain injury as described by Grace *et al.*, (2010), cardiac blood was collected from Sprague-Dawley male rats which were scavenged 28 days following chronic constriction injury of the sciatic nerve (once allodynia had been established) following a lethal i.p. injection with 60mg/kg of sodium pentobarbitone. Using cardiac puncture, blood was drawn from the heart into a 1 ml syringe containing EDTA/PBS solution with either 200 μ l of Sensor 1 (10 μ M), 200 μ l PBS as the vehicle control or 200 μ l of Sensor 1 with Angeli's salt. The collected samples were mixed well in the syringe and allowed to sit in the dark for 20 minutes before being transferred to a 1.5 ml tube and spun at 3000 rpm for 10 minutes. The separated samples (plasma and red blood cell fractions) were then aliquoted in triplicate into a 96 well plate and reading was done on the Biotek SynergyMx spectrophotometer at (Sensor 1) $\lambda_{ex/em} = 470/512$ nm.

3.10.7 Myocardial ischemic reperfusion injury model

Myocardial Ischemic reperfusion injury occurs when heart tissue undergoes an ischemic event thus being deprived of blood flow and oxygen (creating hypoxic conditions) for a period of time, followed by the reperfusion of oxygenated blood. The reintroduction of oxygen causes the injury and results in the necrosis of tissue (Switzer *et al.*, 2009). This phenomenon is reported to occur due to production of ROS and increased oxidative stress as well as increases in NO and other RNS production immediately following reperfusion (Wang & Zweier, 1996). However, although a role for HNO in pre-conditioning the heart prior to ischemia has been established using donors (Pagliaro *et al.*, 2003), lack of tools to measure HNO have meant that little is known about the production of HNO during ischemia and following reperfusion. Therefore, we sought to identify the presence of HNO using Sensor 1 prior to ischemia and following reperfusion.

In a pilot experiment using an animal model of myocardial ischemic-reperfusion injury as described by Wu *et al.*, (2011), blood samples were scavenged from a Sprague-Dawley male

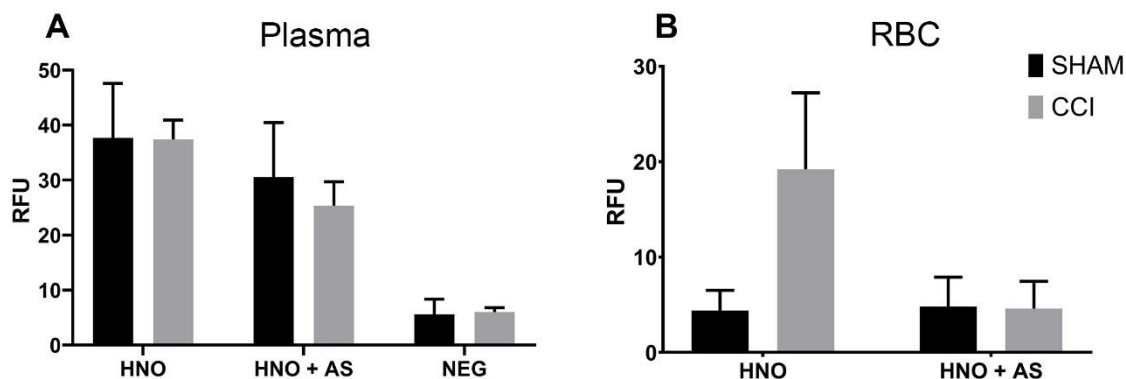
rat undergoing surgery. Blood samples were collected directly from a catheter surgically inserted the aorta at 3 time points; before ischemia, immediate after and 15 minutes after the cardiac ischemia-reperfusion and was drawn up into 1 ml syringes as described above. Sensor 1 (10 μ M) was used in this experiment and only triplicates of the plasma fraction were read on the Biotek SynergyMx spectrophotometer over 4 hours at (Sensor 1) $\lambda_{ex/em} = 470/512$ nm.

3.11 RESULTS

3.11.1 Sensor 1 may detect endogenous HNO signal in blood of neuropathic pain animals

A pilot study was carried out to determine if endogenous HNO could be measure from the blood of animals with neuropathic pain. Blood collected via cardiac puncture from either chronic constriction injury (CCI; N3S1, n = 5) animals displaying allodynia (pain response to non-noxious stimulus) and sham operated animals (control non-injured group, n = 5) was mixed with Sensor 1 before being separated into plasma and red blood cell samples (RBC) (Figure 3.15). Spectrometer readings determined that the separated plasma contained higher fluorescent signals in both sham operated (37.6 ± 9.9 RFU) and CCI (37.4 ± 3.5 RFU) when compared to blood samples without Sensor 1 (6 ± 0.7 RFU) (Figure 3.15; A) however, the addition of AS to the blood mixture to determine the saturation value, generated a slightly lower RFU signal for both sham operated (30.5 ± 9.9 RFU) and CCI group (25.3 ± 4.3 RFU) than plasma with sensor alone. One possibility for this unexpected result may be accounted by the reaction kinetics of AS in whole blood, which may be scavenged by plasma haemoglobin, and therefore was not available to interact with sensor 1 (He et al., 2008).

Interestingly, in the separated RBC portion of blood Sensor 1 (Figure 3.15; B) showed a trending increase in fluorescent signal from blood collected from CCI operated animals (19.2 ± 8 RFU) but not sham operated animals (4.4 ± 2.1 RFU) when compared to samples containing AS (4.8 ± 3.1 RFU). These data suggest that most of Sensor 1 may be separated into the plasma portion of blood, however the residual signal in the RBC fraction may be more indicative of changes in HNO due to disease state.



Supplementary figure 3.15 Sensor 1 may potentially detect increased circulating HNO in red blood cell fraction of neuropathic rats.

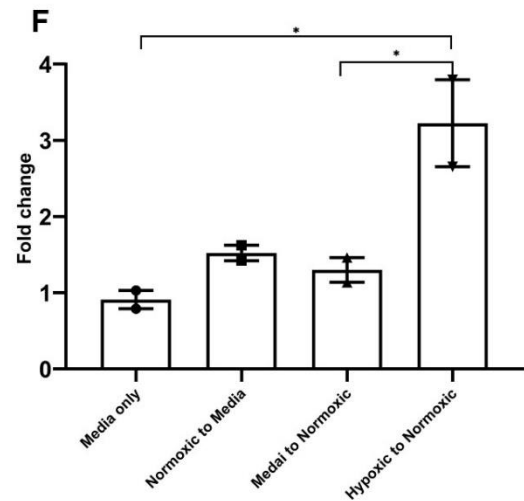
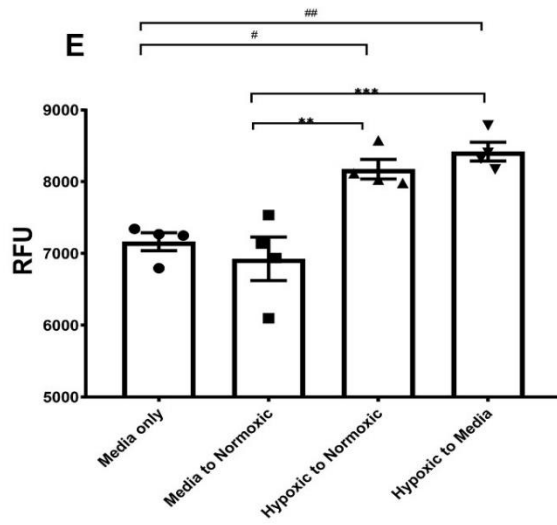
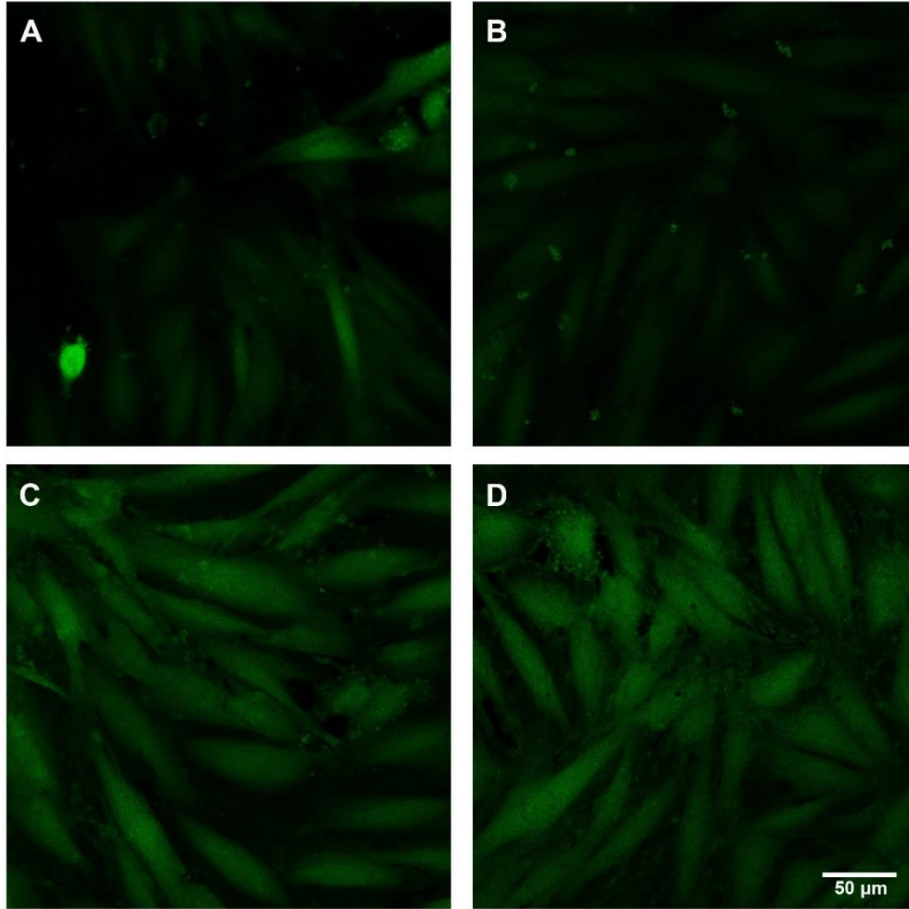
Bar graphs showing the random fluorescent unit (RFU) signal of Sensor 1 in cardiac blood samples separated into plasma (A) and red blood cells (B). Blood samples were taken via cardiac puncture from rats with developed neuropathic pain (grey bars: CCI, n = 5) and sham operated controls (black bars: Sham, n= 5). Samples were measured using a spectrophotometer.

3.11.2 Sensor 1 detects endogenous HNO in, in vitro and in vivo models of ischemic reperfusion injury

To explore further potential use of Sensor 1 to detect endogenous HNO signal, the fluorescent signal derived from human coronary artery endothelial (H9C2) treated cells (Figure 3.16, n = 3) and cardiac blood collected from rat models of ischemic reperfusion injury (Figure 3.17, n = 1) was measured using spectroscopy and confocal microscopy. The coronary endothelial cells were imaged using confocal microscopy in the presence of AS and hypoxic stimuli. H9C2 cells pre-treated with hypoxia solution followed by either normoxic (8175 ± 136RFU) (Figure 3.16; C) or media (8420 ± 130 RFU) (Figure 3.16; D) showed significantly increased intracellular fluorescent signal when compared to cells pre-treated with media followed by either a second media exchange (7164 ± 124) (Hypoxic/Normoxic v Media/Media, p < 0.05; Hypoxic/Media v Media/Media, p < 0.01)(Figure 3.16; A) or normoxic solution (6926 ± 303 RFU) (Hypoxic/Normoxic v Media/Normoxic, p < 0.01; Hypoxic/Media v Media/Normoxic, p < 0.001) (Figure 3.16; B) (as shown in graph E). To further determine the detection capabilities using spectroscopy, a sample of supernatant from H9C2 cells treated with either media, normoxic or hypoxic solution was measured to determine a baseline fluorescent reading, then a second supernatant sample was compared following the switching of solutions to either media or normoxic buffers (Figure 3.16; F). Only cells pre-treated with hypoxic solution followed by

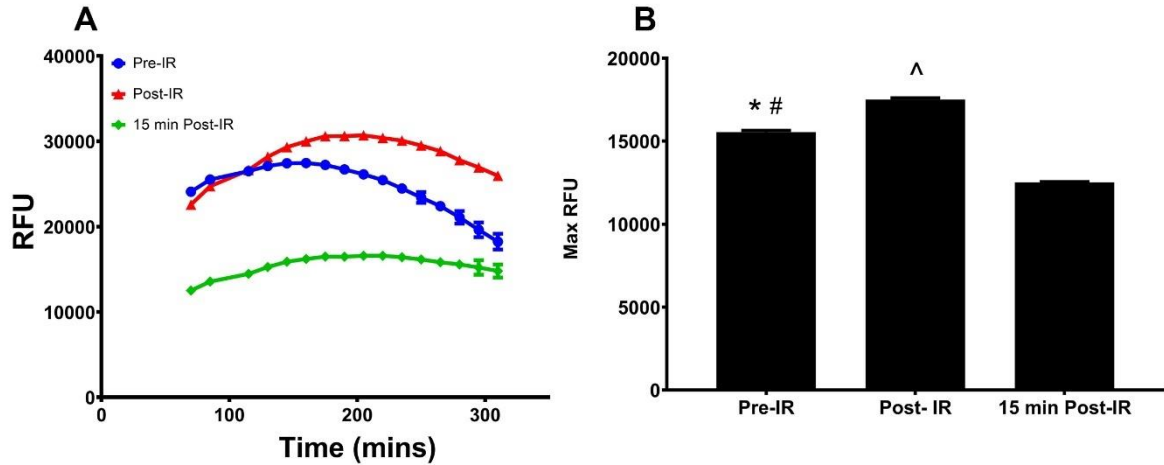
normoxic solution showed a significant fold-change increase (3.22 ± 0.57 fold) in fluorescent signal when compared to media/media treatment only (0.91 ± 0.12 fold) ($p < 0.05$) and media/normoxic treatment (1.3 ± 0.16 fold) ($p < 0.05$). This data suggests that after a period of hypoxia, HNO is released by H9C2 cells following the reintroduction of oxygen.

HNO has been implicated as a factor in the damage generated in cardiac tissue following ischemic reperfusion. Sensor 1 fluorescence signal was measured from rat aortic blood collected before ischemia (Pre-IR), immediately following reperfusion (Post-IR) and 15 min after reperfusion (15 min Post-IR), using spectroscopy (Figure 3.17; A). The mean RFU overtime was compared (Figure 3.17; B) and showed a significant increase in Sensor 1 fluorescent signal immediately following reperfusion (17509 ± 98 RFU), when compared to Pre-IR (15544.5 ± 106.5 RFU) ($p < 0.01$). Fifteen minutes following reperfusion, Sensor 1 fluorescent signal is significantly less (12508.5 ± 44.5 RFU) when compared to both Post-IR ($p < 0.0001$) and Pre-IR ($p < 0.001$). These data indicate that there is a temporal change in HNO production as it is increased immediately following the re-introduction of oxygenated blood to cardiac tissue which has undergone a period of ischemia, that then drops to below baseline levels shortly after. Together this data supports the use of Sensor 1 for the detection of endogenous HNO generated by *in vitro* and *in vivo* models of ischemic reperfusion injury.



Supplementary figure 3.16 HNO increased in H9C2 cells following hypoxic/normoxic treatment

Confocal images (60x) showing Sensor 1 fluorescent signal in H9C2 cells following media/media treatment (A), media/normoxic buffer treatment (B), hypoxic/normoxic treatment (C) and hypoxic/media treatment (D) (n = 3 per treatment). The bar graph E, represents the relative fluorescent signal (RFU) measured from 20 randomly selected cells within each frame and shows hypoxic treatment followed by normoxic solution or media, significantly increases Sensor 1 signal (** p < 0.01, *** p < 0.001, # p < 0.05, ## p < 0.01). A second experiment was carried out with the supernatant of both the 1st and 2nd treatment measured in the presence of Sensor 1 on a spectrophotometer (F). The fold change between conditioned media determined that H9C2 cells challenged with normoxic solution following a period of hypoxia gave a significant increase the fold change of signal of Sensor 1. Together this data suggests that HNO is released by H9C2 cells following the reintroduction of oxygen, following a period of hypoxia.



Supplementary figure 3.17 HNO increases in cardiac blood samples taken immediately following ischemic reperfusion injury.

Data showing the time-course of signal development of Sensor 1 from cardiac blood samples taken, before (blue line), immediately after (red line) and 15 mins post (green line) cardiac ischemic reperfusion injury (A) (n = 1). The mean RFU overtime was compared (B) and showed a significant increase in Sensor 1 fluorescent signal immediately following reperfusion, when compared to Pre-IR (*p < 0.01). Fifteen minutes following reperfusion, Sensor 1 fluorescent signal is significantly less (#p < 0.001) when compared to both Pre-IR and Post-IR (^p < 0.0001). These data indicate that there is a temporal change in HNO production as it is increased immediately following the re-introduction of oxygenated blood to cardiac tissue which has undergone a period of ischemia, that then drops to below baseline levels shortly after.

This page has been left intentionally blank.

Statement of Authorship

Title of Paper	Nitroxyl reduces Cathepsin B enzyme activity in both in vitro and in vivo models of neuropathic pain	
Publication Status	<input type="checkbox"/> Published <input type="checkbox"/> Submitted for Publication	<input type="checkbox"/> Accepted for Publication <input checked="" type="checkbox"/> Unpublished and Unsubmitted work written in manuscript style
Publication Details	Prepared for submission to Journal of Neuroscience	

Principal Author

Name of Principal Author (Candidate)	Vasiliki Staikopoulos		
Contribution to the Paper	Manuscript conception, generated data and figures, statistical analysis, and wrote manuscript.		
Overall percentage (%)	80%		
Certification:	This paper reports on original research I conducted during the period of my Higher Degree by Research candidature and is not subject to any obligations or contractual agreements with a third party that would constrain its inclusion in this thesis. I am the primary author of this paper.		
Signature		Date	2/9/2019

Co-Author Contributions

By signing the Statement of Authorship, each author certifies that:

- i. the candidate's stated contribution to the publication is accurate (as detailed above);
- ii. permission is granted for the candidate to include the publication in the thesis; and
- iii. the sum of all co-author contributions is equal to 100% less the candidate's stated contribution.

Name of Co-Author	Xiaozhou Zhang		
Contribution to the Paper	Provided expert advice towards design and execution of Cathepsin B activity assay.		
Signature		Date	4/9/19

Name of Co-Author	Elizabeth Beckett		
Contribution to the Paper	Provided expert advice on experimental design and reviewed manuscript.		
Signature		Date	3/9/2019

Please cut and paste additional co-author panels here as required.

Name of Co-Author	Mark R Hutchinson		
Contribution to the Paper	Assisted in manuscript conception, provided expert advice on experimental design and revised manuscript.		
Signature		Date	3/9/2019

Name of Co-Author			
Contribution to the Paper			
Signature		Date	

Name of Co-Author			
Contribution to the Paper			
Signature		Date	

Name of Co-Author			
Contribution to the Paper			
Signature		Date	

Name of Co-Author			
Contribution to the Paper			
Signature		Date	

Chapter 4. Nitroxyl reduces Cathepsin B enzyme activity in both *in vitro* and *in vivo* models of neuropathic pain.

This chapter is unpublished and unsubmitted work written in manuscript style.

4.1 Abstract

Peripheral nerve injury leads to spinal adaptations involving cysteine proteases which contribute to the development of neuropathic pain states. Using LPS treated BV2 cells and *in vivo* (chronic constriction injury; CCI) animal model of neuropathic pain we assessed the role of protonated nitric oxide species, nitroxyl (HNO; liberated from Angeli's salt), on enzymatic activity of the lysosomal cysteine protease, cathepsin B (CB), and downstream generation of metalloproteases MMP-2 and MMP-9 and the inflammatory cytokine IL-1 β . Further to this, we measured the effect of Angeli's salt (AS) on mechanical allodynia in sham and CCI-injured animals. AS was able to temporally reduce allodynia in injured animals 4 h following AS (3 mg/kg) administration. AS was also able to reduce CB activity in LPS stimulated BV2 cells and the spinal cord of both Sham operated and CCI-injured animals. Downstream proteins MMP-2 and MMP-9 were not altered in the spinal cord lysates by AS treatment and LPS stimulated IL-1 β protein increase was not inhibited by AS. The current findings support the use of HNO to inhibit CB enzyme activity, however quantitative protein analysis does not support the CB/MMP/IL-1 β pathway in regulating the anti-allodynia effects of HNO donor, AS.

4.2 Introduction

Neuropathic pain is a maladaptive type of chronic pain (Costigan M, et al., 2009) which affects approximately 2% of the adult population (Bennet, 1997; Bowsher, 1991). Described as "pain caused by a lesion or disease of the somatosensory nervous system" (IASP 2018), symptoms include; spontaneous pain (stimulus independent), allodynia (pain generated from non-noxious stimuli) and hyperalgesia (heightened sense of pain to noxious stimuli). Many adaptations occur within the dorsal horn of the spinal cord which lead to the development of neuropathic pain, hence previous studies have focused on understanding central nervous system (CNS) mechanisms for the development and treatment of the disease.

It is well understood that the reactive nitrogen species, nitric oxide (NO), is increased within the CNS following peripheral injury and can contribute to neuropathic pain signalling via several pathways (Bian K, 2016; Schmidtko A, et al., 2009). The soluble guanylate cyclase (sGC)

pathway has been implicated as a key pathway in neuropathic signaling, with studies demonstrating that modulation of NO/sGC/cGMP/PKG components can reduce symptoms of neuropathic pain (Schmidtko A, et al., 2008; Song XJ, et al., 2006; Ferreira J, et al., 1999). Recently nitroxyl (HNO), the reduced, protonated form of NO, was also reported to reduce neuropathic pain symptoms via the cGMP-PKG-K⁺ pathway (Longhi-Balbinot DT et al, 2016), suggesting that alternate reactive nitrogen species contribute to neuropathic pain signalling. Others suggest HNO may reduce chronic pain symptoms via alternative mechanisms, such as by reducing the enzymatic activity of the lysosomal cysteine protease, Cathepsin B (CB) (Väänänen AJ, et al., 2018). Cysteine cathepsins have been implicated in the development of neuropathic pain (Barclay J, et al., 2007; Abbadiea C, et al., 2009). A proposed mechanism involves the cathepsin B-mediated inactivation of MMP-9 and MMP-2 inhibitors, Tissue inhibitor matrix metalloproteinase 1 and 2 (TIMP1 and TIMP2) (Kostoulasa G., et al, 1999). MMP-9, released from the spinal terminals of DRG neurons, and MMP-2, released due to astrocytic activation, potentiate the cleavage of pro-IL-1 β to the inflammatory cytokine IL-1 β , which is associated with increased excitatory synaptic signalling (Kawasaki Y, et al., 2008; Schönbeck U, et al., 1998). Hence, cathepsin B may contribute to chronic pain by promoting the release and cleavage of IL-1 β (Schotte et al., 1998; Hentze et al., 2003; Terada, et al., 2010). However, a direct relationship between HNO and reduction of neuropathic pain via cathepsin B inactivation has yet to be explored. Therefore, we aimed to determine if HNO reduces *in vivo* activity of CB and can lead to changes in expression of MMP-9, MMP-2 and IL-1 β in cellular and animal models of neuropathic pain.

4.3 Methods

4.3.1 Chemicals and assays.

Angeli's salt (Cayman Chemicals, Ann Arbor, MI) was used as an HNO donor and added to either cell-culture media or injected subscapular *in vivo*, to initiate the release of HNO. To produce an appropriate stock solution of the HNO donor, Angeli's salt was dissolved in ice-cold 10 mM NaOH. Both salt and stock solutions were stored at -80°C. Unless otherwise specified, all other kits or reagents were obtained from Sigma-Aldrich (St. Louis, MO).

4.3.2 Enzymatic assay to determine exogenous Cathepsin B activity

The direct effect of HNO on CB enzymatic activity was determined by fluorometric assessment of 7-amino-4-methylcoumarin (liberated from the Cathepsin B substrate Z-Arg-Arg-7-amido-4-

methylcoumarin; Z-Arg-Arg-AMC) using spectroscopy. The protocol outlined below was adapted from the Sigma-Aldrich recommended protocol ([Appendix 1](#)). CB is a lysosomal cysteine protease which will hydrolyse proteins by preferential cleavage at the carboxyl side of Arg-Arg bonds in small molecule substrates. It has been suggested that HNO may exert its biological effect via the oxidised cysteine residues on proteins, therefore this assay was used to test this hypothesis. Increasing amounts of HNO donor, Angeli's salt (to achieve concentrations of 0, 0.05, 0.26, 1.3, 6.6, 30, 150 μ M) were added to the CB enzyme solution (5-10 units/ml) in the presence of Z-Arg-Arg-AMC (0.02 mM) and the resulting fluorescence measured using a spectrophotometer at $\lambda_{ex/em} = 348/440$ nm. Absence of Z-Arg-Arg-AMC and the addition of the HNO scavenger L-cysteine (150 μ M) were used as controls.

4.3.3 Cell culture

Immortalized BV2 cells from a murine microglial cell line were cultured in Dulbecco's modified Eagle's medium (DMEM; Sigma-Aldrich) supplemented with 10% fetal bovine serum (FBS; Gibco, ThermoFisher-Scientific), 100 IU/ml penicillin, 100 μ g/ml streptomycin, (Penicillin-streptomycin; Sigma-Aldrich) 2 mM L-glutamine (Gibco, ThermoFisher-Scientific) and 100 μ g/ml Normocin (InvivoGen). Cells were maintained at 37°C in a saturated humidity atmosphere containing 95% air and 5% CO₂ and used for assays when 75-80% confluent. To prepare samples for spectrophotometer experiments, 10,000 cells/ml of BV2 cells were seeded in poly-D-lysine coated 96 well plate (triplicate) in 200 μ l of media per well. To prepare cell lysates for western blot experiments, 75,000 cells/ml of BV2 were seeded in poly-D-lysine coated 6 well plates (triplicate) in 2 ml of media and allowed to adhere overnight. To prepare samples for confocal imaging, BV2 cells (50,000 cells/ml) were seeded in 8 well Ibidi slides (Cat: 80826, Ibidi, DAKO Australia) in 300 μ l of media per well.

4.3.3.1 Cell experiments

Experiment series 1: The following fluorogenic experiments were conducted in triplicate wells. For CB enzyme assay, BV2 cells were treated with LPS (500 ng/ml) or vehicle (sterile PBS 0.01M) and incubated for 24 h at 37°C. Increasing concentrations of Angeli's salt (0, 50, 100 & 150 μ M) were added to either vehicle or LPS treated cells for the last hour of incubation and kept at 37 °C. Study design: 2 (LPS v Veh) by 4 (Veh, 50, 100 and 150 μ M AS).

Experiment series 2: The following fluorogenic experiments were conducted in triplicate wells. For Cathepsin B enzyme assay experiments, HNO scavenger, L-cysteine (1 mM) was added in

control wells 30 min prior to the addition of AS/vehicle following a 24 h treatment with LPS (100 ng/ml). Study design: 2 (LPS v Veh) by 2 (AS v Veh) by 2 (L-cysteine v Veh).

Experiment series 3: The following western blot experiments were conducted in triplicate. BV2 cells were incubated with LPS (100ng/ml) for 4 h at 37 °C, followed by a 1 h incubation with AS (10, 50, 100 or 200 µM) with or without a 30-minute L-cysteine (1 mM) pre-treatment. Control conditions included AS incubation alone, L-cysteine incubation alone or vehicle (PBS 0.01 M) only treatment. Study design: 2 (LPS v Veh) by 4 (Veh, 50, 100 and 150 µM AS) by 2 (L-cysteine v Veh).

At the end of each experimental protocol outlined above, cells were washed with ice cold PBS (0.01M) and lysed with ice cold lysis buffer and samples collected for either cathepsin B enzyme assay or western blot analysis, described in detail below.

4.3.4 Animal experiments

Male C57B6J mice (8-10 weeks old) were used in all experiments, unless otherwise specified. All mice were maintained under a specific pathogen-free (SPF) barrier facility at the University of Adelaide, Laboratory Animal Services, with *ad libitum* access to food and water and maintained on a 12 h light /12 h dark cycle. All experimental procedures were performed in accordance with the National Health and Medical Research Council Australian code for the care and use of animals for scientific purposes (8th edition, 2013) and the University of Adelaide Animal Ethics Guidelines, and were approved by the University of Adelaide Animal Ethics Committee (Application number: M-2016-123).

4.3.4.1 Experimental protocol

All animals were acclimatised for 7 days following arrival to the animal facility prior to starting experimentation (Table 1). Following the acclimatisation period, animals were habituated to the behavioural testing set-up for 3-5 days prior to testing. Animals underwent baseline behavioural testing (Baseline) to determine their mechanical withdrawal threshold. The following day (Day 0), animals underwent surgery (details in section 4.3.4.2) and were followed up with subsequent behavioural testing assessments (post-surgery Days 1, 3, 5 & 7). On Day 7 following the initial behavioural testing assessment, animals were injected with either vehicle (10 µM NaOH), AS (0.3, 1 or 3 mg/kg s.c.) and/or pre-treated with vehicle (0.9% saline) or L-cysteine (1 mg/kg i.p.) and returned to their home cage for 4 h before a second behavioral assessment was conducted.

Study design: 2 (CCI v Sham) by 4 (Veh, 0.3, 1 & 3 mg/kg AS) by 2 (L-cysteine v Veh). A 24 h follow up behavioural assessment was performed on Day 8, then animals were humanely killed by sodium pentobarbital (60mg/kg; i.p.) overdose and the lumbar 3-5 spinal segments were rapidly removed and kept on ice, hemisected into left (ipsilateral) and right (contralateral) segments, snap frozen in 100 µl of cell lysis buffer and stored at -80°C until required. A timeline of the experimental protocol is shown below, $n = 6$ animals were used in each group.

Table 1: Protocol Timeline

Day	Day -1	Day 0	Day 1, 3, 5 & 7	Day 7	Day 8
Protocol	Baseline behavioural testing	Surgery	Behavioural testing	Treatment injection(s) followed by 4 h post-injection behavioural testing	Behavioural testing followed by tissue collection

4.3.4.2 Graded chronic constriction injury (CCI) model

The CCI model of sciatic nerve injury was performed aseptically at the mid-thigh level of the left hind-leg, as previously described (Walczak et al, 2006; Grace et al., 2010; Kwok et al., 2013), in order to produce clinically relevant pain behaviour. Briefly, animals were anesthetized with 2% isoflurane, the skin of the hindquarters was shaved and the sciatic nerve gently elevated using glass hooks. Zero or 3 sterile chromic gut sutures (cuticular 4-0 chromic gut; Ethicon, Somerville, NJ, USA) were loosely tied around the isolated sciatic nerve (N; approximately 3–4 mm in length). Once the superficial muscle overlying the nerve was sutured with silk, and prior to surgical stapling of the skin incision, additional equal lengths of chromic gut were placed subcutaneously (S; approximately 3 – 4 mm in length), such that each animal was exposed to four equal lengths of chromic gut in total. Thus, the surgery treatment groups, differing in pain behaviour, were sham (N0S4) and medium-high pain (N3S1).

4.3.4.3 von Frey mechanical allodynia behavioural testing

The von Frey test was used to investigate mechanical allodynia using phasic stimulation of von Frey filaments across a range of thresholds. Briefly, mice were subjected to 10 stimulations with 6 calibrated von Frey filaments (0.04, 0.07, 0.16, 0.4, 0.6 & 1 grams of force). Von Frey filaments were applied for 1 s at 1 s intervals in random force assignment at each test session as described by Nicotra *et al* (2014). In order to avoid sensitization, a 10-minute break was given between each set of simulations. The von Frey test investigated the response frequency when each gauge of von Frey filament was applied, and behavioural responses were recorded as the

average number of responses out of 10 for each von Frey filament. Behavioural testing days are outlined in section 4.3.4.1.

4.3.4.4 Tissue collection and preparation

Animals were humanely killed by sodium pentobarbital (60mg/kg; i.p.) overdose, following behavioural testing on Day 8 post-surgery. The lumbar region of the spinal cord was quickly excised, rinsed with ice cold PBS (0.01M) and placed onto an inverted glass petri dish over ice. The section was trimmed to only contain lumbar regions 3-5 and hemisected into left (ipsilateral) and right (contralateral) samples, placed into a 1.5 ml microtube, snap frozen in liquid nitrogen and stored at -80°C until required. Once all required samples were collected, ipsilateral samples were thawed on ice with 100 µl of cell lysis buffer (provided by Cathepsin B enzyme assay kit) and homogenised using a probe homogeniser for 10 sec, followed by 1 min on ice. Samples were then left on ice for 30 min before being centrifuged at 20,000 x g for 5 min at 4°C and the supernatant collected into a clean 1.5 ml microtube. Samples were either kept on ice if immediately used or stored at -80°C until required.

4.3.5 Cathepsin B enzyme assay

Samples collected from both cell and animal experiments were assessed to measure CB enzymatic activity present using a commercial fluorometric kit (Abcam Australia, ab65300). Briefly, the protein concentration of each tissue sample was measured using a colourmetric BCA protein assay kit (Pierce, ThermoFisher-Scientific). 50 µg of tissue protein was added (in triplicate) to a black 96 well plate and the volume adjusted to 50 µl using cell lysis buffer. For cell experiments, 50 µl of each sample was added to each well. The remaining protocol was the same with CB reaction buffer (50 µl) added to each well followed by the cathepsin B substrate (Ac-RR-AFC, 2 µl) and the samples incubated at 37°C for 2 h. The resultant fluorescence was measured using a BioTek SynergyMx spectrophotometer at $\lambda_{ex/em} = 400/505$ nm. Relative fluorescence values were compared between treatment groups.

4.3.6 Western Blotting

Western blot analysis was used to determine the relative abundance of the following proteins in both cell and tissue lysate samples; interleukin-1b (IL-1b; pro- 31 kD, mature- 17 kD), cathepsin B (38 kD), metalloprotease 2 (MMP-2; 72 kD), metalloprotease 9 (MMP-9; 102-105 kD) and beta-actin (β -actin; 42 kD). The protein concentration of both cell and tissue lysate samples were measured using a colourmetric BCA protein assay kit (Pierce, ThermoFisher-Scientific).

Samples were prepared with an equal volume of standard 5x Laemmli buffer (80 mM SDS, 10% glycerol, 50 mM DTT, 0.004% bromophenol blue, 63 mM Tris-HCl) and boiled for 10 minutes at 100°C, before 20 µg of protein was loaded into 4–12% gradient SDS-PAGE gels (NUPAGE, ThermoFisher-Scientific) and transferred to nitrocellulose membranes, which were blocked with skim powdered milk (5% in Tris-buffered saline). Immunoreactive proteins were visualized with antibodies to goat anti-mouse cathepsin B (0.2 µg/ml, AF965; R & D systems), rabbit anti-human MMP-2 (2 µg/ml, ab37150; Abcam Australia), rabbit anti-mouse MMP-9 (2 µg/ml, ab38898; Abcam Australia), rabbit anti-mouse IL-1b (1 µg/ml, ab9722; Abcam Australia) (used for cell lysate samples only) and anti-rabbit β-actin (0.1 µg/ml, A2066; Sigma-Aldrich, Australia) incubated overnight at 4°C, followed by secondary antibody incubation for 1 h at room temperature with donkey anti-rabbit IgG IRDye 680 (0.01 µg/ml, Millennium Science, Australia) or donkey anti-goat IgG Dye Light 800 (0.01 µg/ml, Invitrogen, ThermoFisher-Scientific). The fluorescent bands were detected and quantified using Licor Odyssey CLx scanning system at excitation/ emission wavelengths $\lambda_{ex/em} = 680/694$ nm and $\lambda_{ex/em} = 794/778$ nm respectively. Band intensities were normalised against loading control (βActin) and then compared between treatments for each protein.

4.3.7 Immunohistochemistry

In a separate set of experiments, male CX3CR1^{gfp+} (Kindly provided from Dr. Peter Psaltis, SAHMRI, originally from Jackson Laboratories) mice (8-10 weeks old) were used to generate tissue for IHC. Nine animals underwent the same protocol as outlined in Experimental Protocol section with an $n = 3$ animals in each of the following treatment groups; CCI surgery + Angeli's salt (3 mg/kg) Day 7, CCI surgery + Vehicle (0.01M NaOH) or Sham surgery + no injection. At the end of Day 8, animals were humanely killed by overdose with sodium pentobarbital (60 mg/kg; i.p.) and perfused with PBS (0.01M) followed by ice cold 4% paraformaldehyde (PFA, pH 7.2). The lumbar spinal cord regions (L3-L5) were removed and placed in 4% PFA overnight at 4°C, followed by 3 x 10 min washes with PBS and 1-2-day incubation at 4°C with PBS-sucrose (20%) for cryoprotection. The tissues segments were frozen in OCT (ProSciTech, Australia), sectioned (in triplicate for each animal) using a Leica cryostat at 10 µm, mounted on SuperFrost® glass microscope slides (Menzel-Gläser; Braunschweig, Germany) and processed for IHC. Briefly, following 1 h air drying, sections were rinsed with PBS to remove residual OCT and incubated for 1 h at room temperature with blocking solution (1% BSA 0.3% TritonX in 0.01 M

PBS). Following the blocking step, sections were incubated for 2 nights at 4°C in primary antibodies goat-anti cathepsin B (0.2 µg/ml, AF965; R&D Systems) and rabbit-anti NeuN (0.1 µg/ml; ab177487, Abcam Australia). After washing, sections were incubated for 1 h at room temperature with donkey anti-goat Alexa Fluor® 594 secondary antibody (0,01 µg/ml , A21203; Invitrogen, ThermoFisher-Scientific) and donkey anti-rabbit Alexa Fluor® 647 (0,01 µg/ml, ab150063; Abcam, Australia). Sections were washed using PBS (0.01 M) 3 ×10 min before adding DAPI nuclear stain (0.1 µg/ml, ThermoFisher Scientific) for 5 minutes at room temp before final washes with PBS (0.01 M) 3 × 10 minutes. All sections were mounted with Tris-based Fluoro-Gel medium (IM030; ProSciTech; Queensland, Australia).

4.3.8 Live cell preparation and Cathepsin B staining

BV2 cells (10,000 cells/well) were seeded in 96 well culture plates and left overnight to adhere. To triplicate wells, cells were incubated with either LPS (500 ng/ml) or vehicle (PBS 0.01M) for 24 h at 37°C. At the 23 h timepoint, AS (200 µM) was added to either LPS treated or vehicle treated cells for 1 h at 37°C. At 24h, the intracellular cathepsin B enzymatic activity was assessed by incubation with the fluorogenic substrate, Magic Red® Cathepsin B assay (#ICT938, Immunochemistry Technologies, Bio-Rad, Australia). Briefly, cells were incubated with the Magic Red substrate for 1 h at 37°C, before rinsing the cells with PBS and adding Hoechst (33342) nuclear stain for a further 10 min. After a final rinse with PBS, fluorescence was captured on an Olympus FV3000 laser scanning confocal using the live cell system (heated and oxygenated stage) using appropriate lasers and filters (Magic Red $\lambda_{ex/em}$ = 550-590/610 nm, Hoechst $\lambda_{ex/em}$ = 365/480 nm).

4.3.9 Confocal acquisition

Immunohistochemistry: Slides were viewed with an Olympus FV3000 scanning confocal microscope (Olympus; Japan) using a 20x objective (NA 0.75) and appropriate excitation wavelengths (Alexa Fluor® 594 $\lambda_{ex/em}$ = 592/619 nm, Alexa Fluor® 647 at $\lambda_{ex/em}$ = 645/660 nm, DAPI nuclear stain $\lambda_{ex/em}$ = 350/470 nm and GFP protein $\lambda_{ex/em}$ = 488/510 nm) Images were acquired using FLUOVIEW FV3000 software (Olympus; Japan). Final images (1024 x 1024 pixels) are digital composites of 1.5 - 2 µm Z-series scans (approximately 4 optical sections through a depth of 6-8 µm). All images per antibody label were taken at the same gain and offset parameters between animals. Each spinal dorsal horn per section (both ipsilateral and contralateral) was imaged separately.

Live cell cathepsin B enzyme Magic Red® assay:

Ibidi slides (Cat: 80826, Ibidi, DAKO Australia) containing BV2 cells, were viewed with an Olympus FV3000 scanning confocal microscope (Olympus; Japan) using a 60x objective oil immersion lens (NA 1.4) and appropriate excitation wavelengths (Magic Red: $\lambda_{ex/em}$ = 550-590/610 nm, Hoechst: $\lambda_{ex/em}$ = 365/480 nm). Images were acquired using FLUOVIEW FV3000 software (Olympus; Japan). Final images (512 x 512 pixels) are digital composites of 1.5 μ m Z-series scans (approximately 9 optical sections through a depth of 13.5 μ m). All images per antibody label were taken at the same gain and offset parameters between treatment.

4.3.10. Image analysis

Immunohistochemistry

Semiquantitative analyses were performed on collected images using ImageJ Fiji software (ImageJ 1.52n, NIH, USA). All images were examined blinded as to animal treatment. Maximized Z-stack of images were converted from Olympus image files (.oir) to 8-bit greyscale (.jpg) images, and signal pixels of positive staining areas in the region of interest (ROI) were selected. The ROI was an ellipsoid shape that remained a consistent size for each triplicate image between animals and was positioned over laminae I-V. The number of cells within the ROI and/or percentage of immunofluorescence in the ROI was calculated. The duplicate area measurements for each dorsal horn were averaged to obtain a single percentage area value per ipsilateral and contralateral dorsal horn, per animal.

Live cell cathepsin B enzyme Magic Red® assay:

Semiquantitative analyses were performed on collected images using ImageJ Fiji software (ImageJ 1.52n, NIH, USA). All images were examined blinded as to animal treatment. Maximized Z-stack of images were converted from Olympus image files (.oir) to 8-bit greyscale (.jpg) images, and signal pixels of positive staining areas in the region of interest (ROI) were selected. The ROI was the outline of 40 cells selected using the DIC image and added to the ROI manager. The mask outline was then applied to the other channels and the mean integrated density (sum of the value of the pixels) within each cell was measured.

4.3.11 Statistical analysis

Data were analysed using GraphPad Prism 7 software (GraphPad Software, Inc. La Jolla, CA, USA). The Shapiro-Wilk or Kolmogorov-Smirnov normality test was used to test the normality of data distribution. One-way ANOVA was used to compare three or more groups and the *p-values*

for significant differences were derived from relevant post-hoc test for multiple comparisons. A two-way ANOVA was used to compare multiple treatments across groups and *p-values* for significant differences were derived from relevant post-hoc test for multiple comparisons. Where applicable, linear regression was used to determine the slope of a line. All data are reported as mean \pm standard error of the mean (SEM), along with the individual data points where relevant to demonstrate biological variability. Significance was set at $p < 0.05$

4.4 Results

4.4.1 Nitroxyl deactivates exogenous Cathepsin B enzyme

The enzymatic activity of the CB enzyme (provided from an exogenous source) in the presence of HNO donor was assessed by fluorogenic substrate and measured using spectroscopy. Angeli's salt (AS) was used as an HNO donor and tested at concentrations ranging from 0 to 150 μM (Figure 4.1). The presence of HNO was able to significantly reduce fluorescent signal $F(7, 152) = 947.3$, $p < 0.0001$) as determined by the change in slope over time. Furthermore, the half maximal inhibition concentration (IC₅₀) of Angeli's salt was determined as 41.32 μM . This data, reported for the first time, shows that HNO can directly inhibit CB enzyme activity.

4.4.2 Nitroxyl inhibits LPS derived Cathepsin B enzyme activity in BV2 cells

Following the chemistry-based demonstration of HNO inhibition of exogenous CB enzyme activity, *in vitro* experiments were conducted to evaluate the effects of HNO on endogenous CB activity by LPS (inflammatory agent) challenge of mouse microglia-like cells. BV2 cells were incubated with LPS (500 ng/ml) for 24 h followed by a 1 h incubation with increasing concentrations of AS. CB enzyme activity was measured in cell homogenates using a commercially available fluorometric assay (Figure 4.2). LPS treatment produced a significant increase in fluorescence (2534 ± 109.6 RFU; $p < 0.0002$) compared to vehicle (827 ± 75.2 RFU), which was decreased in the presence of AS in a concentration dependant manner (50 μM AS, 1714 ± 46.5 , $p < 0.0001$; 100 μM AS, 1232 ± 103.5 , $p < 0.0001$; 150 μM AS 1333 ± 56.6 , $p < 0.0001$) (Figure 4.2A). AS alone had no effect on fluorescence on vehicle treated cells (50 μM AS, 798 ± 17.6 , $p > 0.05$; 100 μM AS, 740.3 ± 17.7 , $p > 0.05$; 150 μM AS 712.3 ± 35.7 , $p > 0.05$). To determine if this response was specific to AS, an additional series of experiments was conducted in which BV2 cells were pre-treated with HNO scavenger, L-cysteine (1 mM) for 30 minutes prior to the addition of AS (Figure 4.2B). On LPS (100 ng/ml) treated cells, pre-treatment with L-cysteine (1 mM) effectively abolished the attenuating effect of AS (200 μM) on CB

fluorescence (i.e. LPS only: $17,228 \pm 907$ RFU; LPS + AS: $13,451 \pm 340$ RFU ($p < 0.05$) and L-cysteine + LPS + AS: $25,200 \pm 2964$ RFU ($p < 0.01$ compared to LPS + AS). Control experiments revealed that LPS treatment alone ($17,228 \pm 907$ RFU) and L-cysteine alone ($15,216 \pm 403.7$ RFU) were sufficient to increase CB fluorescence above that detected from naïve, untreated cells (4279 ± 830 RFU, $p < 0.01$ for both comparisons). In contrast, application of AS alone did not elicit an increase in CB fluorescence above that of untreated cells (AS only: 8634 ± 565 RFU; Untreated cells: 4279 ± 830 RFU, $p > 0.05$). To understand the relationship between LPS and AS concentrations in affecting CB enzyme activity, two LPS (10 & 100 ng/ml) concentrations were compared with increasing concentrations of AS. Data showed a right-wards shift in IC₅₀ (LPS 10 ng/ml, IC₅₀ 28.7 μ M; LPS 100 ng/ml, IC₅₀ 77.8 μ M) with increasing concentration of LPS, indicating that a higher concentration of AS is required to reduce the CB fluorescent signal (Figure 4.2C).

To determine the intracellular localisation of these changes in CB enzymatic activity within live cells, non-toxic intracellular fluorogenic substrate Magic Red®, was incubated with BV2 cells treated with LPS (100 & 1000 ng/ml) for 24 h, followed by a 1 h incubation with AS (200 μ M). Cells were counterstained with Hoechst nuclear stain to identify cell nuclei. Representative confocal images are shown in Figure 4.3A. The Magic Red® CB enzyme staining was localised to the cytoplasm of BV2 cells, with dense patches of punctate staining observed just outside the nucleus. The mean integrated density (IntDens) of 40 cells per image, 3 images per treatment, were measured (Figure 4.3B). Results demonstrated that AS was able to significantly reduce the IntDens of 1000 ng/ml LPS incubated cells (LPS only: 7465 ± 487 RFU compared to AS + LPS: 5462 ± 333 RFU; $p < 0.01$), but not following 100 ng/ml LPS treatment (LPS only: 7731 ± 439 RFU compared to AS + LPS 7276 ± 405 RFU; $p > 0.05$). These data indicate that whilst an AS-mediated reduction in LPS induced CB enzyme activity can be detected in intact living cells, more robust changes in enzymatic activity were resolved via the homogenate-based CB assay.

4.4 3 Cathepsin B or IL-1 β protein levels are not altered by LPS treatment in BV2 cells

To determine if observed changes in CB enzyme activity was due to alterations in protein production, western blot analysis of BV2 lysates was conducted (Figure 4.4). Western blot analysis determined that there was no change in CB protein levels caused by any of the treatment conditions compared to control (Figure 4.4A). To address the hypothesis that HNO inhibition of CB enzyme ultimately leads to decreased IL-1 β production, we quantified IL-1 β

protein levels and found that 24 h LPS (100 ng/ml) increased IL-1 β levels in BV2 cells (ratio 1.5 ± 0.13 relative to β -actin compared to 0.26 ± 0.02 in control cells, $p < 0.0001$), but this increase was not altered by a 1 h AS incubation (ratio 1.5 ± 0.06 , $p > 0.05$) (Figure 4.4B).

4.4.4 Nitroxyl reduces neuropathic pain symptoms in mice.

To determine the *in vivo* effect of HNO on neuropathic pain symptoms, a modified chronic constriction injury model was used as described by Grace *et al* (2010). Mechanical allodynia was assessed in mice with (CCI) or without (Sham) injured sciatic nerves until Day 7 post-surgery, using 6 varied strength von Frey filaments adjusted for mouse weight, and applied to the hind paw as described by Nicotra *et al* (2014) (Figure 4.5). Data collected shows allodynia at Day 7 generated by lighter hairs (0.04 g, $10 \pm 2.6\%$; 0.07 g, $15 \pm 2.4\%$; 0.16 g, $21.6 \pm 3.7\%$) in the ipsilateral hind paw of CCI animals when compared to baseline (0.04 g, $0.8 \pm 0.5\%$, $p < 0.05$; 0.07 g, $2.9 \pm 1.4\%$; $p < 0.01$; 0.16 g, $2.9 \pm 1.1\%$, $p < 0.001$). Allodynia was not present in Sham operated animals at Day 7 (Figure 4.5A). A closer inspection of hair strength responses found that hair weighted 0.16 g gave the greatest percentage change in mechanical withdrawal in CCI animals at Day 7 compared to pre-surgery baseline (Day 7: $21.6 \pm 3.7\%$; Baseline: $2.9 \pm 1.1\%$, $p < 0.001$) (Figure 4.5B). To assess the effect on HNO on established allodynia, a subscapular injection of AS (0.3, 1 & 3 mg/kg; as described by Longhi-Balbinot *et al*, 2016) or vehicle (10 μ M NaOH) was given to both CCI and Sham operated animals immediately after behavioural testing in the morning of Day 7 and the animals were returned to their home cages and allowed full access to food and water and monitored for changes in general behaviour. At 4 h and 24 h post-injection, animals underwent subsequent behavioural testing. We observed a significant reduction in mechanical withdrawal response at 4 h post-injection of AS (3 mg/kg) for von Frey filament weights: 0.04, 0.07, 0.16, 0.4 g (0.04 g, $5 \pm 3.4\%$; 0.07 g, $11\% \pm 6\%$; 0.16 g, $6.6 \pm 3.3\%$; 0.4 g, $16.6 \pm 6.6\%$) (Figure 4.5C) when compared to pre-injection (0.04 g, $26.6 \pm 5.5\%$; $p < 0.01$; 0.07 g, $28.3 \pm 3\%$; $p < 0.05$; 0.16 g, $35 \pm 4.2\%$; $p < 0.0001$; 0.4 g, $35 \pm 9\%$, $p < 0.05$), but not the 24 h timepoint (0.04 g, $23.3 \pm 8.4\%$; 0.07 g, $20 \pm 5\%$; 0.16 g, $28.3 \pm 6\%$; 0.4 g, $28.3 \pm 4.7\%$). Vehicle injections did not alter behavioural responses in either CCI or sham operated animals, and AS injections did not change behavioural responses in sham operated animals. Lower concentrations of AS (0.3 & 1 mg/kg) did not produce a significant decrease in mechanical withdrawal response (data not shown). In a separate group of animals, the specificity of the reduced allodynic response to AS was assessed by a pre-injection (i.p) of HNO scavenger,

L-cysteine, 30 minutes prior to AS or vehicle (10 μ M NaOH) injection (Figure 4.5d). L-cysteine abolished the reduced allodynic change generated by AS at the 4 h timepoint.

4.4.5 Nitroxyl reduces Cathepsin B enzyme activity in mouse spinal cord

To determine whether HNO administration affected CB enzyme activity in the homogenates of ipsilateral lumbar 3-5 spinal segments of these mice, a fluorogenic assay was used (Figure 4.6). CB activity (reported as RFU) was significantly reduced following AS administration at all concentrations in both CCI [Vehicle: 19074 ± 1377 ; 0.3 mg/kg AS: 12724 ± 675 ($p < 0.0001$); 1 mg/kg AS: 13993 ± 608 ($p < 0.001$); 3mg/kg AS: 12945 ± 743 ($p < 0.0001$)] and Sham operated mice [Vehicle: 15684 ± 767 ; 0.3 mg/kg AS: 11756 ± 884 ($p < 0.05$); 1 mg/kg AS: 12027 ± 518 , $p < 0.05$; 3 mg/kg AS: 11702 ± 866 ($p < 0.05$)].

4.4.6 HNO reduces CX3CR1 expression but not cathepsin B in mouse spinal cord of CCI - injured animals

To further assess the localisation of CB protein within the spinal cord of CX3CR1^{gfp+} mice (which express GFP within macrophage and microglial cells), immunohistochemical assessment was performed in CCI and sham operated animals. Spinal cords collected on Day 8 post-surgery were stained using the nuclear stain DAPI and antibodies to the neuron-specific nuclear protein NeuN and cathepsin B (CB). Representative confocal images are shown in Figure 4.7.1. Image overlay showed that CB protein was predominately co-localised with NeuN positive cells (white arrowhead) and was also detected in some GFP expressing microglia (white arrowhead with asterisk) (Figure 4.7.2). The mean pixel intensity and number of cells of GFP, Cathepsin B and NeuN in laminae I-V (pain processing regions) of both the ipsilateral and contralateral sides of the spinal dorsal horn were assessed. As this was a global focus within the dorsal pain processing region, no further analysis was done to look at specific laminae outside these regions. Mean percentage of GFP positive cells (%GFP positive cells) and mean pixel intensity of GFP was higher in ipsilateral dorsal horn of CCI operated animals (%GFP positive cells, $6.4\% \pm 0.3$; Mean pixel intensity, 2050 ± 59 RFU) compared to contralateral dorsal horn (%GFP positive cells, $11.7\% \pm 0.2$; Mean pixel intensity, 1659 ± 134 RFU), AS treated CCI ipsilateral dorsal horn (%GFP positive cells, $8.4\% \pm 0.8$; Mean pixel intensity, 1673 ± 117 RFU) and sham ipsilateral dorsal horn (%GFP positive cells, $8.7\% \pm 1.6$; Mean pixel intensity, 1268 ± 94.5 RFU) (Figure 4.7.3a/b). Cathepsin B mean cell percentages (%CB positive cells) and mean pixel intensity, were unchanged between all treatment groups (Table 2a). The mean percentage and mean pixel

intensity of NeuN positive cells did not change between treatment groups (Figure 4.7.2e/f) (Table 2b).

Table 2a %CB positive cells and mean pixel intensity values (RFU)

	Sham ipsi	Sham contr	CCI ipsi	CCI contr	CCI AS ipsi	CCI AS contr
%CB pos cells	43.18 ± 2.3	61.87 ± 4.6	41.73 ± 6.1	47.39 ± 7.8	53.74 ± 7.9	50.14 ± 2.1
Mean Pixel Intensity	1412 ± 213	1306 ± 205	1866 ± 173	1898 ± 131	1312 ± 236	1248 ± 236

Table 2b %NN positive cells and mean pixel intensity values (RFU)

	Sham ipsi	Sham contr	CCI ipsi	CCI contr	CCI AS ipsi	CCI AS contr
%NN pos cells	64.79 ± 1.9	66.11 ± 2.3	69.87 ± 5.2	65.38 ± 3.1	66.93 ± 3.4	62.58 ± 3.9
Mean Pixel Intensity	1479 ± 215	1443 ± 158	1556 ± 60.6	1668 ± 84.6	1134 ± 74.3	1034 ± 202

4.4.7 Nitroxyl treatment did not change Cathepsin B, MMP-2 and MMP-9 protein levels

To determine the changes in proteins which may be involved in downstream signalling of CB enzyme within the spinal cord, western blot analysis of ipsilateral tissue homogenates was conducted (Figure 4.8). Western blot data showed no significant changes in protein ratios of CB, MMP-2 or MMP-9 when comparing CCI operated animals to sham controls in the presence or absence of AS. However, the L-cysteine pre-treatment followed by AS injection, resulted in a decrease in MMP-9 in both sham (0.44 ± 0.05) and CCI animals (ratio 0.51 ± 0.12), when compared to CCI + AS injection only (ratio 1.14 ± 0.13, $p < 0.01$).

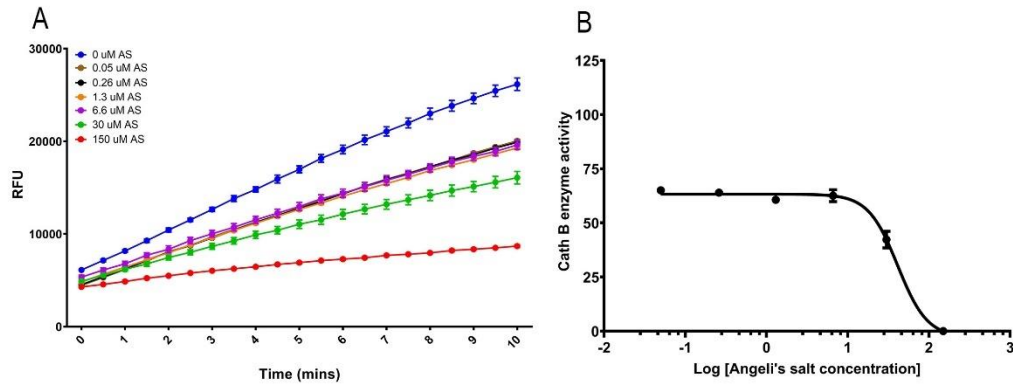


Figure 4.1 HNO inhibits exogenous Cathepsin B enzyme activity.

Fluorometric measure of exogenous Cathepsin B enzymatic activity over time in the presence of a range of Angeli's salt (HNO donor) concentrations (A). In the absence of Angeli's salt, fluorescence increased over the 10 min acquisition time (as shown by blue line). As the concentration of Angeli's salt was increased, the extent by which fluorescence increased from $T = 0$ to $T = 10$ min was attenuated ($F(7, 152) = 947.3, p < 0.0001$). B) Inhibition of Cathepsin B enzyme activity by Angeli's salt after 10 minutes of incubation time. Increasing concentration of Angeli's salt (log conc 0 – 150 μM) was added to cathepsin B enzyme (5-10 units/ml). The half maximal inhibition concentration of Angeli's salt was calculated at 41.32 μM .

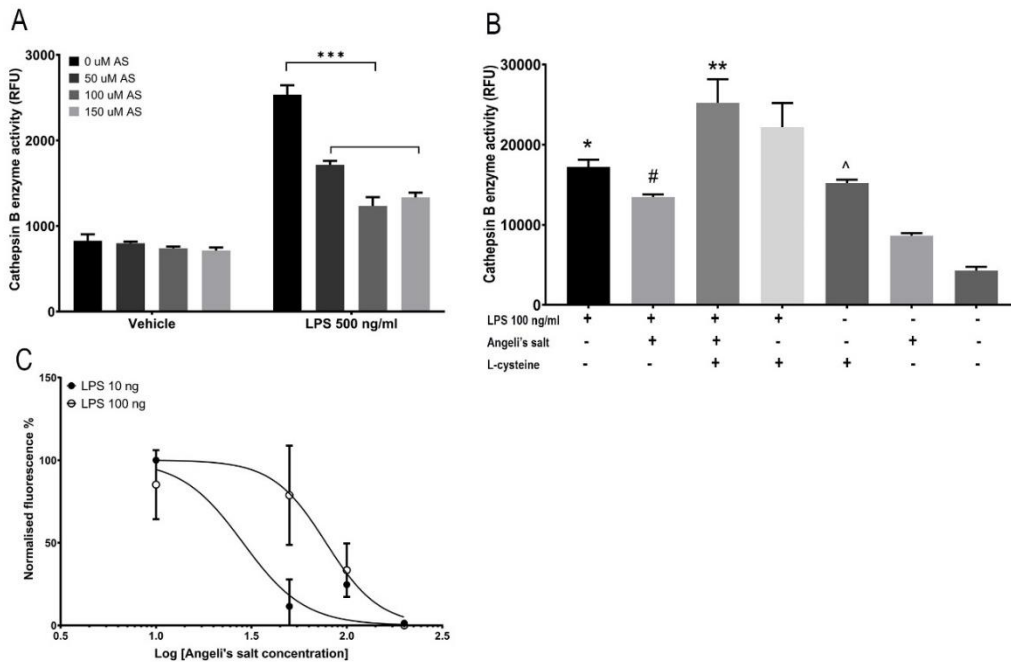


Figure 4.2 HNO inhibits LPS triggered cathepsin B enzyme activity in BV2 cells

(A) Treating BV2 cells with LPS for 24 h increases cathepsin B enzyme activity, the extent of which is reduced by high concentration of Angeli's salt (***) $p < 0.001$. (B) L-cysteine (HNO scavenger) reverses the inhibitory effect of Angeli's salt on cathepsin B enzymatic activity following LPS treatment. (* LPS v Control, $p < 0.01$; # LPS v LPS + AS, $p < 0.05$; ** LPS + AS + LC v LPS + AS, $p < 0.01$; ^ LC v control, $p < 0.01$). (C) Increasing LPS concentration produced a right-ward shift in IC50 (LPS 10 ng/ml, IC50 28.7 μM; LPS 100 ng/ml, IC50 77.8 μM) of Angeli's salt required to reduce cathepsin B enzyme activity.

A

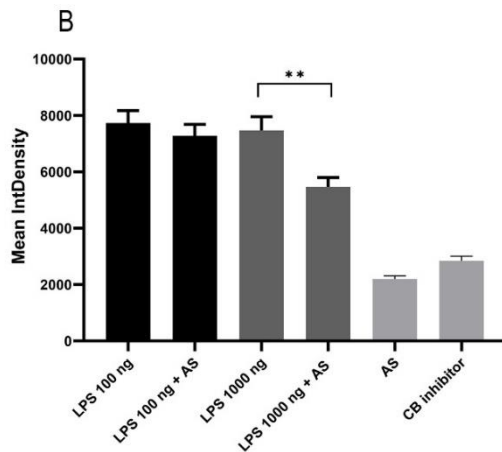
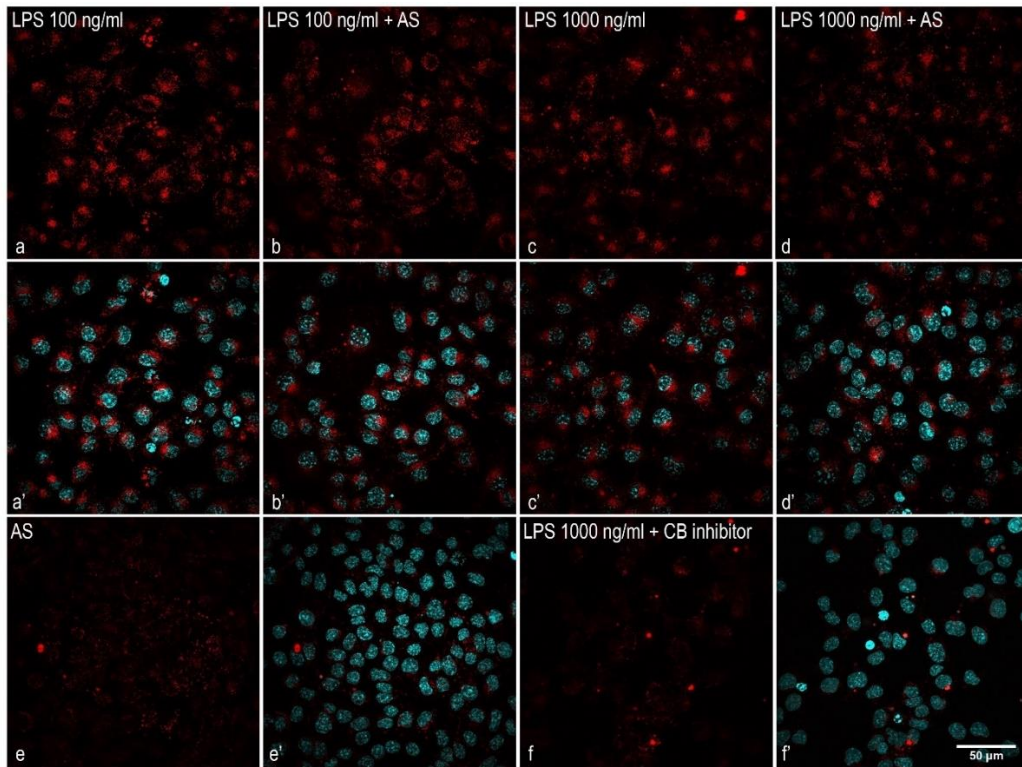


Figure 4.3 Angeli's salt reduces cathepsin B enzyme activity in LPS treated cells in vitro.

Representative z-stack confocal images of BV2 cells taken at 60x magnification showing (A) Cathepsin B enzyme stain (red) and nuclear DAPI stain (cyan). Panels show LPS treatment only; 100 ng/ml (a, a') and 1000 ng/ml (c, c') and with Angeli's salt pre-treatment followed by LPS incubation at 100 ng/ml (b, b') and 1000 ng/ml (d, d'). Control images show cathepsin B enzyme activity fluorescence in the presence of Angeli's salt only (e, e') and with pre-treatment of cathepsin B enzyme inhibitor prior to LPS 1000 ng/ml incubation (f, f'). Scale bar = 50 μ m. (B) The bar graph represents the mean integrated density measurements taken of cathepsin B enzyme activity fluorescence within cells from each treatment. AS (200 μ M) was sufficient to reduce CB activity in live cells treated with 1000 ng/ml LPS, but not 100 ng/ml (** $p < 0.01$).

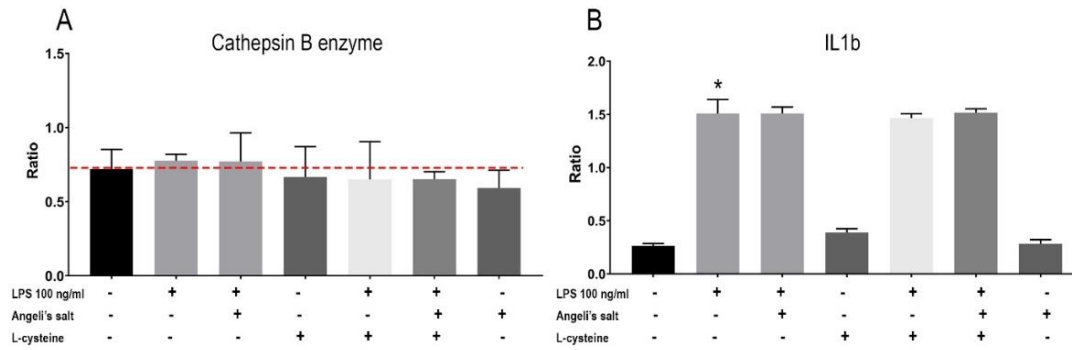


Figure 4.4 Angeli's salt treatment does not reduce cathepsin B or IL-1 β protein levels.

(A) Relative levels of cathepsin B protein in BV2 cell lysates following 24 h treatment with LPS (100 ng/ml) +/- Angeli's salt. Cathepsin B levels were not altered by either LPS or Angeli's salt treatment. (B) A 24 h treatment with LPS (100 ng/ml) increased the relative amount of IL-1 β protein in BV2 cell lysates (*p < 0.0001). Pre-treatment with Angeli's salt did not alter IL-1 β protein expression compared to LPS treatment or control. Data is represented as a ratio of protein of interest expression to β -actin loading control.

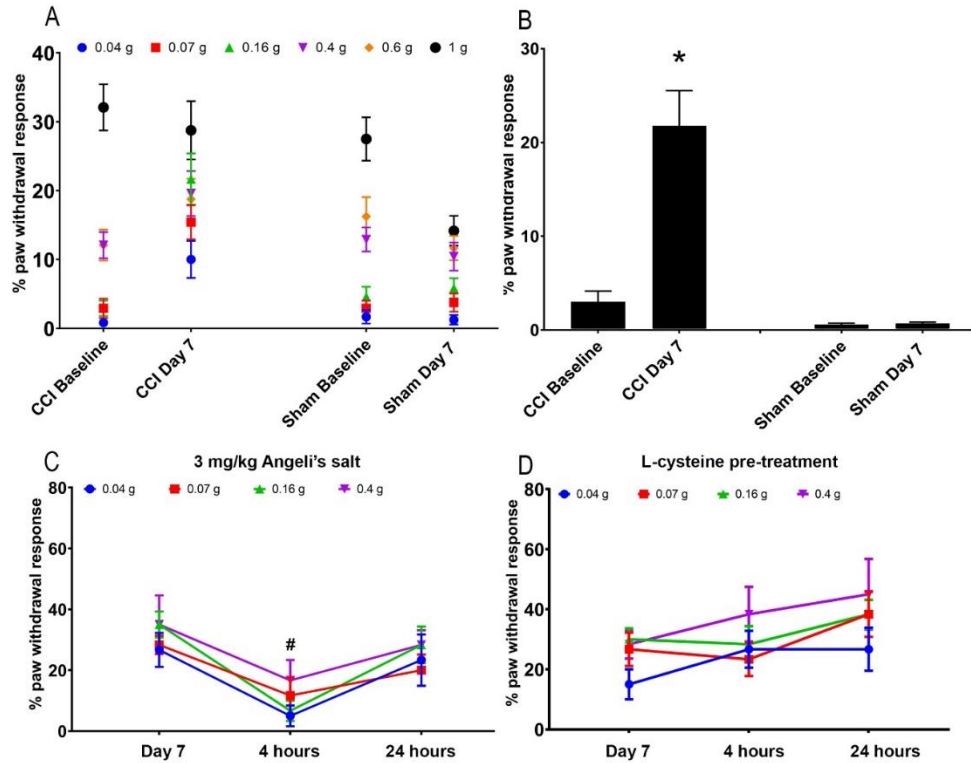


Figure 4.5 Angeli's salt reduces mechanical allodynia in CCI operated mice.

Mechanical allodynia was determined using von Frey testing. (A) Summary graph showing the percentage paw withdrawal response to each of the von Frey hairs used at Baseline and Day 7 post-surgery for CCI operated ($n = 6$) and sham operated animals ($n = 6$). (B) Graph showing the development of allodynia in the hind-paw of injured animals at Day 7 post-surgery. CCI animals displayed a significantly increased withdrawal response to the 0.16 g filament compared to sham operated animals, indicating the development of allodynia. Sub-scapular injection of Angeli's salt (3 mg/kg) reduced allodynia at 4 h, but not 24 h when measured with von Frey hairs (0.04, 0.07, 0.16 and 0.4 g) (C). Pre-injection with nitroxyl scavenger, L-cysteine (1 mM) was able to attenuate the Angeli's salt inhibition at the 4 h time-point (D) for all 4 von Frey hairs. * $p < 0.001$, # $p < 0.05 - 0.0001$ (see Results section 4.3.4 for details)

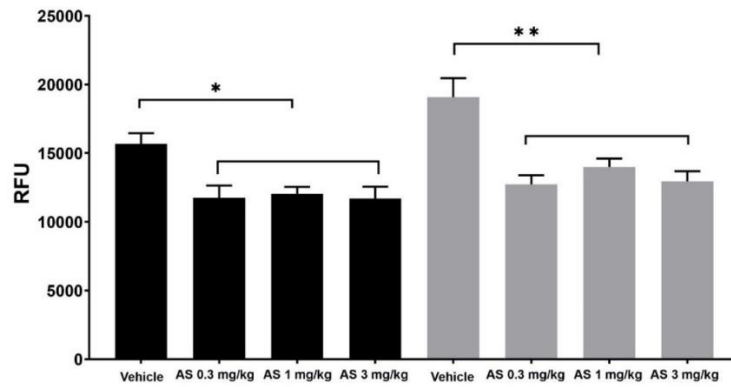


Figure 4.6 Angeli's salt reduces Cathepsin B enzyme activity in the spinal cord of mice.

A colourmetric assay was used to determine relative cathepsin B enzyme activity in homogenates of L3-5 ipsilateral spinal cord from sham (black bars) and CCI (grey bars) animals. Angeli's salt reduced cathepsin B enzymatic activity in both CCI and sham operated animals for all concentrations of Angeli's salt (0.3, 1 and 3 mg/kg), when compared to vehicle control (0.01M NaOH). *p < 0.05, **p < 0.001-0.0001, see results section 4.4.5 for details. N = 6 per treatment group.

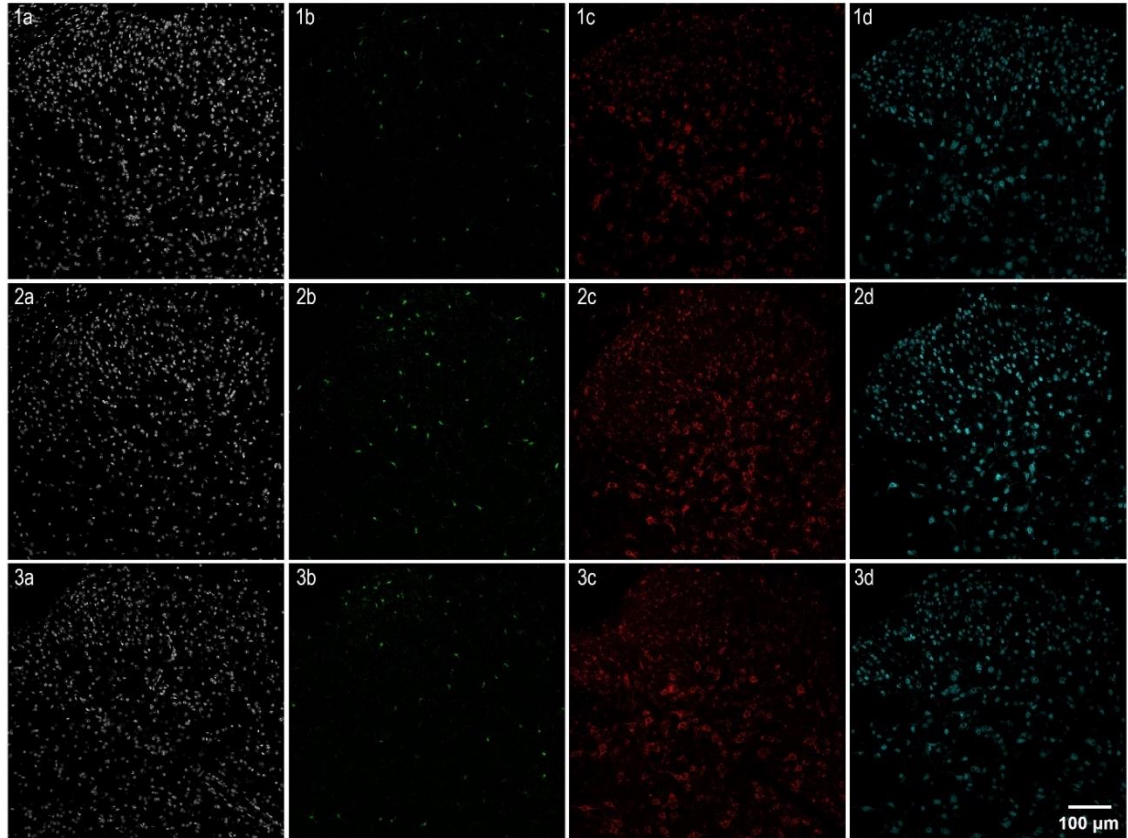


Figure 4.7.1 Localisation of cathepsin B and NeuN immunopositive cells in dorsal spinal cord of CCI and sham operated CX3CR1^{gfp+} mice.

Representative z-stack confocal images of ex vivo ipsilateral dorsal horn from lumbar spinal cord slices taken at 20x magnification showing nuclear DAPI stain (white), GFP (green) expression indicative of microglial CX3CR1 expression (green), cathepsin B enzyme protein (red) and neuronal marker NeuN (cyan). Panel shows ipsilateral spinal dorsal horn region from sham operated animals (1a, 1b, 1c and 1d), CCI operated animals with vehicle injection (2a, 2b, 2c and 2d) and CCI operated animals with Angeli's salt (3mg/kg) injection (3a, 3b, 3c and 3d). Scale bar = 100 μm.

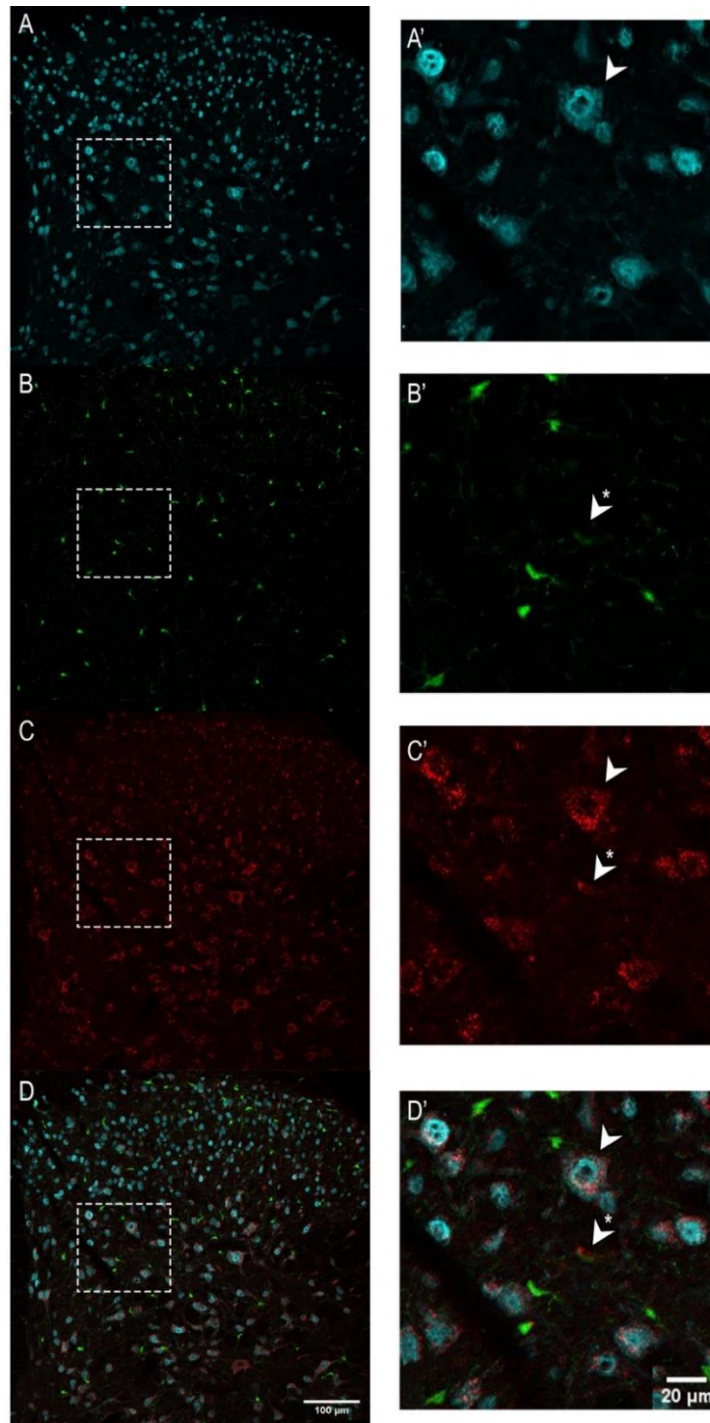


Figure 4.7.2 Overlay of immunohistological labelling of cathepsin B and NeuN in dorsal spinal cord of CX3CR1^{GFP+} mice.

Representative z-stack confocal images of ex vivo lumbar spinal cord slices taken at 20x magnification showing GFP (green) expression in microglial cells on the CX3CR1 gene, Cathepsin B enzyme protein (red) and neuronal marker NeuN (cyan). Panel shows ipsilateral spinal dorsal horn region CCI operated animals. Cathepsin B immunoreactivity localised to both neuronal (white arrowhead) and microglial cells (white arrowhead with asterisk). Scale bar = 100 μm for panel, scale bar = 20 μm for expanded images.

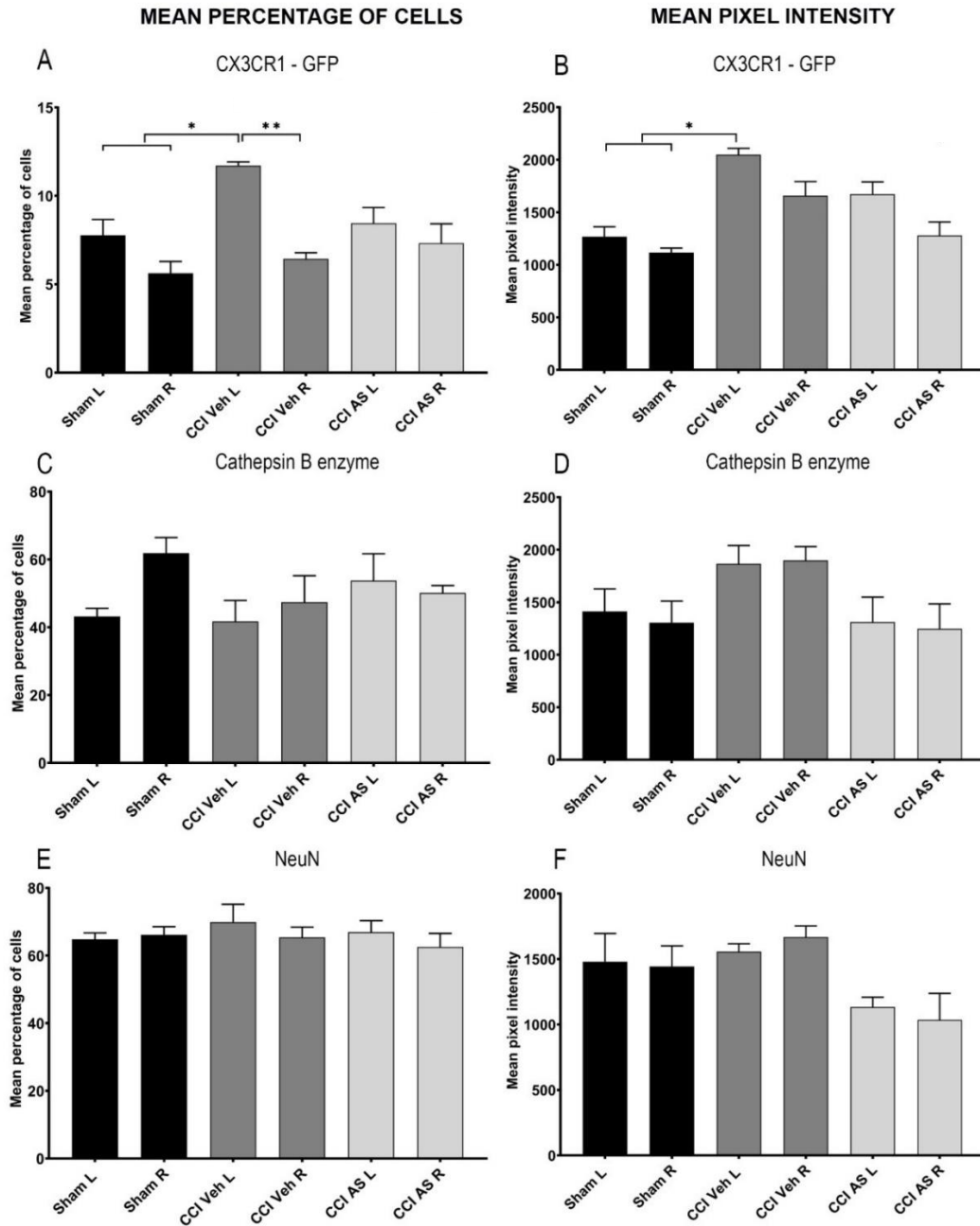


Figure 4.7.3 Angeli's salt treatment reduces percentage of CX3CR1 positive cells.

Graphs representing the mean percentage of cells and mean pixel intensity of the spinal dorsal horn region expressing (A, B) GFP – CX3CR1 (microglial marker), (C, D) Cathepsin B enzyme protein and (E, F) NeuN (neuronal marker). The mean percentage (A; * $p < 0.05$) and mean pixel intensity (B * $p < 0.01$) of microglial cells is increased in the ipsilateral dorsal horn of CCI injured animals compared with Sham operated and contralateral dorsal horn of CCI injured animals (A; ** $p < 0.01$)($n = 3$).

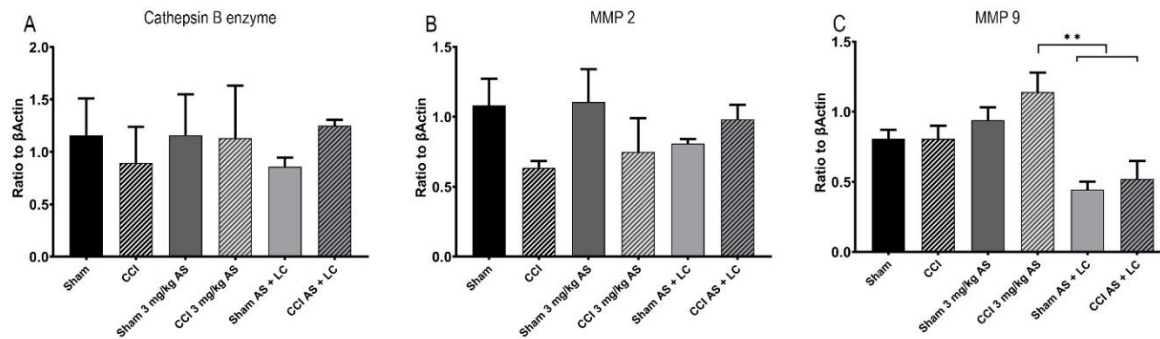


Figure 4.8 Cathepsin B, MMP-2 and MMP-9 protein levels within spinal cord tissue homogenates 24h following Angeli's salt treatment.

Relative levels of Cathepsin B enzyme protein (A/B), metalloprotease 2 (C/D) and metalloprotease 9 (E/F) in homogenates of ipsilateral L3-5 spinal cord tissue from sham-operated (solid bars, n = 6) and CCI-operated (lined bars, n = 6) animals. A) Cathepsin B expression levels in both sham and CCI operated animals were unchanged by Angeli's salt (AS) or L-cysteine (LC) treatment. B) There was no change in MMP-2 expression levels regardless of surgery or AS/LC treatment. C) MMP-9 protein expression levels did not change following CCI surgery or AS treatment, however a decreased expression was noted in both sham and CCI, AS + LC treated samples when compared to CCI injured AS treated samples (**p < 0.01). Data is represented as a ratio of protein of interest expression to β -Actin loading control.

4.5 Discussion

Here we demonstrate that 1) the direct action of HNO on reducing cathepsin B enzyme activity, 2) a HNO dependent decrease in cathepsin B activity in both BV2 cells and ipsilateral spinal cord of CCI-injured and sham-operated mice, 3) reduced allodynia 4h post HNO administration, 4) the detection of CB protein within BV2 cells and mouse dorsal spinal cord tissue, which was not altered by LPS treatment, CCI-injury or subsequent HNO administration, and 5) no changes in MMP-2, MMP-9 or IL-1 β protein levels following HNO treatment.

The involvement of reactive nitrogen species in central mechanisms of neuropathic pain are being increasingly explored. The one electron reduced NO species, HNO has been implicated in reducing neuropathic pain symptoms via different pathways, however the central mechanism is still uncertain. HNO is reported to inhibit the LPS driven inflammatory response in BV2 cells, via NF κ B and p38 MAPK pathways, and specifically targeting the Cys-179 residue of IKK β and preventing the phosphorylation and degradation of I κ B α and subsequent release of NF κ B (Zhou et al., 2016). It has also been proposed that HNO can alter NMDA receptor activity by modifying a critical thiol residue leading to a decrease in Ca²⁺ influx (Kim et al., 1999). As NMDA activation is critical in the development of the increased post-synaptic excitatory signalling in neuropathic pain, this may provide an alternative mechanism of action. Furthermore, in animal models of neuropathic pain HNO was also reported to reduce glial inflammatory markers (GFAP and Iba1) and inflammatory mediators (IL-1 β , TNF α) in the spinal cord (Longhi-Balbinot et al., 2016). Another possible pathway is via the inactivation of lysosomal cysteine, CB, which has been reported to aid the release of cytokine IL-1 β in models of neuropathic pain (Longhi-Balbinot et al., 2016). The active-site cysteines in cysteine proteases are suggested to be highly sensitive for modification by HNO.

Our study found that HNO can directly inhibit CB enzyme activity, which was restored by the HNO scavenger, L-cysteine. We determined that the concentration of HNO required to reduce CB enzymatic activity by 50% (IC₅₀) was 41.32 μ M. In support of our findings, previous studies report a similar IC₅₀ for the AS-mediated reduction of CB activity in THP-1 and RAW 264.7 macrophages (IC₅₀; 51 μ M) (Väänänen et al., 2006, 2008), Pro-inflammatory mediator LPS, can increase CB activity in various cells (Li et al., 2009; Creasy et al., 2010) triggering cell apoptosis and playing a major role in many disease models. LPS is used as an inflammatory stimulant for *in vitro* models of inflammatory and neuropathic diseases and is the major ligand for Toll-like

receptor 4 (TLR4) predominantly found on macrophage like cells, which when activated, releases many pro-inflammatory cytokines and NO (Nakamura et al., 1999). We also report that HNO (liberated from Angeli's salt) was able to inhibit LPS stimulated CB activity in BV2 cells, in a concentration dependent manner. The specificity of Angeli's salt to reduce CB activity was confirmed via the pre-treatment with the HNO scavenger, L-cysteine, which not only reversed the inhibitory effect of the HNO donor, but also potentiated CB activity. As L-cysteine cannot discriminate between Angeli's salt derived, or endogenously generated HNO, this suggests that BV2 cells produce a basal level of endogenous HNO which modulates CB activity. Recent unpublished work from our laboratory observed an increase in iNOS derived endogenous HNO signal in BV2 cells following LPS stimulation, using a novel arylphosphine based fluorescent HNO probe (see Chapter 3). However, the local concentration of endogenous HNO may be in the nM to μ M range, as approximately 40 μ M of Angeli's salt was required to reduce CB activity by 50%. We also showed that the concentration of AS required to reduce CB activity was positively correlated with LPS concentration, suggesting that the more CB is active, the higher amount of HNO is required to inhibit it. Despite increased CB activity in response to LPS stimulation, western blot analysis of BV2 cell lysates revealed that CB protein levels remain unchanged, suggesting that increased CB activity detected by the fluorescence assay may be due to enhanced enzymatic activity and not an increase in CB protein *per se*. A lack of mRNA transcript changes for CB following 24 h LPS stimulation in macrophage cells despite increases in CB activity (Creasy et al., 2010) also support post- rather than pre-transcriptional modifications.

A change in CB activity in chronic pain is suggested to drive the release and cleavage of cytokine IL-1 β , thus, enhancing excitatory synaptic signalling (Schotte et al., 1998; Hentze et al., 2003; Terada, et al., 2010). Further to this, IL-1 β levels are reduced in CB knock-out models of chronic pain (Sun et al., 2012). We observed an increase in pro-IL-1 β protein levels in cell lysates following 24 h LPS (100 ng/ml) treatment, however Angeli's salt did not alter IL-1 β production suggesting that it is not driven by HNO. This is in contrast to the finding that pro- IL-1 β mRNA expression in spinal cord of CCI-injured mice was significantly reduced following acute AS treatment (Longhi-Balbinot et al., 2016). It is worth noting that the spinal samples in Longi-Balbinot, 2016 study were collected at 5 h post-AS treatment when the anti-allodynic effect was at peak, compared to the current study in whereby samples were collected 24 h post AS

treatment and the anti-allodynic effect had resolved. Future experiments using sensitive ELISA analysis of supernatants may assist in quantifying IL-1 β levels in cell lysates.

Our study also found that acute administration of HNO can reduce allodynia in CCI-injured animals, however this effect appears to be transient as it is present at 4 h post injection and resolved by 24 h, which has been previously reported (Longhi-Balbinot et al., 2016). Although previous study has shown that AS can disrupt the blood brain barrier and potentially reach the spinal cord following treatment, future experiments using intrathecal administration may increase the duration of reduced allodynia (Boje, 2000).

As cathepsins have been previously implicated in the development of neuropathic pain (Barclay J, et al., 2007; Abbadiea C, et al., 2009) we examined HNO's effect on CB activity within the ipsilateral spinal cord of both sham-operated and CCI-injured animals. Interestingly, HNO decreased CB activity in both surgery groups in a non-concentration dependant manner but did not alter mechanical withdrawal thresholds of sham operated animals. This suggests that the anti-allodynic effect of HNO is not mediated by its actions on CB activity. This is supported by pervious work showing pharmacological inhibition and gene knock-out of CB reduced tactile allodynia in models of inflammatory pain but not neuropathic pain (Sun et al., 2012). Similarly, to BV2 cells, we also observed no change in CB protein levels in mouse spinal cord following CCI-injury or subsequent HNO treatment, as determined by both immunohistological and western analysis. However, this is contradicted by a study which reported increases in both CB mRNA and protein from spinal cord tissue lysates of spinal injured rats (Ellis et al., 2004). Similar studies which reported increases in CB protein levels, appeared to use pain models which have a high impact traumatic CNS injury (Fan et al., 2001; Hu et al., 2002) and may be providing a greater stimulus than our current study, thus driving more CB activated cellular pathways required for apoptosis and tissue degradation. We observed that CB enzyme was predominantly located in discrete punctate bundles just outside of the nucleus of BV2 cells or diffused throughout the cytoplasm (Figure 4.3) which has been previously reported in bone marrow derived macrophage (BMDM) cells (Lopez-Castejon et al., 2010). However, immunohistological observations from dorsal spinal cord tissue of CCI injured animals, indicate a high proportion of CB immunoreactivity in NeuN positive cells (neurons) as well as some GFP expressing microglial cells. Similar to our findings, a report by Ellis et al, (2005) shows CB staining localised only to

the lysosomes of spinal neurons in normal rats and observing CB in OX42 positive microglia only following spinal cord injury.

Further to this, we also observed an increase in mean cell percentage and mean pixel intensity of GFP expressing microglial cells in ipsilateral dorsal horn of CCI-injured mice when compared to Sham controls. Microglial activation is a well characterised phenomenon following sciatic nerve injury in various animal models (Colburn et al., 1997; Mika et al., 2009). Longhi-Balbinot *et al.*, (2016) observed a reduction in IBA1 mRNA levels in the spinal cord of HNO treated CCI-injured mice, following both acute (single AS injection 3 mg/kg) and chronic (daily AS injection up to 7 days, 3 mg/kg) administration, supporting the idea that HNO reduces spinal microglial activation in response to nerve injury.

Our data shows that MMP-2 & -9 protein was not increased in the ipsilateral spinal cord of CCI-injured mice compared to Sham operated mice. Further to this HNO treatment (AS 3 mg/kg) did not alter MMP-2 or -9 levels. These findings do not support our hypothesis, however similar to our CB observations, HNO may be involved in S-nitrosylation of cysteine residues on these metalloproteases, hence reducing activity but not translation of these proteases. Further investigation may elucidate whether HNO can regulate MMP-9 and MMP-2 enzyme function, similar the inactivation of MMP-9 function observed by NO during cerebral ischemia (Gu et al., 2002). Interestingly, HNO scavenger, L-cystine pre-treatment reduced MMP-9 levels in both CCI and Sham operated mice. MMP-9 is an extracellular protease released from various cells types in the CNS (neuron, glia and leukocytes) and is an important regulator of synaptic activity and excitatory signalling (Vafadari et al., 2016). Enzymatic activity, protein abundance and gene expression of MMP-9 is markedly increased following various physiological stimulus, including peripheral nerve injury (Vafadari et al., 2016). Previous studies have shown that L-cysteine pre-incubation can reduced stimulated levels of MMP-9 mRNA and protein in rat astrocytes (Wang et al., 2017) and lung fibroblast cells (Wang et al., 2006), suggesting that MMP-9 activity is mediated by reactive oxygen species and supports our current observations.

4.6 Conclusion

Understanding the various adaptations which occur in the spinal cord during neuropathic pain development may provide potential therapeutic targets. Lysosomal cysteine proteases play a critical role in the regulation of cytokines such as IL-1 β and other extracellular matrix molecules, such as metalloprotease in chronic pain pathologies. HNO, the protonated form of NO is able to

cleave cysteine residues on thiols and was shown to directly reduce cysteine protease, Cathepsin B activity in both BV2 cells and mouse spinal cord tissue. However, there was no change observed in protein levels of MMP-2 & -9 or IL-1 β which suggests that CB may not have a direct role in IL-1 β regulation in neuropathic pain, however MMP-2 and MMP-9 enzyme function requires further assessment. It should be noted, that the cysteine protease cathepsin S is another potential candidate which may be inactivated by HNO and has also been implicated in IL-1 β production in neuropathic pain, which warrants further investigation. However, as HNO incubation in BV2 cells did not reduced LPS stimulated IL-1 β levels in this study, careful assessment should be made as to whether HNO reduces allodynia via inactivation of either cathepsin substrate. The ability of HNO to reduce allodynia in CCI-injured animals highlights its importance as a future therapeutic treatment option for persistent pain patients.

4.7 References

Abbadie C, Bhangoo S, De Koninck Y, Malcangio M, Melik-Parsadaniantz S, White FA. (2009) Chemokines and pain mechanisms. *Brain Research Reviews*; 60(1): 125-134.

Barclay J, Clark AK, Ganju P, Gentry C, Patel S, Wotherspoon G, Buxton F, Song C, Ullah J, Winter J, Fox A, Bevan S, Malcangio M. (2007) Role of the cysteine protease cathepsin S in neuropathic hyperalgesia. *Pain*; 130(3): 225-234.

Bennett GJ. (1997) Neuropathic pain: an overview. In: Borsook D, editor. *Molecular biology of pain*. Seattle: IASP Press: 109–13.

Bian K, Ke Y, Kamisaki Y, Murad F. (2006) Proteomic Modification by Nitric Oxide. *Journal of Pharmacological Sciences*; 101(4): 271-279.

Boje KM, Lakhman SS (2000) Nitric oxide redox species exert differential permeability effects on the blood brain barrier. *J Pharmacol Exp Ther*; 293(2): 545-50.

Bowsher D. (1991) Neurogenic pain syndromes and their management. *Br Med Bull*; 47: 644–66.

Colburn RW, DeLeo JA, Rickman AJ, Yeager MP, Kwon P, Hickey WF. (1997) Dissociation of microglial activation and neuropathic pain behaviors following peripheral nerve injury in the rat. *Journal of Neuroimmunology*; 79: 163–175.

Costigan M, Scholz J and Woolf CJ. (2009) Neuropathic Pain: A Maladaptive Response of the Nervous System to Damage. *Annu Rev Neurosci*; 2009(32): 1–32.

Ellis RC, Earnhardt JN, Hayes RL, Wang KK, Anderson DK. (2004). Cathepsin B mRNA and protein expression following contusion spinal cord injury in rats. *J. Neurochem*; 88: 689 – 697.

Ellis RC, O'Steen WA, Hayes RL, Nick HS, Wang KKW, Anderson DK. (2005) Cellular localization and enzymatic activity of cathepsin B after spinal cord injury in the rat. *Experimental Neurology*;193(1): 19-28.

Fan M, Mi R, Yew DT, Chan WY. (2001) Analysis of gene expression following sciatic nerve crush and spinal cord hemisection in the mouse microarray expression profiling. *Cell Mol. Neurobiol*; 21: 497-508.

Ferreira J, Santos ARS, Calixto JB. (1999) The role of systemic, spinal and supraspinal l-arginine–nitric oxide–cGMP pathway in thermal hyperalgesia caused by intrathecal injection of glutamate in mice. *Neuropharmacology*; 38(6):835-842.

Grace PM, Hutchinson MR, Manavis J, Somogyi AA, Rolan PE (2010) A novel animal model of graded neuropathic pain: Utility to investigate mechanisms of population heterogeneity. *Journal of Neuroscience Methods*; 193(1): 47-53.

Gu Z, Kaul M, Yan B, Kridel SJ, Cui J, Strongin A, Smith JW, Liddington RC, Lipton SA. (2002) S-nitrosylation of matrix metalloproteinases: signaling pathway to neuronal cell death. *Science*; 297: 1186–90.

Hentze H; Lin XY; Choi MSK; Porter AG. (2003) Critical role for cathepsin B in mediating caspase-1-dependent interleukin-18 maturation and caspase-1-independent necrosis triggered by the microbial toxin nigericin. *Cell Death and Differentiation*; 10(9): 956.

Hu J, Fink D, Mata M. (2002) Microarray analysis suggests the involvement of proteasomes, lysosomes, and matrix metalloproteinases in the response of motor neurons to root avulsion. *Eur J Neurosci*; 18: 1409-1416.

Kawasaki Y, Xu ZZ, Wang X, Park JY, Zhuang ZY, Tan PH. (2008) Distinct roles of matrix metalloproteases in the early- and late-phase development of neuropathic pain. *Nat.Med*; 14: 331–336.

Kim WK; Choi YB; Rayudu PV; Das P; Asaad W; Arnelle DR; Stamler JS; Lipton SA. (1999) Attenuation of NMDA Receptor Activity and Neurotoxicity by Nitroxyl Anion, NO⁻. *Neuron*; 24(2): 461-469.

Kostoulas G, Lang A, Nagase H, Baici A. (1999) Stimulation of angiogenesis through cathepsin B inactivation of the tissue inhibitors of matrix metalloproteinases. *FEBS Letters*; 455(3): 286-290.

Kwok YH; Tuke J; Nicotra LL; Grace PM; Rolan PE; Hutchinson MR. (2013) TLR 2 and 4 responsiveness from isolated peripheral blood mononuclear cells from rats and humans as potential chronic pain biomarkers. *PLoS ONE*; 8(10): e77799.

Li JH, D'Alessio A, Pober JS. (2009) Lipopolysaccharide Can Trigger a Cathepsin B-Dependent Programmed Death Response in Human Endothelial Cells. *Am J Pathol*; 175(3): 1124–1135.

Longhi-Balbinot DT, Rossaneis AC, Pinho-Ribeiro FA, Bertozzi MM, Cunha FQ, Alves-Filho JC, Cunha TM, Peron JPS, Miranda KM, Casagrande R and Verri Jr. WA, (2016) The nitroxyl donor, Angeli's salt, reduces chronic constriction injury-induced neuropathic pain. *Chemico-Biological Interactions*; doi: 10.1016/j.cbi.2016.06.009.

Lopez-Castejon G, Theaker J, Pelegrin P, Clifton AD, Braddock M, Surprenant A. (2010) P2X7 Receptor-Mediated Release of Cathepsins from Macrophages Is a Cytokine-Independent Mechanism Potentially Involved in Joint Diseases. *J Immunol*; 185(4): 2611-2619.

Mika J, Osikowicz M, Rojewska E, Korostynski M, Wawrzczak-Bargiela A, Przewlocki R, Przewlocka B. (2009) Differential activation of spinal microglial and astroglial cells in a mouse model of peripheral neuropathic pain. *European Journal of Pharmacology*; 623: 65–72.

Nakamura Y, Si QS, Kataoka K. (1999) Lipopolysaccharide-induced microglial activation in culture: temporal profiles of morphological change and release of cytokines and nitric oxide. *Neurosci Res*; 35(2): 95-100.

Nicotra L; Tuke J; Grace PM; Rolan PE; Hutchinson MR. (2014) Sex Differences in Mechanical Allodynia: How Can it be Preclinically Quantified and Analysed? *Frontiers in Behavioral Neuroscience*; 8.

Schmidtko A, Tegeder I, Geisslinger G (2009) 'No NO, no pain? The role of nitric oxide and cGMP in spinal pain processing.' *Trends Neurosci*; 32(6): 339–346.

Schmidtko A, Wei Gao W, Ko'nig P, Heine S, Motterlini R, Ruth P, Schlossmann J, Koesling D, Niederberger E, Tegeder I, Friebe A and Geisslinger G. (2008) 'cGMP produced by NO-sensitive guanylyl cyclase essentially contributes to inflammatory and neuropathic pain by using targets different from cGMP-dependent protein kinase I.' *J. Neurosc*; 28: 8568–8576.

Schönbeck U, Mach F and Libby P. (1998) Generation of biologically active IL-1 beta by matrix metalloproteinases: a novel caspase-1-independent pathway of IL-1 beta processing. *J Immunol*; 161: 3340–3346.

Schotte P, Van Criekinghe W, Van de Craen M, Van Loo G, Desmedt M, Grooten J, Cornelissen M, De Ridder L, Vandekerckhove J, Fiers W, Vandenabeele P, Beyaert R. (1998) Cathepsin B-

Mediated Activation of the Proinflammatory Caspase-11. *Biochemical and Biophysical Research Communications*; 251(1): 379-387.

Song XJ, Gan Q, Cao JL, Wang ZB, Rupert RL. (2006) Spinal Manipulation Reduces Pain and Hyperalgesia After Lumbar Intervertebral Foramen Inflammation in the Rat. *Journal of Manipulative and Physiological Therapeutics*; 29(1): 5-13.

Sun L, Wu Z, Hayashi Y, Peters C, Tsuda M, Inoue K and Nakanishi H. (2012) Microglial Cathepsin B Contributes to the Initiation of Peripheral Inflammation-Induced Chronic Pain. *The Journal of Neuroscience*; 32(33): 11330 –11342.

Terada K, Yamada J, Hayashi Y, Wu Z, Uchiyama Y, Peters C, Nakanishi H. (2010) Involvement of cathepsin B in the processing and secretion of interleukin-1 β in chromogranin A-stimulated microglia. *Glia*; 58(1): 114-124.

Väänänen AJ, Salmenperä P, Hukkanen M, Miranda KM, Harjula A, Rauhala P, Kankuri E. (2008) Persistent susceptibility of cathepsin B to irreversible inhibition by nitroxyl (HNO) in the presence of endogenous nitric oxide. *Free Radical Biology & Medicine*; 45: 749–755.

Väänänen AJ, Salmenperä P, Hukkanen M, Rauhala P, Kankuri E. (2006) Cathepsin B is a differentiation-resistant target for nitroxyl (HNO) in THP-1 monocyte/macrophages. *Free Radical Biology and Medicine*; 41(1): 120-131.

Vafadari B, Salamian A, Kaczmarek L. (2016) MMP-9 in translation: from molecule to brain physiology, pathology, and therapy. *Journal of Neurochemistry*; 139: 91-114.

Walczak JB, Pierre B. (2006) Comparison of three models of neuropathic pain in mice using new method to assess cold allodynia: The double plate technique. *Neuroscience Letters*; 399 (3): 240-244.

Wang HT, Gao JL, Tian YX, Kan Q. (2006) Inhibition of N-acetyl-L-cysteine on expressions of matrix metalloproteinases increased by exposure to silicon dioxide in lung fibroblasts in rats. *Chinese Journal of Industrial Hygiene and Occupational Diseases*; 24(9): 514-517.

Wang T, Liao Y, Sun Q, Tang H, Wang G, Zhao F, Jin Y. (2017) Upregulation of Matrix Metalloproteinase-9 in Primary Cultured Rat Astrocytes Induced by 2-Chloroethanol Via MAPK Signal Pathways; *Frontiers in Cellular Neuroscience*; 11.

Zhou Y, Wu Z, Cao X, Ding L, Wen ZS, Bian JS. (2016) HNO suppresses LPS-induced inflammation in BV-2 microglial cells via inhibition of NF- κ B and p38 MAPK pathways. *Pharmacological Research*; 111: 885-895.

Statement of Authorship

Title of Paper	Graded peripheral nerve injury alters the progression and severity of microglial activity within the spinal cord of CX3CR1-GFP mice
Publication Status	<input type="checkbox"/> Published <input type="checkbox"/> Accepted for Publication <input checked="" type="checkbox"/> Submitted for Publication <input type="checkbox"/> Unpublished and Unsubmitted work written in manuscript style
Publication Details	Submitted to: Neurobiology of Disease

Principal Author

Name of Principal Author (Candidate)	Vasiliki Staikopoulos			
Contribution to the Paper	Manuscript conception, wrote manuscript, generated figures and provided training to collaborators for 3 of 5 techniques used.			
Overall percentage (%)	20%			
Certification:	This paper reports on original research I conducted during the period of my Higher Degree by Research candidature and is not subject to any obligations or contractual agreements with a third party that would constrain its inclusion in this thesis. I am the primary author of this paper.			
Signature	<table border="1"> <tr> <td>_____</td> <td>Date</td> <td>2/9/2019</td> </tr> </table>	_____	Date	2/9/2019
_____	Date	2/9/2019		

Co-Author Contributions

By signing the Statement of Authorship, each author certifies that:

- i. the candidate's stated contribution to the publication is accurate (as detailed above);
- ii. permission is granted for the candidate to include the publication in the thesis; and
- iii. the sum of all co-author contributions is equal to 100% less the candidate's stated contribution.

Name of Co-Author	Sha Qiao			
Contribution to the Paper	Carried out experiments, provided data and images for figures, contributed to writing of methods section and review of manuscript.			
Signature	<table border="1"> <tr> <td>_____</td> <td>Date</td> <td>4/9/19</td> </tr> </table>	_____	Date	4/9/19
_____	Date	4/9/19		

Name of Co-Author	Jiajun Liu			
Contribution to the Paper	Provided advice towards and carried out linear regression statistical analysis.			
Signature	<table border="1"> <tr> <td>_____</td> <td>Date</td> <td>04/09/2019</td> </tr> </table>	_____	Date	04/09/2019
_____	Date	04/09/2019		

Please cut and paste additional co-author panels here as required.

Name of Co-Author	Xianlin Song		
Contribution to the Paper	Provided advice on experimental design.		
Signature		Date	11/9/2019

Name of Co-Author	Xiaoqun Yang		
Contribution to the Paper	Provided advice on experimental design.		
Signature		Date	9/9/2019

Name of Co-Author	Qingming Luo		
Contribution to the Paper	Provided advice on experimental design.		
Signature		Date	7/9/2019

Name of Co-Author	Mark R Hutchinson		
Contribution to the Paper	Manuscript conception, reviewed manuscript and carried out statistical analysis.		
Signature		Date	3/9/2019

Name of Co-Author	Zhihong Zhang ²		
Contribution to the Paper	Manuscript conception, reviewed manuscript and acting as corresponding author.		
Signature		Date	7/9/2019

Chapter 5 - Graded peripheral nerve injury alters the progression and severity of microglial activity within the spinal cord of CX3CR1-GFP mice.

This chapter has been submitted as a primary research paper in Neurobiology of Disease and is currently under review. [Staikopoulos V, Qiao S, Liu J, Song X, Yang X, Luo Q, Hutchinson MR, Zhang Z. Graded peripheral nerve injury alters the progression and severity of microglial activity within the spinal cord of CX3CR1-GFP mice. Neurobiology of disease. 2019]

5.1 Abstract

The reactivity of microglia within the spinal cord in response to nerve injury, has been associated with the development and maintenance of neuropathic pain. However, the temporal establishment of spinal microglial reactivity following injury remains to be fully defined. Using a heterozygous CX3CR1^{gfp+} transgenic mouse strain, we monitored microglial activity as measured by cell density, morphology, movement and process length over 14 days via *in vivo* confocal microscopy. Uniquely, this was explored in groups of mice which had graded nerve injury and associated graded behavioural mechanical nociceptive sensitivity. Significant mechanical allodynia was quantified from ipsilateral hind paw and was shown to interact with the extent of nerve injury from day 5 to day 14 ($p < 0.009$) and the extent of this ipsilateral allodynia was proportional to the nerve injury from day 5 to 14 (Spearman rho = -0.58 to -0.77; $p < 0.002$). This approach allowed for the assessment of the association of spinal microglial changes with the magnitude of quantified mechanical sensitivity. Additionally, the hemodynamic response in the somatosensory cortex was also quantified as a surrogate measure of brain activity. We found that spinal dorsal horn microglia underwent changes unilateral to the injury in density (Spearman rho = 0.47; $p = 0.01$), velocity (Spearman rho = -0.68; $p = 0.00009$), and circularity (Spearman rho = 0.55; $p = 0.01$) proportional with the degree of the neuronal injury. Importantly, these data demonstrate that the allodynic behaviour is not a binary all or nothing state and that microglial reactivity are changing proportional to this. Increased total haemoglobin levels in the somatosensory cortex of higher-grade injured animals was observed when compared to sham controls. The degree of phenotypic microglial changes throughout the injury lifespan may provide an explanation for how microglia can

induce both rapid onset and sustained functional changes in the spinal cord dorsal horn, following peripheral injury.

5.2 Introduction

Damage to somatosensory nerves can create exaggerated nociception which is expressed by the individual as pain behaviour responses. Within 24 hours following peripheral nerve injury, neuronal adaptations occur in the dorsal horn of the spinal cord including, altered expression of receptors, ion channels and neurotransmitters, which leads to an increased generation and firing of action potentials and associated presentation of exaggerated pain behaviours (Latremoliere and Woolf, 2009; Scholz and Woolf, 2007). In addition to the neuronal adaptations, it is now well accepted that peripheral nerve injury also leads to the recruitment of a reactive microglial phenotype within the spinal cord dorsal horn, which can occur within hours of injury (Tanga et al., 2004) and last up to several months (Clark et al., 2007; Coyle, 1998).

Microglia are resident immune-like cells of the central nervous system. When challenged, microglia undergo molecular changes, including the release of various pro-inflammatory cytokines and take on a more phagocytic phenotype (Austin and Moalem-Taylor, 2010). After nerve injury, several molecular factors released from neurons contribute to spinal cord dorsal horn microglia transitioning to a reactive state (also known as microgliosis), causing changes in morphology (developing a more amoeboid appearance), allowing them to migrate easily to sites of reactivity and increase proliferation (Cavlo and Bennett, 2012; von Hehn et al., 2012). The temporal resolution of these microglial transitions during the initiation and maintenance of chronic pain states remains unclear. Unfortunately, refining the knowledge around these critically timed transitions with standard approaches that require terminal tissue collection and analysis would require unacceptably large experimental designs and the use of excessive numbers of animals. Understanding the real time, longitudinal molecular and cellular changes within individuals, would offer a clearer appreciation of the transitional phenomena that occurs as exaggerated pain behaviours (e.g. mechanical allodynia) develop. This may identify a critical time point at which therapeutic interventions could circumvent the establishment of long-term neuropathic pain. As new interventional therapies are being sought to target microglial contributions to hyper-nociception, it is critical to differentiate the cellular adaptations

within the spinal cord during the early phases (first 24-36 hours) and later phase (days to weeks) following peripheral nerve injury. Importantly, these changes need to account for inter- and intra-individual responses rather than assuming group mean responses represent the breadth of mechanisms that may be involved in establishing a phenotypically similar response. The animal models of peripheral nerve injury, which are often used to model the human neuropathic pain pathology, use a binary approach (pain versus no-pain) to create the extremes of the disease. The limitation with this approach is that binary methods cannot capture the dynamic range of the degrees of symptoms that are observed in clinical presentation of neuropathic pain which vary from mild to severe. Nor can they address the hypothesised molecular mediators that contribute differentially to different magnitudes of exaggerated pain. We have previously developed an animal model of neuropathic pain, adapted from the well validated Bennet and Xie (1988) chronic constriction injury model (CCI), that allows for the development of graded behavioural response to mechanical stimuli (Grace et al., 2010). Importantly, this model explores mechanical hypersensitivity across hypothesised clinically relevant ranges, rather than focusing on sparsely observed extremes of potential pain behaviours. We previously demonstrated that by using a graded CCI injury approach, animals produced both distinct pathological responses that aligned with the increased expression of glial markers, CD11b (microglia) and GFAP (astrocytes) within the ipsilateral lumbar dorsal spinal cord. Although the behavioural pathology could be assessed from the same animals throughout the study, the molecular changes within the spinal cord were only determined at the endpoint (day 14 post-op), once mechanical allodynia had been established. Using endpoint based experimental protocols such as the aforementioned study, would require a significant number of animals to be used to observe the progressive spinal changes (both cellular and molecular) which occur during the transition between acute and chronic pain states. Novel *in vivo* imaging can circumvent the previous methodology limitations by allowing researchers to observe the spinal cord throughout the experimentation period, such as repeated observations of GFP expressing cells within the spinal cord using 2-photon imaging (Farrar et al., 2012; Ali et al., 2017). These implanted windows into the spine, allow for up to 60 days of observation of the animal, giving spatial and temporal information regarding cellular activity of tagged cells, such as microglia, encoding information such as shape and numbers of cells and their movement over time.

Further to this, owing to the known multi-neuroanatomical compartment processing of ascending nociceptive signals, understanding the functional changes occurring in multiple regions of the somatosensory cortex across similar time-course would add valuable information towards understanding corresponding changes in neuronal activity of higher order processing, following the development of mechanical allodynia. An example of a technology that would enable this, is photoacoustic tomography (PAM). PAM measures haemodynamic responses to neural activity, allowing non-invasive quantification of cerebral haemodynamic changes (Qiao et al., 2017).

In this study we created a convergence experimental design through the use of three innovative experimental and analytical techniques to further understand 1) microglial reactivity changes following nerve constriction injury as mechanical allodynia develops; 2) haemodynamic changes within the somatosensory cortex following the establishment of mechanical allodynia; and 3) how these changes relate to the degree of nerve injury and the graded behavioural response.

5.3 Methods

5.3.1 Animals

Male CX3CR1^{gfp+} (Stock No. 005582, purchased from Jackson Lab) mice (8 weeks old) were used in all experiments. All mice were maintained under a specific pathogen-free (SPF) barrier facility at Animal Centre of Wuhan National Laboratory for Optoelectronics. All animal studies were conducted in compliance with protocols that had been approved by the Hubei Provincial Animal Care and Use Committee and in compliance with the experimental guidelines of the Animal Experimentation Ethics Committee of Huazhong University of Science and Technology. During surgeries 0.2 g/kg chloral hydrate + 1 g/kg urethane was used as anaesthesia, and 1-2 % isoflurane as anaesthesia during spinal and brain imaging.

5.3.2 Experimental design

5.3.2.1 Surgery (spinal window)

The surgery has been described in detail previously (Farrar et al., 2012 Nature Methods; Figure 5.1). Under general anaesthesia (i.p. 0.2 g/kg chloral hydrate and 1 g/kg urethane), the dorsal surface above the lumbar spine (L4-5) was shaved and the exposed skin washed three times alternatively with 70% (v/v) ethanol and iodine to reduce risk of infection. Intraperitoneal

injections of 1 ml/100 g mouse of 5% glucose in saline (for hydration) and 0.2 mg/kg mouse dexamethasone (an anti-inflammatory steroid to reduce inflammation) were administered prior to surgery. A subcutaneous injection of 0.1 ml of 0.125% (v/v) lidocaine was administered at the site of skin incision. A small incision in the skin at the lumbar level of the mouse's spine and the skin retracted. An incision along three vertebrae on either side of L5 was made and the bone scraped clean on the top and the sides. The attached tendons to the three vertebrae were severed and all incongruous tissue was trimmed to reduce necrosis. Three vertebrae were clamped by magnetic stainless-steel bars with a notched groove and held under pressure on 30 mm stainless steel posts with a three-pronged plug, consisting of two pins to prevent rotation and a central magnet to hold the bar. The dorsal lamina of L5 was removed, the lateral edges of the bone back were trimmed as close as possible to the edges of the bars and the surface of the bone sealed with dental acrylic and cyanoacrylate. Where possible, the dura was left intact.

Keeping the cord irrigated with normal saline, the top plate was positioned, and screws inserted into the metal bars. Kwik-Sil silicone elastomer (World Precision Instruments) was injected into the space between the cord and the top plate and the chamber was sealed with a 5 mm diameter coverslip. Dental acrylic (Liquid, Teets,8501. Powder, TCI) and cyanoacrylate (Loctite 495) was used to seal the chamber at the rostral and caudal vertebrae. With pressure maintained by the screws, the three-pronged steel posts were then removed. The skin was pulled to the edge of the implant and secured with cyanoacrylate glue and dental acrylic. The set screws were inserted into the wings of the top plate.

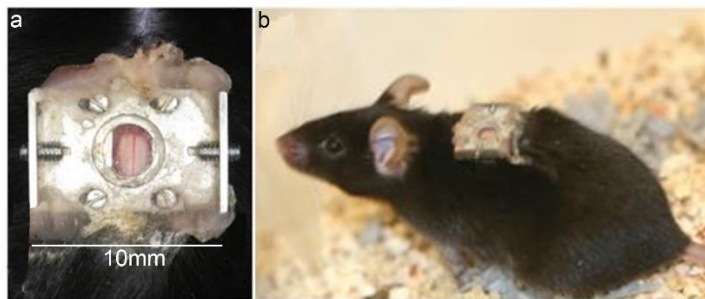


Figure 5.1 An imaging chamber for longitudinal optical access to mouse spinal cord without the need for repeated surgeries, adapted from *Farrar et al., 2012 Nature Methods*. (a) Photograph of the imaging chamber. Scale bar, 10 mm. (b) Photograph of a mouse with an implanted chamber (same mouse from panel a)).

Study 1: Spinal window imaging

Day -7	Day -1	Day 0	Days 2, 5, 7 & 14 PO
<i>Spinal window surgery</i>	<i>Baseline von Frey testing and spinal confocal imaging</i>	<i>CCI surgery</i>	<i>Von Frey behavioural testing and spinal confocal imaging</i>

5.3.2.2. Surgery (sensory cortex window)

This surgery has been described in detail previously (Shih et al., 2012). Under general anaesthesia (i.p. 0.2 g/kg chloral hydrate and 1 g/kg urethane), the mouse was fixed on a brain stereotactic apparatus to avoid motion disturbance. The region covering the somatosensory cortex hind limb was thinned using a dental drill with low speed after removing the scalp over the entire dorsal skull surface, to create a thinned-skull window for photoacoustic imaging, described here below.

Study 2: Photoacoustic cortex imaging

Day 0	Day 30+ PO
<i>CCI surgery</i>	<i>Photoacoustic imaging</i>

5.3.3. Graded chronic constriction injury (CCI) model

The CCI model of graded sciatic nerve injury was performed aseptically at the mid-thigh level of the left hind-leg, as previously described (Grace et al., 2010), in order to produce a graded intensity of pain behaviour. Briefly, animals were anesthetized with 1-2 % isoflurane, the skin of the hindquarters was shaved and the sciatic nerve gently elevated using glass hooks. Zero, 1, 2, 3 or 4 sterile chromic gut sutures (cuticular 4-0 chromic gut; Ethicon, Somerville, NJ, USA) were loosely tied around the isolated sciatic nerve (N; approximately 3–4 mm in length). Once the superficial muscle overlying the nerve was sutured with silk, and prior to surgical stapling of the skin incision, additional equal lengths of chromic gut were placed subcutaneously (S; approximately 3 – 4 mm in length), such that each animal was exposed to four equal lengths of chromic gut in total. Thus, the treatment groups, differing in pain

behaviour, were: sham (N0S4; n = 4); low pain (N1S3; n = 4); low-medium pain (N2S2; n = 4); medium-high pain (N3S1; n = 4) and high pain (N4S0; n = 4).

5.3.4 von Frey mechanical allodynia behavioural testing

The von Frey test investigated mechanical allodynia using phasic stimulation of von Frey filaments across a range of thresholds. Briefly, mice were subjected to 10 stimulations with 6 calibrated von Frey filaments (0.04, 0.07, 0.16, 0.4, 0.6 & 1; grams of force). von Frey filaments were applied for 1 s at 1 s intervals in random force assignment at each test session as described by Nicotra *et al* (2012). In order to avoid sensitization, a 10-minute break was given between each set of simulations. von Frey Testing investigated the response frequency at each von Frey filament and behavioural responses were recorded as the average number of responses out of 10 for each von Frey filament.

5.3.5 Confocal imaging of spinal cord:

CX3CR1^{gfp+} mice were imaged at different time points: pre (the date before the CCI injury), day 2, day 5, day 7, day 14 (the date when CCI injury operation finished was denoted as day 0). Mice were anaesthetized with 1-2% isoflurane in oxygen flow at 0.6 L/min controlling by a Matrix VMS small animal anaesthesia machine (Midmark, Kettering, Ohio, USA) and was placed on an imaging bracket in which the spinal cord chamber was fixed through the screw hole in the lateral of top plate. Imaging was performed using a multiphoton microscope (LSM 780, Axio Examiner, Zeiss) with a 20× water-immersion objective lens (numerical aperture (NA) = 1.0; Zeiss). Imaging was performed using 488 nm wavelength with an Ar laser. Emission filters at 525/50 nm were used to isolate fluorescence GFP. The large scale of imaging stacks, 3000 μm × 1500 μm (in the xy plane) × 200 μm (in the z plane) with 10 μm axial spacing, were acquired first, from which the dorsal vein was clearly shown and the bilateral of spinal cord were distinguished. Then 20 min imaging sequences with an interval of 5 seconds were monitored in both ipsi- and contra-lateral aspects of the spinal cord.

5.3.6 Photoacoustic microscopy of somatosensory cortex imaging

The Sensory 1, hindlimb region (S1HL) of mice were imaged through the thinned-skull window between day 30-40 post-injury using a custom photoacoustic microscopy (Jiang *et al.*, 2016; Yang *et al.*, 2017) with a step size of 2 μm. To image the cerebral microvascular structure through the thinned skull window, during each experiment, an isosbestic wavelength of 584 nm was used. A separate 2 mm x 2 mm cross-sectional area of the S1HL cortex was chosen for

both the ipsilateral and contralateral side. The selected cross scan was used for dynamic monitoring of the diameter, HbT, and SO₂. Three wavelengths of 576, 580, and 584 nm were used for the monitoring. Each monitoring trial lasted for ~23 min per wavelength (150 B-scans at three wavelengths).

5.3.7. Confocal imaging

Imaging stacks and time series were analysed with Imaris (Version 7.6, Bitplane) and ImageJ (Version 1.49, Fiji). Volume density of microglia in each lateral of spinal cord were acquired from large scale z stacks through counting the average cell numbers from 5 random cubes with a volume of 250 μm \times 250 μm \times 60 μm per cube in each mouse and are presented here as cells/ $3.75 \times 10^6 \mu\text{m}^3$. The morphology change (circularity) was evaluated according to the formula of form factor. Form factor = $4\pi A/P^2$ (A; area; P, perimeter). The area and perimeter of microglia were calculated with Fiji. Cells that are more circular or ameboid in shape are given a score closer to 1 (with a circle being = 1), in contrast, a cell that is highly ramified or less circular is scored closer to zero. When analysing the movement of microglial processes, intact processes were randomly chosen. The motility (velocity) of microglial processes during a 20 min time series was tracked manually with Imaris software (version 9.2, Advance Tracking). We randomly selected intact processes, and tracked the processes in each frame, over a whole image sequence containing 240 frames, using the SPOT selection tool. The velocity is described below as the microglial process velocity in micrometres per min ($\mu\text{m}/\text{min}$). The average process length originating from the soma was also determined from these frames and described below as microglial process length in micrometres (μm).

5.3.8 Photoacoustic imaging

The total haemoglobin (HbT) signal (denoted as, PA amplitude) of cerebral micro vessels were mapped in images through scanning under the wavelength of 584 nm. The PA amplitude value were acquired from random regions of micro vessels with MATLAB. SO₂ of S1HL cortex micro vessels were calculated using a multi-wavelength method. With the use of three wavelengths shown above, the formula following were acquired by least-squares fitting.

$$[HbR] = (M^T M)^{-1} M^T \Phi(x,y,z) K \quad (1)$$

$$[HbO_2]$$

$$SO_2 = \frac{[HbO_2]}{[HbO_2] + [HbR]} \quad (2)$$

where

$$M = \begin{bmatrix} \varepsilon_{HbR}(\lambda_1) & \varepsilon_{HbO_2}(\lambda_1) \\ \vdots & \vdots \\ \varepsilon_{HbR}(\lambda_n) & \varepsilon_{HbO_2}(\lambda_n) \end{bmatrix}, \Phi(x, y, z) = \begin{bmatrix} \Phi(\lambda_1, x, y, z) \\ \vdots \\ \Phi(\lambda_n, x, y, z) \end{bmatrix}$$

HbR is deoxygenated haemoglobin. HbO₂ is oxygenated haemoglobin. K is the proportionality coefficient that is considered to be constant. ε is the molar extinction coefficient. φ is the amplitude of photoacoustic signal. Further data processing was the same as that used in HbT to get the relative change in SO₂. Then the SO₂ of S1HL cortex micro vessels were collected from micro vessels randomly with MATLAB.

5.3.9. Statistical analysis

The 50% response threshold was calculated from the von Frey mechanical stimulation of both ipsi and contralateral hind paw plantar surfaces. A repeated measure (within individual) linear mixed-effects model was used to determine the effect of time (days post-surgery), the extent of nerve injury on the quantified mechanical allodynia, and any possible interaction between them (ipsi and contralateral responses assessed separately). Similar repeated measures linear mixed effects modelling was performed for each imaging measure collected to determine if any significant time or nerve injury effects had been observed (ipsi and contralateral responses assessed separately). Given some data for specific imaging measures were missing, the subsets of data and the behavioural statistical tests were re-run to ensure the main behavioural effects were still represented in the remaining animals (any loss of significance was reported). For the day 14 imaging and behavioural data, a Spearman rank correlation of allodynia x extent of nerve injury, imaging data x extent of nerve injury, and allodynia x imaging data were performed to determine if any relationship between the level of nerve injury and other behavioural and imaging parameters existed (ipsi and contralateral responses assessed separately). All statistics were performed using the 64-bit distribution of R statistical program,

version 3.6 (R Development Core Team, 2011) via the graphical user interface: R-studio (RStudio). Statistical analyses of Photoacoustic measurements were carried out using GraphPad Prism 7.03 software. PAM data were analysed using a Two-way ANOVA with a Tukey's test as post hoc test. Results are means +/- standard error of the mean (SEM). A value of $p < 0.05$ was considered statistically significant.

5.4 Results

5.4.1 Development of graded mechanical allodynia following nerve injury.

Prior to CCI surgery, mice showed similar 50% response withdrawal threshold on the left (ipsilateral; $p = 0.87$) and right (contralateral; $p = 0.996$) hind paws. Following surgery, the change in the 50% response withdrawal (PWR) to tactile stimulus of the ipsilateral hind paw showed a main effect of time and degree of nerve injury with significant interactions between the degree of nerve injury and days post-surgery at day 5 ($p = 0.009$), day 7 ($p = 0.0006$) and day 14 ($p < 0.00001$). In contrast, no such time or injury effect was observed on the contralateral hind paw ($p = 0.28$) (Figure 5.2). Further assessment of the relationship between the degree of the nerve injury and the development of graded mechanical allodynia demonstrated that whilst no correlation was found on day 0 (Spearman rho = -0.22; $p = 0.2$) and day 2 post-surgery (Spearman rho = -0.31; $p = 0.08$), by day 5 (Spearman rho = -0.60; $p = 0.0003$) and onwards through 7 (Spearman rho = -0.72; $p < 0.00001$) and day 14 (Spearman rho = -0.80; $p < 0.00001$) post-surgery significant correlations between the number of neuronal sutures and the extent of mechanical allodynia was evident. No such relationship was evident for the contralateral paw (Spearman rho = -0.12 to 0.30; $p = 0.15$).

5.4.2 Microglial density, circularity, process length and movement following graded nerve injury.

Microglial density, circularity, process length and velocity were measured from the ipsilateral and contralateral dorsal lumbar regions of the spinal cord of mice pre- and post- surgery for up to 14 days post-injury. At baseline, the density, circularity and velocity of the microglia were the same for all animals in both the ipsilateral and contralateral side of the spinal cord.

Representative confocal images of microglia taken from the contralateral and ipsilateral dorsal spinal cord are shown in Figure 5.3E. Microglial density within the ipsilateral side of the spinal cord increased depending on the grade of the nerve of injury as well as the time following

surgery from day 7 ($p < 0.0001$) until day 14 ($p < 0.01$) (Figure 5.3A). Importantly, this increase in density was significantly correlated with the degree of nerve injury (day 14 Spearman rho = -0.77; $p < 0.0001$). These relationships were not evident for the contralateral side ($p = 0.18$ for day by nerve relationship and Spearman rho = -0.1, $p = 0.6$).

Circularity of microglia was used to measure the change in microglial morphology from a ramified shape to an amoeboid shape, which is reported to be related to the functional change from dormant or surveillance properties, to more active or phagocytic properties as seen in pain states (Zanier et al., 2015). Briefly, cells that are more circular or amoeboid in shape are given a score closer to 1 (with a circle = 1), in contrast, a cell that is highly ramified or less circular is scored closer to zero. A linear mixed-effects model was constructed analysing the effect of day of assessment and CCI surgery model on ipsilateral microglial circularity (Figure 5.3B). The test revealed a significant day by nerve injury effect from day 2 to 14 ($p < 0.03$) on the ipsilateral side but not the contralateral side ($p > 0.21$). As for microglial density, a significant correlation was observed for the degree of microglial circularity with the extent of nerve injury from day 5 (Spearman rho = 0.58; $p = 0.008$) until day 14 (Spearman rho = 0.55; $p = 0.01$). No such effect was observed on the contralateral side ($p > 0.21$ for day by nerve relationship and Spearman rho = -0.1, $p = 0.8$).

The velocity of microglia was measured by tracking the movement of individual microglial processes during a 20 min video capture. The data is expressed as movement in micrometres per minute ($\mu\text{m}/\text{min}$). A linear mixed-effects model was constructed analysing the effect of day of assessment and CCI surgery model on ipsilateral microglial process velocity (Figure 5.3C). The test revealed a significant day by nerve injury effect from day 7 to 14 ($p < 0.03$) on the ipsilateral side but not the contralateral side ($p > 0.38$). As for microglial density and circularity, a significant correlation was observed for the degree of microglial velocity on day 14 (Spearman rho = -0.68; $p < 0.0001$). No such effect was observed on the contralateral side ($p > 0.21$ for day by nerve relationship and Spearman rho = -0.16, $p = 0.4$).

Length of microglial processes was measured as distance originating from the cell soma to the end of the extended tip and the data is expressed in micrometres. A linear mixed-effects model was constructed analysing the effect of day of assessment and CCI surgery model on ipsilateral microglial process length. The test failed to detect any significant effect of time since nerve injury or degree of injury on the ipsilateral ($p > 0.26$) or contralateral ($p > 0.92$). Unlike

the other measures of microglial state, no relationship to nerve injury was observed on either side of the spinal cord (Spearman rho = -0.02 to 0.02; $p > 0.95$).

5.4.3 Sensory motor cortex oxygen levels increase due to injury.

The cerebral haemodynamic responses in both the ipsilateral and contralateral sides of sensory 1, hindlimb region (S1HL) primary somatosensory cortex, was measured from N0S4 (sham control), N2S2 (med pain) and N4S0 (high pain) animals. A two-way ANOVA was constructed to analyse the effect of graded CCI surgery on both contralateral and ipsilateral photoacoustic amplitude (PA) and oxygen saturation (SO₂). The test revealed an overall effect of CCI surgery ($p < 0.0001$) on PA. A post-hoc test using Tukey's correction showed that there was a significant increase in PA signal in both ipsilateral ($p < 0.01$) and contralateral ($p < 0.01$) blood vessels of N4S0 S1HL sensory cortex when compared to sham (N0S4) animals (Figure 5.4A & B). This indicates a higher total haemoglobin level and blood flow in the cortex of N4S0 injured animals. The test also revealed that there was an overall effect of CCI surgery ($p < 0.01$) on SO₂. However, the Tukey's post-hoc test showed no difference between surgery groups (Figure 5.4C & D).

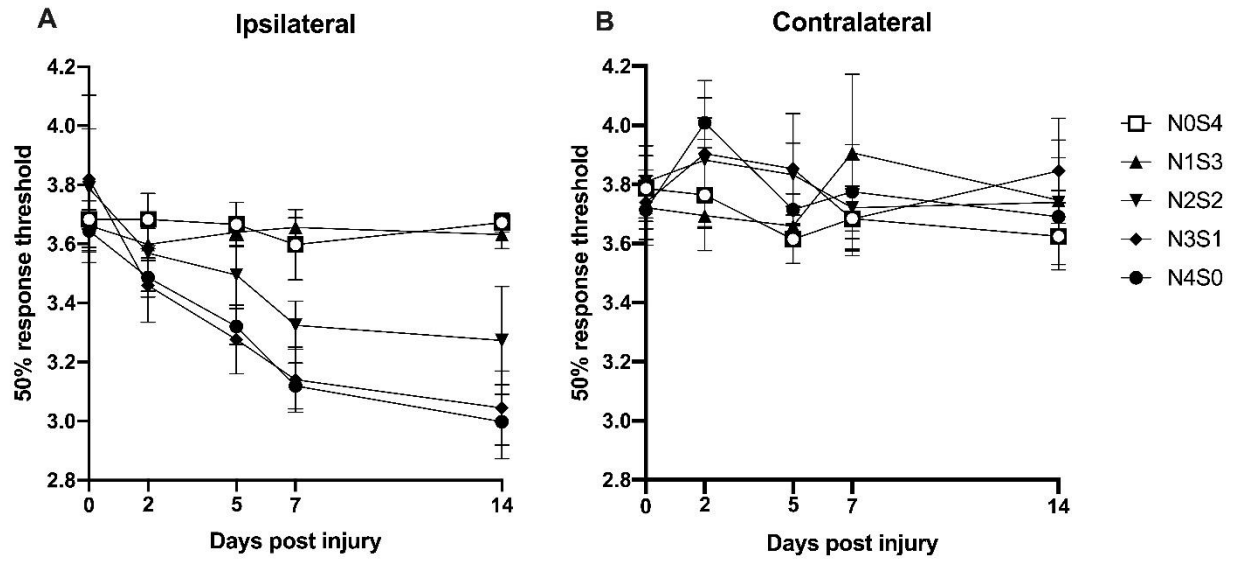


Figure 5.2 Graded nerve injury creates graded mechanical allodynia. Graded sciatic nerve injury (N0S4, N1S3, N2S2, N3S1, N4S0) causes the presentation of mechanical allodynia to von Frey stimuli over the 14 days of the study which is correlated with the extent of nerve injury. Error bars are SEM with n = 4.

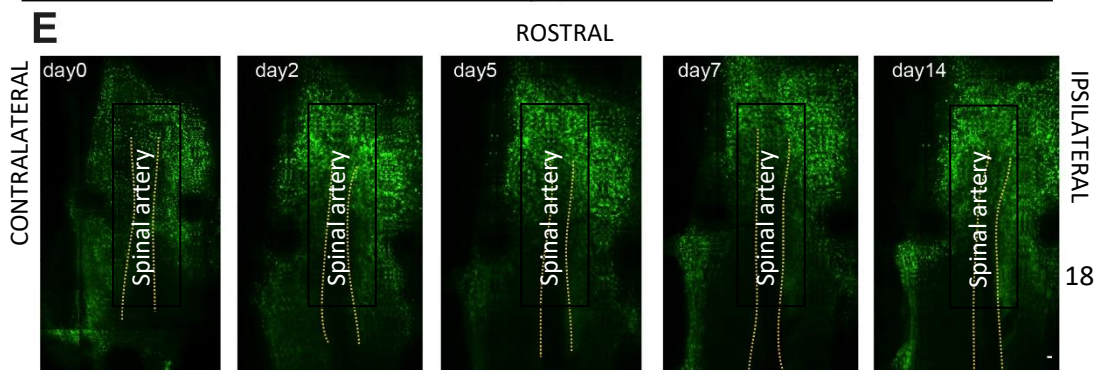
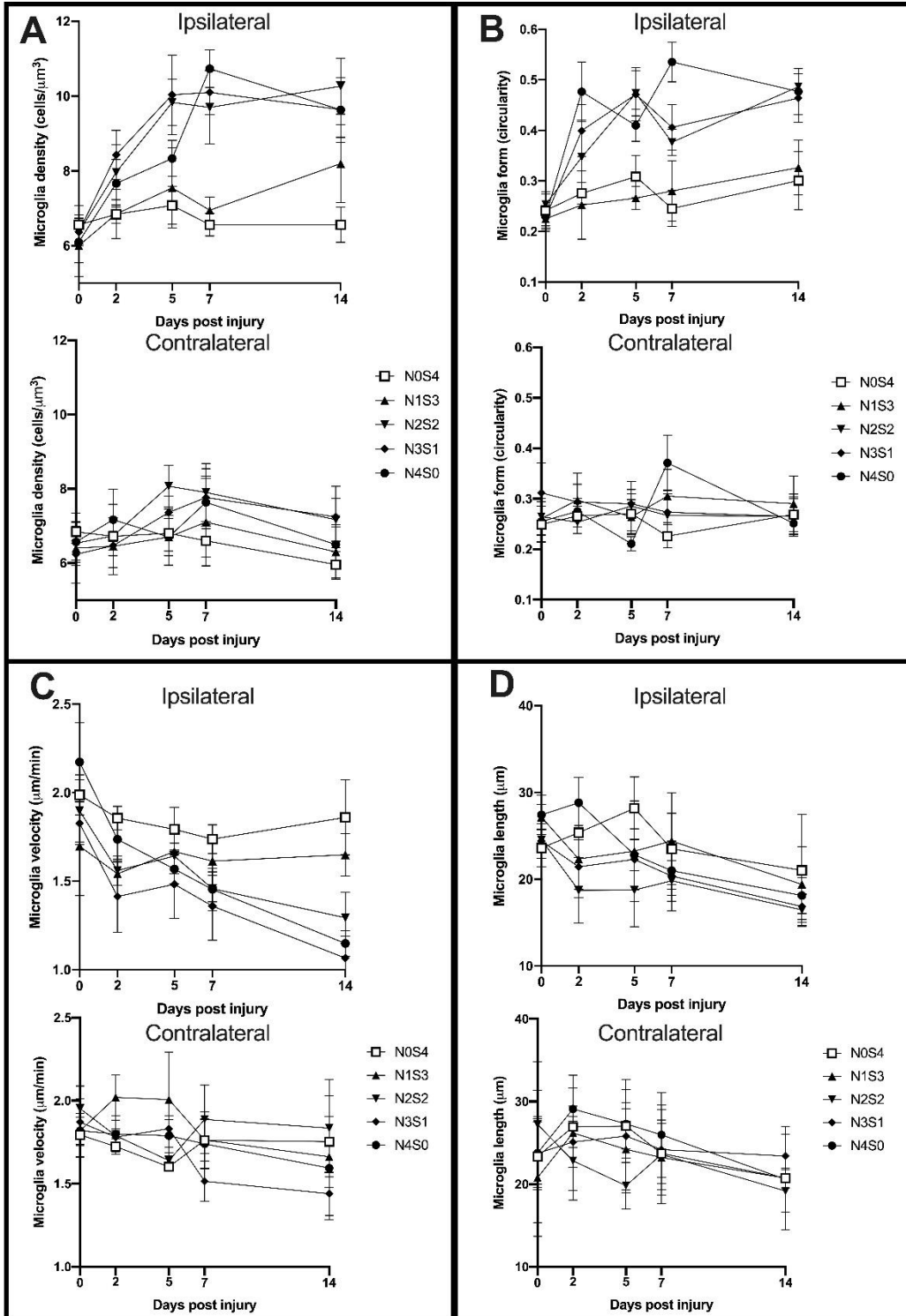


Figure 5.3. Graded peripheral injury results in changes in spinal microglial density, morphology, velocity but not process length.

Graphs representing measures of microglia density (A), form (B) velocity (C) and (D) process length for each graded sciatic nerve injury group over time (Day). Error bars are SEM with n = 4. (E) Confocal images taken of the dorsal aspect of the L4/L5 contralateral and ipsilateral dorsal spinal cord at Day 0, 2, 5, 7 and 14 post-injury. The rostral aspect is to the top of the image with more caudal towards the bottom. Scale bar = 50 μ m.

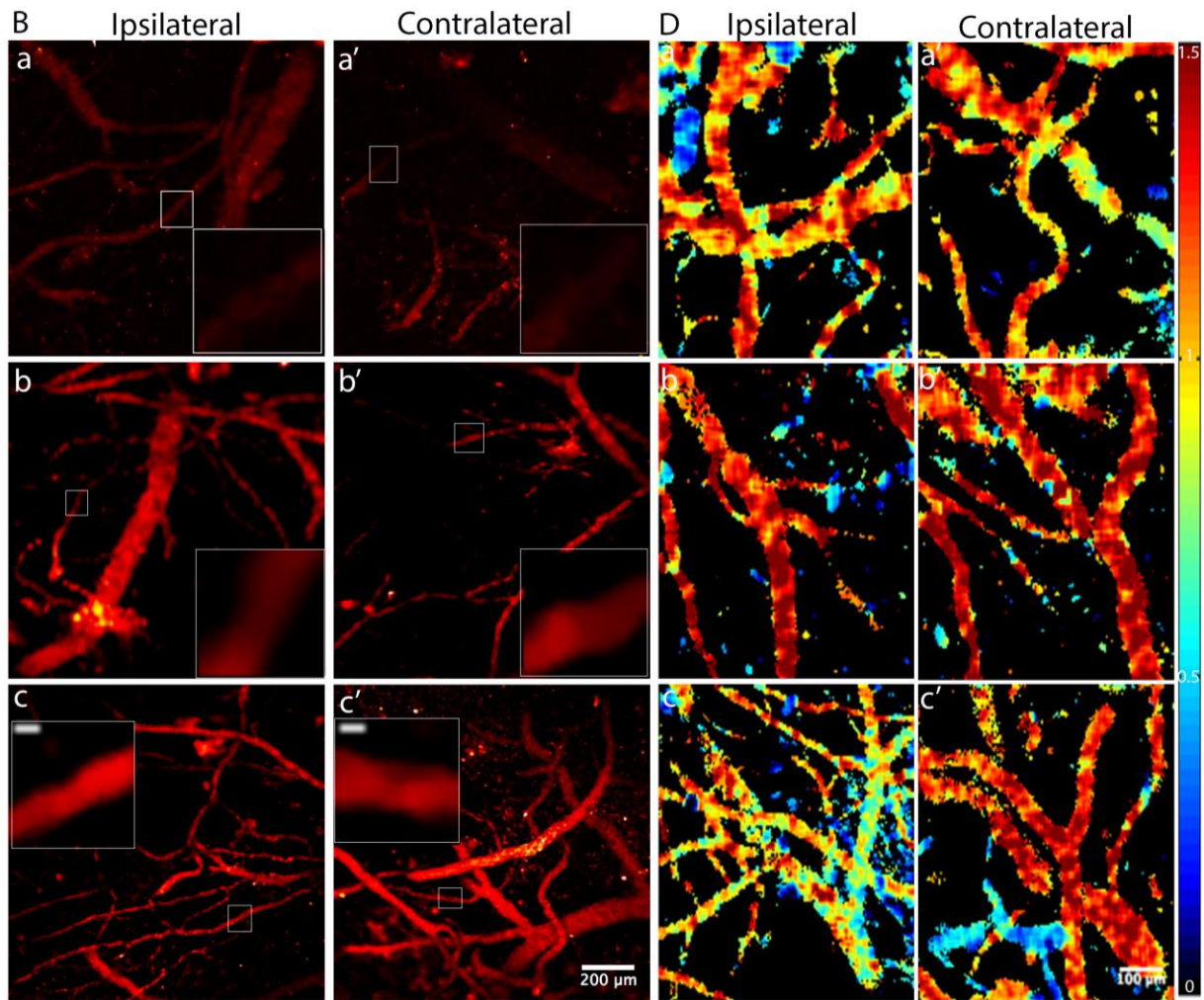
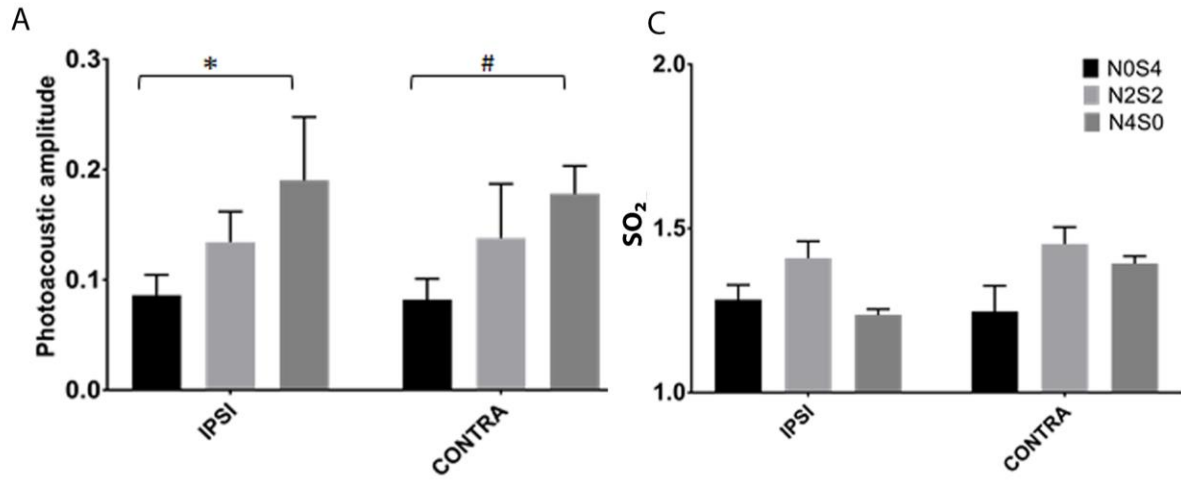


Figure 5.4 Photoacoustic amplitude is increased in the S1HL somatosensory cortex of high grade (N4S0) injured animals

(A) Quantitation of photoacoustic amplitude from vasculature in S1HL. (B) Typical MAP (maximum amplitude projection) images in different injury groups are showed and magnification of single vessels are shown in white box. Ipsilateral refers to peripheral injury side. Injury groups: N0S4 (a; ipsilateral, a'; contralateral), N2S2 (b; ipsilateral, b'; contralateral) and N4S0 (c; ipsilateral, contralateral). Scale bar = 200 μ m. (C) Oxygen saturation (SO₂) in S1HL somatosensory cortex of injured animals is not different from control animals. (D) Typical MAP (maximum amplitude projection) images are shown. Colour bar of SO₂ shows changes from normoxia (0) to hyperoxia (1.5). Ipsilateral refers to peripheral injury side. Injury groups: N0S4 (a; ipsilateral, a'; contralateral), N2S2 (b; ipsilateral, b'; contralateral) and N4S0 (c; ipsilateral, contralateral). Scale bar = 100 μ m. Error bars are SEM with n = 3, significance is reported as p < 0.05.

5.5 Discussion

We have established, using a graded nerve injury model with repeated imaging of spinal microglia, that the degree of nerve injury influences (i) the development of graded allodynia from days 5 - 14 post-surgery (ii) the extent of microglial density from day 7 – 14 post-surgery (iii) the extent of microglial circularity from day 5 -14 post-surgery (iv) the velocity of microglial processes at day 14 post-surgery. However, there were no observable changes associated with overall process length. Further to this, higher level sciatic injury (N4S0), resulted in an increased haemoglobin levels and blood flow in the somatosensory cortex (S1HL).

Our study found that the extent of peripheral nerve injury, as determined by the number of sciatic sutures, was correlated with graded mechanical allodynia from days 5 14 following injury. Previous work (Grace et al., 2010) has shown that graded chronic constriction injury of the sciatic nerve, can generate hind paw allodynia that is correlated to the number of neural sutures in rats. We confirmed these results in our study using mice. However, it is worth noting that our injured mice did not develop allodynia on the contralateral hind paw, as was reported in the same study. The correlation observed by Grace et al (2010), also extended to the expression levels of CD11b (a known microglial reactivity marker) in the ipsilateral dorsal horn of the spinal cord, but not on the contralateral side. To understand the relationship between increased microglial reactivity and functional changes that are occurring, such as the release of inflammatory mediators that act on the local neurons, further investigation is warranted.

This study was able to observe and measure microglial reactivity within the superficial region of the lumbar spinal cord and compare ipsilateral and contralateral changes, from before injury, through to the development of allodynia within the same animal. We observed a change in cell morphology from a more ramified shape to that resembling a circular or amoeboid shape, indicative of cell reactivity within 48 hours following injury in the high neural injury group (N4S0) when compared to the surgical sham animals (N0S4). A significant correlation between the degree of microglial circularity and the extent of nerve injury was observed from day 5 to 14 post-injury. Previous studies have also observed changes in morphology of microglia to a reactive state, 24 hours after peripheral nerve injury (Eriksson et al., 1993). It is worth noting, in other groups, the extent and time course of microgliosis changes varied between studies depending on the type of injury and the location (Colberg et al., 1999; Parkhurst & Gan, 2010 Review).

The importance of the timing of microgliosis in the context of neuropathic pain was recently demonstrated in a study that inhibited the development of mechanical allodynia following spinal nerve injury by depleting microglial (CX3CR1⁺) cells within 5 days. However, this reversal was not seen if the depletion was done at later time points (7- & 9-days following injury) (Peng et al., 2016). Additionally, pharmacological inhibition of microglia attenuated the development but not existing hypersensitivity following peripheral nerve injury (Ledeboer et al., 2005; Raghavendra et al., 2003). These past studies and the new evidence generated here support the growing body of evidence, that microglial cells contribute to the initiation, but not maintenance of neuropathic pain development (Colburn et al., 1999; DeLeo et al., 2004; Jin et al., 2003; Narita et al., 2006; Tanga et al., 2004, Mika et al., 2009).

Knowledge of whether the increased density of microglia following injury was due to either proliferation or peripheral infiltration was limited by our ability to identify between these cell types *in vivo*. However, previous studies have observed an increase in microglial proliferation in the ipsilateral spinal cord of rats following nerve ligation which peaked at day 3 post-surgery, with the newly generated cells continuing to proliferate over time peaking at 14 days post-surgery (Echeverry et al., 2008). Furthermore, a recent study using transgenic reporter mice, and resident microglial versus monocyte cell specific immunostaining, found that there were no monocytes entering the spinal dorsal horn within 14 days of spinal cord injury (Gu et al., 2016). This is in contrast to previous work that showed peripheral monocytes infiltrating the parenchyma of the spinal cord following peripheral nerve injury. The authors of the study concluded that the chemokine, monocyte chemoattractant protein-1 (MCP-1) cause local microglial activation as well as drove the infiltration of bone-derived monocytes into the spinal cord (Zhang et al., 2007). Taken together, this evidence suggests that the increased microglial density observed in this study requires further investigation to identify the source of the increased cell numbers.

This study observed a decreased in microglial process velocity from day 7 to 14 post-surgery. However, a correlation with the degree of injury was only observed at day 14. Under normal physiological conditions, microglia display a constant motility of their highly branched cellular processes within the intact mouse CNS (Stence et al., 2001; Nimmerjahn et al., 2005). Experiments in mice, have shown that microglial processes contact and pause on active neuronal synapses *in vivo*, suggesting a possible role of microglia motility in synaptic

remodelling and/or function (Wake et al., 2009). Following acute CNS damage, Stence et al (2001), has elegantly described a series of morphological stages that microglia undergo, which sees the highly ramified processes of resting microglia completely retract into the cell body within approximately an hour after initial observations begin, using confocal time lapse capture. This retraction occurs before transitioning, into what was described as a dynamic motile stage, where new extending and retracting processes develop. In this study, it is likely that these secondary processes, are what we are observing in the spinal cord, 48 hours following peripheral injury. At the molecular level, this dynamic motile stage, appears to proceed a series of stages, which differ in their expression of molecules for cell adhesion, cytoskeletal organization and antigen presentation (Raivich et al., 1999).

Within days to weeks following this dynamic motile stage, microglia then transition into the phagocytic amoeboid morphology and can move quite rapidly to clean up axonal damage. Microglial processes are capable of rapid extension (1 - 4 $\mu\text{m}/\text{min}$) towards the site of injury (Stence et al., 2001; Nimmerjahn et al., 2005), our study found that there was no difference in baseline velocity of microglial processes in all groups prior to surgery (2.0 \pm 0.1 $\mu\text{m}/\text{min}$, ipsilateral and 1.9 \pm 0.1 $\mu\text{m}/\text{min}$, contralateral). However, we observed a significant change in the velocity of microglial processes within the ipsilateral dorsal spinal cord at day 14 following injury. The reduction in process movement may be occurring due to the retraction of processes, as the microglia transition into a more phagocytic morphological phenotype.

Previous work reporting changes in microglial process velocity only measure acute responses (1-2 hours post-injury) following focal injury in the brain. This is the first study to look at longer term changes in motile behaviour of spinal microglia following peripheral nerve injury.

Microglial process length has previously been reported as a morphological marker of activation. Resting microglia display small compact somata and long, thin, ramified processes, whereas activated microglia exhibit marked cellular hypertrophy and retraction of processes (Zhang et al., 2008). Following the microglial changes detected in circularity and process velocity, we expected to observe similar changes in overall process length. However, our results showed that there was no relationship between graded injury and process length over time. Furthermore, linear mixed effects analysis did not identify any injury group differences. A previous study (Gu et al., 2016) reported a decrease in spinal microglial process length at 3- and 7-days post-injury, which is in contrast with our study. However, our study employed a

less extreme and more clinically relevant mode of neuropathic pain which may attribute to these differences and highlight the relevant association between the intensity of injury and overall microglial response. As it is now understood that microglia are fundamental to neuropathic pain processing in male rodents. There is a differential role for this cell type in female rodents (Mapplebeck et al, 2016; Watkins et al, 2003), as it has been reported that pharmacological inhibition of microglia produces a reversal of hypersensitivity in male but not female mice (Sorge et al, 2015). Futures studies into the activation of spinal microglia following injury, similar to this study, would allow us to further understand how microglia characteristics change over time in the spinal cord of CCI injured female mice, compared to male cohorts. We observed an increase in PA signal (measure of total haemoglobin) to both the contralateral and ipsilateral aspects of the S1HL region of the primary somatosensory cortex in N4S0 injured animals (compared to N0S4), indicating an increase in blood flow to these regions following peripheral injury. It is worth noting, that these measurements were done approximately 30 days following the initiation of peripheral injury, and any changes in neural activity relating to the injury, may have resolved by this time. A limitation of this study is that although these animals were established as allodynic at day 14 post-injury, they did not undergo von Frey testing at the same time (day 30) as the PAM imaging, therefore, we cannot report if the animals were allodynic at that time. However, previous studies have reported persistent allodynia in rodent models of neuropathic pain for up to and beyond 20 weeks post injury (Decosterd & Woolf., 2000; Seminowicz et al., 2009), therefore we conclude that our animals used for PAM imaging at 30 days post-injury, were most-likely still allodynic. This is the first study to measure hemodynamic changes in the sensory cortex of neuropathic pain animals. We observed increased haemoglobin levels in the somatosensory cortex of animals with a high degree of injury (N4S0) when compared to sham controls. This suggests that higher levels of injury result in changes in neuronal activity within the somatosensory cortex. These changes were observed in both the ipsi- and contralateral sides of the cortex despite the unilateral injury. Bi-lateral changes in cortical neural activity have previously been reported in CCI operated rats when compared to sham operated, as inferred from increased local glucose utilization rate, measured using ¹⁴C-2-deoxyglucose (2-DG) autoradiography (Mao et al., 1993). Mao et al., (1993) looked at topographical changes of 2-DG throughout sections of the whole brain and reported increased neuronal metabolic activity only in deeper

contralateral brain regions, including the mid and deep S1HL region. As PAM measurements of the cortical blood vessels are taken through the thinned skull, we may have not reached the required imaging depths to determine the haemodynamic activity of the deeper layers of S1HL region and highlights a possible limitation of our system.

Previous work using fMRI scans of the primary sensory cortex of spinal cord injured (SCI) patients, observed changes in cerebral blood flow in patients with neuropathic pain compared without reported pain. The authors reported a reorganization of the primary somatosensory cortex that correlated with pain intensity in subjects with complete SCI and neuropathic pain when compared to SCI subjects without pain (Wrigley et al., 2009). Similarly, a study using functional Near-Infrared Spectroscopy (fNIRS) measured distinguishable changes in signal from the S1 region of the somatosensory cortex following painful and non-painful electrical skin stimuli. Functional NIRS is a non-invasive method to measure cerebral hemodynamic activity and is sensitive enough to differentiate painful and non-painful stimuli, based on their signal size and profile (Yucel et al., 2015). These findings suggest that non-invasive measurements of hemodynamic changes in the cortex could potentially be used as an objective measure of pain levels in patients and supports our current animal findings.

5.6. Conclusion

The aims of this study were to investigate, 1) the cellular characteristics of microglia during the development of allodynia; 2) the haemodynamic changes of the somatosensory cortex following the establishment of allodynia; and 3) how these changes relate to the degree of nerve injury and/or graded behavioural responses. This was carried out using an animal model of graded neuropathic pain and a combination of the latest techniques in *in vivo* spinal cord imaging. The density, morphology and velocity of microglia was altered within the ipsilateral dorsal spinal cord of injured animals, and dependent upon the severity of the grade of sciatic nerve injury at varying time-points throughout the course of the experiment. These immune-like cells remained both abundant and exhibited morphological characteristics suggestive of being 'active' for up to 14 days post-injury, suggesting a concerted development of both microglial and behavioural adaptations throughout the first 14 days of injury. In addition, the altered hemodynamic changes occurring in the somatosensory cortex of the brain are also correlated with the degree of injury and allodynia and may provide an adjunct method for measuring the extent of pain.

This study contributes to the understanding of the progression of the characteristic changes of microglia within the spinal cord of the same animal, throughout the development of neuropathic pain.

5.7 References

Ali, I., Avdic, U., Chugh, D., and Ekdahl, C.T. (2017). Decreased post-synaptic density-95 protein expression on dendrites of newborn neurons following CX3CR1 modulation in the epileptogenic adult rodent brain. *Cellular and Molecular Immunology* 14, 1-4.

Austin, P.J., and Moalem-Taylor, G. (2010). The neuro-immune balance in neuropathic pain: involvement of inflammatory immune cells, immune-like glial cells and cytokines. *J Neuroimmunol* 229, 26–50.

Calvo, M., and Bennett, D.L. (2012). The mechanisms of microgliosis and pain following peripheral nerve injury. *Exp Neurol* 234, 271–82.

Colburn, R.W., Rickman, A.J., and DeLeo, J.A. (1999). The Effect of Site and Type of Nerve Injury on Spinal Glial Activation and Neuropathic Pain Behavior. *Experimental Neurology* 157, 289–304.

Clark, A.K., Gentry, C., Bradbury, E.J., McMahon, S.B., and Malcangio, M. (2007). Role of spinal microglia in rat models of peripheral nerve injury and inflammation. *Eur. J. Pain* 11, 223–230.

Colburn, R.W., Rickman, A.J., and DeLeo, J.A. (1999). The effect of site and type of nerve injury on spinal glial activation and neuropathic pain behavior. *Exp. Neurol.* 157, 289–304.

Costigan, M., Moss, A., Latremoliere, A., Johnston, C., Verma-Gandhu, M., Herbert, T.A., Barrett, L., Brenner, G.J., Vardeh, D., Woolf, C.J., and Fitzgerald, M. (2009a). T-cell infiltration and signaling in the adult dorsal spinal cord is a major contributor to neuropathic pain-like hypersensitivity. *J. Neurosci.* 29, 14415–14422.

Costigan, M., Scholz, J. and Woolf, C.J. (2009b). Neuropathic pain: A maladaptive response of the nervous system to damage. *Annu Rev Neurosci.* 32: 1-32.

Coyle, D.E. (1998). Partial peripheral nerve injury leads to activation of astroglia and microglia which parallels the development of allodynic behavior. *Glia* 23: 75–83.

Decosterd, I., and Woolf, C.J. (2000). Spared nerve injury: an animal model of persistent peripheral neuropathic pain. *Pain* 87(2), 149-158.

DeLeo, J.A., Tanga, F.Y., and Tawfik, V.L. (2004). Neuroimmune activation and neuroinflammation in chronic pain and opioid tolerance/hyperalgesia. *Neuroscientist.* 10, 40–52

Echeverry, S., Shi, X.Q., and Zhang, J. (2008). Characterization of cell proliferation in rat spinal cord following peripheral nerve injury and the relationship with neuropathic pain. *Pain* 135 (1-2), 37-47.

Eriksson, N.P., Persson, J.K.E., Svensson, M., Arvidsson, J., Molander, C., and Aldskogius, H. (1993). A quantitative analysis of the microglial cell reaction in central primary sensory projection territories following peripheral nerve injury in the adult rat. *Exp. Brain Res* 96, 19–27.

Grace, P., Hutchinson, M.R., Manavis, J., Somogyi, A.A., and Rolan, P.E. (2010). A novel animal model of graded neuropathic pain: Utility to investigate mechanisms of population heterogeneity. *Journal of Neuroscience Methods* 193, 47-53.

Gu, N., Eyo, U.B., Murugan, M., Peng, J., Matta, S., Dong, H., Wu, L.J. (2016). Microglial P2Y₁₂ Receptors regulate microglial activation and surveillance during neuropathic pain. *Brain Behav Immun.* 55, 82-92.

Gu, N., Peng, J., Murugan, M., Wang, X., Eyo, U.B., Sun, D., Ren, Y., DiCicco-Bloom, E., Young, W., Dong, H., and Wu, L.J. (2016). Spinal Microgliosis Due to Resident Microglial Proliferation Is Required for Pain Hypersensitivity after Peripheral Nerve Injury. *Cell Reports* 16, 605–614.

Jiang, B., Yang, X., and Luo, Q. (2016). Reflection-mode Bessel beam photoacoustic microscopy for in vivo imaging of cerebral capillaries. *Optics Express* 24, 270785.

Jin, S.X., Zhuang, Z.Y., Woolf, C.J., and Ji, R.R. (2003). p38 mitogen-activated protein kinase is activated after a spinal nerve ligation in spinal cord microglia and dorsal root ganglion neurons and contributes to the generation of neuropathic pain. *J. Neurosci.* 23, 4017–4022.

Jones, M., Berwick, J., and , J. (2002). Changes in blood flow, oxygenation, and volume following extended stimulation of rodent barrel cortex. *Neuroimage.* 15 (3), 474-87.

Latremoliere, A., and Woolf, C.J. (2009). Central sensitization: a generator of pain hypersensitivity by central neural plasticity. *J. Pain* 10, 895–926.

Ledeboer, A., Sloane, E.M., Milligan, E.D., Frank, M.G., Mahony, J.H., Maier, S.F., and Watkins, L.R. (2005). Minocycline attenuates mechanical allodynia and proinflammatory cytokine expression in rat models of pain facilitation. *Pain* 115, 71–83.

Mika, J., Osikowicz, M., Rojewska, E., Korostynski, M., Wawrzczak-Bargiela, A., Przewlocki, R., and Przewlocka, B. (2009). Differential activation of spinal microglial and astroglial cells in a mouse model of peripheral neuropathic pain. 623, 65-72.

Moore, D.C. Stanisstreet, M., and Evans, G.E. (1987). Morphometric analyses of changes in cell shape in the neuroepithelium of mammalian embryos. *Journal of Anatomy* 155, 87–99.

Morsch, M., Radford, R., Lee, A., Don, E.K., Badrock, A.P., Hall, T.E., Cole, N.J., and Chung, R. (2015). In vivo characterization of microglial engulfment of dying neurons in the zebrafish spinal cord. *Frontiers in Cellular Neuroscience* 9, 321.

Narita, M., Yoshida, T., and Nakajima, M. (2006). Direct evidence for spinal cord microglia in the development of a neuropathic pain-like state in mice. *J. Neurochem.* 97, 1337–1348.

Nicotra, L., Tuke, J., Grace, P.M., Rolan, P.E., Hutchinson, M.R. (2014). Sex differences in mechanical allodynia: how can it be preclinically quantified and analyzed? *Frontiers in Behavioral Neuroscience*, 8 (40).

Nimmerjahn, A., Kirchhoff, F., and Helmchen, F. (2005). Resting microglial cells are highly dynamic surveillants of brain parenchyma in vivo. *Science (New York, N.Y.)* 308 (5726), 1314–1318.

Parkhurst, C.N., Gan, W.B. (2010). Microglia dynamics and function in the CNS. *Curr Opin Neurobiol.* 20(5), 595–600.

Peng, J., Gu, N., Zhou, L., B. Eyo, U., Murugan, M., Gan, W.B., and Wu, L. (2016). Microglia and monocytes synergistically promote the transition from acute to chronic pain after nerve injury. *Nat Communication* 28 (7), 12029.

Pfeiffer, T., Avignone, E., and Nägerl, U.V. (2016). Induction of hippocampal long-term potentiation increases the morphological dynamics of microglial processes and prolongs their contacts with dendritic spines. *Scientific Reports* 6, 32422.

Raghavendra, V., Tanga, F., and DeLeo, J.A. (2003). Inhibition of microglial activation attenuates the development but not existing hypersensitivity in a rat model of neuropathy. *J. Pharmacol. Exp. Ther.* 306, 624–630.

Raivich, G., Bohatschek, M., Kloss, C.U.A., Werner, A., Jones, L.L., and Kreutzberg, G.W. (1999). Neuroglial activation repertoire in the injured brain: graded response, molecular mechanisms and cues to physiological function. *Brain Research Reviews* 30, 77–105.

Qiao, W., and Chen, Z. (2017). All-optically integrated photoacoustic and optical coherence tomography: A review. *Journal of Innovative Optical Health Sciences* 10, 1-10.

Scholz, J., and Woolf, C.J. (2007). The neuropathic pain triad: neurons, immune cells and glia. *Nature Neuroscience* 10 (11), 1361-1368.

Seminowicz, D.A., Laferriere, A.L., Millecamps, M., Yu, J.S.C., Coderre, T.J., and Bushnell, M.C. (2009). MRI structural brain changes associated with sensory and emotional function in a rat model of long-term neuropathic pain. *NeuroImage* 47, 1007–1014.

Shih, A.Y., Mateo, C., Drew, P.J., Tsai, P.S., and Kleinfeld, D. (2012). A polished and reinforced thinned-skull window for long-term imaging of the mouse brain. *J Vis Exp* 61, 3742.

Sorge RE, Mapplebeck JCS, Rosen S, Beggs S, Taves S, Alexander JK, Martin LJ, Austin J-S, Sotocinal SG, Chen D, Yang M, Shi XQ, Huang H, Pillon NJ, Bilan PJ, Tu Y, Klip A, Ji R-R, Zhang J, Salter MW, Mogil JS. (2015) Different immune cells mediate mechanical pain hypersensitivity in male and female mice. *Nat Neurosci*; 18:1081–3.

Stein, E.W., Maslov, K., and Wang, L.V. (2009). Non-invasive, in vivo imaging of blood-oxygenation dynamics within the mouse brain using photoacoustic microscopy. *J Biomed Opt.* 14 (2), 020502

Stence, N., Waite, M., and Dailey, M.E. (2001). Dynamics of microglial activation: a confocal time-lapse analysis in hippocampal slices. *Glia*. 33, 256–266.

Tanga, F.Y., Raghavendra, V., and DeLeo, J.A. (2004). Quantitative real-time RT-PCR assessment of spinal microglial and astrocytic activation markers in a rat model of neuropathic pain. *Neurochem. Int.* 45, 397–407.

von Hehn, C.A., Baron, R., and Woolf, C.J. (2012). Deconstructing the neuropathic pain phenotype to reveal neural mechanisms. *Neuron* 73, 638–52

Wake, H., Moorhouse, A.J., Jinno, S., Kohsaka, S., and Nabekura, J. (2009). Resting microglia directly monitor the functional state of synapses *in vivo* and determine the fate of ischemic terminals. *J Neurosci.* 29 (13), 3974-80.

Wang, X., Pang, Y., Ku, G., Xie, X., Stoica, G., and Wang, L.V. (2003). Non-invasive laser-induced photoacoustic tomography for structural and functional *in vivo* imaging of the brain. *Nat. Biotechnol.* 21, 803–806.

Watkins L, Maier S. (2003) Glia: a novel drug discovery target for clinical pain. *Nat Rev Drug Discov*; 2:973–85.

Woolf, C.J. (2004). Dissecting out mechanisms responsible for peripheral neuropathic pain: implications for diagnosis and therapy. *Life Sci.* 74, 2605–2610.

Woolf, C.J., and Salter, M.W. (2000). Neuronal plasticity: increasing the gain in pain. *Science* 288, 1765–1769.

Wrigley P, Press S, Gustin S, Gandevia S, Middleton J, Cousins M, Henderson L, Siddall P. (2009). Neuropathic pain and primary somatosensory cortex reorganization following spinal cord injury. *Pain*; 141(1-2): 52-59

Yang, X., Jiang, B., Song, X., Wei, J., and Luo, Q. (2017). Fast Axial-scanning Photoacoustic microscopy using tunable acoustic gradient lens. *Optics Express* 25 (7), 284507.

Yu, H., Lim, K.P., Xiong, S., Tan, L.P., and Shim, W. (2013). Functional morphometric analysis in cellular behaviors: shape and size matter. *Advanced Healthcare Materials* 2 (9), 1188–1197.

Yucel, M.A., Aasted, C.M., Petkov, M.P., Borsook, D., Boas, D.A., and Becerra, L. (2015). Specificity of Hemodynamic Brain Responses to Painful Stimuli: A functional near-infrared spectroscopy study. *Sci. Rep.* 5, 9469.

Zanier, E.R., Fumagalli, S., Perego, C., Pischiutta, F., and De Simoni, M.G. (2015). Shape descriptors of the “never resting” microglia in three different acute brain injury models in mice. *Intensive Care Medicine Experimental*, 3, 7.

Zhang, F., Vadakkan, K.I., Kim, S.K., Wu, L.J., Shang, Y., Zhuo, M. (2008). Selective activation of microglia in spinal cord but not higher cortical regions following nerve injury in adult mouse. *Molecular Pain*, 4, 15.

Zhang, H.F., Maslov, K., and Physics, M.S.A. (2007). Imaging of hemoglobin oxygen saturation variations in single vessels in vivo using photoacoustic microscopy. *Appl. Phys. Lett.* 90, 053901.

Zhang, J., Shi, X.Q., Echeverry, S., Mogil, J.S., De Koninck, Y., and Rivest, S. (2007). Expression of CCR2 in both resident and bone marrow-derived microglia plays a critical role in neuropathic pain. *Journal of Neuroscience* 27 (25), 12396-406.

Chapter 6: Discussion

The studies described in this thesis were conducted to explore the use of novel techniques to further our understanding of persistent pain development and molecular signaling within the CNS. The results provide insight into the activity of the immune-like glial cells within the CNS, and the reactive nitrogen species, nitroxyl (HNO). The work contributes novel findings which add to the literature on persistent pain, and shape future investigations. Specifically, the key results from these studies have identified:

- An acrylphosphine based novel fluorescent probe and validated its use for the detection of endogenously produced HNO in cell and animal models of persistent pain (Aim 1);
- Changes in the activity of lysosomal cysteine protease Cathepsin B in the spinal cord, due to inactivation by exogenous HNO, are not involved in the anti-nociceptive behavioural adaptations observed in animals with persistent pain (Aim 2);
- A relationship between the degree of spinal microglial activation and graded peripheral injury during the development of persistent pain in animals (Aim 3).
- An increase in total haemoglobin levels in the somatosensory cortex of animals with a high degree of injury (Aim 4).

6.1 Detection of endogenous nitroxyl in persistent pain models

Much of our understanding of pain mechanisms is based on the technology available to us for detecting molecules involved such as DNA, RNA and proteins. However, short-lived, rapid acting gaseous molecules can also be produced via metabolic pathways which can act as transmitters and exhibit biological functions of their own. Their presence is often suggested via surrogate methods such as upregulation of associate enzymes; detection of reactive by-products; loss of function by scavengers or predictive chemistry (Shoman et al, 2016; Fukuto et al., 2005).

Direct detection of gaseous molecules is notoriously difficult due to their rapid diffusion away from the site of release, conversion to other species or self-dimerisation. Further to this, their activity can often be scavenged by other biological molecules present as part of their modulation, making it difficult to resolve the actual bio-available amount of endogenous product. Therefore, the rate of reaction and specificity of the species of interest, coupled to the

detection moiety is critical to ensuring the most accurate representation of endogenous levels. This will provide opportunities to further understand the endogenous role of particular gaseous molecules such as HNO. In recent years, the development of fluorescent based chemosensors has created useful tools for direct (or indirect) detection of these nitrogen species (see Chapter 2; Table 2.1 & 2.2).

As such, using arylphosphine based fluorescent probes which specifically detect HNO described in Chapter 3, we have demonstrated the presence of endogenous HNO in multiple cell populations (microglia and myocardial cells) and in blood samples taken from animals with either persistent pain or myocardial ischemic-reperfusion injury.

HNO was detectable from both BV2 cells, an immortalized line of murine cultured microglial cells (when stimulated with LPS and LPA) and H9C2 cells, an immortalized line of rat myocardial cells (following the re-oxygenation of cells after a period of hypoxia). Our finding supports the hypothesis that HNO is derived by the iNOS enzyme as 1400W (iNOS inhibitor) was able to prevent the detection of both LPS and LPA stimulated HNO release in BV2 cells. Although we demonstrated the generation of HNO following LPS and LPA stimulation was derived by enzyme iNOS, many alternative NOS-independent sources of production have also been previously suggested (Shoman et al, 2016; Fukuto et al., 2005; Irvine et al., 2008). Oxidized products of NO such as peroxynitrite, nitrite, nitrate, nitrogen dioxide and dinitrogen trioxide have long been considered the main mediators of various physiological responses. However, it is now understood that reduced intermediate species such as HNO, elicit their own biophysiological responses via various pathways (Irvine et al., 2008; Miranda, 2005). Thus, the nitroxyl signaling pathway represents another target to be explored for intervention in various pathologies including persistent pain and cardiovascular disease, where modulation of NO and related oxidized species may produce broad 'off-target' effects. Differential reactivity of NO and HNO towards metals and thiols has been demonstrated in cardiovascular disease.

Furthermore, where traditional NO donors are failing clinically due to tolerance development and decreased effectiveness, HNO donors are proving to be a superior alternative due to their ability to increase myocardial function and reduce the workload of the heart, due to potent vasodilation properties (Andrews et al., 2015; Sabbah et al., 2013). Further to this, HNO donors have also been implicated as a potential anti-nociceptive treatment given their actions to attenuate the activation of spinal glia in persistent pain models (Longhi-Balbinot et al., 2016;

Zarpelon et al., 2013). However, despite the clear clinical application of HNO, little is known about the potential endogenous formation, biological targets and regulation of function due to the lack of tools available for measuring its presence.

Through the multi-disciplinary environment of the ARC Centre of Excellence for Nanoscale Biophotonics at the University of Adelaide, I was able to directly engage with chemist Dr Zhang and physicist Dr Reineck and work together to produce multiple generations of HNO fluorescent sensors. Being a part of the creation and testing process allowed us to have a better appreciation of some of the limitations within both chemistry and physics. Conversely, it also allowed Drs Zhang and Reineck, to better understand the complex environment biologists work with, when trying to identify specific targets in a multifarious system. This is an important distinction, as quite often chemists and physicists will only generally test their products in either water or in-organic solvent, neither of which is directly relevant to biological solutes. This experience also afforded us an appreciation of the rigorous life cycles of research, development and testing chemists conduct to reach the desired end-product. Once we had a good understanding of each other's needs and wants, together we were able to develop the right tools and systems to test the presence of HNO in vitro.

Our findings in Chapter 3 demonstrated the presence of endogenous HNO in persistent pain and cardiovascular disease models Using a novel arylphosphine based fluorescent probe, we were able to detect endogenously produced HNO in both BV2 and H9C2 cells using LPS/LPA and hypoxia, respectively. Future studies should focus on further characterizing the role of endogenous HNO in these systems and provide direct functional links between HNO production, bioactivity and disease development. Such experiments could include examination of persistent pain behaviour in the presence of HNO scavengers (L-cysteine, N-acetyl-L-cysteine, DTT), allowing researchers to specifically determine whether sequestering endogenous HNO can modulate this condition. Functional experiments in which the synthesis of HNO has been disrupted, for example by inhibiting the synthesis enzymes iNOS (expressed by microglia/astrocytes), or nNOS (expressed in neurons) will however need to be interpreted with caution as these synthesis enzymes and pathways are common to other reactive nitrogen species.

Indeed, the intraperitoneal, intrathecal and oral administration of N-acetyl-L-cysteine has already been shown to alleviate pain in CCI-induced neuropathic pain in rats (Naik et al., 2006;

Chen et al., 2000). These reports would indicate that endogenous production of HNO may contribute to neuropathic pain development, however, as mentioned recent literature has also reported that exogenous administration of HNO via donor AS, can also reduce allodynic pain behaviours in rodent CCI-induced neuropathic pain. These conflicting outcomes may be due to concentration specific actions of HNO, similar to that observed for NO and warrants further examination. With future investigations, these agents may provide additional support as analgesics so desperately needed for many people with persistent pain.

An interesting observation of the experiments in Chapter 3 was the ability to detect elevated levels of HNO in the red blood fraction of neuropathic pain animals. Although this work requires further experimentation, it highlights the possibility of using circulating HNO levels as a biomarker for pain. The term biomarker has been defined by The National Institutes of Health as “a characteristic that is objectively measured and evaluated as an indicator of normal biological processes, pathogenic processes, or pharmacological responses to a therapeutic intervention”. As reactive nitrogen species are involved in many pathologies, it would be challenging to use circulating levels of HNO to detect specific diseases, however it may potentially be used in conjunction with other specific markers, such as plasma CGRP which has been shown to be a biomarker of HNO activity (Paolucci et al., 2001).

To support our findings, it would be ideal to include additional groups of animals with graded pain and observe if the HNO level detected in CCI-induced pain animals are relative to allodynic measures. Further to this, additional control experiments would determine if the sensor used was specifically targeting HNO in circulation. This was unfeasible during the experimental period due to constraints with time and resources. Our findings support the hypothesis that endogenous HNO is produced both in vitro and in vivo and demonstrates a potential role in various pathologies including persistent pain.

6.2 Exogenous HNO in persistent pain and its cysteine interactions

Spinal glial cells can release pro-inflammatory cytokines following peripheral injury which can contribute to the establishment of persistent pain. This cytokine release may be further modulated by lysosomal cysteine proteases (such as Cathepsin B and S) and as such, a role for lysosomal cysteine proteases in pain has been demonstrated in pathophysiological conditions (Barclay et al., 2007; Abbadie et al., 2009). Nitrosylation of enzyme regulatory

cysteines is one of the key posttranslational modification mechanisms of enzyme function. HNO has been suggested to irreversibly inhibit lysosomal cysteine protease Cathepsin B, via modification of the active-site cysteine (Väänänen et al., 2008), and our results from Chapter 4 suggest that this direct inactivation of enzyme activity may occur within microglia cells at the spinal cord level. We hypothesized that HNO would reduce allodynia via a cathepsin B enzyme mediated pathway. Our findings in Chapter 4, only partially support our original hypothesis that HNO directly inactivates Cathepsin B enzyme activity, however the Cathepsin B pathway does not appear to effect IL-1 β production in BV2 cells or contribute to the reduced allodynia observed in CCI-injured animals. In these experiments, LPS stimulated murine microglial cells (BV2) displayed increased lysosomal cathepsin B activity which was reduced when co-incubated in the presence of HNO. However, LPS stimulated IL-1 β cytokine levels were not reduced by HNO.

Further to this, in vivo experiments showed that CCI-operated animals administered high concentration of HNO donor (3 mg/kg), displayed less allodynia than vehicle treated CCI animals. Sham operated animals did not develop allodynia and showed no behavioural changes with HNO. However, both non-injured and CCI-injured animals receiving the HNO donor displayed reduced spinal cathepsin B activity. This implies that cathepsin B is not involved in the reduced allodynia observed in CCI-injured animals, although literature suggests it may be involved in inflammatory models of persistent pain (Sun et al., 2012). Furthermore, our observations may be a result of HNO mediated inactivation of another lysosomal cysteine enzyme Cathepsin S, which is implicated in neuropathic pain peripheral and spinal modulation (Barclay et al., 2007; Clark et al., 2009). It would be beneficial to determine if HNO can irreversibly in-activate cathepsin S enzyme. In the spinal cord, cathepsin S is secreted by activated spinal microglia and upregulated after nerve injury to cleave the soluble chemokine ligand CX3CL1 (also known as fractalkine) from spinal local neurons and primary afferent fibers (Zhang et al., 2017). Released CX3CL1 activates CX3C-chemokine receptor 1 (CX3CR1) on microglial cells and leads to IL-1 β secretion via p38 MAPKs (Inoue et al., 2018), however as HNO incubation in BV2 cells did not reduced LPS stimulated IL-1 β levels, careful consideration should be made as to whether HNO reduces allodynia via inactivation of either cathepsin substrate. Further to this, it would be important to measure spinal IL-1 β protein levels via ELISA to confirm the BV2 observations. This was not carried out during the

experimental period as the samples generated were prioritized towards cathepsin B enzymatic activity assays and western blot assessment. Western blot experiments did not generate usable IL-1 β protein data from spinal cord lysates and hence were not included in Chapter 4.

6.3 Spinal microglial activation is dependent upon degree of injury

The reactivity of microglia within the spinal cord, in response to nerve injury, has been associated with the development and maintenance of neuropathic pain. However, the temporal establishment of spinal microglial reactivity following injury remains to be fully defined.

Therefore, in Chapter 5 we observed the changes in spinal microglial activity (as measured by cell density, morphology, movement and process length), using a heterozygote CX3CR1 gfp+ transgenic mouse strain, monitored over 14 days via in vivo confocal microscopy. Changes in microglial activity was explored in groups of mice which had graded nerve injury and associated graded behavioural mechanical nociceptive sensitivity, allowing for association of spinal microglial changes to be related to the extent of quantified mechanical sensitivity.

Measuring GFP positive cells, we found that the density, circularity and process velocity of spinal dorsal horn microglia were altered following sciatic injury and correlated with the extent of nerve injury at various time points post-surgery. Some changes were observed as early as 2 days post-injury (circularity) with other characteristics taking longer to develop, such as density changes (5 days post-surgery) and process length decline (14 days post-injury). Furthermore, higher-grade injured animals generally produced earlier onset of changes in microglial density and morphology compared to both lower-grade injured animals and sham controls.

Our findings suggest that microglial reactivity is not a binary all or nothing state, but rather is a spectrum of response proportional to the degree insult or injury. Varying levels of injury and subsequent development of graded mechanical allodynia are also associated with positively correlated changes in the expression of spinal glial markers, GFAP (astrocytes) and CD11b (microglia) (Grace et al., 2010). These findings suggest that there is a threshold in the extent of microgliosis (and astrogliosis) required to develop persistent pain, possibly via changes in neuronal plasticity within the spinal cord. Knowing what this threshold is, would provide critical information about which injuries are most likely to develop into persistent pain or not, and

enable personalised therapeutic intervention at specific time points and doses that would prevent the onset of long-term pain. Further to this, the degree of phenotypic microglial changes throughout the injury lifespan may provide an explanation for how microglia can induce both rapid onset and sustained functional changes in the spinal cord dorsal horn, following peripheral injury.

Our spinal cord observations would benefit further from exploring the effect of pharmacological intervention on the observed changes in microglial activity, when administered at the 2 to 5-day time window and observe which time-point generates the greatest prevention of persistent pain. As such, pharmacological inhibition of microglia using minocycline at 24 hours post-injury, has been shown to attenuate the development but not existing hypersensitivity following peripheral nerve injury when administered following 1 week (Ledeboer et al., 2005; Raghavendra et al., 2003). Minocycline is a tetracycline derivative antibiotic used to treat of bacterial infections which also possesses potent anti-inflammatory activity. It has been demonstrated to strongly suppress microglial activation in a variety of neuroinflammatory and neurodegenerative disorders (reviewed in Garrido-Mesa et al., 2013). However, although proven to be safe for human use, it is not readily prescribed for persistent pain. Therefore, exploring more commonly prescribed therapeutic agents such as opioids and non-steroidal anti-inflammatory drugs (NSAID) during this 2 to 5-day window, would further our understanding of their effect on microglial activity following injury. Our findings support our first and second hypothesis that microglial activation is evident following peripheral injury and is correlated to the degree of peripheral injury and subsequent graded mechanical allodynia. Changes in microglial activity can occur both in response to and can contribute to increased spinal neuronal activity following peripheral injury. Spinal dorsal horn regions including superficial laminae I-II and deep laminae V – VI show increased neural activity in CCI animals and transmit somatosensory information via ascending spinothalamic tracts (Boadas-Vaello et al., 2016; Colloca et al., 2017). A limitation of this study is the use of male cohorts only. It is well understood that microglia are fundamental to neuropathic pain processing in male rodents however, there appears to be a differential role for this cell type in female rodents (Mapplebeck et al, 2016; Watkins et al, 2003). Studies have shown that pharmacological inhibition of microglia produces a reversal of hypersensitivity in male but not female mice (Sorge et al, 2015). Futures studies into the activation of spinal microglia following injury, similar to this

study, would allow us to further understand how microglia characteristics change over time in the spinal cord of CCI injured female mice, compared to male cohorts. Changes in somatosensory activity can be measured by functional spectroscopy and photoacoustic tomography (PAM). These techniques are non-invasive methods used to measure cerebral hemodynamic responses (such as blood flow and oxygen saturation) to neural activity and is sensitive enough to differentiate painful and non-painful stimuli (Qiao et al., 2017). We observed increased haemoglobin levels in the somatosensory cortex of animals with a high degree of injury (N4S0) when compared to sham controls. This suggests that higher levels of injury result in changes in neuronal activity within the somatosensory cortex. These changes were observed in both the ipsi- and contralateral sides of the cortex despite the unilateral injury. Bi-lateral changes in cortical neural activity have previously been reported in CCI operated rats when compared to sham operated, as inferred from increased local glucose utilization rate, measured using ¹⁴C-2-deoxyglucose (2-DG) autoradiography (Mao et al., 1993). Mao et al., (1993) looked at topographical changes of 2-DG throughout sections of the whole brain and reported increased neuronal metabolic activity only in deeper contralateral brain regions, including the mid and deep S1HL region. As PAM measurements of the cortical blood vessels are taken through the thinned skull, we may have not reached the required imaging depths to determine the haemodynamic activity of the deeper layers of S1HL region and highlights a possible limitation of our system.

Our findings suggest that changes in haemoglobin levels in the S1HL region of the somatosensory cortex could be used to measure the presence of pain in non-verbal patients following peripheral injury. This may be used in conjunction with other brain activity measures to create a suite of minimally invasive tools for assessing pain.

As with the longitudinal spinal microglial observations, future work observing the change in haemoglobin levels and blood flow in the somatosensory cortex during the development of persistent pain, would further our understanding of the time scale involved in cortical changes following injury. However, this was outside the scope of our current study and would have created too many interventions to the cohorts of animals being used. To our knowledge, this is first study to measure these changes in rodents following injury, as previous literature has generally reported similar findings in humans. Our findings support our third hypothesis that peripheral nerve injury will create haemodynamic changes within the somatosensory cortex.

6.4 Concluding remarks

Persistent pain is a global debilitating condition brought on by various underlying etiologies such as neuronal lesions and many other diseases, which impose a significant burden upon the quality of daily life for millions of people as well as contributing towards major social economic deficit. Diagnosis and treatment of neuropathic pain and other chronic pain conditions are confounded by the underlying disease and quite often, treatment of the causal disease does not resolve the persistent pain. Contributing to the complexity and challenging nature of persistent pain, pharmacological therapies used to treat nociceptive pain, often have limited success in treating persistent pain symptoms, likely due to the diverging and variable spinal mechanisms which are involved. Understanding the underlying pathogenesis of persistent pain will better aid future outcomes for both prevention and treatment. In order to develop understanding, often we first need to develop new tools and methods to allow researchers to ask and answer questions which were not before possible.

The studies reported in this thesis have provided evidence indicating that reactive nitrogen species, nitroxyl, may influence persistent pain in both an endogenous and exogenous setting via spinal glial involvement. Furthermore, a detailed analysis of spinal glial changes during persistent pain development has contributed to our understanding of the tightly regulated activation status of microglia based on the degree of peripheral injury.

Briefly, we have created a tool that can detect the presence of nitroxyl in immune-like cells which may be derived via the inducible NOS receptor following pain generating stimulus. Further research into this finding could expand the understanding of the reactive nitrogen species in chronic pain development. In addition, our studies support the recent finding that exogenous application of nitroxyl can reduce pain symptoms, however the mechanism of action still remains elusive. Future work on the impact of nitroxyl on alleviating pain symptoms could facilitate the development of novel centrally targeted analgesic therapies, providing much needed relief for patients with untreatable neuropathies using current available treatments. Finally, our studies have shown that there is a relationship between the severity of nerve injury and the resulting spinal glial changes which may predict the severity of pain-like symptoms within in the first 2 - 7 days following the initial injury. This creates a window into which therapeutic management should be targeted to prevent the development of persistent pain in

these patients. It is hoped that the present work will drive future research with a significant focus on improving the knowledge of treatment and possible prevention of neuropathic and other chronic pain conditions, giving back quality of life to millions of chronic pain sufferers and preventing many more.

6.5. References

Abbadie C, Bhangoo S, De Koninck Y, Malcangio M, Melik-Parsadaniantz S, White FA. (2009) Chemokines and pain mechanisms. *Brain Research Reviews*; 60(1): 125-134.

Andrews KL, Lumsden NG, Farry J, Jefferis AM, Kemp-Harper BK, and Chin-Dusting JP. (2015) 'Nitroxyl: a vasodilator of human vessels that is not susceptible to tolerance,' *Clinical Science*; 129(2): 179–187.

Barclay J, Clark AK, Ganju P, Gentry C, Patel S, Wotherspoon G, Buxton F, Song C, Ullah J, Winter J, Fox A, Bevan S, Malcangio M. (2007) Role of the cysteine protease cathepsin S in neuropathic hyperalgesia. *Pain*; 130(3): 225-234.

Boadas-Vaello P, Castany S, Homs J, Alvarez-Perez B, Deulofeu M, Verdu E. (2016) Neuroplasticity of ascending and descending pathways after somatosensory system injury: reviewing knowledge to identify neuropathic pain therapeutic targets. *Spinal Cord*; 54: 330-340.

Chen SR, Eisenach, JC, Pan HL. (2000) Intrathecal S-nitroso-Nacetylpenicillamine and L-cysteine attenuate nerve injury induced allodynia through noradrenergic activation in rats. *Neuroscience*; 101(3): 759-765.

Clark AK, Yip PK, Malcangio M (2009) The liberation of fractalkine in the dorsal horn requires microglial cathepsin S. *J Neurosci*; 29: 6945–6954.

Colloca L, Ludman T, Bouhassira D, Baron R, Dickenson AH, Yarnitsky D, Freeman R, Truin A, Attal N, Finnerup NB, Eccleston C, Kalso E, Bennett DL, Dworkin RH and Raja SN. (2017) *Nature Reviews Disease Primers* volume 3, Article number: 17002.

Fukuto JM, Switzer CH, Miranda KM and Wink DA. (2005) NITROXYL (HNO): Chemistry, Biochemistry, and Pharmacology. *Annu. Rev. Pharmacol. Toxicol*; 45: 335–55

Garrido-Mesa N, Zarzuelo A, Galvez Jz. (2013) Minocycline: far beyond an antibiotic. *British journal of pharmacology*; 169(2): 337-352.

Grace PM, Hutchinson MR, Manavis J, Somogyi AA, Rolan PE (2010) A novel animal model of graded neuropathic pain: Utility to investigate mechanisms of population heterogeneity. *Journal of Neuroscience Methods*; 193(1): 47-53.

Inoue K, Tsuda M. (2018) Microglia in neuropathic pain: cellular and molecular mechanisms and therapeutic potential. *Nature reviews, Neuroscience*; 19(3): 138.

Irvine JC, Ritchie RH, Favaloro JL, Andrews KL, Widdop RE, Kemp-Harper BK. (2008) Nitroxyl (HNO): the Cinderella of the nitric oxide story. *Trends in Pharmacological Sciences*; 29(12): 601-608.

Ledeboer, A., Sloane, E.M., Milligan, E.D., Frank, M.G., Mahony, J.H., Maier, S.F., and Watkins, L.R. (2005). Minocycline attenuates mechanical allodynia and proinflammatory cytokine expression in rat models of pain facilitation. *Pain* 115, 71–83.

Longhi-Balbinot DT, Rossaneis AC, Pinho-Ribeiro FA, Bertozzi MM, Cunha FQ, Alves-Filho JC, Cunha TM, Peron JPS, Miranda KM, Casagrande R and Verri Jr. WA, (2016) 'The nitroxyl donor, Angeli's salt, reduces chronic constriction injury-induced neuropathic pain'. *Chemico-Biological Interactions*; doi: 10.1016/j.cbi.2016.06.009.

Mao J, Mayer DJ, Price DD. (1993) Patters of increased brain activity indicative of pain in a rat model of peripheral mononeuropathy. *The journal of neuroscience*; 13(6): 2689-2702.

Miranda KM. (2005) The chemistry of nitroxyl (HNO) and implications in biology. *Coordination Chemistry Reviews*; 249: 433–455

Naik AK, Tandan SK, Dudgaonkar SP, Jadhav SH, Kataria M, Prakash VR, Kumar D. (2006) Role of oxidative stress in pathophysiology of peripheral neuropathy and modulation by N-acetyl-L-cysteine in rats. *European journal of pain*; 10(7): 573.

Paolocci N, Jackson MI, Lopez BE, Miranda K, Tocchetti CG, Wink DA, Hobbs AJ, Fukuto JM., (2007) 'The pharmacology of nitroxyl (HNO) and its therapeutic potential: Not just the janus face of NO.' *Pharmacology & Therapeutics*; 113: 442–458.

Qiao, W., and Chen, Z. (2017). All-optically integrated photoacoustic and optical coherence tomography: A review. *Journal of Innovative Optical Health Sciences* 10, 1-10.

Raghavendra V, Tanga F and De Leo JA. (2003) Inhibition of Microglial Activation Attenuates the Development but Not Existing Hypersensitivity in a Rat Model of Neuropathy. *J. Pharmacol. Exp. Ther*; 306: 624–630.

Sabbah HN, Tocchetti CG, Wang M, Daya S, Gupta RC, Tunin RS, Mazhari R, Takimoto E, Paolocci N, Cowart D, Colucci WS. and Kass DA. (2013) 'Nitroxyl (HNO) a Novel Approach for the Acute Treatment of Heart Failure.' *Circ Heart Fail*; 6(6): 1250–1258.

Shoman ME and Aly OM. (2016) Nitroxyl (HNO): A Reduced Form of Nitric Oxide with Distinct Chemical, Pharmacological, and Therapeutic Properties. *Oxidative Medicine and Cellular Longevity*; Article ID 4867124.

Sun L, Wu Z, Hayashi Y, Peters C, Tsuda M, Inoue K and Nakanishi H. (2012) Microglial Cathepsin B Contributes to the Initiation of Peripheral Inflammation-Induced Chronic Pain. *The Journal of Neuroscience*; 32(33): 11330 –11342.

Väänänen AJ, Salmenperä P, Hukkanen M, Miranda KM, Harjula A, Rauhala P, Kankuri E. (2008) Persistent susceptibility of cathepsin B to irreversible inhibition by nitroxyl (HNO) in the presence of endogenous nitric oxide. *Free Radical Biology & Medicine*; 45: 749–755.

Zarpelon AC, Souza GR, Cunha TM, Schivo IRS, Marchesi M, Casagrande R, Pinge-Filho P, Cunha FQ, Ferreira SH, Miranda KM and Verri Jr. WA, (2013) 'The nitroxyl donor, Angeli's salt, inhibits inflammatory hyperalgesia in rats.' *Neuropharmacology*; 71: 1–9.

Zhang ZJ, Jiang BC, Gao YJ. (2017) Chemokines in neuron-glia cell interaction and pathogenesis of neuropathic pain. *Cellular and Molecular life sciences*; 74(18): 3275-3291.

APPENDICIES

Appendix 1. Exogenous Cathepsin B enzyme assay protocol (Sigma- Aldrich)

<https://www.sigmaaldrich.com/technical-documents/protocols/biology/enzymatic-assay-of-cathepsin-b.printerview.html>

Enzymatic Assay of Cathepsin B

1. Objective

To standardize a procedure for determining the enzymatic activity of Cathepsin B.

2. Scope

This procedure applies to all products that have a specification for Cathepsin B activity, such as [Sigma-Aldrich Product Numbers C0150](#) and [C8571](#), determined by the liberation of 7-amino-4-methylcoumarin from Z-Arg-Arg 7-amido-4-methylcoumarin.

3. Definitions

3.1 Purified Water = water from a deionizing system, resistivity $\geq 18\text{M}\Omega\cdot\text{cm}$ @ 25°C

3.2 CBZ – carbobenzoxy.

3.3 Arg-Arg – arginylarginine

3.4 7-AMC – 7-amino-4-methylcoumarin.

3.5 Unit definition – one unit will liberate 1 nanomole of 7-amino-4-methylcoumarin from Z-Arg-Arg 7-amido-4-methylcoumarin per min at pH 6.0 at 40°C.

4. Discussion

4.1 Cathepsin B is a lysosomal cysteine proteinase which will hydrolyse proteins with a broad specificity for peptide bonds, but will preferentially cleave at the carboxyl side of Arg-Arg bonds in small molecule substrates. Lysosomal Cathepsin B has also been shown to degrade soluble monomeric collagen and insoluble polymeric collagen *in vitro*.



4.2 The substrate N α -CBZ-Arg-Arg-7-amido-4-methylcoumarin is used for the fluorometric detection of Cathepsin B activity. The K_m value for this substrate is 0.39 mM, with an optimum pH of 6.0. The fluorescence of the free aminomethylcoumarin released.

5. Responsibilities

It is the responsibility of trained Analytical Services laboratory personnel to follow this procedure as written.

6. Safety

Refer to Safety Data Sheets (SDS) for hazards and appropriate handling precautions.

7. Procedure

7.1 CONDITIONS:

7.1.1 T = 40°C, pH = 6.0, Excitation = 348 nm, Emission = A_{440nm}, Light path = 1 cm

7.2 METHOD:

7.2.1 Fluorometric Rate Determination

7.3 REAGENTS:

7.3.1 352 mM Potassium Phosphate Buffer, 48 mM Sodium Phosphate, and 4.0 mM Ethylenediaminetetraacetic Acid; pH 6.0 at 40°C (**Buffer**).

Prepare a solution in purified water using 47.9 mg/ml of Potassium Phosphate Monobasic, such as [Sigma-Aldrich Product Number P5379](#); 6.8 mg/ml of Sodium Phosphate Dibasic, such as [Sigma-Aldrich Product Number S0876](#); 1.7 mg/ml of Ethylenediaminetetraacetic Acid, such as [Sigma-Aldrich Product Number ED4SS](#). Adjust the pH to 6.0 at 40°C using 1N HCl or 1N KOH.

7.3.2 8.0 mM L-Cysteine HCL Solution, pH 6.0 at 40°C (**L-Cys**).

Prepare a fresh solution in Reagent 7.3.1 (**Buffer**) using 1.4 mg/ml of L-Cysteine hydrochloride, such as [Sigma-Aldrich Product Number C7880](#). Adjust to pH 6.0 at 40°C with 1N NaOH.

7.3.3 0.1% (v/v) Brij 35 Solution (**Brij 35**).

Prepare a 0.1% (v/v) solution in purified water using Brij 35 Solution, 30% (w/v) solution, such as [Sigma-Aldrich Product Number B4184](#).

7.3.4 0.02 mM Na-CBZ-Arg-Arg-7-amido-4-methylcoumarin (**Arg-Arg-7-AMC**).

Prepare a *fresh* solution in Dimethyl Sulfoxide such as [Sigma-Aldrich Product Number D5879](#) using 7.1 mg/ml of Na-CBZ-Arg-Arg-7-amido-4-methylcoumarin, such as [Sigma-Aldrich Product Number C5429](#). Dilute to a final concentration of 0.02 mM with Reagent 7.3.3 (**Brij 35**) and use within 3 hours of preparation. *Protect this solution from light.*

7.3.5 5.0 μM 7-amino-4-methylcoumarin (**Standard**).

Prepare a solution in Dimethyl Sulfoxide, such as [Sigma-Aldrich Product Number D5879](#), using 1 mg/ml of 7-amino-4-methylcoumarin such as [Sigma-Aldrich Product Number A9891](#). Dilute to a final concentration of 5.0 μM with Reagent 7.3.3 (**Brij 35**). Protect this solution from light.

7.3.6 Cathepsin B Enzyme Solution (**Enzyme**).

Immediately before use, prepare a solution containing 5-10 units/ml of Cathepsin B in cold Reagent 7.3.3 (**Brij 35**).

7.4 PROCEDURE

7.4.1 For measuring enzymatic activity, pipette (in milliliters) the following reagents into fluorometric cuvettes:

	Blank	Test
Reagent 7.3.2 (L-Cys)	0.75	0.75
Reagent 7.3.3 (Brij 35)	0.90	1.00
Reagent 7.3.6 (Enzyme)	0.10	----

7.4.2 Mix by inversion and equilibrate to 40°C. Monitor the intensity of fluorescence at the excitation wavelength of 348 nm and the emission wavelength of 440 nm until constant using a suitably thermostatted fluorometer.

7.4.3 Then pipette (in milliliters) the following reagents into fluorometric cuvettes:

	Blank	Test
Reagent 7.3.4 (Arg-Arg-7-AMC)	0.75	0.75

7.4.4 Immediately mix by inversion and record the increase in intensity of fluorescence at the excitation wavelength of 348 nm and the emission wavelength of 440 nm for 5 minutes. Obtain the maximum Δ Intensity/min using the maximum linear rate for both the test and the blank.

7.4.5 For standard curve determination, pipette (in milliliters) the following reagents into fluorometric cuvettes:

	STD1	STD2	STD3	STD4	STD5	STD BLANK
Reagent 7.3.2 (L-Cys)	0.75	0.75	0.75	0.75	0.75	0.75
Reagent 7.3.3 (Brij 35)	1.55	1.35	1.15	0.95	0.75	1.75
Reagent 7.3.5 (Standard)	0.20	0.40	0.60	0.80	1.00	----

7.4.6 Mix by inversion and equilibrate to 40°C. Measure the fluorescence intensity at the excitation wavelength of 348 nm and the emission wavelength of 440 nm for all standards and standard blank.

7.5 CALCULATIONS

7.5.1 Correct standard intensities versus the standard blank.

$$\Delta \text{ Intensity Standard} = \text{Intensity STD} - \text{Intensity STD blank}$$

Obtain the linear regression of the standards by plotting the Δ Intensity Standard versus nanomoles of 7-amino-4-methylcoumarin for each standard.

7.5.2 Determine the nanomoles of 7-amino-4-methylcoumarin liberated using the linear regression obtained from the standard data:

nanomoles of 7-AMC liberated =	$(\Delta\text{Intensity}/\text{min sample} - \Delta\text{Intensity}/\text{min blank}) - y \text{ intercept slope}$
--------------------------------	--

Units/ml enzyme =	nanomoles of 7-AMC liberated) (DF) 0.100 ml
-------------------	---

where:

DF = dilution factor

0.100 ml = volume of enzyme used

7.6 FINAL ASSAY CONCENTRATION:

7.6.1 In a 2.50 ml reaction mix, the final concentrations are 105.6 mM potassium phosphate, 14.4 mM sodium phosphate, 1.2 mM ethylenediamine tetraacetic acid, 2.4 mM L-cysteine, 0.07% (v/v) Brij 35, 0.006 mM N α -CBZ-Arg-Arg-7-amido-4-methylcoumarin, 0.0525% (v/v) dimethyl sulfoxide, and 0.2 – 0.4 units of Cathepsin B.

8. References & Attachments

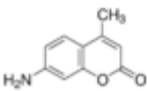
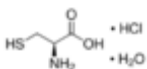
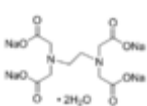
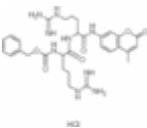
8.1 Barret, A.J.; Kirschke, H. *Methods in Enzymology* 80, 535-538 (1981).

8.2 Cathepsin B from human placenta, Product Information, C0150.

9. Approval

Review, approvals and signatures for this document will be generated electronically using the EDMS. Print a "For Use" copy if hardcopy with signature verification is required.

Materials

Product #	Image	Description	Molecular Formula
A9891		7-Amino-4-methylcoumarin Chromophore for substrates	$C_{10}H_9NO_2$
B4184		Brij® L23 solution 30 % (w/v) in H₂O	
C8571		Cathepsin B from human liver buffered aqueous solution, ≥1,500 units/mg protein (E1%/280)	
C0150		Cathepsin B from human placenta lyophilized powder, ≥5 units/mg protein	
C7880		L-Cysteine hydrochloride monohydrate reagent grade, ≥98% (TLC)	$C_3H_7NO_2S \cdot HCl \cdot H_2O$
ED4SS		Ethylenediaminetetraacetic acid tetrasodium salt dihydrate 99.0-102.0% (titration)	$C_{10}H_{12}N_2Na_4O_8 \cdot 2H_2O$
P5379	KH_2PO_4	Potassium phosphate monobasic <i>ReagentPlus</i>®	H_2KO_4P
S0876	Na_2HPO_4	Sodium phosphate dibasic <i>ReagentPlus</i>®, ≥99.0%	HNa_2O_4P
C5429		Z-Arg-Arg-7-amido-4-methylcoumarin hydrochloride	$C_{30}H_{39}N_9O_6$

Appendix 2. Publications arising from this thesis.

This thesis was written as a combination of traditional (Chapters 1 & 6) and manuscript style (Chapters 2-5) sections. The peer-reviewed, formally published manuscript (Chapter 2) is presented in its original format. Here, the final PDF (.pdf) file of the published manuscript is presented.

Review

Nitroxidative Signaling Mechanisms in Pathological Pain

Peter M. Grace,^{1,4,*} Andrew D. Gaudet,¹ Vasiliki Staikopoulos,² Steven F. Maier,¹ Mark R. Hutchinson,² Daniela Salvemini,³ and Linda R. Watkins¹

Tissue injury can initiate bidirectional signaling between neurons, glia, and immune cells that creates and amplifies pain. While the ability for neurotransmitters, neuropeptides, and cytokines to initiate and maintain pain has been extensively studied, recent work has identified a key role for reactive oxygen and nitrogen species (ROS/RNS; nitroxidative species), including superoxide, peroxynitrite, and hydrogen peroxide. In this review we describe how nitroxidative species are generated after tissue injury and the mechanisms by which they enhance neuroexcitability in pain pathways. Finally, we discuss potential therapeutic strategies for normalizing nitroxidative signaling, which may also enhance opioid analgesia, to help to alleviate the enormous burden of pathological pain.

The Link Between Nitroxidative Signaling and Pain

Investigation of oxidative processes, such as rusting, began with the 'phlogiston theory', developed by Georg Ernest Stahl during the scientific revolution, which postulated that a fire-like element (phlogiston) is released during combustion. Oxidation was formally linked to biology during the early 20th Century, when it was found to underpin cellular metabolism [1–3]. The connection between ROS and altered sensory processing was empirically identified around the same time [4]. Since then, research has shown that prolonged, unchecked increases in ROS/RNS (nitroxidative species) after infection or tissue damage can promote cytotoxicity and inflammation. These processes can cause peripheral and central sensitization which underlie **pathological pain** (see *Glossary*) [5,6]. Thus, restoring nitroxidative balance in peripheral and central nervous systems (PNS, CNS) is a possible therapeutic approach for ameliorating neuropathology [6–10].

In this review, we summarize recent research on how nitroxidative species participate in **neuroimmune signaling** throughout the neuraxis to drive pathological pain. We additionally discuss potential therapeutic strategies for normalizing nitroxidative signaling by activating endogenous antioxidant systems, which may also enhance opioid analgesia. Because pathological pain is often intractable to current therapies, new strategies to normalize nitroxidative signaling may help to alleviate the enormous burden of pain [11].

Production of Nitroxidative Species by Neurons, Glia, and Immune Cells

The role of nitroxidative signaling in pain has been studied using rodent experimental models of inflammatory pain [e.g., intraplantar complete Freund's adjuvant (CFA), formalin] and neuropathic pain [e.g., peripheral nerve injury (PNI), chemotherapy-induced peripheral neuropathy

Trends

Nitroxidative species (RNS, ROS, and their products) contribute to peripheral and central sensitization after tissue injury, which leads to pathological pain.

There is a reciprocal relationship between nitroxidative and inflammatory signaling that drives peripheral and central sensitization.

New approaches to restoring nitroxidative balance may reveal effective strategies to treat pathological pain.

The development of new tools may enhance our understanding of the crucial relationships between real-time local creation of nitroxidative species, their concentration at the effect site, and the distribution of their direct effects.

¹Department of Psychology and Neuroscience, and the Center for Neuroscience, University of Colorado, Boulder, CO, USA

²Discipline of Physiology, School of Medicine, and the Australian Research Council (ARC) Centre for Nanoscale BioPhotonics (CNBP), University of Adelaide, Adelaide, SA, Australia

³Department of Pharmacology and Physiology, Saint Louis University School of Medicine, St. Louis, MO, USA

⁴Current address: Department of Critical Care Research, University of Texas MD Anderson Cancer Center, Houston, TX, USA

*Correspondence: pgrace@mdanderson.org (P.M. Grace).

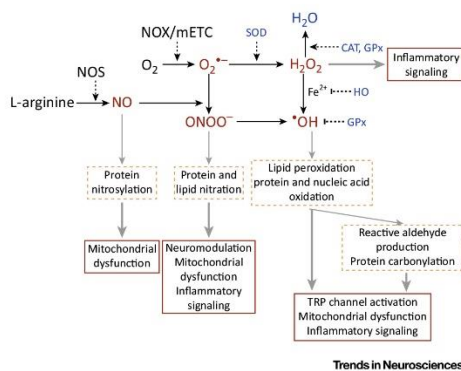


Figure 1. Induction of Nitroxidative Species after Tissue Injury. Nitroxidative species can induce post-translational modifications of proteins and lipids, which subsequently drive pathological pain by modulating nociceptive neurotransmission, activating TRP channels, and inducing mitochondrial dysfunction, and thereby induce inflammatory signaling. In healthy cells, endogenous antioxidant systems prevent nitroxidative damage. Cell damage/pathology can perturb this balance, driving the accumulation of potentially damaging nitroxidative species. Abbreviations: CAT, catalase; GPx, glutathione; H_2O_2 , hydrogen peroxide; HO, heme oxygenase; mETC, mitochondrial electron transport chain; NO, nitric oxide; NOS, nitric oxide synthase; NOX, NADPH oxidase; $O_2^{\bullet-}$, superoxide; $^{\bullet}OH$, hydroxyl radical; ONOO $^-$, peroxynitrite; SOD, superoxide dismutase.

Glossary

Neuroimmune signaling:

bidirectional communication between leukocytes, glia, and neurons.

Pathological pain: maladaptive pain that serves no useful purpose.

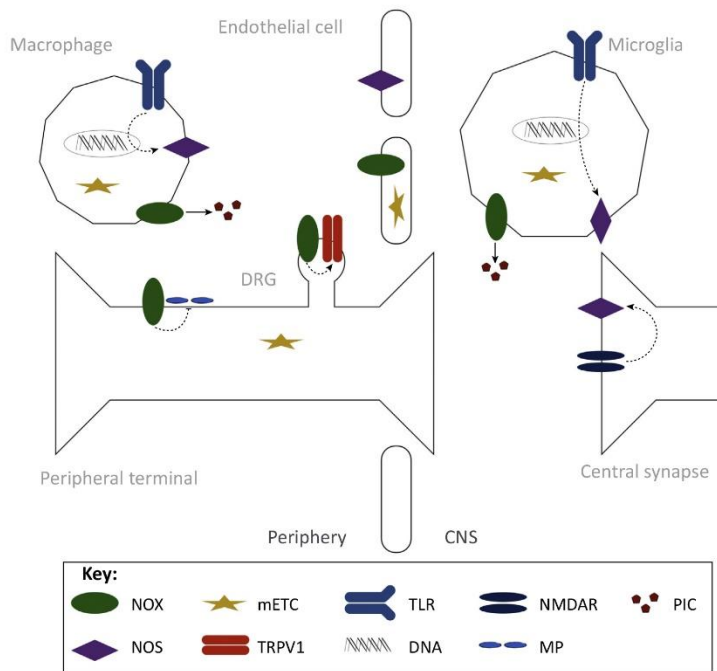
(CIPN), diabetic neuropathy (DN), spinal cord injury (SCI), experimental autoimmune encephalomyelitis (EAE), which have recently been reviewed elsewhere [12]. There are numerous endogenous sources of ROS and nitric oxide (NO) that are engaged during pain processing [13]. NADPH oxidases, NO synthases, and mitochondrial respiration are among the best characterized ROS/NO producers, and will be discussed here (Figures 1 and 2).

NADPH Oxidases

NADPH oxidases (NOX) are membrane-bound enzyme complexes. They transport electrons donated from cytosolic NADPH to generate extracellular or luminal superoxide anions or hydrogen peroxide that can be transported into the cytosol via aquaporin channels [13,14]. In contrast to other sources of ROS that are generated as a byproduct of catabolism, ROS generation is the primary function of NOX. There are seven members in the NOX family; NOX1, 2, and 4 have been implicated in pathological inflammatory and neuropathic pain models [13,15,16]. NOX1 and 2 are expressed at the cellular membrane, and produce superoxide anions following phosphorylation of cytosolic subunits [17]. NOX4 is expressed on organelles, such as the endoplasmic reticulum, and constitutively produces hydrogen peroxide [17].

NOX1 is inducibly expressed by microglia, neurons, astrocytes, and macrophages in the dorsal root ganglion (DRG) and CNS [17–19]. Nociceptive hypersensitivity induced by the inflammatory stimuli formalin and carrageenan is attenuated in *Nox1*-deficient mice [18]. NOX1-derived ROS induce translocation of PKC ϵ to the membrane to enhance transient receptor potential (TRP) V1 activity in DRG neurons [18], a change consistent with pain amplification (Figure 2). By contrast, another study showed that NOX1 mRNA failed to upregulate in the DRG following peripheral nerve injury (PNI) [20]. These results indicate that DRG NOX1 may have a preferential role in inflammatory versus neuropathic pain.

NOX2 is predominantly expressed by phagocytic cells – peripheral macrophages and CNS microglia [13]. PNI induces a rapid upregulation of NOX2 mRNA by DRG macrophages and spinal microglia, which is correlated with increased intracellular superoxide [20,21]. PNI-induced nociceptive hypersensitivity was attenuated in *Nox2*-deficient mice [20,21]. *Nox2* deficiency attenuated TNF, but not IL-1 β , mRNA expression, as well as expression of the neuronal injury marker ATF3 in DRG (Figure 2) [20]. However, *Nox2* deficiency did not influence macrophage recruitment to the injured DRG, suggesting a role for NOX2 in macrophage function rather than in



Trends in Neurosciences

Figure 2. Sources of Nitroxidative Species after Tissue Injury. Principal sources of nitroxidative species include NADPH oxidase (NOX), nitric oxide synthase (NOS), and electron leakage from the mitochondrial electron transport chain (mETC). The NOX1, 2, and 4 isoforms are differentially expressed across cell types and tissues after injury. NOX1-derived reactive oxygen species (ROS) induce enhance transient receptor potential (TRP) V1 activity in dorsal root ganglia (DRG) neurons. NOX2 activity in macrophages and microglia drives proinflammatory cytokine (PIC) gene expression in DRG of the spinal dorsal horn. NOX4 expression at the site of peripheral nerve injury decreases the expression of myelin proteins (MP). The three NOS isoforms – NOS1 (neuronal), 2 (inducible), and 3 (endothelial) – are also differentially expressed by cell type. In abnormal pain states, *N*-methyl-D-aspartate receptors (NMDARs) are activated, resulting in calcium influx and activation of NOS1. Transcription of NOS2 is initiated by Toll-like receptors (TLRs). These enzymes and processes have a well-established role in pathological pain.

chemotaxis [20]. *Nox2* deficiency attenuated PNI-induced Iba1 expression and the attendant expression of proinflammatory cytokines TNF and IL-1 β in the spinal dorsal horn [21]. Because these studies were performed in global knockouts, it is still unclear whether alterations in the DRG and dorsal horn are subject to NOX-dependent changes in macrophage function at the injury site. In contrast to NOX1, NOX2 activity in monocytes appears to play no role in inflammatory pain [22].

NOX4 is expressed by DRG neurons – both myelinated (A-fibers) and unmyelinated (C-fibers) DRG neurons – as well as by microglia, astrocytes, and macrophages [13,23,24]. Nociceptive hypersensitivity following PNI is attenuated in *Nox4*-deficient mice, with attenuation of hydrogen peroxide at the sciatic nerve injury site [23]. These results are supported by the absence of NOX4 upregulation in the DRG after PNI [20]. The myelin proteins MPZ and PMP22 are decreased at

the sciatic nerve injury site over time in a NOX4-dependent fashion, suggesting that myelin degeneration by hydrogen peroxide may maintain neuropathic pain (Figure 2). However, attenuated damage at the injury site did not alter expression of the nitroxidative stress and neuroinflammation indices at the spinal dorsal horn or DRG (microglia proliferation, hydrogen peroxide levels) [23]. This contrasts with other studies showing that such processes are dependent on manipulations at the sciatic nerve [25–27]. Finally, a role for NOX4 may be limited to neuropathic rather than inflammatory pain [23].

Together, these data suggest that NOX1, 2, and 4 isoforms contribute to pathological pain. Future studies could expand the role of various NOX isoforms to other sites in the neuraxis and well as identifying a role for other NOX isoforms in pain. These data may help to guide the development of therapeutics that target the activity of specific NOX isoforms to reduce nitroxidative stress and pain.

Nitric Oxide Synthases

NO is a diffusible gas mediator that is synthesized from L-arginine by one of three nitric oxide synthase (NOS) isoforms: NOS1 (neuronal), 2 (inducible), and 3 (endothelial). NO and all three NOS isoforms have a well-established role in nociception (Figure 2) [28]. It easily passes through membranes to directly impact on nearby cells.

NOS1 is constitutively expressed in the cytosolic compartment of postsynaptic terminals of neurons, and of stressed Schwann cells, and requires calcium for its activation [29–31]. In abnormal pain states, *N*-methyl-D-aspartate (NMDA) receptors are activated, resulting in calcium influx and activation of NOS1 [28]. Nociceptive hypersensitivity induced by PNI and CIPN is attenuated by genetic ablation and pharmacological inhibition of NOS1 [32–35].

NOS2 is a cytosolic isoform that is widely expressed in many immune cells and in glia. Transcription of NOS2 is initiated by Toll-like receptors (TLRs) and, once translated, is constitutively active – that is, unlike NOS1 and 3, its activity is independent of calcium [28]. NOS2 inhibition attenuates nociceptive hypersensitivity associated with inflammatory and neuropathic pain models [15,36,37].

NOS3 is best known for its expression in the cardiovascular system as a regulator of vascular tone. NOS3 is a membrane-bound enzyme that is constitutively expressed; however, it requires the interaction of calcium and calmodulin for its activation [28]. NOS3 expression is increased in the DRG after subcutaneous administration of CFA, and is correlated with allodynia, suggestive of increased NOS3 activity [38]. CFA-induced inflammatory pain is attenuated by NOS3 inhibition [38].

Cellular Respiration

One crucial function of mitochondria is in energy metabolism. The mitochondrial electron transport chain (mETC) is a series of five molecular complexes through which electrons are transported to synthesize ATP from ADP. Premature electron leakage can occur during cellular respiration, particularly at complexes I and III, resulting in superoxide production (Figure 2) [39].

Mitochondrial ROS levels are elevated in spinal neurons, microglia, and astrocytes in neuropathic pain models [21,40,41]. Furthermore, blocking the mETC attenuates hyperalgesia associated with a range of inflammatory and neuropathic pain models [42–45]. However, a direct link between mETC-dependent pain and mitochondrial ROS has yet to be shown. These results suggest that cellular respiration is increased, but is inefficient owing to enhanced ROS-generating electron leakage from the mETC because ATP production by sciatic nerves is impaired during CIPN [46].

Mechanisms of Nitroxidative Signaling in Neuronal Hyperexcitability

Injury or disease can provoke intense, repeated, and sustained activity of primary afferent (sensory) neurons. This activity, together with the release of mediators from reactive glia and immune cells, elicits well-characterized changes in neuronal and biochemical processing at peripheral terminals and central synapses [5,47–50]. This is termed ‘sensitization’, and results in nociceptive hypersensitivity. We discuss here how nitroxidative signaling engages neurons in pain pathways, leading to peripheral and central sensitization (Figures 1 and 3).

Nitroxidative Species as Neuromodulators in Pain Pathways

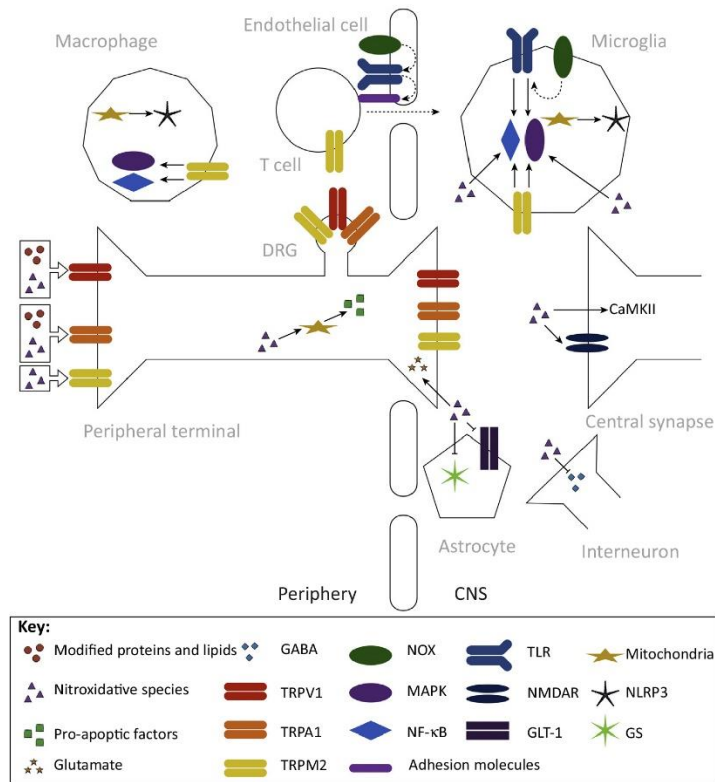
Nitroxidative species can directly increase the excitability of nociceptive neurons. Intraplantar administration of superoxide or peroxynitrite, or intrathecal delivery of the ROS donor *tert*-butyl hydroperoxide (tBOOH), is sufficient to induce nociceptive hypersensitivity in naïve rats [51–54]. These studies demonstrated that ROS activates calcium/calmodulin-dependent protein kinase II (CaMKII) in glutamatergic spinal neurons, and induced presynaptic inhibition of GABAergic interneurons (disinhibition). Furthermore, hydrogen peroxide enhanced the frequency and amplitude of action potentials of DRG neurons from neuropathic rats (Figure 3) [55].

In neuropathic pain models, administration of the non-selective ROS scavenger phenyl-*N*-*tert*-butylnitron (PBN), selective small-molecule superoxide and peroxynitrite decomposition catalysts such as M40403, FeTMPyP⁵⁺, and MnTE-2-PyP⁵⁺, or selective peroxynitrite decomposition catalysts such as SRI6 and SRI110, attenuated nociceptive hypersensitivity [15,51,53,54,56–58]. Accordingly, PBN attenuated injury-induced hyperexcitability of spinal dorsal (sensory) horn ‘pain’-responsive neurons and phosphorylation of CaMKII [51,57], an effect consistent with pain normalization. Several mechanisms of enhanced excitatory signaling have been identified. Hydrogen peroxide can activate cGKII α , resulting in increased neurotransmitter release from the terminals of primary afferent neurons in the dorsal horn [59,60]. Peroxynitrite and ROS disrupt glutamate homeostasis, leading to potentiation of synaptic currents and calcium influx, and ultimately excitotoxicity [56,61]. Mechanisms include nitration and phosphorylation of several NMDA receptor subunits, as well as inhibition of glutamine synthetase and the glutamate transporter GLT-1 that limit the synaptic half-life of glutamate [15,56,62,63]. Nitroxidative products also induce disinhibition after PNI because PBN normalized the decrease in GAD-67⁺ GABAergic dorsal horn neurons, and increased GABA release (Figure 3) [53,64]. Together, these data suggest that nitroxidative species directly enhance neuroexcitability in pain pathways.

Nitroxidative Species Activate TRP Channels

The TRP family of nonselective cation channels play a vital role in the molecular integration of multiple endogenous and exogenous sensory stimuli [65]. Several of these channels, expressed at the peripheral and central terminals and cell bodies of primary afferent neurons, are activated by nitroxidative species and products. TRP channel activation by nitroxidative species can also initiate neurogenic inflammation – recruitment and activation of immune cells following release of neuropeptides by neurons – which is a key process underlying pathological pain (Figure 3) [5,66]. We focus here on the known roles of TRPA1, TRPM2, and TRPV1.

TRPA1 is a chemoreceptor expressed exclusively by peptidergic C-fibers [65]. Nitroxidative species induce protein carbonylation, and membrane phospholipid peroxidation and nitration, as well as subsequent production of reactive aldehydes such as acrolein (Figure 1). These products all share the ability to induce nociceptive hypersensitivity by directly activating TRPA1 [67–72]. Acrolein is elevated in the DRG and spinal cord after SCI, and blockade with hydralazine or phenelzine partially attenuated allodynia [73,74]. Moreover, nociceptive hypersensitivity induced by CIPN was abolished in *Trpa1*-deficient mice or by a TRPA1 antagonist [75]. In this



Trends in Neurosciences

Figure 3. Nitrooxidative Mechanisms of Neuroexcitability after Tissue Injury. Reactive nitrooxidative species, such as hydrogen peroxide and peroxynitrite, and modified proteins and lipids, including carbonylated proteins, peroxidated and nitrated lipids, and reactive aldehydes, all contribute to peripheral and central sensitization after tissue injury. These processes drive pathological pain. Several of the transient receptor potential (TRP) family of nonselective cation channels are activated by nitrooxidative species and by modified proteins and lipids (see Nitrooxidative Species Activate TRP Channels). TRPA1 is expressed by peptidergic C-fibers, and is activated by modified proteins and lipids. TRPM2, which is expressed by neurons, monocytes/macrophages, microglia, and T cells, is directly activated by nitrooxidative species. TRPM2 also activates intracellular signaling pathways, including mitogen-activated protein kinase (MAPK) pathways and nuclear translocation of nuclear factor κ light-chain enhancer of activated B cells (NF- κ B). TRPV1 is found on C-fibers and is directly activated by some modified proteins and lipids, as well as being a target of oxidation and nitration events by nitrooxidative species that increase the responsiveness of the channel. Reactive nitrooxidative species can directly modulate neuroexcitability in central synapses by promoting glutamate release from primary afferent terminals, by activating calcium/calmodulin-dependent protein kinase II (CaMKII) in glutamatergic spinal neurons, and by inhibiting GABAergic interneurons (see Nitrooxidative Species as Neuromodulators in Pain Pathways). Nitrooxidative species also disrupt glutamate homeostasis by nitration and phosphorylation of NMDA receptor (NMDAR) subunits, as well as by inhibiting glutamine synthetase (GS) and the glutamate transporter GLT-1. Mitochondrial DNA is a target for oxidation and nitration, while some nitrooxidative species can form adducts with many mitochondrial proteins, which together impair the structural integrity and function of mitochondria (see Nitrooxidative Species Induce Mitochondrial Dysfunction). Nitrooxidative species can also trigger release of proapoptotic factors from mitochondria by disrupting organelle dynamics. Nitrooxidative species induce the production of proinflammatory mediators, and can activate NF- κ B and MAPK intracellular signaling pathways (see Nitrooxidative Species Induce Neuroinflammatory Signaling). Toll-like receptors (TLRs) bind to a variety of endogenous danger signals, including those released from nitrooxidative-damaged mitochondria, to activate NF- κ B and MAPKs. NOX-derived ROS are second

(Figure legend continued on the bottom of the next page.)

model, the chemotherapeutic bortezomib did not directly activate TRPA1, suggesting that ROS may act as an intermediate [75].

TRPM2 is expressed by neurons, and abundantly by immune cells including monocytes/macrophages, neutrophils, T cells, and microglia. This channel is directly activated by hydrogen peroxide and by cytosolic ADP-ribose that is generated after nitroxidative damage to mitochondria [76–81]. Furthermore, TRPM2 activation is crucial for activation of spinal microglia and for macrophage infiltration into the spinal cord after PNI [82]. TRPM2 also activates the ERK/MAPK pathway and induces nuclear translocation of NF- κ B, resulting in the production of proinflammatory cytokines and chemokines [76,77,81,83,84]. Consequently, pharmacological and genetic studies have demonstrated that TRPM2 contributes to inflammatory and neuropathic nociceptive hypersensitivity [77–79,82,85].

TRPV1 is found on unmyelinated, slowly-conducting neuronal C-fibers, and is an essential component underlying injury-elicited thermal hyperalgesia and nociceptive hypersensitivity [65]. TRPV1 expression is upregulated by an exogenous ROS donor (tBOOH), and is a target of oxidation and nitration events that increase the responsiveness of the channel [18,86–88]. Moreover, linoleic acid metabolites, created during the production of eicosanoids, are endogenous TRPV1 agonists when oxidized, and contribute to nociceptive signaling [89,90].

Nitroxidative Species Induce Mitochondrial Dysfunction

Mitochondria have pivotal roles in a variety of cellular functions, including energy metabolism, calcium homeostasis, lipid synthesis, and apoptosis. As noted above, cellular respiration can be elevated under neuropathic pain conditions, with an attendant elevation of ROS derived from neuronal and microglial mitochondria [21,40,41]. Together with nitroxidative species derived from NOX and NOS enzymes, these species disrupt mitochondrial homeostasis via several mechanisms, leading to bioenergetic crisis (due to impaired mETC efficiency) and degeneration of primary afferents (Figure 3) [91].

Mitochondrial DNA is a target of oxidation and nitration, while peroxidated lipid end-products, such as reactive aldehydes, can form covalent modifications (adducts) with an array of mitochondrial proteins, including antioxidants [92,93]. Together, these changes impair the structural integrity and function of mitochondria. Nitroxidative species can also trigger release of proapoptotic factors from mitochondria. For example, NO can disrupt mitochondrial dynamics (fission and fusion; responsible for maintaining metabolic homeostasis), resulting in translocation of Bcl-2-associated X protein from the cytosol to the organelle membrane, where it activates apoptosis pathways [94–96]. Activation of apoptosis pathways contributes to neuropathic pain because inhibition of several caspase enzymes attenuates vincristine- and dideoxycytidine-induced nociceptive hypersensitivity [97]. Neuropathic pain is associated with impaired mitochondrial function, and nociceptive hypersensitivity is accordingly attenuated by pharmacologically normalizing mitochondrial dynamics or preventing mitotoxicity [46,98–100].

Nitroxidative Species Induce Neuroinflammatory Signaling

Proinflammatory mediators released by glial and immune cells increase neuroexcitability in pain pathways after injury (e.g., TNF, IL-1 β , BDNF) [5,50,101–103]. Several mechanisms include enhanced glutamate release, increased AMPA receptor expression, phosphorylated NMDA receptor subunits, and downregulated astrocyte glutamate transporters [5]. These

messengers for NF- κ B- and p38 MAPK-dependent TLR signaling, and TLR expression. The TLR2–NOX1 interaction also upregulates adhesion molecules via CCL3, which facilitates transendothelial cell migration into the CNS. Mitochondria-derived ROS also activate NLRP3 inflammasomes, which are protein complexes responsible for the proteolytic activation of IL-1 β .

proinflammatory mediators can also induce disinhibition of neuronal excitability by attenuating GABA and glycine release from interneurons and inhibitory descending projections, and by downregulating KCC2 on postsynaptic terminals [5].

Nitroxidative species regulate the production of proinflammatory mediators during pathological pain. For example, NF- κ B and p38 MAPK are responsible for the production of a wide array of proinflammatory mediators in immune cells. Nitroxidative products degrade/inhibit I κ B and MAPK phosphatases, resulting in activation of NF- κ B and p38 that both mediate inflammatory and neuropathic pain [52,104–107]. Furthermore, nitroxidative species may promote the release of neuron-to-glia signals such as matrix metalloproteases (MMPs) (Figure 3) [108].

Nitroxidative species also elicit proinflammatory responses via TLR signaling. TLRs bind a variety of endogenous ligands (danger-associated molecular patterns, DAMPs), including DNA and *N*-formyl peptides from nitroxidatively damaged mitochondria, to trigger innate immune responses that contribute to pathological pain [5,109]. ROS serve a vital role as second messengers for TLR signaling. A rapid (minutes) respiratory burst occurs upon activation of TLR2 and 4, which is mediated by a direct interaction with the intracellular domains of NOX1, 2, and 4 enzymes. This NOX activity is essential for downstream NF- κ B- and p38 MAPK-dependent cytokine production [110–114]. Furthermore, activation of NOX enzymes by TLR signaling induces transcription of TLRs, and promotes membrane expression in lipid rafts, which is necessary for efficient signaling [111,115,116]. In concert with disruption of blood–brain barrier tight junctions by nitroxidative species, the TLR2–NOX1 interaction also upregulates adhesion molecules via CCL3 to facilitate transendothelial cell migration, which contributes to nociceptive hypersensitivity after PNI (Figure 3) [102,110,117].

ROS have been implicated in the activation of NLRP3 inflammasomes [118] – protein complexes responsible for the proteolytic activation of IL-1 β , a proinflammatory cytokine with a well-established role in pathological pain [5,101,119]. Among the various sensor molecules that trigger the formation of inflammasomes, NLRP3 has been most widely investigated and has a recently described role in neuropathic pain [120]. The relative contributions of ROS to the activation versus priming of NLRP3 inflammasomes remains to be elucidated [119]. Mitochondria are key participants in the activation of NLRP3 inflammasomes: they are a source of ROS that can directly activate NLRP3, as well as of oxidized mitochondrial DNA that can also activate NLRP3 (Figure 3) [118,121–123]. Furthermore, TRPM2 activation by nitroxidative species induces a calcium flux that activates the NLRP3 inflammasome [124].

Finally, there is a reciprocal relationship between nitroxidative species and inflammatory signaling. For example, the transcription of NOX and NOS enzymes is upregulated by TLR4 and 9 signaling, as well as by NF- κ B and p38 activation [19,125–129]. The purinergic receptor P2X7, which has a documented role in pathological pain, also induces ROS production [5,120,130]. ATP signaling through P2X7R activates NOX2 in a calcium and p38-dependent fashion [131–133].

Endogenous Regulators of Nitroxidative Signaling

Under healthy conditions, nitroxidative species and antioxidants exist in a balanced state because nitroxidative products play a vital physiological role in cellular processes (e.g., signal transduction, pathogen defense [134–136]). In response to increased production of nitroxidative species during injury or infection, antioxidant and regulatory systems are activated in an attempt to recover homeostasis (Figure 1) [14].

Antioxidant Defense

Transcription of antioxidant genes is a crucial step in controlling nitroxidative signaling. One key transcription factor is nuclear factor E2-related factor 2 (Nrf2). Nrf2 is expressed in CNS and PNS

neurons, macrophages, Schwann cells, astrocytes, and microglia [137–139]. Under homeostatic conditions, cytosolic Nrf2 is sequestered by the protein Keap1 and ubiquitinated for degradation. However, in the presence of oxidants and electrophiles, Nrf2 is released from Keap1 and translocates to the nucleus [140]. Nrf2 binds to the antioxidant response element (ARE) promoter region to elicit expression of >200 antioxidant genes, including those encoding superoxide dismutases (SOD1, cytosolic; SOD2, mitochondrial), catalase, glutathione, and heme-oxygenases [140]. Another transcription factor, forkhead box class O (FoxO), is also responsible for the production of SOD2 and catalase [141]. Many of these antioxidants are ubiquitously expressed, and their catabolic function is summarized in Figure 1 [142].

These endogenous antioxidant systems collaborate to detoxify reactive nitroxidative species (Figure 1). The evidence is mixed whether neuroinflammatory or traumatic events increase nervous system antioxidant levels [143–152]. This likely reflects a temporally- and injury-specific antioxidant response, and the fact that injury-induced nitroxidative species can negatively regulate antioxidant production [15,76]. Antioxidant system activation can limit pathological pain: deletion of SOD1 exacerbates neuropathic pain, while exogenous antioxidants attenuate nociceptive hypersensitivity in a range of inflammatory and neuropathic pain models [37,108,153–155]. Similarly, heme-oxygenases, which elicit the expression of various antioxidants, protect cells and could improve inflammation and neuropathic pain [21]. Therefore, therapies that increase antioxidant systems could resolve neuroinflammation and pain symptoms.

Anti-Inflammatory Cytokine and Adenosine Signaling

Cytokines such as IL-10 and TGF- β counter-regulate proinflammatory signaling and contribute to the resolution of neuropathic pain hypersensitivity [5,156,157]. One mechanism of action is via the regulation of nitroxidative signaling. For example, IL-10 and TGF- β inhibit NOX2 activity and promote antioxidant production [158–160]. This is a reciprocal relationship because antioxidants can also drive the production of anti-inflammatory cytokines [161,162]. Adenosine signaling is also anti-nociceptive in pathological pain models [163–165]. Signaling through A_{2A} and A₃ receptors inhibits NOX activity, and drives the production of anti-inflammatory cytokines and antioxidants [163,166,167].

Opposition of Opioid Analgesia by Nitroxidative Species

Opioid analgesics remain the cornerstone of management of moderate-to-severe pain. However, the clinical utility of opioids is limited by tolerance, which is characterized by dose escalation as a result of reduced sensitivity to an opioid agonist, as well as by hyperalgesia, a paradoxical increase in pain sensitivity induced by opioid exposure [168,169]. Recent evidence has identified a role for nitroxidative signaling in these phenomena [6,170].

NOX activity is elevated by morphine, and genetic or pharmacological disruption of these enzymes attenuates tolerance and hyperalgesia [171–173]. Superoxide and peroxynitrite have been implicated as downstream mediators because decomposition catalysts also attenuate tolerance and hyperalgesia [174–176]. It remains unclear how morphine engages these enzymes, but it may be mediated by classical μ -opioid receptors and/or TLR4 [168]. The pronociceptive mechanisms of nitroxidative species, described above, may act as an opposing process of neuronally-mediated opioid analgesia to create tolerance, or may overshadow analgesia to induce hyperalgesia. Therefore, correcting nitroxidative imbalance may improve the clinical profile of opioids [170].

Nitroxidative signaling also disrupts endogenous opioid analgesia in supraspinal sites that are engaged to inhibit spinal nociception via descending projections. For example, upregulation of peroxynitrite during inflammatory pain results in nitration of met-enkephalin in the rostral

ventromedial medulla (RVM), and this reduces opioid receptor binding affinity [177]. This may be normalized by intra-RVM microinjections of FeTMPyP⁵⁺, which was antinociceptive in inflammatory and neuropathic pain models [177].

Nitroxidative Signaling as a Therapeutic Target for Pathological Pain

Under pathological conditions, endogenous antioxidant responses can be insufficient, leading to an accumulation of toxic nitroxidative species. As mentioned above, unchecked increases in nitroxidative species can promote cytotoxicity and inflammation via cascading pronociceptive signaling. Therefore, discovering therapeutic treatments that enhance cellular antioxidant capacity could help to achieve nitroxidative balance to recover homeostasis.

Initial efforts to combat increases in nitroxidative species in a wide range of neurological disorders used direct antioxidant compounds (e.g., vitamins C and E, coenzyme Q). The consensus view is that the possible beneficial effects are outweighed by unfavorable pharmacokinetic and pharmacodynamic profiles [13,178,179]. A variety of redox-active therapeutics are being developed to overcome these issues, and are effective in treating cancer-induced bone pain as well as inflammatory and neuropathic pain, and can also potentiate opioid analgesia [9,10,180].

Newer approaches have instead aimed to inhibit sources of nitroxidative species, stimulate endogenous antioxidants, and prevent nitroxidative damage [13,178]. To this end, inhibitors of specific NOX and NOS isoforms, and ROS toxifiers such as MPO, are being developed and may prove effective for pain treatment [13,181]. As noted above, A_{2A} and A₃ adenosine receptor agonists attenuate spinal NOX activity and promote antioxidant production, with a concomitant decrease in neuropathic pain [163–165]. Another promising approach is the development of small molecules that catalyze the clearance of reactive aldehydes [182].

Indirect antioxidants augment the redox response without being antioxidants themselves. For example, sulforaphane, resveratrol, and curcumin induce nuclear translocation of Nrf2, a transcription factor responsible for the production of a wide array of antioxidants, and attenuate nociceptive hypersensitivity in neuropathic pain models [21,183–186]. Non-pharmacological approaches may also function in this capacity. For example, exercise increases Nrf2 expression and promotes the expression of antioxidants in the CNS as well as peripherally [187–189]. Consequently, voluntary wheel running has been shown to both prevent and reverse neuropathic pain [187,190].

Finally, ROS have a role in normal physiological processes [134–136], and there is some evidence that ROS may have protective effects after injury. For example, inflammation induced by endotoxin is exacerbated in NADPH-impaired mice relative to their wild-type counterparts [191]. In another study, yeast survival to hydrogen peroxide stress was dependent on superoxide [192]. Further work will be necessary to determine whether ROS may also have a protective role after sterile nervous system injury. However, agents have been developed to spare superoxide (e.g., peroxynitrite decomposition catalysts SRI110 and SRI6 [15]), and such approaches may prove to be important for restoring homeostasis after nervous system injury.

Concluding Remarks

Nitroxidative species are generated by mitochondria and by NOX and NOS enzymes. They enhance neuroexcitability in pain pathways through direct neuronal interactions, and indirectly by impairing mitochondria and inducing neuroinflammation. Normalizing nitroxidative signaling may be an alternative strategy to help to alleviate the enormous burden of pathological pain, which affects ~20% of the population and is poorly treated [11,193,194]. There are several

Outstanding Questions

How ubiquitous are nitroxidative signaling mechanisms within the neuraxis, beyond the classical sites already tested (peripheral nerve injury site, DRG, spinal cord)?

Are nitroxidative signaling mechanisms common or different between different preclinical pain models?

What is the relationship between the antioxidant and anti-inflammatory cytokine systems?

Do indirect antioxidants have improved translational potential for treatment of pathological pain?

areas of basic science research that may move us towards that goal (see Outstanding Questions).

Despite the extensive research implicating nitroxidative species in pathological pain states, no studies to date have quantified the crucial relationships between real-time local cellular creation of nitroxidative species, their concentration at the effect site, and the distribution of their direct effects. This challenge has not been overcome owing to the volatility of these nitroxidative species and hence their very short lifetimes *in vivo* and *ex vivo*. Several new technologies are being developed to address these issues and are discussed in [Box 1](#) and [Table 1](#).

Lessons from the failure of direct antioxidants to improve clinical disease need to be recognized within the pain field: the effects of direct antioxidants on preclinical pain models continue to be reported despite the strong probability that the results will not translate clinically. Several studies suggest that more-robustly engaging antioxidant systems after injury can help alleviate pain: for instance, in animal pain models, increasing the action of master antioxidant transcription factors Nrf2 or FoxO, or activating the heme-oxygenase system, show promising pain-relieving effects. Future studies could explore whether combinatorial strategies – aimed at boosting multiple antioxidants or targeting both antioxidant and nitroxidative systems simultaneously – dampen inflammation and pain. Nitroxidant dysregulation clearly contributes to neuropathology; thus, discovering new targets and therapies that restore nitroxidative balance could help to relieve pathological pain.

Box 1. New and Emerging Tools To Study Nitroxidative Species

Colorimetric and fluorescent methods for detecting the 'shadow' of the presence of nitroxidative species production is well established by the quantification of attendant cellular events (e.g., oxidative stress such as lipid peroxidation: thiobarbituric acid reactive substances (TBARS) [195]; DNA damage (8-oxoguanine, 8-OxoG) [196,197]) or the quantification of more stable metabolites (e.g., nitrite/nitrate using the Griess reaction [198]). These methods are not only limited in their temporal and spatial resolution, but also because of their insufficient ability to define the concentrations and time-courses of specific nitroxidative species. Establishing differential regulation of distinct nitroxidative species would be useful because specific oxygen or nitrogen species have unique outcomes in the neuroinflammatory responses. A recent example demonstrated that specifically targeting peroxynitrite reduced inflammatory progression via NLRP3 inflammasome-dependent IL-1 β /IL-18 release following intracerebral hemorrhage injury [199]. Thus, new biosensors will be necessary to improve our mechanistic understanding of how nitroxidative species affect the nervous system.

The chemistry of fluorescent probes for specific detection of both *ex vivo* and *in vivo* production of nitroxidative species has grown rapidly. A range of approaches and hence biosensors have been created that exploit platform sensing modalities, such as photoinduced electron transfer (PET) and Förster resonance energy transfer (FRET) signaling. In addition, composite biosensors that incorporate a sensor functionalized to a nanoparticle [gold particles, upconversion nanoparticles (UCNPs), and QDots] are being used to detect and/or measure ROS/RNS species (detailed in [Table 1](#)). Such ROS probes can quantify hypochlorite [200,201], hydroxyl [202,203], superoxide [204], hydrogen peroxide [205], and singlet oxygen [206]. Biosensors for nitric oxide [207,208], nitroxyl [209–211], peroxynitrite [212] are also being developed.

These probes detect targeted species in cell lines, in *ex vivo* tissue, or in *in vivo* models of inflammation. However, these biosensor tools require further optimization. Further refinement of biosensors will help to improve the stability of the probe, the brightness of the fluorescing molecule, the specificity to defined species, the sensitivity of detection, and the consumption of the probe in the sensing process. However, real-time visualization and/or quantification of nitroxidative species within the CNS of a behaving preclinical rodent model of pathological pain remains an elusive goal.

The ultimate nitroxidative species biosensor would have real-time sensing capacity, with signal brightness that can detect the subcellular localization of the nitroxidative species; ideally, this probe would not be consumed/bleached in the sensing process, thereby allowing repeated measurements *in vivo*. Next-generation probes will address some of these limitations. For instance, a redox-sensitive fluorescent protein (xrFP1), whose fluorescence intensity is positively related to the extent of oxidation of the probe, can detect varying amounts of oxidative stress within separate cellular compartments [213]. Further refining these tools will enable an improved understanding of how particular species contribute to oxidative or nitrosative stress, and will allow researchers to define how the spatiotemporal regulation of nitroxidative activity contributes to pathological pain.

Table 1. Probes Able To Detect Specific ROS and RNS Species *In Vitro*, *Ex Vivo*, or *In Vivo*^a

	Probe type	Imaging platform used	Tested <i>in vitro</i>	Tested <i>ex vivo</i> / <i>in vivo</i>	ROS/RNS stimulation	Refs
<i>ROS species</i>						
Hypochlorite	Iridium (III) complex-based two-photon phosphorescent probe	Two-photon laser scanning fluorescence microscope and confocal laser microscope	HeLa cells/RAW 264.7 cells	Zebrafish	10 mM NaClO (HeLa) 1 mg/ml LPS (RAW 264.7 and zebrafish)	[201]
Hypochlorite	Rhodamine-based hydrazide protein fluorescent probe	Fluorescence microscope	HeLa cells		50 μ M OCl ⁻	[200]
Hydroxyl	Ratiometric fluorescence biosensor (gold particles conjugated with organic fluorophore)	Confocal laser microscope	HeLa cells		10 μ g/ml LPS	[203]
Hydroxyl	Ratiometric fluorescence biosensor (upconversion nanoparticles conjugated with organic fluorophore)	Fluorescence microscope equipped with 980 nm laser	HeLa cells	Mouse liver	500 ng/ml PMA (<i>in vitro</i>) 1–4 mg LPS/100 g body weight (<i>in vivo</i>)	[202]
Superoxide	Fluorescein protein-based fluorescent probe	Confocal laser microscope	HCT116/BV-2/RAW 264.7 cells	Zebrafish	500 ng/ml LPS and 50 ng/ml IFN- γ (<i>in vitro</i>) PMA 200 ng/ml or antimycin A 500 nM (<i>in vivo</i>)	[204]
Hydrogen peroxide	Chemoselective fluorescent naphthylimide peroxide probe	Two-photon laser scanning fluorescence microscope	RAW 264.7 cells	Mouse lung and skin	1 μ g/ml LPS (<i>in vitro</i>) 20 μ g LPS (<i>in vivo</i>)	[205]
Singlet oxygen	Far-red silicon-rhodamine-based chemical fluorescent probe	Fluorescence microscope with 640 nm laser	HeLa cells/RAW 264.7 cells		Photosensitizers: 150 μ g/ml 5-ALA and 5 μ M TMPyP4	[206]
<i>RNS species</i>						
Nitric oxide	Chemoselective copper(II)-based fluorescence probe	Confocal laser microscope	HeLa cells/RAW 264.7 cells		50–200 μ M DEA-NONate (HeLa) 200 ng/ml LPS (RAW 264.7)	[208]
Nitric oxide	Far-red two-photon chemical fluorescent probe	Two-photon laser scanning fluorescence microscope	HeLa cells/RAW 264.7 cells	Mouse liver	25 μ M NOC-9 (HeLa) 20 μ g/ml LPS, 200 U/ml IFN- γ and 0.5 mg/ml L-arginine (RAW 264.7) 1–4 mg/ml LPS (<i>in vivo</i>)	[207]
Nitroxyl	FRET-based ratiometric chemical fluorescent probe	Confocal laser microscope	HeLa cells		100 μ M AS	[211]

Table 1. (continued)

	Probe type	Imaging platform used	Tested <i>in vitro</i>	Tested <i>ex vivo/ in vivo</i>	ROS/RNS stimulation	Refs
Nitroxyl	Near infrared chemical fluorescent probe	Confocal laser microscope and <i>in vivo</i> imaging system	RAW 264.7 cells	Mouse (<i>in vivo</i>)	100 μ M AS (RAW 264.7) 500 μ M AS (i.p. Mouse)	[210]
Nitroxyl	Lysosome-targetable near infrared chemical fluorescent probe	Confocal laser microscope and <i>in vivo</i> imaging system	RAW 264.7 cells	Mouse (<i>in vivo</i>)	200 μ M AS (RAW 264.7) 1 mM AS (i.p. mouse)	[209]
Peroxynitrite	Boronate-based chemical fluorescent probe	Confocal laser microscope	HeLa cells/RAW 264.7 cells		5 and 20 μ M peroxyxynitrite solution (HeLa) 1 μ g/ml LPS, 50 ng/ml IFN- γ , 2.5 ng/ml PMA (RAW 264.7)	[212]

^aAbbreviations: AS, Angeli's salt (nitroxyl donor); 5-ALA, 5-aminolevulinic acid (drug used in photodynamic therapy, known to produce singlet oxygen); antimycin A, produces endogenous ROS/RNS by driving apoptosis; DEA-NONOate, 2-(*N,N*-diethylamino)-diazolotetrazol-2-oxide (nitric oxide donor); IFN- γ , interferon γ (produces endogenous ROS/RNS); LPS, lipopolysaccharide (produces endogenous ROS/RNS); NOC-9, 6-[2-hydroxy-1-methyl-2-nitrosodiazirino]-*N*-methyl-1-hexanamine (nitric oxide donor); PMA, phorbol 12-myristate-13-acetate (activates protein kinase C *in vivo* and *in vitro*); TMPyP4, 5,10,15,20-tetra-(*N*-methyl-4-pyridyl)porphyrin (drug used in photodynamic therapy, known to produce singlet oxygen).

Acknowledgments

This work was supported by an Australian Postgraduate Research scholarship (V.S.), an ARC Research Fellowship (DP110100297; M.R.H.), funding from the ARC Centre of Excellence for Nanoscale Biophotonics (CE140100003; M.R.H.), National Institutes of Health (NIH) grant DE021966 (L.R.W.), and a Wings for Life Project Grant (L.R.W./A.D.G.).

References

- Krebs, H.A. and Johnson, W.A. (1937) The role of citric acid in intermediate metabolism in animal tissues. *Enzymologia* 4, 148–156
- Gozsy, B. and Szent-Gyorgyi, A. (1934) On the mechanism of primary respiration in pigeon breast muscle. *Hoppe. Seylers Z. Physiol. Chem.* 224, 1–10 (in German)
- Harden, A. and Young, W.J. (1906) The alcoholic ferment of yeast-juice. *Proc. R. Soc. Lond. B Biol. Sci.* 77, 405–420
- Maass, O. and Hatcher, W.H. (1920) The properties of pure hydrogen peroxide. I. *J. Am. Chem. Soc.* 42, 2548–2569
- Grace, P.M. *et al.* (2014) Pathological pain and the neuroimmune interface. *Nat. Rev. Immunol.* 14, 217–231
- Salvemini, D. *et al.* (2011) Roles of reactive oxygen and nitrogen species in pain. *Free Radic. Biol. Med.* 51, 951–966
- Janes, K. *et al.* (2012) Anti-superoxide and anti-peroxynitrite strategies in pain suppression. *Biochim. Biophys. Acta* 1822, 815–821
- Little, J.W. *et al.* (2012) Reactive nitroxidative species and nociceptive processing: determining the roles for nitric oxide, superoxide, and peroxynitrite in pain. *Amino Acids* 42, 75–94
- Symons-Liguori, A. *et al.* (2016) The contribution of nitroxidative stress to pathophysiological pain and opioid analgesic failure. In *Redox-Active Therapeutics* (Batinic-Haberle, I. *et al.*, eds), pp. 563–595, Springer International Publishing
- Batinic-Haberle, I. *et al.* (2016) Mn porphyrin-based redox-active therapeutics. In *Redox-Active Therapeutics* (Batinic-Haberle, I. *et al.*, eds), pp. 165–211, Springer International Publishing
- Pizzo, P.A. and Clark, N.M. (2012) Alleviating suffering 101 – pain relief in the United States. *N. Engl. J. Med.* 366, 197–199
- Burma, N.E. *et al.* (2016) Animal models of chronic pain: advances and challenges for clinical translation. *J. Neurosci. Res.* Published online July 4, 2016. <http://dx.doi.org/10.1002/jnr.23768>
- Casas, A.I. *et al.* (2015) Reactive oxygen-related diseases: therapeutic targets and emerging clinical indications. *Antioxid. Redox Signal.* 23, 1171–1185
- Holmström, K.M. and Finkel, T. (2014) Cellular mechanisms and physiological consequences of redox-dependent signalling. *Nat. Rev. Mol. Cell Biol.* 15, 411–421
- Doyle, T. *et al.* (2012) Targeting the overproduction of peroxynitrite for the prevention and reversal of paclitaxel-induced neuropathic pain. *J. Neurosci.* 32, 6149–6160
- Hassler, S.N. *et al.* (2014) Reactive oxygen species and lipid peroxidation inhibitors reduce mechanical sensitivity in a chronic neuropathic pain model of spinal cord injury in rats. *J. Neurochem.* 131, 413–417
- Nayernia, Z. *et al.* (2014) New insights on NOX enzymes in the central nervous system. *Antioxid. Redox Signal.* 20, 2815–2837
- Ibi, M. *et al.* (2008) Reactive oxygen species derived from NOX1/NADPH oxidase enhance inflammatory pain. *J. Neurosci.* 28, 9486–9494
- Kim, J.-S. *et al.* (2010) Glycogen synthase kinase-3 β and β -catenin pathway is involved in Toll-like receptor 4-mediated NADPH oxidase 1 expression in macrophages. *FEBS J.* 277, 2830–2837
- Kallenborn-Gerhardt, W. *et al.* (2014) Nox2-dependent signaling between macrophages and sensory neurons contributes to neuropathic pain hypersensitivity. *Pain* 155, 2161–2170
- Kim, D. *et al.* (2010) NADPH oxidase 2-derived reactive oxygen species in spinal cord microglia contribute to peripheral nerve

- injury-induced neuropathic pain. *Proc. Natl. Acad. Sci. U.S.A.* 107, 14851–14856
22. Hackel, D. *et al.* (2013) The connection of monocytes and reactive oxygen species in pain. *PloS ONE* 8, e63564
 23. Kallenborn-Gerhardt, W. *et al.* (2012) NADPH oxidase-4 maintains neuropathic pain after peripheral nerve injury. *J. Neurosci.* 32, 10136–10145
 24. Lee, C.F. *et al.* (2010) Nox4 is a novel inducible source of reactive oxygen species in monocytes and macrophages and mediates oxidized low density lipoprotein-induced macrophage death. *Circ. Res.* 106, 1489–1497
 25. Grace, P.M. *et al.* (2010) A novel animal model of graded neuropathic pain: utility to investigate mechanisms of population heterogeneity. *J. Neurosci. Methods* 193, 47–53
 26. Wen, Y.-R. *et al.* (2007) Nerve conduction blockade in the sciatic nerve prevents but does not reverse the activation of p38 mitogen-activated protein kinase in spinal microglia in the rat spared nerve injury model. *Anesthesiology* 107, 312–321
 27. Xie, W. *et al.* (2009) Early blockade of injured primary sensory afferents reduces glial cell activation in two rat neuropathic pain models. *Neuroscience* 160, 847–857
 28. Cury, Y. *et al.* (2011) Pain and analgesia: the dual effect of nitric oxide in the nociceptive system. *Nitric Oxide Biol. Chem.* 25, 243–254
 29. Brecht, D.S. *et al.* (1990) Localization of nitric oxide synthase indicating a neural role for nitric oxide. *Nature* 347, 768–770
 30. Cao, J. *et al.* (2005) The PSD95–nNOS interface: a target for inhibition of excitotoxic p38 stress-activated protein kinase activation and cell death. *J. Cell Biol.* 168, 117–126
 31. Askwith, T. *et al.* (2012) Taurine reduces nitrosative stress and nitric oxide synthase expression in high glucose-exposed human Schwann cells. *Exp. Neurol.* 233, 154–162
 32. Annedi, S.C. *et al.* (2011) Discovery of N-(3-(1-methyl-1,2,3,6-tetrahydropyridin-4-yl)-1H-indol-6-yl) thiophene-2-carboximide as a selective inhibitor of human neuronal nitric oxide synthase (nNOS) for the treatment of pain. *J. Med. Chem.* 54, 7408–7416
 33. Keilhoff, G. *et al.* (2013) Time-course of neuropathic pain in mice deficient in neuronal or inducible nitric oxide synthase. *Neurosci. Res.* 77, 215–221
 34. Mihara, Y. *et al.* (2011) Involvement of spinal NR2B-containing NMDA receptors in oxaliplatin-induced mechanical allodynia in rats. *Mol. Pain* 7, 8
 35. Mukherjee, P. *et al.* (2014) Development of nitric oxide synthase inhibitors for neurodegeneration and neuropathic pain. *Chem. Soc. Rev.* 43, 6814–6838
 36. Bonnelous, C. *et al.* (2009) Discovery of inducible nitric oxide synthase (iNOS) inhibitor development candidate KD7332. Part 1. Identification of a novel, potent, and selective series of quinoline NOS dimerization inhibitors that are orally active in rodent pain models. *J. Med. Chem.* 52, 3047–3062
 37. Tanabe, M. *et al.* (2009) Pharmacological assessments of nitric oxide synthase isoforms and downstream diversity of NO signaling in the maintenance of thermal and mechanical hypersensitivity after peripheral nerve injury in mice. *Neuropharmacology* 56, 702–708
 38. Borsani, E. *et al.* (2013) Endothelial nitric oxide synthase in dorsal root ganglia during chronic inflammatory nociception. *Cells Tissues Organs* 197, 159–169
 39. Galluzzi, L. *et al.* (2012) Mitochondria: master regulators of danger signalling. *Nat. Rev. Mol. Cell Biol.* 13, 780–788
 40. Schwartz, E.S. *et al.* (2008) Oxidative stress in the spinal cord is an important contributor in capsaicin-induced mechanical secondary hyperalgesia in mice. *Pain* 138, 514–524
 41. Schwartz, E.S. *et al.* (2009) Persistent pain is dependent on spinal mitochondrial antioxidant levels. *J. Neurosci.* 29, 159–168
 42. Chu, C. *et al.* (2011) Mitochondrial dependence of nerve growth factor-induced mechanical hyperalgesia. *Pain* 152, 1832–1837
 43. Ferrari, L.F. and Levine, J.D. (2010) Alcohol consumption enhances antiretroviral painful peripheral neuropathy by mitochondrial mechanisms. *Eur. J. Neurosci.* 32, 811–818
 44. Joseph, E.K. and Levine, J.D. (2006) Mitochondrial electron transport in models of neuropathic and inflammatory pain. *Pain* 121, 105–114
 45. Joseph, E.K. and Levine, J.D. (2010) Multiple PKC α -dependent mechanisms mediating mechanical hyperalgesia. *Pain* 150, 17–21
 46. Zheng, H. *et al.* (2011) Functional deficits in peripheral nerve mitochondria in rats with paclitaxel- and oxaliplatin-evoked painful peripheral neuropathy. *Exp. Neurol.* 232, 154–161
 47. Basbaum, A.I. *et al.* (2009) Cellular and molecular mechanisms of pain. *Cell* 139, 267–284
 48. Gold, M.S. and Gebhart, G.F. (2010) Nociceptor sensitization in pain pathogenesis. *Nat. Med.* 16, 1248–1257
 49. Latremoliere, A. and Woolf, C.J. (2009) Central sensitization: a generator of pain hypersensitivity by central neural plasticity. *J. Pain* 10, 895–926
 50. Ren, K. and Dubner, R. (2010) Interactions between the immune and nervous systems in pain. *Nat. Med.* 16, 1267–1276
 51. Gwak, Y.S. *et al.* (2013) Reactive oxygen species contribute to neuropathic pain and locomotor dysfunction via activation of CaMKII in remote segments following spinal cord contusion injury in rats. *Pain* 154, 1699–1708
 52. Ndengele, M.M. *et al.* (2008) Cyclooxygenases 1 and 2 contribute to peroxynitrite-mediated inflammatory pain hypersensitivity. *FASEB J.* 22, 3154–3164
 53. Yovtak, J. *et al.* (2011) Reactive oxygen species contribute to neuropathic pain by reducing spinal GABA release. *Pain* 152, 844–852
 54. Wang, Z.-Q. *et al.* (2004) A newly identified role for superoxide in inflammatory pain. *J. Pharmacol. Exp. Ther.* 309, 869–878
 55. Sözbir, E. and Nazroglu, M. (2016) Diabetes enhances oxidative stress-induced TRPM2 channel activity and its control by N-acetylcysteine in rat dorsal root ganglion and brain. *Metab. Brain Dis.* 31, 385–393
 56. Chen, Z. *et al.* (2010) NMDA-receptor activation and nitrosative regulation of the glutamatergic pathway during nociceptive processing. *Pain* 149, 100–106
 57. Lee, I. *et al.* (2007) The role of reactive oxygen species in capsaicin-induced mechanical hyperalgesia and in the activities of dorsal horn neurons. *Pain* 133, 9–17
 58. Rausaria, S. *et al.* (2011) Retooling manganese(III) porphyrin-based peroxynitrite decomposition catalysts for selectivity and oral activity: a potential new strategy for treating chronic pain. *J. Med. Chem.* 54, 8658–8669
 59. Lorenz, J.E. *et al.* (2014) Oxidant-induced activation of cGMP-dependent protein kinase I α mediates neuropathic pain after peripheral nerve injury. *Antioxid. Redox Signal.* 21, 1504–1515
 60. Luo, C. *et al.* (2012) Presynaptically localized cyclic GMP-dependent protein kinase 1 is a key determinant of spinal synaptic potentiation and pain hypersensitivity. *PLoS Biol.* 10, e1001283
 61. Muscoli, C. *et al.* (2013) Posttranslational nitration of tyrosine residues modulates glutamate transmission and contributes to N-methyl-D-aspartate-mediated thermal hyperalgesia. *Mediators Inflamm.* 2013, 950947
 62. Gao, X. *et al.* (2007) Reactive oxygen species (ROS) are involved in enhancement of NMDA-receptor phosphorylation in animal models of pain. *Pain* 131, 262–271
 63. Zanelli, S.A. *et al.* (2002) Nitration is a mechanism of regulation of the NMDA receptor function during hypoxia. *Neuroscience* 112, 869–877
 64. Yovtak, J. *et al.* (2013) Effect of antioxidant treatment on spinal GABA neurons in a neuropathic pain model in the mouse. *Pain* 154, 2469–2476
 65. Julius, D. (2013) TRP channels and pain. *Annu. Rev. Cell Dev. Biol.* 29, 355–384
 66. Xanthos, D.N. and Sandkühler, J. (2014) Neurogenic neuroinflammation: inflammatory CNS reactions in response to neuronal activity. *Nat. Rev. Neurosci.* 15, 43–53
 67. Andersson, D.A. *et al.* (2015) Streptozotocin stimulates the ion channel TRPA1 directly: involvement of peroxynitrite. *J. Biol. Chem.* 290, 15185–15196

66. Bautista, D.M. *et al.* (2006) TRPA1 mediates the inflammatory actions of environmental irritants and proalgesic agents. *Cell* 124, 1269–1282
69. Bessac, B.F. *et al.* (2009) Transient receptor potential ankyrin 1 antagonists block the noxious effects of toxic industrial isocyanates and tear gases. *FASEB J.* 23, 1102–1114
70. Taylor-Clark, T.E. and Undem, B.J. (2010) Ozone activates airway nerves via the selective stimulation of TRPA1 ion channels. *J. Physiol.* 588, 423–433
71. Taylor-Clark, T.E. *et al.* (2009) Nitrooleic acid, an endogenous product of nitrate stress, activates nociceptive sensory nerves via the direct activation of TRPA1. *Mol. Pharmacol.* 75, 820–829
72. Trevisani, M. *et al.* (2007) 4-Hydroxynonenal, an endogenous aldehyde, causes pain and neurogenic inflammation through activation of the irritant receptor TRPA1. *Proc. Natl. Acad. Sci.* 104, 13519–13524
73. Due, M.R. *et al.* (2014) Acrolein involvement in sensory and behavioral hypersensitivity following spinal cord injury in the rat. *J. Neurochem.* 128, 776–786
74. Chen, Z. *et al.* (2016) Mitigation of sensory and motor deficits by acrolein scavenger phenethylzine in a rat model of spinal cord contusive injury. *J. Neurochem.* 138, 328–338
75. Trevisan, G. *et al.* (2013) Novel therapeutic strategy to prevent chemotherapy-induced persistent sensory neuropathy by TRPA1 blockade. *Cancer Res.* 73, 3120–3131
76. Chen, S. *et al.* (2013) Role of TRPM2 in cell proliferation and susceptibility to oxidative stress. *Am. J. Physiol. Cell Physiol.* 304, C548–C560
77. Haraguchi, K. *et al.* (2012) TRPM2 contributes to inflammatory and neuropathic pain through the aggravation of pronociceptive inflammatory responses in mice. *J. Neurosci.* 32, 3931–3941
78. Naziroglu, M. *et al.* (2013) Role of TRPM2 cation channels in dorsal root ganglion of rats after experimental spinal cord injury. *Muscle Nerve* 48, 945–950
79. Özdemir, Ü.S. *et al.* (2015) *Hypericum perforatum* attenuates spinal cord injury-induced oxidative stress and apoptosis in the dorsal root ganglion of rats: involvement of TRPM2 and TRPV1 channels. *Mol. Neurobiol.* 53, 3540–3551
80. Perraud, A.-L. *et al.* (2005) Accumulation of free ADP-ribose from mitochondria mediates oxidative stress-induced gating of TRPM2 cation channels. *J. Biol. Chem.* 280, 6138–6148
81. Yamamoto, S. *et al.* (2008) TRPM2-mediated Ca^{2+} influx induces chemokine production in monocytes that aggravates inflammatory neutrophil infiltration. *Nat. Med.* 14, 738–747
82. Isami, K. *et al.* (2013) Involvement of TRPM2 in peripheral nerve injury-induced infiltration of peripheral immune cells into the spinal cord in mouse neuropathic pain model. *PLOS ONE* 8, e66410
83. Chung, M.-K. *et al.* (2015) The role of TRPM2 in hydrogen peroxide-induced expression of inflammatory cytokine and chemokine in rat trigeminal ganglia. *Neuroscience* 297, 160–169
84. Naziroglu, M. *et al.* (2014) Modulation of oxidative stress and Ca^{2+} mobilization through TRPM2 channels in rat dorsal root ganglion neuron by *Hypericum perforatum*. *Neuroscience* 263, 27–35
85. So, K. *et al.* (2015) Involvement of TRPM2 in a wide range of inflammatory and neuropathic pain mouse models. *J. Pharmacol. Sci.* 127, 237–243
86. Chuang, H. and Lin, S. (2009) Oxidative challenges sensitize the capsaicin receptor by covalent cysteine modification. *Proc. Natl. Acad. Sci. U.S.A.* 106, 20097–20102
87. Susankova, K. *et al.* (2006) Reducing and oxidizing agents sensitize heat-activated vanilloid receptor (TRPV1) current. *Mol. Pharmacol.* 70, 383–394
88. Westlund, K.N. *et al.* (2010) Impact of central and peripheral TRPV1 and ROS levels on proinflammatory mediators and nociceptive behavior. *Mol. Pain* 6, 46
89. Patwardhan, A.M. *et al.* (2009) Activation of TRPV1 in the spinal cord by oxidized linoleic acid metabolites contributes to inflammatory hyperalgesia. *Proc. Natl. Acad. Sci. U.S.A.* 106, 18820–18824
90. Patwardhan, A.M. *et al.* (2010) Heat generates oxidized linoleic acid metabolites that activate TRPV1 and produce pain in rodents. *J. Clin. Invest.* 120, 1617–1626
91. Bennett, G.J. *et al.* (2014) Mitotoxicity in distal symmetrical sensory peripheral neuropathies. *Nat. Rev. Neurol.* 10, 326–336
92. MacMillan-Crow, L.A. and Thompson, J.A. (1999) Tyrosine modifications and inactivation of active site manganese superoxide dismutase mutant (Y34F) by peroxynitrite. *Arch. Biochem. Biophys.* 366, 82–88
93. Zarkovic, N. *et al.* (2013) Pathophysiological relevance of aldehydic protein modifications. *J. Proteomics* 92, 239–247
94. Sinha, K. *et al.* (2013) Oxidative stress: the mitochondria-dependent and mitochondria-independent pathways of apoptosis. *Arch. Toxicol.* 87, 1157–1180
95. Yuan, H. *et al.* (2006) Mitochondrial fission is an upstream and required event for bax foci formation in response to nitric oxide in cortical neurons. *Cell Death Differ.* 14, 462–471
96. Scheving, R. *et al.* (2012) Protein S-nitrosylation and denitrosylation in the mouse spinal cord upon injury of the sciatic nerve. *J. Proteomics* 75, 3967–4004
97. Joseph, E.K. and Levine, J.D. (2004) Caspase signalling in neuropathic and inflammatory pain in the rat. *Eur. J. Neurosci.* 20, 2896–2902
98. Ferrari, L.F. *et al.* (2011) Role of Drp1, a key mitochondrial fission protein, in neuropathic pain. *J. Neurosci.* 31, 11404–11410
99. Janes, K. *et al.* (2013) Bioenergetic deficits in peripheral nerve sensory axons during chemotherapy-induced neuropathic pain resulting from peroxynitrite-mediated post-translational nitration of mitochondrial superoxide dismutase. *Pain* 154, 2432–2440
100. Lim, T.K.Y. *et al.* (2015) Mitochondrial and bioenergetic dysfunction in trauma-induced painful peripheral neuropathy. *Mol. Pain* 11, 58
101. Austin, P.J. and Moalem-Taylor, G. (2010) The neuro-immune balance in neuropathic pain: involvement of inflammatory immune cells, immune-like glial cells and cytokines. *J. Neuroimmunol.* 229, 26–50
102. Grace, P.M. *et al.* (2011) Peripheral immune contributions to the maintenance of central glial activation underlying neuropathic pain. *Brain, Behav. Immun.* 25, 1322–1332
103. Gaudet, A.D. *et al.* (2011) Wallerian degeneration: gaining perspective on inflammatory events after peripheral nerve injury. *J. Neuroinflammation* 8, 110
104. Genovese, T. *et al.* (2009) Effects of a metalloporphyrinic peroxynitrite decomposition catalyst, ww-85, in a mouse model of spinal cord injury. *Free Radic. Res.* 43, 631–645
105. Kamata, H. *et al.* (2005) Reactive oxygen species promote TNF α -induced death and sustained JNK activation by inhibiting MAP kinase phosphatases. *Cell* 120, 649–661
106. Matata, B.M. and Galifianes, M. (2002) Peroxynitrite is an essential component of cytokines production mechanism in human monocytes through modulation of nuclear factor-kappa B DNA binding activity. *J. Biol. Chem.* 277, 2330–2335
107. Zhou, H. *et al.* (2013) CD11b/CD18 (Mac-1) is a novel surface receptor for extracellular double-stranded RNA to mediate cellular inflammatory responses. *J. Immunol.* 190, 115–125
108. Li, J. *et al.* (2016) N-acetyl-cysteine attenuates neuropathic pain by suppressing matrix metalloproteinases. *Pain* 157, 1711–1723
109. Zhang, Q. *et al.* (2010) Circulating mitochondrial DAMPs cause inflammatory responses to injury. *Nature* 464, 104–107
110. Lee, J.H. *et al.* (2013) Interaction of NADPH oxidase 1 with Toll-like receptor 2 induces migration of smooth muscle cells. *Cardiovasc. Res.* 99, 483–493
111. Nakahira, K. *et al.* (2006) Carbon monoxide differentially inhibits TLR signaling pathways by regulating ROS-induced trafficking of TLRs to lipid rafts. *J. Exp. Med.* 203, 2377–2389
112. Park, H.S. *et al.* (2004) Direct interaction of TLR4 with NAD(P)H oxidase 4 isozyme is essential for lipopolysaccharide-induced production of reactive oxygen species and activation of NF- κ B. *J. Immunol.* 173, 3589–3593
113. Yang, C.-S. *et al.* (2008) ASK1-p38 MAPK-p47phox activation is essential for inflammatory responses during tuberculosis via TLR2-ROS signalling. *Cell. Microbiol.* 10, 741–754

114. Yang, C.-S. *et al.* (2009) NADPH oxidase 2 interaction with TLR2 is required for efficient innate immune responses to mycobacteria via cathelicidin expression. *J. Immunol.* 182, 3696–3705
115. Matsuzawa, A. *et al.* (2005) ROS-dependent activation of the TRAF6-ASK1-p38 pathway is selectively required for TLR4-mediated innate immunity. *Nat. Immunol.* 6, 587–592
116. Wong, S.W. *et al.* (2009) Fatty acids modulate Toll-like receptor 4 activation through regulation of receptor dimerization and recruitment into lipid rafts in a reactive oxygen species-dependent manner. *J. Biol. Chem.* 284, 27384–27392
117. Lochhead, J.J. *et al.* (2012) Tempol modulates changes in xenobiotic permeability and occludin oligomeric assemblies at the blood-brain barrier during inflammatory pain. *Am. J. Physiol. Heart Circ. Physiol.* 302, H582–593
118. Zhou, R. *et al.* (2010) Thioredoxin-interacting protein links oxidative stress to inflammasome activation. *Nat. Immunol.* 11, 136–140
119. Latz, E. *et al.* (2013) Activation and regulation of the inflammasomes. *Nat. Rev. Immunol.* 13, 397–411
120. Grace, P.M. *et al.* (2016) Morphine paradoxically prolongs neuropathic pain in rats by amplifying spinal NLRP3 inflammasome activation. *Proc. Natl. Acad. Sci. U.S.A.* 113, E3441–E3450
121. Nakahira, K. *et al.* (2011) Autophagy proteins regulate innate immune responses by inhibiting the release of mitochondrial DNA mediated by the NALP3 inflammasome. *Nat. Immunol.* 12, 222–230
122. Shimada, K. *et al.* (2012) Oxidized mitochondrial DNA activates the NLRP3 inflammasome during apoptosis. *Immunity* 36, 401–414
123. Zhou, R. *et al.* (2011) A role for mitochondria in NLRP3 inflammasome activation. *Nature* 469, 221–225
124. Zhong, Z. *et al.* (2013) TRPM2 links oxidative stress to NLRP3 inflammasome activation. *Nat. Commun.* 4, 1611
125. Anrather, J. *et al.* (2006) NF- κ B regulates phagocytic NADPH oxidase by inducing the expression of gp91phox. *J. Biol. Chem.* 281, 5657–5667
126. Guo, Z. *et al.* (2007) Identification of a classic cytokine-induced enhancer upstream in the human iNOS promoter. *FASEB J.* 21, 535–542
127. Lee, J.-G. *et al.* (2008) A combination of Lox-1 and Nox1 regulates TLR9-mediated foam cell formation. *Cell. Signal.* 20, 2266–2275
128. Li, Y. *et al.* (2007) Regulation of neuronal nitric oxide synthase exon 1f gene expression by nuclear factor- κ B acetylation in human neuroblastoma cells. *J. Neurochem.* 101, 1194–1204
129. Yoo, B.K. *et al.* (2008) Activation of p38 MAPK induced peroxynitrite generation in LPS plus IFN- γ -stimulated rat primary astrocytes via activation of iNOS and NADPH oxidase. *Neurochem. Int.* 52, 1188–1197
130. Sorge, R.E. *et al.* (2012) Genetically determined P2X7 receptor pore formation regulates variability in chronic pain sensitivity. *Nat. Med.* 18, 595–599
131. Apolloni, S. *et al.* (2013) The NADPH oxidase pathway is dysregulated by the P2X7 receptor in the SOD1-G93A microglia model of amyotrophic lateral sclerosis. *J. Immunol.* 190, 5187–5195
132. Kim, S.Y. *et al.* (2007) ATP released from beta-amyloid-stimulated microglia induces reactive oxygen species production in an autocrine fashion. *Exp. Mol. Med.* 39, 820–827
133. Parvathani, L.K. *et al.* (2003) P2X7 mediates superoxide production in primary microglia and is up-regulated in a transgenic mouse model of Alzheimer's disease. *J. Biol. Chem.* 278, 13309–13317
134. Sena, L.A. and Chandel, N.S. (2012) Physiological roles of mitochondrial reactive oxygen species. *Mol. Cell* 48, 158–167
135. Zuo, L. *et al.* (2015) Biological and physiological role of reactive oxygen species – the good, the bad and the ugly. *Acta Physiol.* 214, 329–348
136. Massaad, C.A. and Klann, E. (2011) Reactive oxygen species in the regulation of synaptic plasticity and memory. *Antioxid. Redox Signal.* 14, 2013–2054
137. Dang, J. *et al.* (2012) Nrf2 expression by neurons, astroglia, and microglia in the cerebral cortex of ischemic rats. *J. Mol. Neurosci.* 46, 578–584
138. Ishii, T. *et al.* (1999) Oxidative stress-inducible proteins in macrophages. *Free Radic. Res.* 31, 351–355
139. Vincent, A.M. *et al.* (2009) Sensory neurons and Schwann cells respond to oxidative stress by increasing antioxidant defense mechanisms. *Antioxid. Redox Signal.* 11, 425–438
140. Hayes, J.D. and Dinkova-Kostova, A.T. (2014) The Nrf2 regulatory network provides an interface between redox and intermediary metabolism. *Trends Biochem. Sci.* 39, 199–218
141. Klotz, L.-O. *et al.* (2015) Redox regulation of FoxO transcription factors. *Redox Biol.* 6, 51–72
142. Vihardt, F. *et al.* (2016) Microglia antioxidant systems and redox signaling. *Br. J. Pharmacol.* Published online January 11, 2016. <http://dx.doi.org/10.1111/bph.13426>
143. Goecks, C.S.B. *et al.* (2012) Assessment of oxidative parameters in rat spinal cord after chronic constriction of the sciatic nerve. *Neurochem. Res.* 37, 1952–1958
144. Guedes, R.P. *et al.* (2006) Neuropathic pain modifies antioxidant activity in rat spinal cord. *Neurochem. Res.* 31, 603–609
145. Guedes, R.P. *et al.* (2009) Sciatic nerve transection increases glutathione antioxidant system activity and neuronal nitric oxide synthase expression in the spinal cord. *Brain Res. Bull.* 80, 422–427
146. Hu, P. *et al.* (2015) Secoisolaricresinol diglycoside, a flavone lignan, exerts analgesic effects in a mouse model of type 1 diabetes: engagement of antioxidant mechanism. *Eur. J. Pharmacol.* 767, 183–192
147. Kallenborn-Gerhardt, W. *et al.* (2013) Antioxidant activity of seselin 2 controls neuropathic pain after peripheral nerve injury. *Antioxid. Redox Signal.* 19, 2013–2023
148. Liu, X. *et al.* (2015) Spinal heme oxygenase-1 (HO-1) exerts antinociceptive effects against neuropathic pain in a mouse model of L5 spinal nerve ligation. *Pain Med.* 17, 220–229
149. Naik, A.K. *et al.* (2006) Role of oxidative stress in pathophysiology of peripheral neuropathy and modulation by N-acetyl-L-cysteine in rats. *Eur. J. Pain* 10, 573–579
150. Pabreja, K. *et al.* (2011) Minocycline attenuates the development of diabetic neuropathic pain: possible anti-inflammatory and antioxidant mechanisms. *Eur. J. Pharmacol.* 661, 15–21
151. Pathak, N.N. *et al.* (2014) Atorvastatin attenuates neuropathic pain in rat neuropathy model by down-regulating oxidative damage at peripheral, spinal and supraspinal levels. *Neurochem. Int.* 68, 1–9
152. Scheidt, T. *et al.* (2013) Sciatic nerve transection modulates oxidative parameters in spinal and supraspinal regions. *Neurochem. Res.* 38, 935–942
153. Berger, J.V. *et al.* (2011) Enhanced neuroinflammation and pain hypersensitivity after peripheral nerve injury in rats expressing mutated superoxide dismutase 1. *J. Neuroinflammation* 8, 33
154. Kong, Q. *et al.* (2012) Heme oxygenase-1 inhibits neuropathic pain in rats with diabetic mellitus. *Neural Regen. Res.* 7, 2305–2311
155. Shen, Y. *et al.* (2015) Exogenous induction of HO-1 alleviates vincristine-induced neuropathic pain by reducing spinal glial activation in mice. *Neurobiol. Dis.* 79, 100–110
156. Chen, G. *et al.* (2015) Intrathecal bone marrow stromal cells inhibit neuropathic pain via TGF- β secretion. *J. Clin. Invest.* 125, 3226–3240
157. Kwilasz, A.J. *et al.* (2015) The therapeutic potential of interleukin-10 in neuroimmune diseases. *Neuropharmacology* 96, 55–69
158. Lee, T.-S. and Chau, L.-Y. (2002) Heme oxygenase-1 mediates the anti-inflammatory effect of interleukin-10 in mice. *Nat. Med.* 8, 240–246
159. Qian, L. *et al.* (2006) Interleukin-10 protects lipopolysaccharide-induced neurotoxicity in primary midbrain cultures by inhibiting the function of NADPH oxidase. *J. Pharmacol. Exp. Ther.* 319, 44–52
160. Qian, L. *et al.* (2008) Potent anti-inflammatory and neuroprotective effects of TGF- β 1 are mediated through the inhibition of

- ERK and p47phox-Ser345 phosphorylation and translocation in microglia. *J. Immunol.* 1950 181, 660–668
161. Jadhav, A. *et al.* (2013) The heme oxygenase system selectively enhances the anti-inflammatory macrophage-M2 phenotype, reduces pericardial adiposity, and ameliorated cardiac injury in diabetic cardiomyopathy in Zucker diabetic fatty rats. *J. Pharmacol. Exp. Ther.* 345, 239–249
162. Plantadosi, C.A. *et al.* (2011) Heme oxygenase-1 couples activation of mitochondrial biogenesis to anti-inflammatory cytokine expression. *J. Biol. Chem.* 286, 16374–16385
163. Janes, K. *et al.* (2014) A3 adenosine receptor agonist prevents the development of paclitaxel-induced neuropathic pain by modulating spinal glial-restricted redox-dependent signaling pathways. *Pain* 155, 2560–2567
164. Little, J.W. *et al.* (2015) Endogenous adenosine A3 receptor activation selectively alleviates persistent pain states. *Brain* 138, 28–35
165. Loram, L.C. *et al.* (2009) Enduring reversal of neuropathic pain by a single intrathecal injection of adenosine 2A receptor agonists: a novel therapy for neuropathic pain. *J. Neurosci.* 29, 14015–14025
166. Sun, W. *et al.* (2007) Pharmacologic characterization of novel adenosine A2A receptor agonists in equine neutrophils. *Am. J. Vet. Res.* 68, 981–987
167. Sun, W. *et al.* (2007) Effects of stimulation of adenosine A2A receptors on lipopolysaccharide-induced production of reactive oxygen species by equine neutrophils. *Am. J. Vet. Res.* 68, 649–656
168. Grace, P.M. *et al.* (2015) Opioid-induced central immune signaling: implications for opioid analgesia. *Headache* 55, 475–489
169. Hutchinson, M.R. *et al.* (2011) Exploring the neuroimmunopharmacology of opioids: an integrative review of mechanisms of central immune signaling and their implications for opioid analgesia. *Pharmacol. Rev.* 63, 772–810
170. Salvemini, D. and Neumann, W.L. (2009) Peroxynitrite: a strategic linchpin of opioid analgesic tolerance. *Trends Pharmacol. Sci.* 30, 194–202
171. Doyle, T. *et al.* (2010) Spinal NADPH oxidase is a source of superoxide in the development of morphine-induced hyperalgesia and antinociceptive tolerance. *Neurosci. Lett.* 483, 85–89
172. Doyle, T. *et al.* (2013) NADPH-oxidase 2 activation promotes opioid-induced antinociceptive tolerance in mice. *Neuroscience* 241, 1–9
173. Ibi, M. *et al.* (2011) Involvement of NOX1/NADPH oxidase in morphine-induced analgesia and tolerance. *J. Neurosci.* 31, 18094–18103
174. Little, J.W. *et al.* (2013) Spinal mitochondrial-derived peroxynitrite enhances neuroimmune activation during morphine hyperalgesia and antinociceptive tolerance. *Pain* 154, 978–986
175. Muscoli, C. *et al.* (2007) Therapeutic manipulation of peroxynitrite attenuates the development of opiate-induced antinociceptive tolerance in mice. *J. Clin. Invest.* 117, 3530–3539
176. Batinić-Haberle, I. *et al.* (2009) Lipophilicity is a critical parameter that dominates the efficacy of metalloporphyrins in blocking the development of morphine antinociceptive tolerance through peroxynitrite-mediated pathways. *Free Radic. Biol. Med.* 46, 212–219
177. Little, J.W. *et al.* (2012) Supraspinal peroxynitrite modulates pain signaling by suppressing the endogenous opioid pathway. *J. Neurosci.* 32, 10797–10808
178. Schmidt, H.H.H.W. *et al.* (2015) Antioxidants in translational medicine. *Antioxid. Redox Signal.* 23, 1130–1143
179. Salvemini, D. *et al.* (2002) SOD mimetics are coming of age. *Nat. Rev. Drug Discov.* 1, 367–374
180. Slosky, L.M. *et al.* (2016) The cystine/glutamate antiporter system xc⁻ drives breast tumor cell glutamate release and cancer-induced bone pain. *Pain* 157, 2605–2616
181. Dao, V.T. *et al.* (2015) Pharmacology and clinical drug candidates in redox medicine. *Antioxid. Redox Signal.* 23, 1113–1129
182. Zambelli, V.O. *et al.* (2014) Aldehyde dehydrogenase-2 regulates nociception in rodent models of acute inflammatory pain. *Sci. Transl. Med.* 6, 251ra118
183. Fattori, V. *et al.* (2015) Curcumin inhibits superoxide anion-induced pain-like behavior and leukocyte recruitment by increasing Nrf2 expression and reducing NF- κ B activation. *Inflamm. Res.* 64, 993–1003
184. Juan, S.H. *et al.* (2005) Mechanism of concentration-dependent induction of heme oxygenase-1 by resveratrol in human aortic smooth muscle cells. *Biochem. Pharmacol.* 69, 41–48
185. Negi, G. *et al.* (2011) Nrf2 and NF- κ B modulation by sulforaphane counteracts multiple manifestations of diabetic neuropathy in rats and high glucose-induced changes. *Curr. Neurovasc. Res.* 8, 294–304
186. Yang, Y. *et al.* (2016) Resveratrol suppresses glial activation and alleviates trigeminal neuralgia via activation of AMPK. *J. Neuroinflammation* 13, 84
187. Benson, C. *et al.* (2015) Voluntary wheel running delays disease onset and reduces pain hypersensitivity in early experimental autoimmune encephalomyelitis (EAE). *Exp. Neurol.* 271, 279–290
188. Navarro, A. *et al.* (2004) Beneficial effects of moderate exercise on mice aging: survival, behavior, oxidative stress, and mitochondrial electron transfer. *Am. J. Physiol. Regul. Integr. Comp. Physiol.* 286, R505–R511
189. Souza, P.S. *et al.* (2016) Physical exercise attenuates experimental autoimmune encephalomyelitis by inhibiting peripheral immune response and blood-brain barrier disruption. *Mol. Neurobiol.* Published online July 22, 2016. <http://dx.doi.org/10.1007/s12035-016-0014-0>
190. Grace, P.M. *et al.* (2016) Prior voluntary wheel running attenuates neuropathic pain. *Pain* 157, 2012–2023
191. Deng, J. *et al.* (2012) Protective role of reactive oxygen species in endotoxin-induced lung inflammation through modulation of IL-10 expression. *J. Immunol.* 188, 5734–5740
192. Thorpe, G.W. *et al.* (2013) Superoxide radicals have a protective role during H₂O₂ stress. *Mol. Biol. Cell* 24, 2876–2884
193. Blyth, F.M. *et al.* (2001) Chronic pain in Australia: a prevalence study. *Pain* 89, 127–134
194. Breivik, H. *et al.* (2006) Survey of chronic pain in Europe: prevalence, impact on daily life, and treatment. *Eur. J. Pain* 10, 287–333
195. Patton, S. and Kurtz, G.W. (1951) 2-Thiobarbituric acid as a reagent for detecting milk fat oxidation. *J. Dairy Sci.* 34, 669–674
196. Bospalov, I.A. *et al.* (1999) Fabs specific for 8-oxoguanine: control of DNA binding. *J. Mol. Biol.* 293, 1085–1095
197. Soultanakis, R.P. *et al.* (2000) Fluorescence detection of 8-oxoguanine in nuclear and mitochondrial DNA of cultured cells using a recombinant Fab and confocal scanning laser microscopy. *Free Radic. Biol. Med.* 28, 987–998
198. Griess, P. (1879) Bemerkungen zu der Abhandlung der H.H. Weselsky und Benedikt 'Ueber einige Azoverbindungen'. *Berichte Dtsch. Chem. Ges.* 12, 426–428
199. Feng, L. *et al.* (2015) P2X7R blockade prevents NLRP3 inflammasome activation and brain injury in a rat model of intracerebral hemorrhage: involvement of peroxynitrite. *J. Neuroinflammation* 12, 190
200. Goswami, S. *et al.* (2014) Nanomolar detection of hypochlorite by a rhodamine-based chiral hydrazide in absolute aqueous media: application in tap water analysis with live-cell imaging. *Anal. Chem.* 86, 6315–6322
201. Li, G. *et al.* (2015) A mitochondrial targeted two-photon iridium(III) phosphorescent probe for selective detection of hypochlorite in live cells and in vivo. *Biomaterials* 53, 285–295
202. Li, Z. *et al.* (2015) A rationally designed upconversion nanoprobe for in vivo detection of hydroxyl radical. *J. Am. Chem. Soc.* 137, 11179–11185
203. Zhuang, M. *et al.* (2014) Ratiometric fluorescence probe for monitoring hydroxyl radical in live cells based on gold nano-clusters. *Anal. Chem.* 86, 1829–1836
204. Hu, J.J. *et al.* (2015) Fluorescent probe HKSX-1 for imaging and detection of endogenous superoxide in live cells and in vivo. *J. Am. Chem. Soc.* 137, 6837–6843
205. Rong, L. *et al.* (2016) Hydrogen peroxide detection with high specificity in living cells and inflamed tissues. *Regen. Biomater.* Published online June 11 2016. <http://dx.doi.org/10.1093/rb/rbw022>

206. Kim, S. *et al.* (2014) Far-red fluorescence probe for monitoring singlet oxygen during photodynamic therapy. *J. Am. Chem. Soc.* 136, 11707–11715
207. Mao, Z. *et al.* (2016) NIR in, far-red out: developing a two-photon fluorescent probe for tracking nitric oxide in deep tissue. *Chem. Sci.* 7, 5230–5235
208. Sun, X. *et al.* (2016) A water-soluble copper(II) complex for the selective fluorescence detection of nitric oxide/nitroxyl and imaging in living cells. *ChemPlusChem* 81, 30–34
209. Jing, X. *et al.* (2014) Visualization of nitroxyl (HNO) in vivo via a lysosome-targetable near-infrared fluorescent probe. *Chem. Commun.* 50, 14253–14256
210. Liu, P. *et al.* (2015) A near-infrared fluorescent probe for the selective detection of HNO in living cells and in vivo. *Analyst* 140, 4576–4583
211. Zhang, H. *et al.* (2015) A FRET-based ratiometric fluorescent probe for nitroxyl detection in living cells. *ACS Appl. Mater. Interfaces* 7, 5438–5443
212. Sun, X. *et al.* (2014) A water-soluble boronate-based fluorescent probe for the selective detection of peroxynitrite and imaging in living cells. *Chem. Sci.* 5, 3368–3373
213. Fan, Y. and Ai, H. (2016) Development of redox-sensitive red fluorescent proteins for imaging redox dynamics in cellular compartments. *Anal. Bioanal. Chem.* 408, 2901–2911